

3. SITE 658¹

Shipboard Scientific Party²

HOLE 658A

Date occupied: 4 March 1986, 1515 UTC

Date departed: 7 March 1986, 0231 UTC

Time on hole: 59.25 hr

Position: 20°44.95'N, 18°34.85'W

Water depth (sea level; corrected m, echo-sounding): 2262.8

Water depth (rig floor; corrected m, echo-sounding): 2273.3

Bottom felt (rig floor; m, drill pipe measurement): 2274.7

Distance between rig floor and sea level (m): 10.5

Total depth (rig floor, m): 2575.5

Penetration (m): 300.4

Number of cores (including cores with no recovery): 33

Total length of cored section (m): 300.4

Total core recovered (m): 295

Core recovery (%): 98.2

Oldest sediment cored:

Depth (mbsf): 300

Nature: clayey calcareous nannofossil ooze

Age: early Pliocene, NN14/15, ~3.5–3.8 Ma

HOLE 658B

Date occupied: 7 March 1986, 0244 UTC

Date departed: 8 March 1986, 0045 UTC

¹ Ruddiman, W., Sarnthein, M., Baldauf, J., et al., 1988. *Proc., Init. Repts. (Pt. A), ODP*, 108.

² William Ruddiman (Co-Chief Scientist), Lamont-Doherty Geological Observatory, Palisades, NY 10964; Michael Sarnthein (Co-Chief Scientist), Geologisch-Paläontologisches Institut, Universität Kiel, Olshausenstrasse 40, D-2300 Kiel, Federal Republic of Germany; Jack Baldauf, ODP Staff Scientist, Ocean Drilling Program, Texas A&M University, College Station, TX 77843; Jan Backman, Department of Geology, University of Stockholm, S-106 91 Stockholm, Sweden; Jan Bloemendal, Graduate School of Oceanography, University of Rhode Island, Narragansett, RI 02882-1197; William Curry, Woods Hole Oceanographic Institution, Woods Hole, MA 02543; Paul Farrimond, School of Chemistry, University of Bristol, Cantocks Close, Bristol BS8 1TS, United Kingdom; Jean Claude Faugeres, Laboratoire de Géologie-Océanographie, Université de Bordeaux I, Avenue des Facultés Talence 33405, France; Thomas Janacek, Lamont-Doherty Geological Observatory, Palisades, NY 10964; Yuzo Katsura, Institute of Geosciences, University of Tsukuba, Ibaraki 305, Japan; Hélène Manivit, Laboratoire de Stratigraphie des Continents et Océans, (UA 319) Université Paris VI, 4 Place Jussieu, 75230 Paris Cedex, France; James Mazzullo, Department of Geology, Texas A&M University, College Station, TX 77843; Jürgen Mienert, Geologisch-Paläontologisches Institut, Universität Kiel, Olshausenstrasse 40, D-2300 Kiel, Federal Republic of Germany, and Woods Hole Oceanographic Institution, Woods Hole, MA 02543; Edward Pokras, Lamont-Doherty Geological Observatory, Palisades, NY 10964; Maureen Raymo, Lamont-Doherty Geological Observatory, Palisades, NY 10964; Peter Schultheiss, Institute of Oceanographic Sciences, Brook Road, Wormley, Godalming, Surrey GU8 5UG, United Kingdom; Rüdiger Stein, Geologisch-Paläontologisches Institut, Universität Giessen, Senckenbergstrasse 3, 6300 Giessen, Federal Republic of Germany; Lisa Tauxe, Scripps Institution of Oceanography, La Jolla, CA 92093; Jean-Pierre Valet, Centre des Faibles Radioactivités, CNRS, Avenue de la Terrasse, 91190 Gif-sur-Yvette, France; Philip Weaver, Institute of Oceanographic Sciences, Brook Road, Wormley, Godalming, Surrey GU8 5UG, United Kingdom; Hisato Yasuda, Department of Geology, Kochi University, Kochi 780, Japan.

Time on hole: 22 hr

Position: 20°44.95'N, 18°34.85'W

Water depth (sea level; corrected m, echo-sounding): 2262.8

Water depth (rig floor; corrected m, echo-sounding): 2273.3

Bottom felt (rig floor; m, drill pipe measurement): 2274.7

Distance between rig floor and sea level (m): 10.5

Total depth (rig floor, m): 2438.5

Penetration (m): 163.8

Number of cores (including cores with no recovery): 18

Total length of cored section (m): 163.8

Total core recovered (m): 175.83

Core recovery (%): 107.35

Oldest sediment cored:

Depth (mbsf): 163.8

Nature: clayey siliceous ooze

Age: late Pliocene, NN17, ~2.4 Ma

HOLE 658C

Date occupied: 8 March 1986, 0045 UTC

Date departed: 8 March 1986, 1600 UTC

Time on hole: 15.75 hr

Position: 20°44.95'N, 18°34.85'W

Water depth (sea level; corrected m, echo-sounding): 2262.8

Water depth (rig floor; corrected m, echo-sounding): 2273.3

Bottom felt (rig floor; m, drill pipe measurement): 2274.7

Distance between rig floor and sea level (m): 10.5

Total depth (rig floor, m): 2346.3

Penetration (m): 72.9

Number of cores (including cores with no recovery): 8

Total length of cored section (m): 72.9

Total core recovered (m): 70.3

Core recovery (%): 96.4

Oldest sediment cored:

Depth (mbsf): 70.3

Nature: nannofossil ooze

Age: NN19 top, ~0.5 Ma

Principal results: Site 658 is located at 20°44.95'N, 18°34.85'W, on the continental slope 160 km west of Cap Blanc at 2263.6 m water depth. For the first time in the history of the Deep Sea Drilling Project/Ocean Drilling Program, Site 658 cored hemipelagic sediments lying directly underneath one of the major nearshore cells of permanent oceanic upwelling in the world ocean. These sediments also are deposited in the central region of the dust supply from northern trade winds that control upwelling intensity. The site was drilled into a largely undisturbed pillow-shaped seismic sediment section near the outer margin of a protruding terrace on the slope—a position that should restrict lateral sediment input from near-bottom downslope transport.

From Holes 658A, 658B, and 658C we recovered a total of 44 advanced piston cores (APC) to depths of 157.9 meters below seafloor

(mbsf) (Hole 658A), 163.8 mbsf (Hole 658B), and 72.9 mbsf (Hole 658C) and 15 extended-core-barrel (XCB) cores from Hole 658A to a total penetration depth of 300.4 mbsf. The eight cores from Hole 658C were reserved for special organo-chemical analyses. Drilling results are summarized in a stratigraphic section (Fig. 1).

The upper Pliocene-Holocene sediment section at Site 658 comprises three major hemipelagic lithologic units, the upper of which is divided into two subunits. All units have good paleomagnetic and biostratigraphic time control despite increased carbonate dissolution in Unit II. Parastriatigraphic curves from magnetic-susceptibility data enabled us to establish a detailed composite-depth section for Holes 658A and 658B down to 90 mbsf. These curves promise further downhole correlations in the future, despite numerous artificial voids in the core recovery because of extensive degassing in the core liners.

Unit I. 0–91.2 mbsf. Pleistocene (lowermost Brunhes) to Holocene. Dark olive gray to gray nannofossil ooze with minor amounts of quartz silt, foraminifers, and siliceous microfossils. Cyclic variations of measured carbonate content (28%–69%) and of organic carbon (up to 2.3%). Sedimentation rates are exceedingly high at

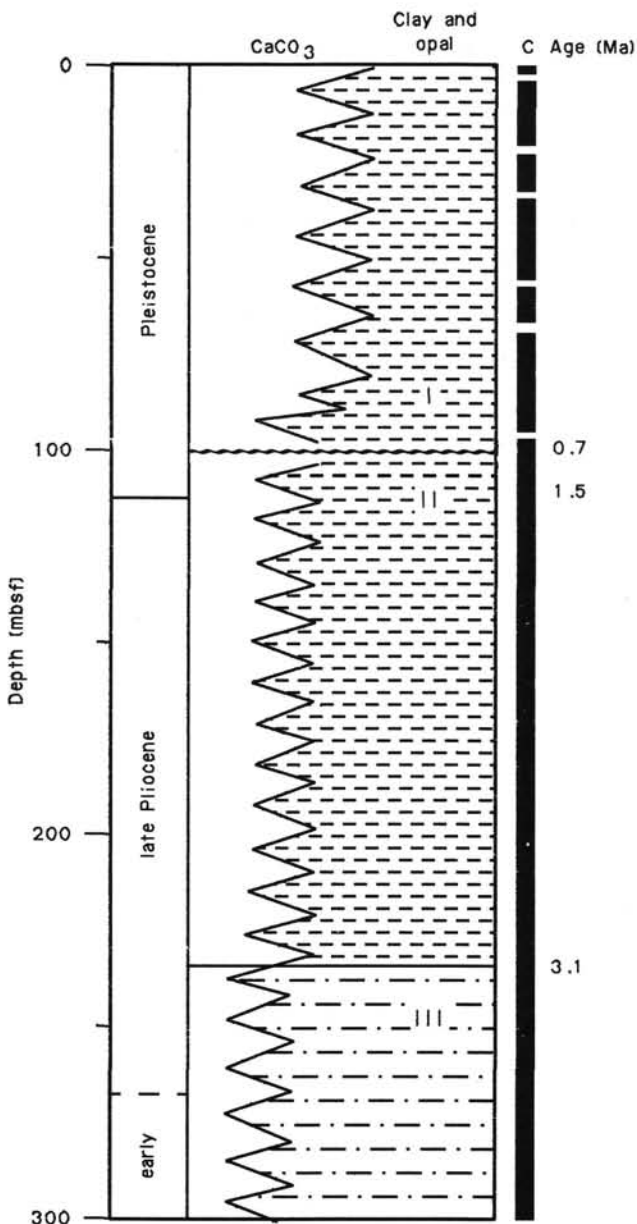


Figure 1. Summary of the stratigraphic section at Site 658. Presentation of CaCO_3 cycles is schematic and based on widely spaced shipboard laboratory analyses. $C = > 1.0\%$ organic carbon.

147 m/m.y. Subunit IA (0–34.2 mbsf) is nannofossil ooze with minor amounts of quartz silt and foraminifers; Subunit IB (34.2–91.2 mbsf) is nannofossil ooze grading into diatom nannofossil ooze and nannofossil diatom ooze. A major hiatus with a duration of 0.8 m.y. forms the base of Unit I.

Unit II. 91.2–233.9 mbsf. Upper Pliocene to lower Pleistocene. Cyclic nannofossil ooze interbedded with mixtures of calcareous, siliceous, and siliciclastic sediments, olive to olive gray. High content of opaline matter according to bulk-grain-density data and up to 3.3% organic carbon. From 19% to 50% carbonate. Bulk-sedimentation rate is 72 m/m.y. in the upper part, 108 m/m.y. in the lower part of Unit II.

Unit III. 233.9–300.4 mbsf. Lower to upper Pliocene. Nannofossil and nannofossil-bearing mud and nannofossil ooze with only minor amounts of siliceous biogenic debris and up to 3% organic carbon. Cyclic variations from gray to dark gray parallel fluctuations of carbonate content (10%–45%). Bulk-sedimentation rate is 112 m/m.y.

The major hiatus at the base of the Brunhes chron can be related to two adjoining slump-style, pinch-out structures on the seismic record near the site. The resulting mass flow is similar in composition and age to slump deposits occurring at companion Site 657 on the continental rise. Below the hiatus, two independent quantitative estimates suggest a correlation of lithologic Unit II with a bowl-shaped, almost transparent seismic section, assuming sound velocities near 900–950 m/s, which would indicate free gas in the sediment. This assumption agrees with the high content of biogenic gas in the sediment cores, particularly below 90 mbsf, and is probably the result of a high content of organic carbon, with the methane/ethane ratio increasing downcore from 5000 to 6000 at 60 mbsf and to 1250 at 300 mbsf.

Overall, coring at Site 658 was highly successful. The ongoing hemipelagic depositional environment during the last 3.5 m.y., combined with high sedimentation rates, provided an excellent record of the history of the Cap Blanc upwelling cell. After 0.7 Ma, its productivity fluctuated in (approximately) 100 k.y. cycles, as shown by variations in carbon content and in the content of biogenic silica, especially diatoms. Both variables were particularly abundant prior to 1.5 Ma. However, only estimates of mass accumulation rates for detailed sediment intervals can provide insights into the actual variations of upwelling productivity. In addition, the low-temperature regime of the upwelling cell may account for unusual first- and last-occurrence datums of some planktonic species similar at times to those found in transitional and higher latitudes of the Atlantic. Finally, the varying nearshore input of wind-borne (and possibly river-borne) terrigenous matter is reflected in the quartzose silt and mud fraction, which was most abundant prior to 3.0 Ma and less frequent from 3.0 to 1.5 Ma. Detection of the actual trade-wind signal in this fraction will require detailed laboratory work.

BACKGROUND AND SCIENTIFIC OBJECTIVES

Introduction

The scientific objectives for Site 658 ($20^{\circ}44.95'N$, $18^{\circ}34.85'W$) are closely related to those for companion Site 657 and have already been explained in great detail elsewhere (see Site 657 chapter, this volume). Site 658 was drilled on the continental slope at the outer margin of a terrace approximately 163 km (90 nmi) west of Cap Blanc, at 2263.6 m water depth (Fig. 2). A major 40-m-high escarpment of a geologically recent sediment slide lies 6–7 km downslope from the position of the site (Figs. 3 and 4) and can be traced on seismic records more than 35 km from north northwest to south southeast. The angle of the slope at the site is 150 m for a 4500-m distance (equal to 3.5% or 1.75°).

For the first time in DSDP/ODP history, Site 658 cored sediments that lie directly underneath a highly productive cell of permanent oceanic upwelling. This upwelling cell offshore from Cap Blanc (Fig. 5) is one of the four major upwelling zones of the world ocean attached to an eastern (passive) continental margin (Schemainda et al., 1975; Tomczak and Hughes, 1980). Hence, the site position provides an ideal opportunity for the following investigations:

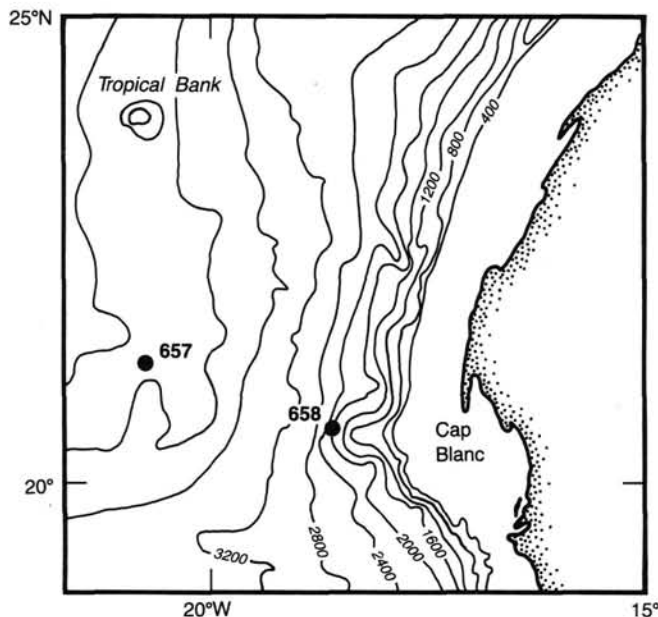


Figure 2. Location map of Sites 658 and 657. Bathymetric values in meters.

1. To monitor the history of the upwelling cell in a fairly continuous, high-resolution hemipelagic sediment record and to compare it with the "non-upwelling" sediment record of neighboring Sites 657 and 659 through late Neogene and Quaternary time (see Fig. 3, Site 657 chapter, this volume; Site 659 chapter, this volume).

2. To analyze the accumulation rates of organic carbon and biogenic opal as a measure of oceanic productivity in a key region (Thiede et al., 1982) and to estimate their influence on the atmospheric CO₂ balance and climatic change through time.

3. To study in detail the early diagenesis of organic compounds in the sediment.

4. To characterize the unusual physical and magnetic properties of a thick sediment body anomalously rich in organic carbon.

5. To investigate the evolution of cold-water organisms within an almost isolated and highly fertile water mass in low latitudes (Thiede, 1975; Cifelli and Stern-Bernier, 1977).

6. To trace back through time the sources of the upwelled water as a signal of intermediate-water paleoceanography (Codispoti and Friederich, 1978).

7. To study eolo-marine dust deposits as a clear signal of the fluctuating trade-wind regime, which in turn controls the intensity of oceanic upwelling (Sarnthein et al., 1982) (see Fig. 3, Site 657 chapter, this volume).

8. To apply spectral analysis to the time series of various paleoceanographic and climatic proxy data related to upwelling.

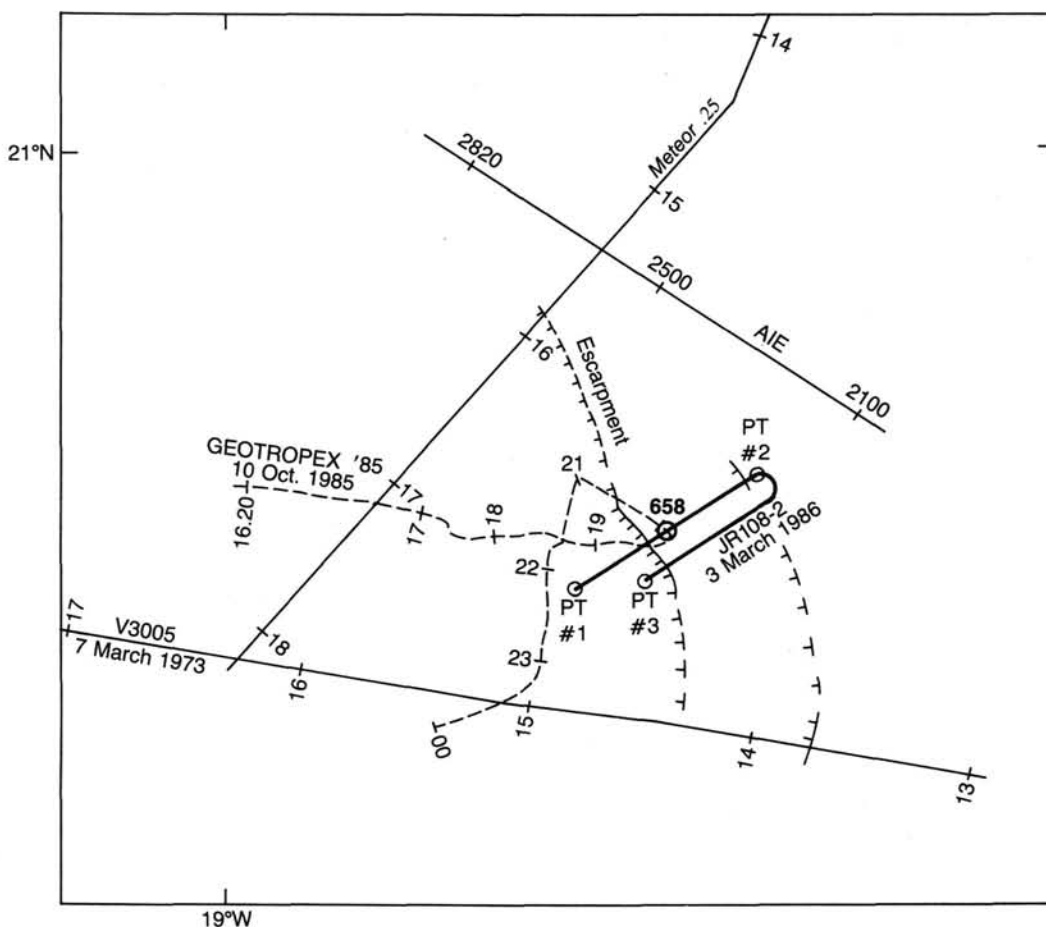


Figure 3. Seismic track lines near Site 658.

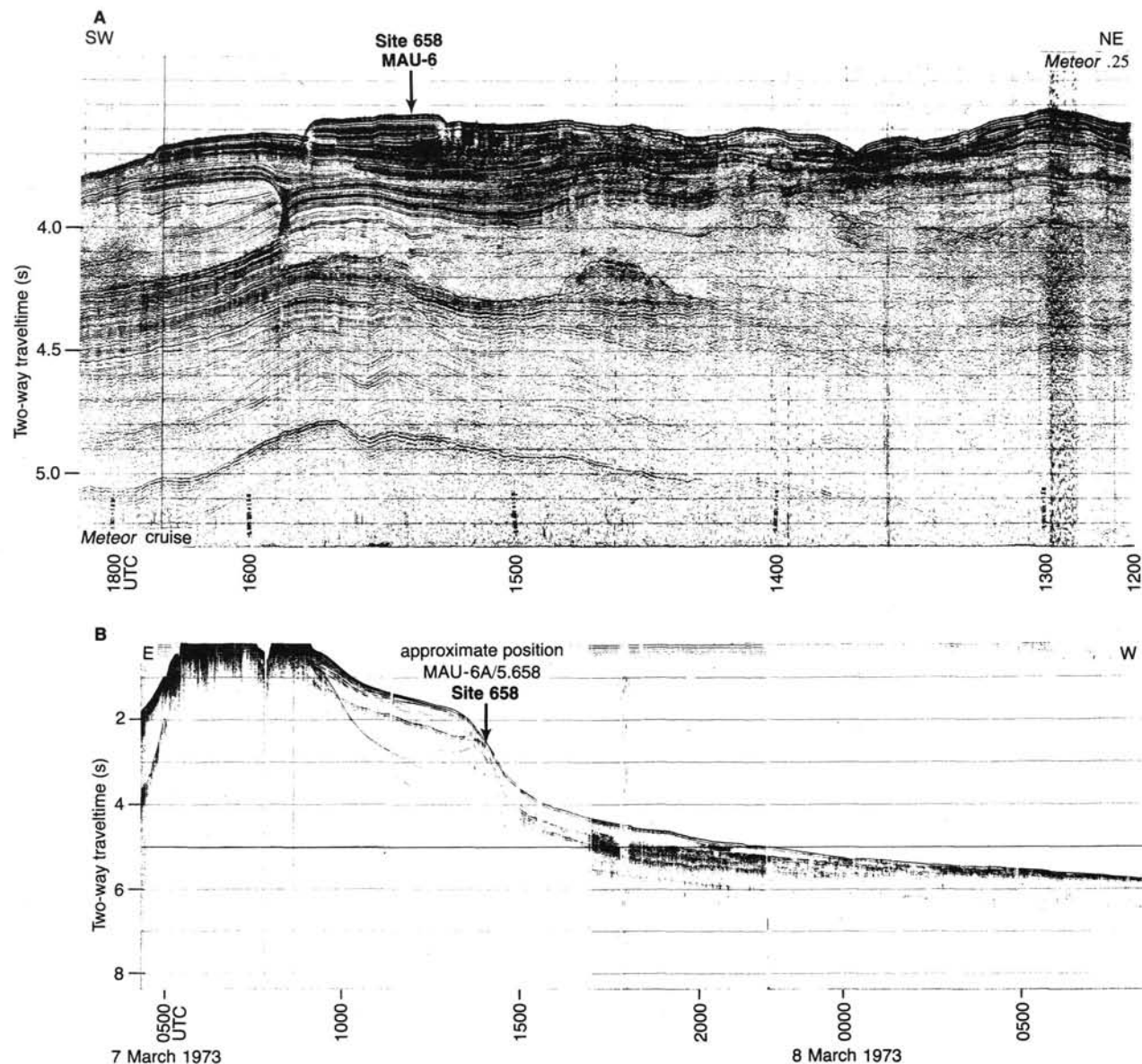


Figure 4. Seismic reflection records near Site 658. All times are Universal Time Coordinated, UTC, formerly Greenwich Mean Time, GMT. A. *Meteor* 25 cruise line, 8 December 1971. B. *Vema* cruise line, 3014. C. GEOTROPEX '85 cruise line MAU-6, B-C. D. *JOIDES Resolution* cruise line on site approach 4 March 1986 (close-up). E. 3.5-Hz echogram from *Meteor* 65-129, 25 km northwest of Site 658 (close-up).

Geologic and Topographic Setting

The position of Site 658 was selected on the basis of unpublished *Meteor* and *Vema* cruise records (Figs. 3, 4A, and 4B) and lies on unpublished GEOTROPEX'85 and *JOIDES Resolution* air-gun and water-gun seismic records (Figs. 4C and 4D). The *JOIDES Resolution* records were obtained while approaching the site. Here, a 300-m-thick, almost undisturbed hemipelagic, pillow-shaped sediment section promised an optimum paleoceanographic record with detailed time resolution. The position of the site at a protrusion of the continental slope between two major canyon systems also promised minimum disturbance of the hemipelagic sediment record by lateral downslope transport of shallow-water sediments.

A distinct, widely spaced double reflector is observed on the well-layered seismic record with its base at 0.20-s two-way traveltimes on top of a slight disconformity overlying offlap structures. Conformable narrowly spaced reflectors occur at approx-

imately 0.20 and 0.23 s. Below 0.35 s, a section with three widely spaced reflectors and transparent zones in between may indicate three levels of slumped sediment or, again, a number of very narrowly spaced fine reflectors lost in the record. Multiple undisturbed reflectors down to 80 m in the 3.5-kHz echogram signify a long-term continuous (hemi-)pelagic sedimentation regime (Fig. 4E).

OPERATIONS

From Site 657, we steamed 12 hr east to Site 658 (target Site MAU-6A), the survey area of *Vema* cruise 30-05, *Meteor* cruises 25/1971 and 65/1983, and *Polarstern* cruise ANT IV/1b (GEOTROPEX'85) on 10 October 1985, 2000 UTC. (All times are expressed as UTC, Universal Time Coordinated, formerly expressed as GMT, Greenwich Mean Time.)

On 4 March 1986, 0000-0300, we obtained an additional pre-site survey line running upslope at 5 kt from Point 1 to Point 2 across the proposed site (Fig. 3; Table 1) to keep the site away

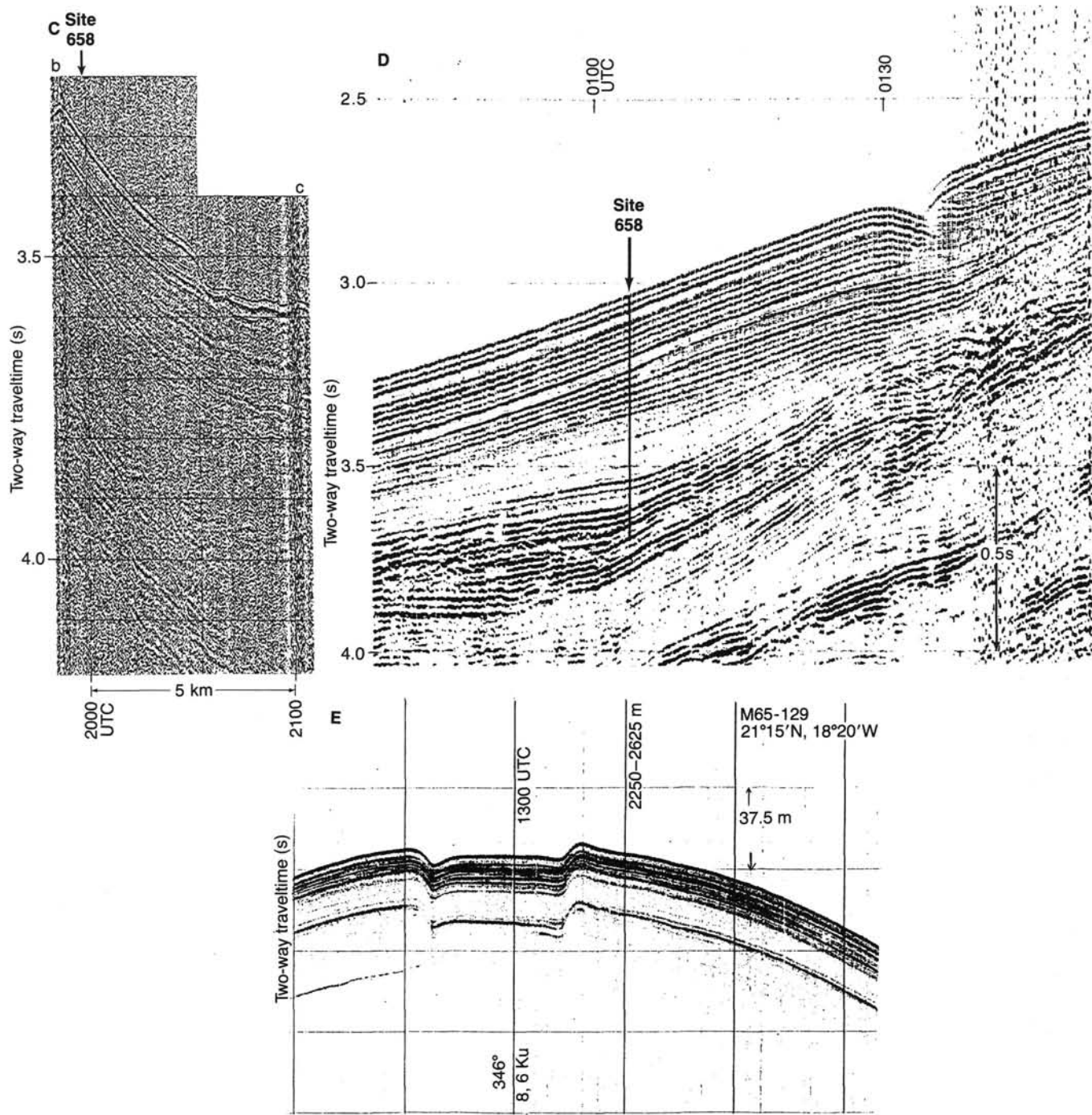


Figure 4 (continued).

from a 40-m-high escarpment 7 km farther west. The survey deployed 80-in.³ water-guns, a 3.5-kHz sub-bottom profiler, and a magnetometer. After the ship turned via Points 2 and 3, a beacon was dropped at 0300 at the proposed site position on the *JOIDES Resolution* seismic line. The survey gear was retrieved until 0330, when the ship stopped and drill string was run into the hole. We tried to establish the mud line from 0800 to 1100 but obtained only two "water cores." In fact, we were 2 nmi south of our intended position because we had no satellites between 0100 and 0730 and because of strong northerly trade winds blowing when the beacon was dropped. Accordingly, we had to reposition the ship 2 nmi farther north from 1130 to 1515 and to deploy a second beacon at 1508.

After stopping the ship over the beacon, we began coring and brought the first APC core on deck at 1710 on 4 March. The mud line (water depth) in Hole 658 was established by drill pipe at 2263.6 m. Coring continued uneventfully for 10 cores (Table 2). Farther down, high methane-gas pressure resulted in unusually high core recovery with core separation creating voids as well as blowing the core out on the catwalk. In some cases methane peaks were too high to measure accurately. Methane/ethane ratios remained between 5000 and 1200. We changed to XCB coring at 0758 on 5 March and continued coring in Hole 658A until Core 108-658A-33 was brought on deck from 300.4 mbsf at 1310 on 6 March. This was the greatest penetration depth that conditions permitted. From 1315 to 1500 hr, the aban-

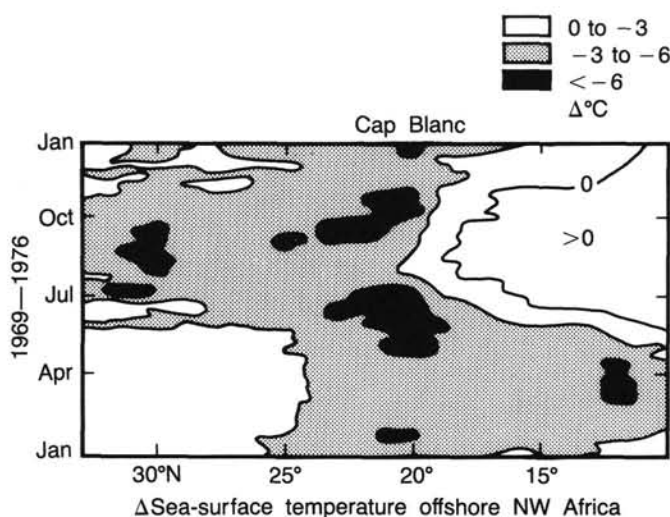


Figure 5. Nearshore oceanic upwelling along the eastern Atlantic continental margin as depicted by mean differences of sea-surface temperatures between nearshore areas off Africa and the non-upwelling mid-Atlantic at the same latitude. Values shown are average seasonal differences for the years 1969 to 1976 (after Speth et al., 1978).

Table 1. Position of site-survey turning points.

Point no.	Location
1	20°41.43'N, 18°41.3'W
2	20°46'N, 18°43'W
3	20°43.5'N, 18°34.52'W

doned hole was plugged with cement. A new free-fall reentry cone was tested successfully and observed with an underwater television camera before clearing the mud line of Hole 658A at 0115 on 7 March. A 30-m offset to Hole 658B was finished at 0215.

The first core of Hole 658B was on deck at 0630 on 7 March, and coring continued successfully for 18 APC cores until 2200, when the corer penetrated only 0.2 m because of stiff mud. High methane-gas pressure posed much less of a problem with core preservation in Hole 658B than in Hole 658A. We prepared to abandon Hole 658B with a cement plug from 2230 to 2400, cleared the mud line, and finished a 15-m offset to Hole 658C at 0045 on 8 March.

The first of eight APC cores from Hole 658C came on deck at 0333, and the last core was on deck at 1015 on 8 March. All eight cores from this hole were reserved for special organochemical studies. Accordingly, the recovered sections were not opened but were stored away as closed sections 75 cm long in our freezer storage space. We began tripping out of the hole at 1015, brought the drill pipe on deck, and headed southwest to Site 659 at 1600 on 8 March.

Strong disturbance during core recovery by high methane-gas pressure at Site 658 caused us special concern in connection with ODP conventions for recording sample depths, as numerous artificial gaps were created during the core recovery. We recommend a general reconsideration of these rules. For an adequate evaluation of our site data, we systematically entered all voids on the computer and shifted all sediment blocks upward to close the gaps within cores. As a result, the actual core recovery of most "expanded" cores was reduced to approximately 100%.

Table 2. Site 658 coring summary (drilling depths).

Core no.	Date (March 1986)	Time (UTC)	Depths (mbsf)	Length cored (m)	Length recovered (m)	Recovery (%)
108-658A-1H	4	1710	0-5.7	5.7	5.7	99.8
108-658A-2H	4	1824	5.7-15.2	9.5	0.0	0.0
108-658A-3H	4	1912	15.2-24.7	9.5	8.8	92.5
108-658A-4H	4	1954	24.7-34.2	9.5	9.1	95.3
108-658A-5H	4	2034	34.2-43.7	9.5	9.8	103.0
108-658A-6H	4	2117	43.7-53.2	9.5	9.8	103.0
108-658A-7H	4	2158	53.2-62.7	9.5	6.6	69.6
108-658A-8H	4	2242	62.7-72.2	9.5	8.8	92.9
108-658A-9H	5	2337	72.2-81.7	9.5	9.3	98.0
108-658A-10H	5	0033	81.7-91.2	9.5	8.6	90.0
108-658A-11H	5	0125	91.2-100.7	9.5	10.9	114.8
108-658A-12H	5	0218	100.7-110.2	9.5	11.2	117.6
108-658A-13H	5	0312	110.2-119.7	9.5	11.2	117.7
108-658A-14H	5	0406	119.7-129.2	9.5	11.7	123.1
108-658A-15H	5	0451	129.2-138.7	9.5	11.2	118.1
108-658A-16H	5	0553	138.7-148.2	9.5	10.0	105.2
108-658A-17H	5	0657	148.2-157.7	9.5	8.5	89.5
108-658A-18H	5	0758	157.7-157.9	0.2	0.2	100.0
108-658A-19X	5	1158	157.9-167.4	9.5	11.5	120.9
108-658A-20X	5	1319	167.4-176.9	9.5	15.1	159.3
108-658A-21X	5	1434	176.9-186.4	9.5	11.7	122.8
108-658A-22X	5	1615	186.4-195.9	9.5	10.8	114.1
108-658A-23X	5	1810	195.9-205.4	9.5	11.7	123.5
108-658A-24X	5	1933	205.4-214.9	9.5	10.7	112.5
108-658A-25X	5	2105	214.9-224.4	9.5	9.9	104.0
108-658A-26X	5	2237	224.4-233.9	9.5	12.3	129.7
108-658A-27X	5	0037	233.9-243.4	9.5	9.7	102.0
108-658A-28X	6	0239	243.4-252.9	9.5	10.2	107.2
108-658A-29X	6	0502	252.9-262.4	9.5	10.1	106.6
108-658A-30X	6	0715	262.4-271.9	9.5	8.1	85.2
108-658A-31X	6	0908	271.9-281.4	9.5	4.2	44.1
108-658A-32X	6	1125	281.4-290.9	9.5	1.3	13.7
108-658A-33X	6	1310	290.9-300.4	9.5	6.4	67.5
108-658B-1H	7	0630	0-2.3	2.3	2.3	98.7
108-658B-2H	7	0740	2.3-11.8	9.5	9.7	102.0
108-658B-3H	7	0840	11.8-21.3	9.5	9.8	103.0
108-658B-4H	7	0930	21.3-30.8	9.5	9.4	99.3
108-658B-5H	7	1015	30.8-40.3	9.5	9.8	103.0
108-658B-6H	7	1100	40.3-49.8	9.5	10.1	105.8
108-658B-7H	7	1135	49.8-59.3	9.5	10.1	106.2
108-658B-8H	7	1255	59.3-68.8	9.5	10.0	105.2
108-658B-9H	7	1331	68.8-78.3	9.5	10.3	108.6
108-658B-10H	7	1408	78.3-87.8	9.5	11.5	121.1
108-658B-11H	7	1448	87.8-97.3	9.5	9.8	103.0
108-658B-12H	7	1545	97.3-106.8	9.5	11.9	125.3
108-658B-13H	7	1620	106.8-116.3	9.5	10.1	106.6
108-658B-14H	7	1716	116.3-125.8	9.5	10.1	106.1
108-658B-15H	7	1830	125.8-135.3	9.5	10.8	113.3
108-658B-16H	7	1926	135.3-144.8	9.5	9.4	98.6
108-658B-17H	7	2107	144.8-154.3	9.5	9.4	98.5
108-658B-18H	7	2215	154.3-163.8	9.5	11.8	123.7
108-658C-1H	8	0333	0-6.4	6.4	6.4	99.4
108-658C-2H	8	0425	6.4-15.9	9.5	8.6	90.9
108-658C-3H	8	0515	15.9-25.4	9.5	9.3	97.8
108-658C-4H	8	0600	25.4-34.9	9.5	9.0	94.9
108-658C-5H	8	0655	34.9-44.4	9.5	9.2	97.2
108-658C-6H	8	0815	44.4-53.9	9.5	9.5	99.8
108-658C-7H	8	0915	53.9-63.4	9.5	9.0	95.1
108-658C-8H	8	1015	63.4-72.9	9.5	9.3	98.0

H = hydraulic piston. X = extended core barrel. UTC = Universal Time Coordinated.

LITHOSTRATIGRAPHY AND SEDIMENTOLOGY

Introduction

Three major sedimentary units are recognized at Site 658 (Figs. 6 and 7). Unit I is composed of nannofossil ooze and minor beds of diatom ooze and ranges in age from middle Pleistocene through Holocene. Unit II is composed of interbedded nannofossil ooze, silt and/or clay, and mixtures of calcareous, siliceous, and siliciclastic grains and is late Pliocene through middle Pleistocene in age. Unit III is composed of nannofossil and nannofossil-bearing mud and nannofossil ooze and ranges in age from early to late Pliocene.

The sediments within these three units are commonly bioturbated, relatively rich in organic matter (from 0.5% to 3.2% total organic carbon [TOC]), and very gaseous below approximately 90 mbsf. The high gas content caused expansion of the core within the core liner and thus created artificial voids within

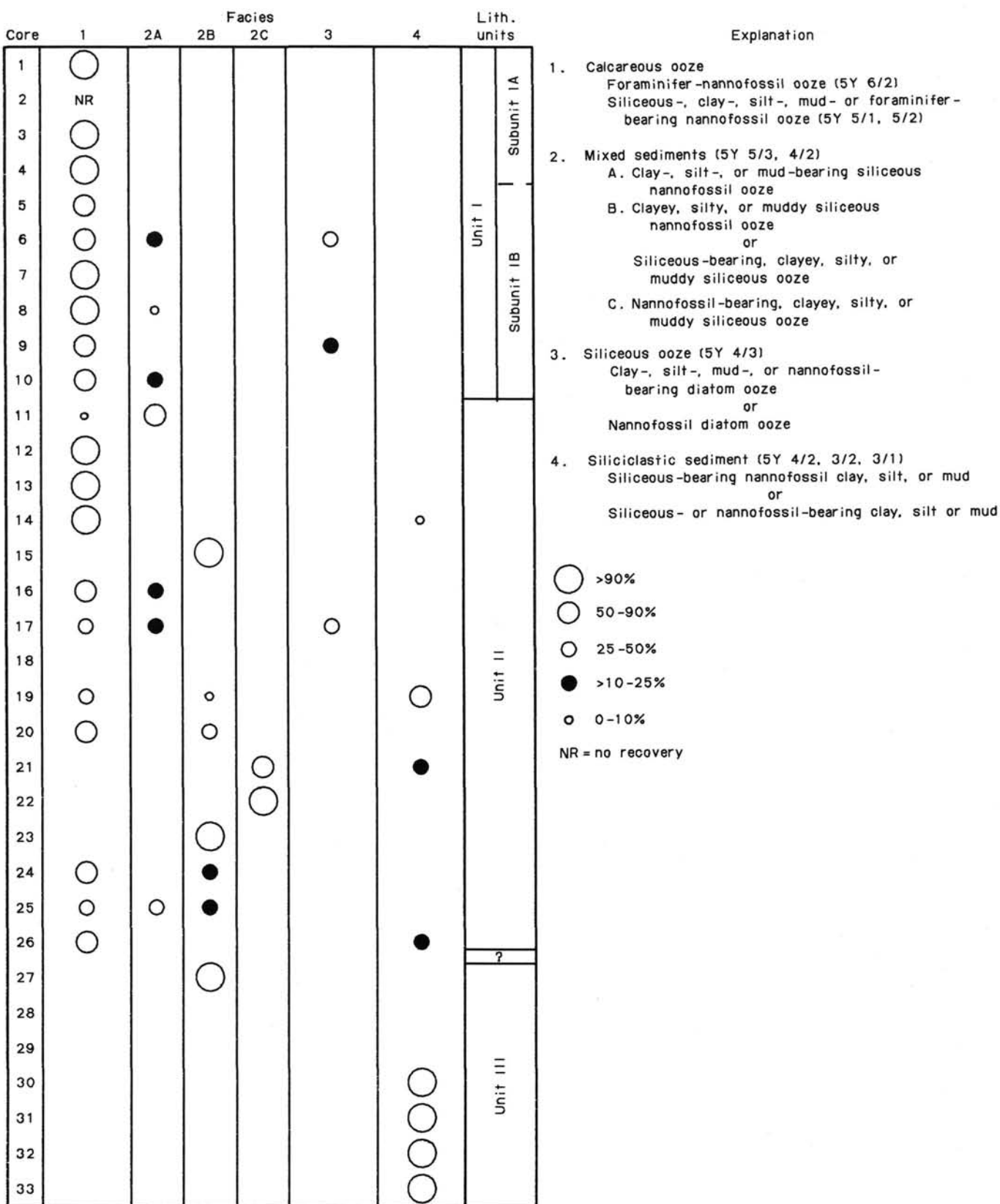


Figure 6. Summary of lithologies of sediments encountered at Site 658A.

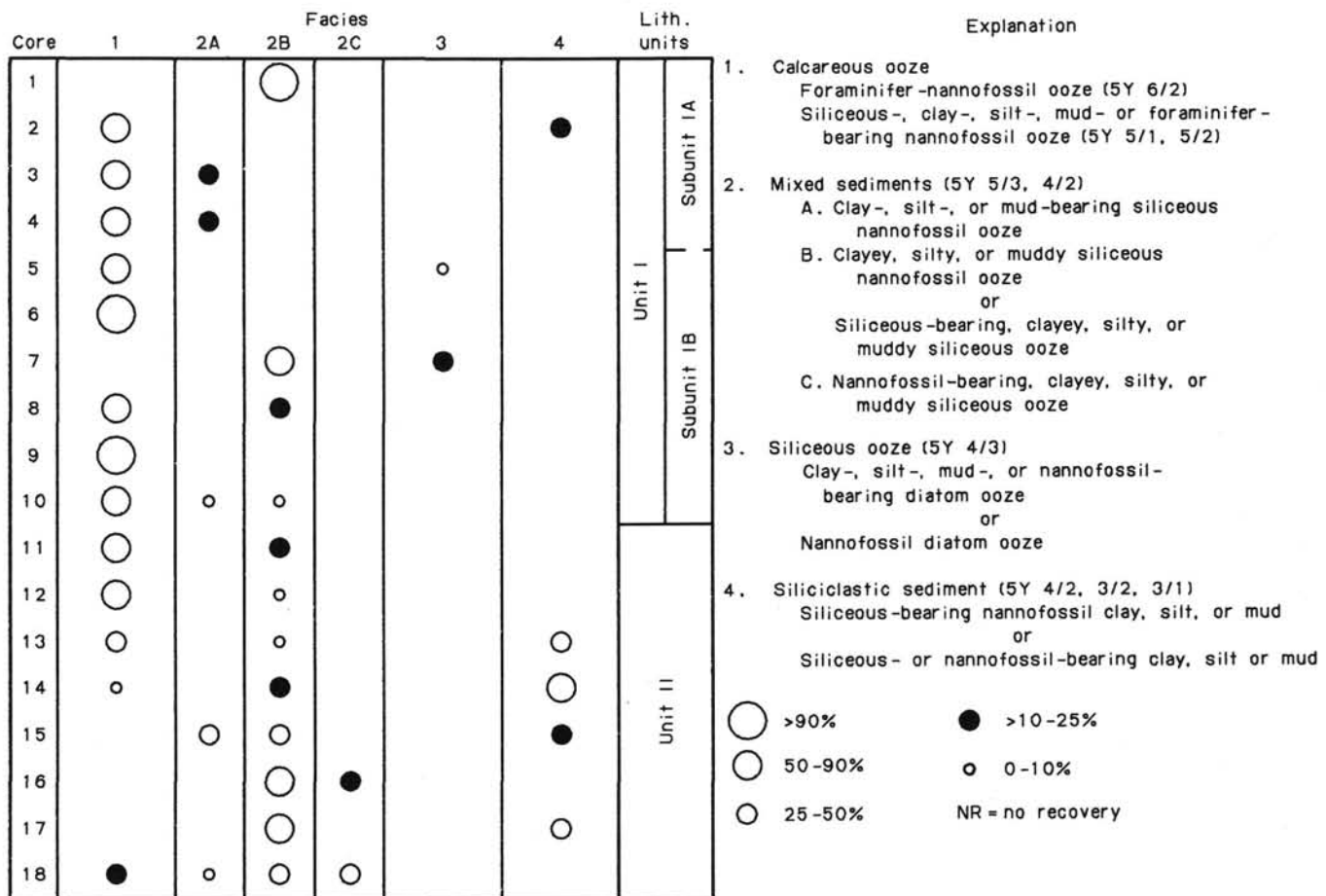


Figure 7. Summary of lithologies of sediments encountered at Site 658B.

each core. The sediments within the three units are also characterized by apparent cyclic variations in color and/or carbonate content, which are presumably the products of variations in the content of minor or major pelagic and terrigenous grain components. Each sedimentary unit is described in detail in the following sections.

Unit I

Cores 108-658A-1H through -658A-10H; depth, 0-91.2 mbsf; thickness, 91.2 m; age, middle Pleistocene (< 0.6 Ma) through Holocene.

Cores 108-658B-1H through -658B-10H; depth, 0-87.8 mbsf; thickness, 87.8 m; age, middle Pleistocene (< 0.6 Ma) through Holocene.

Unit I is composed of nannofossil ooze with variable but minor amounts of quartz silt, foraminifers, diatoms, radiolarians, and sponge spicules (Figs. 6, 7, and 8) and has a measured carbonate content between 28% and 69% (Fig. 9). In this unit, quartz- and feldspar-rich intervals, which are carbonate poor, alternate with intervals of the opposite composition (Fig. 9). The unit has a slight to moderate density of preserved bioturbation traces, but a high density of preserved bioturbation traces is found in Cores 108-658A-3H and -658B-3H. Unit I also has been slightly to moderately disturbed by drilling.

Unit I can be divided into two subunits:

Hole 658A *Hole 658B*

Subunit IA is composed of nannofossil ooze that contains minor amounts of quartz and feldspar silt, foraminifers, and siliceous biogenic debris. The sediment varies cyclically in measured carbonate content (35% to 53%; Fig. 9) and in color (between dark olive gray, olive, gray, and light olive gray). The sediment has a slight to moderate density of preserved bioturbation traces.

Subunit IB is composed of nannofossil ooze and lesser amounts of diatom ooze, diatom nannofossil ooze, and nannofossil diatom ooze. The subunit varies cyclically in measured carbonate content (28% to 69%) and gradually increases in average carbonate content toward its base. The nannofossil ooze within Subunit IB contains minor amounts of quartz silt, foraminifers, and diatoms, and varies cyclically from grays and olive grays to greenish grays. This sediment has a moderate density of preserved bioturbation traces, and the larger burrows are commonly filled with foraminifer-rich ooze. The diatomaceous oozes contain minor amounts of silt, foraminifers, radiolarians, and sponge spicules. These sediments are generally olive in color, and have a slight to moderate density of preserved bioturbation traces.

Unit II

Cores 108-658A-11H through -658A-26X; depth, 91.2-233.9 mbsf; thickness, 142.7 m; age, late Pliocene.

Cores 108-658B-11H through -658-18H; depth, 87.8-163.8 mbsf; thickness, 76.0 m; age, late Pliocene.

Unit II is composed of interbedded nannofossil ooze, mixed sediment, and siliciclastic sediment (Figs. 6, 7, and 8) and is separated from the overlying Unit I by an unconformity that

Core-section	Q	Fsp	K	M	I	Lith-unit	Age
108-658A-1H-1	●						
108-658A-1H-2	●●●●●	●●●	●●●	●●●●●	●●●		
108-658A-1H-3	●●●●●	●●●	●●●	●●●●●	●●●		
108-658A-1H-4	●●●●●	●●●	●●●	●●●●●	●●●		
108-658A-3H-1	●●●●●	●●●	●●●	●●●●●	●●●		
108-658A-3H-3	●●●●●	●●●	●●●	●●●●●	●●●		
108-658A-3H-4	●●●●●	●●●	●●●	●●●●●	●●●		
108-658A-3H-5	●●●●●	●●●	●●●	●●●●●	●●●		
108-658A-3H-6	●●●●●	●●●	●●●	●●●●●	●●●		
108-658A-7H-1	●●●●●	●●●	●●●	●●●●●	●●●		
108-658A-7H-2	●●●●●	●●●	●●●	●●●●●	●●●		
108-658A-7H-3	●●●●●	●●●	●●●	●●●●●	●●●		
108-658A-7H-4	●●●●●	●●●	●●●	●●●●●	●●●		
108-658A-10H-1	●●●●●	●●●	●●●	●●●●●	●●●		
108-658A-10H-2	●●●●●	●●●	●●●	●●●●●	●●●		
108-658A-10H-3	●●●●●	●●●	●●●	●●●●●	●●●		
108-658A-10H-4	●●●●●	●●●	●●●	●●●●●	●●●		
108-658A-10H-5	●●●●●	●●●	●●●	●●●●●	●●●		
108-658A-10H-6	●●●●●	●●●	●●●	●●●●●	●●●		
108-658A-13H-1	●●●●●	●●●	●●●	●●●●●	●●●		
108-658A-13H-2	●●●●●	●●●	●●●	●●●●●	●●●		
108-658A-13H-3	●●●●●	●●●	●●●	●●●●●	●●●		
108-658A-13H-4	●●●●●	●●●	●●●	●●●●●	●●●		
108-658A-13H-5	●●●●●	●●●	●●●	●●●●●	●●●		
108-658A-13H-6	●●●●●	●●●	●●●	●●●●●	●●●		
108-658A-13H-7	●●●●●	●●●	●●●	●●●●●	●●●		
108-658A-17H-1	●●●●●	●●●	●●●	●●●●●	●●●		
108-658A-17H-2	●●●●●	●●●	●●●	●●●●●	●●●		
108-658A-17H-3	●●●●●	●●●	●●●	●●●●●	●●●		
108-658A-17H-4	●●●●●	●●●	●●●	●●●●●	●●●		
108-658A-17H-5	●●●●●	●●●	●●●	●●●●●	●●●		
108-658A-17H-6	●●●●●	●●●	●●●	●●●●●	●●●		
108-658A-23X-1	●●●●●	●●●	●●●	●●●●●	●●●		
108-658A-23X-2	●●●●●	●●●	●●●	●●●●●	●●●		
108-658A-23X-3	●●●●●	●●●	●●●	●●●●●	●●●		
108-658A-23X-4	●●●●●	●●●	●●●	●●●●●	●●●		
108-658A-23X-5	●●●●●	●●●	●●●	●●●●●	●●●		
108-658A-23X-6	●●●●●	●●●	●●●	●●●●●	●●●		
108-658A-23X-7	●●●●●	●●●	●●●	●●●●●	●●●		
108-658A-23X-8	●●●●●	●●●	●●●	●●●●●	●●●		
108-658A-26X-1	●●●●●	●●●	●●●	●●●●●	●●●		
108-658A-26X-2	●●●●●	●●●	●●●	●●●●●	●●●		
108-658A-26X-3	●●●●●	●●●	●●●	●●●●●	●●●		
108-658A-26X-4	●●●●●	●●●	●●●	●●●●●	●●●		
108-658A-26X-5	●●●●●	●●●	●●●	●●●●●	●●●		
108-658A-26X-6	●●●●●	●●●	●●●	●●●●●	●●●		
108-658A-26X-7	●●●●●	●●●	●●●	●●●●●	●●●		
108-658A-26X-8	●●●●●	●●●	●●●	●●●●●	●●●		
108-658A-26X-9	●●●●●	●●●	●●●	●●●●●	●●●		
108-658A-29X-2	●●●●●	●●●	●●●	●●●●●	●●●		
108-658A-29X-3	●●●●●	●●●	●●●	●●●●●	●●●		
108-658A-29X-4	●●●●●	●●●	●●●	●●●●●	●●●		
108-658A-29X-5	●●●●●	●●●	●●●	●●●●●	●●●		
108-658A-29X-6	●●●●●	●●●	●●●	●●●●●	●●●		
108-658A-29X-7	●●●●●	●●●	●●●	●●●●●	●●●		
108-658A-29X-8	●●●●●	●●●	●●●	●●●●●	●●●		
108-658A-31X-1	●●●●●	●●●	●●●	●●●●●	●●●		
108-658A-31X-2	●●●●●	●●●	●●●	●●●●●	●●●		
108-658A-31X-3	●●●●●	●●●	●●●	●●●●●	●●●		
108-658A-32X-1	●●●●●	●●●	●●●	●●●●●	●●●		
108-658A-33X-1	●●●●●	●●●	●●●	●●●●●	●●●		
						Unit III	early Pliocene
						Unit II	late Pliocene
						Subunit IA	Pleistocene
						Subunit IB	

Figure 8. Summary of X-ray-diffraction data of bulk-sediment samples at Site 658A (qualitative estimates). Q = quartz, Fsp = feldspar, K = kaolinite, M = montmorillonite, and I = illite; H = hydraulic piston, X = extended core barrel.

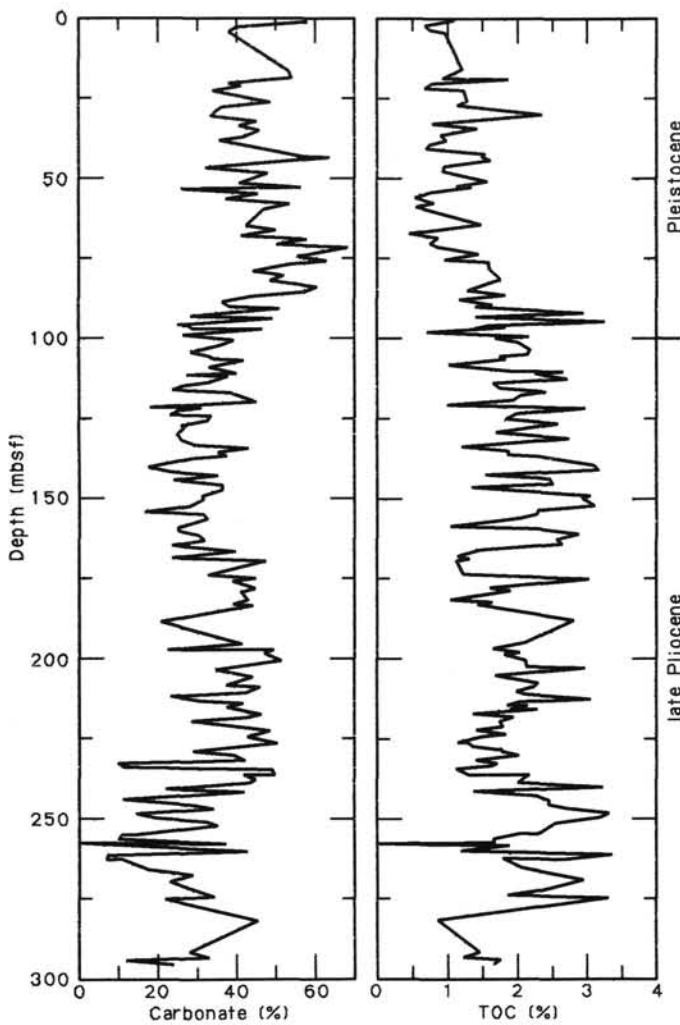


Figure 9. Carbonate content of sediment encountered at Site 658A.

represents a period of >0.6 to 1.5 m.y. Unit II is characterized by cyclic variations in carbonate content ranging from 19% to 50% and is distinguished from the overlying Unit I by its lower average carbonate content (Fig. 9), its higher average TOC content (see "Organic Geochemistry" section, this chapter), and its higher content of siliceous biogenic debris and mud. Unit II has a slight to moderate density of preserved bioturbation traces and generally has been slightly disturbed by drilling.

Nannofossil ooze is the most common sediment type in Unit II. It contains variable but minor amounts of quartz silt, clay, foraminifers, spicules, diatoms, and radiolarians. This sediment varies cyclically from olive gray to olive and has a slight to moderate density of preserved bioturbation traces.

Mixed sediment is the second most common sediment type in Unit II. This sediment type contains major to minor amounts of calcareous biogenic debris (nannofossils and, less commonly, foraminifers), siliceous biogenic debris (diatoms, sponge spicules, and, less commonly, radiolarians), and quartz silt and/or clay (mud). It is generally olive to olive gray and has a slight to moderate density of preserved bioturbation traces.

Siliciclastic sediment is the least common sediment type in Unit II. It is present in major (greater than 50%) amounts only in Cores 108-658A-19H and 108-658B-14H. This sediment is composed of quartz silt and/or clay (mud) and contains variable but minor amounts of foraminifers, nannofossils, sponge

spicules, radiolarians, and diatoms. It is generally olive to olive gray and has a slight density of preserved bioturbation traces.

Unit III

Cores 108-658A-27X through -658A-33X; depth, 233.9–300.4 mbsf; thickness, 66.5 m; age, early to late Pliocene.

Unit III is composed of nannofossil and nannofossil-bearing silt, clay, or mud, and nannofossil ooze (Figs. 6, 7, and 8). It is characterized by cyclic variations in measured carbonate content (10%–45%) and is distinguished from the overlying Unit II by its lower average carbonate content (Fig. 9). Unit III has a slight to moderate density of preserved bioturbation traces and generally has been moderately to greatly disturbed by drilling.

The nannofossil to nannofossil-bearing silt, clay, or mud is generally gray, olive gray, dark gray, or very dark gray. This sediment rarely (in Core 108-658A-30X) contains minor amounts of siliceous biogenic debris (diatoms and sponge spicules), and the silt-sized clasts are composed of quartz, accessory minerals, and (less commonly) feldspar. The nannofossil ooze contains minor amounts of diatoms, silt, and clay and is generally olive gray to dark gray.

Depositional Environment

The three sedimentary units that were recovered at Site 658 record a hemipelagic depositional environment during the Pliocene, Pleistocene, and Holocene epochs. This depositional environment was characterized by high organic productivity, the apparent product of the upwelling of nutrient-rich waters and the influx of fine-grained siliciclastic sediment through eolian, fluvial, and marine processes. The small-scale cyclic variations in color and carbonate content observed in the three sedimentary units are probably the products of short-term fluctuations in climate. Lastly, the unconformity that separates Units I and II may be the product of the erosion of lower Quaternary sediment by mass-flow processes (e.g., slumps). This latter hypothesis is based upon (1) the relatively high slope of the site (1.7°), which is conducive to mass flow, and (2) the occurrences of slump deposits at Site 657 similar in age and composition to the missing section at Site 658.

BIOSTRATIGRAPHY

Site 658 lies in a water depth of 2263.6 m. Three holes were cored at this site underneath the highly productive waters upwelling offshore from Cap Blanc. Hole 658A was cored to a depth of 300.4 mbsf, Hole 658B to a depth of 163.8 mbsf, and Hole 658C to a depth of 72.9 mbsf. Sediments range in age from early Pliocene through Holocene and consist of nannofossil ooze and muddy siliceous nannofossil ooze, both of which are rich in organic carbon. Figures 10 through 12 show the age and zonal assignments of those cores recovered at Site 658.

Although this site is located at latitude 20°N, the microfossil assemblages observed are atypical—more similar in composition to those described from the middle and high latitudes of the North Atlantic (e.g., DSDP Sites 552A, 609, and 610). Because of the sporadic occurrence of low-latitude diatom marker species, low-latitude diatom zonation was abandoned in favor of zonations applicable for the middle latitudes.

Preservation of all microfossil groups varied, but extensive dissolution of both calcium carbonate and biogenic silica occurred in the lower parts of Holes 658A and 658B.

Calcareous Nannofossils

Site 658 was cored to directly below the lower/upper Pliocene boundary. The Pleistocene sequence above the extinction level of *Pseudoemiliania lacunosa* contains well-preserved calcareous nannofossil assemblages. Farther downhole, the lower

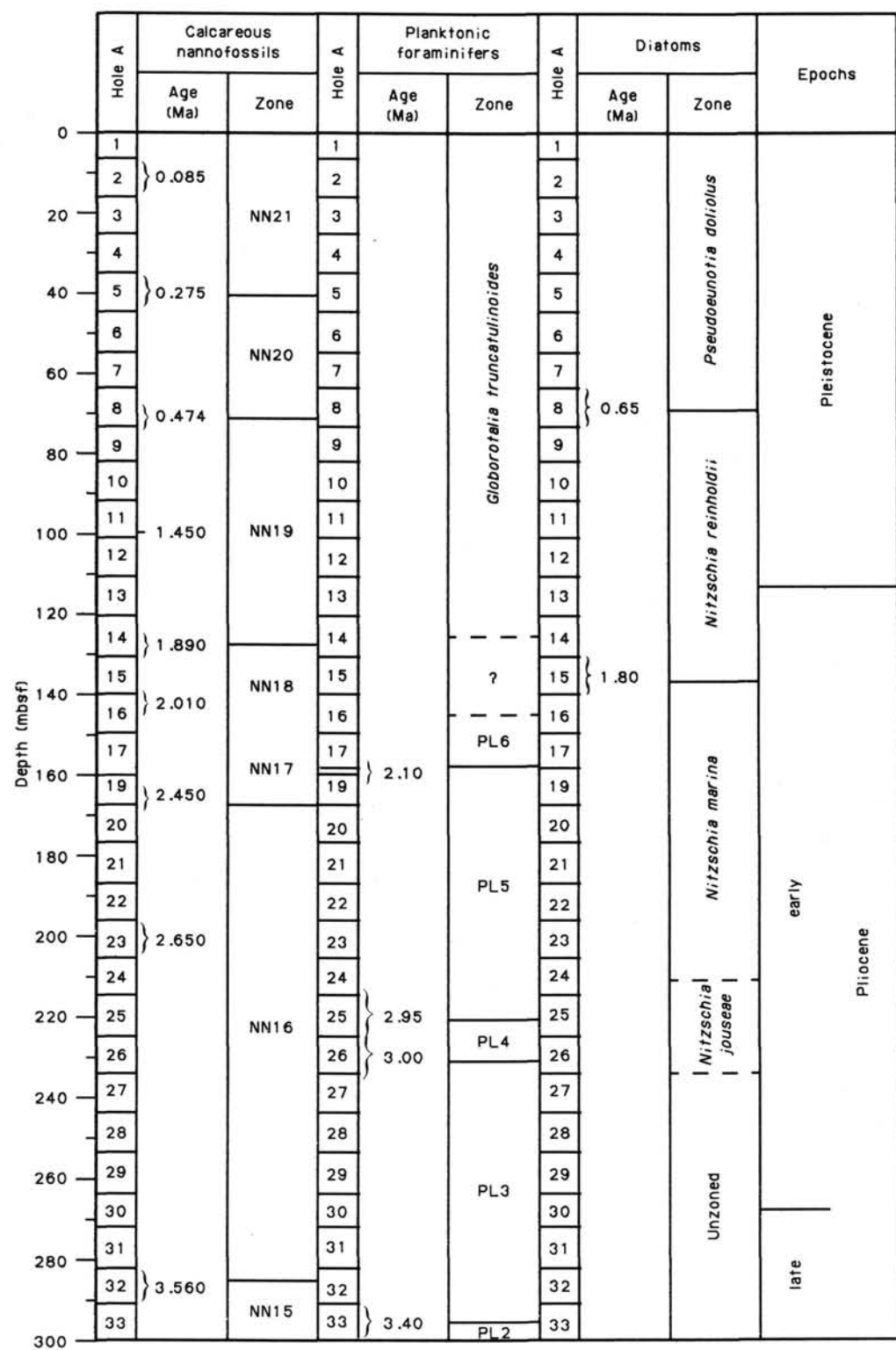


Figure 10. Zonal assignments for cores recovered from Hole 658A.

Pleistocene and Pliocene assemblages become progressively more dissolved, and the deepest cores show severely dissolved and taxonomically impoverished placolith assemblages. Site 658 was drilled in an area of intense upwelling coupled with high productivity; therefore, sediments differ from most other open-ocean oozes in that they are enriched with organic carbon and biogenic opal. The depositional environment also was character-

ized by a high input of terrigenous material. These two factors and their diagenetic consequences are probably major causes for the calcium carbonate dissolution that has occurred, rather than the water depth of 2263.6 m.

The Pliocene discoasters show exceptionally low relative abundances in Hole 658A, considering the tropical position of Site 658 (20°N) and the warm-water preference of discoasters through-

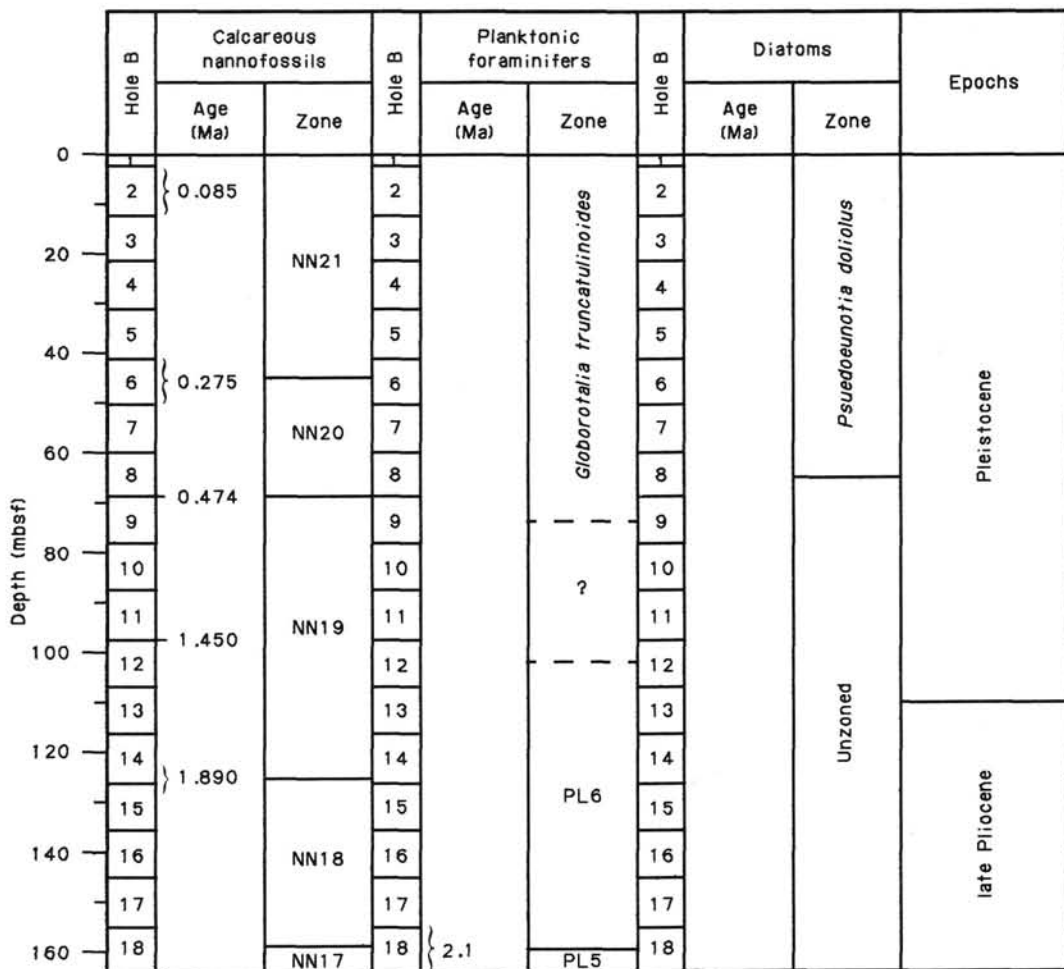


Figure 11. Zonal assignments for cores recovered from Hole 658B.

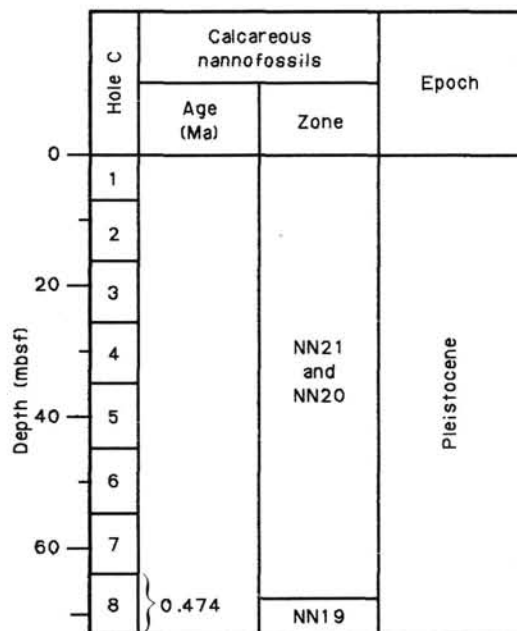


Figure 12. Zonal assignments for cores recovered from Hole 658C.

out the Tertiary. A conservative estimate suggests that discoasters hardly contribute more than 1% of the total assemblage in any discoaster-bearing sample. Such a low figure is typical for the northernmost North Atlantic (e.g., the Pliocene of DSDP Site 552A at 56°N), rather than for tropical areas. Post-depositional dissolution can be ruled out as the cause of the low discoaster abundances because discoasters represent one of the least dissolution-susceptible calcareous nannofossil genera. Hence, the reduced abundances were probably controlled by the specific paleoenvironmental conditions that characterized surface waters of the upwelling zone, the most likely causes being relatively lower sea-surface temperatures and extreme competition among the primary producers. We can only speculate as to which of these two factors had the greatest effect in reducing discoaster abundances, or if the reduction was created by the interaction of both factors.

Site 658 shows a stratigraphic record characterized by high sediment-accumulation rates, ranging from 70 m/m.y. to nearly 150 m/m.y. The only exception to this occurred during the early to middle Pleistocene. This time interval probably is represented by a hiatus encompassing roughly 0.8 m.y. (1.5 Ma to 0.7 Ma).

Pleistocene

The Pleistocene sequence at Site 658 is completely dominated by gephyrocapsids. Common assemblages found are *Calcidiscus leptoporus*, *Coccolithus pelagicus*, and *Helicosphaera carteri*, although more than one of these three species is seldom common in any given sample. The number of specimens of *Emi-*

lianina huxleyi exceeds the number of gephyrocapsids in Cores 108-658A-1H and -658B-1H, indicating an age younger than 0.085 Ma. The first occurrence (FO) of *E. huxleyi* was found in Cores 108-658A-5H and -658B-6H, thus indicating the base of Zone NN21. The top of Zone NN19 (extinction of *P. lacunosa*) is located between 68.7 and 70.2 mbsf in Hole 658A (bottom of Core 108-658A-8H), and between 68.8 and 69.1 mbsf in Hole 658B (top of Core 108-658B-9H). Shortly below these levels, a marked increase in etching of the nannofossil assemblages was observed in both holes.

Calcidiscus macintyreai and *Helicosphaera sellii* disappear between Samples 108-658A-11H-6, 35 cm, and -658A-11H-6, 65 cm. A depth of 99.2 mbsf thus may represent a hiatus because the stratigraphic ranges of these two species are known to differ. In Hole 658B, *C. macintyreai* and *H. sellii* disappear between Samples 108-658B-11H-8, 136 cm, and -658B-11H-9, 64 cm, at a depth of about 97 mbsf. The lower Pleistocene assemblages are similar to those of the middle and upper Pleistocene, with the addition of *C. macintyreai* and *H. sellii*.

Pliocene

The Pliocene assemblages are fairly uniform in taxonomic composition, with abundant small reticulofenestrids, and *C. leptoporus*, *C. macintyreai*, *C. pelagicus*, *H. carteri*, *H. sellii*, and *Pontosphaera japonica* more or less common. Rhabdosphaerids and discoasters are rare.

All determinations of the discoaster disappearances were made by counting their abundance in 50 fields of view at X 790 magnification, using one sample per section. The last occurrences of *Discoaster brouweri* and *Discoaster triradiatus* were observed between Samples 108-658A-14H-3, 145 cm, and -658A-14H-5, 145 cm, (124.15–127.15 mbsf), and between Samples 108-658B-14H-6, 110 cm, and -658B-14H-8, 87 cm (about 124–125.8 mbsf), at an age of 1.89 Ma. The low abundances of the discoasters in Core 108-658A-16H made it impossible to determine the increase of *D. triradiatus* (relative to *D. brouweri*) to better than 6 m, between Samples 108-658A-15H, CC and -658A-16H-4, 150 cm.

Farther downhole, the first specimens of *Discoaster surculus* were observed at the base of Core 108-658A-17H, although the first consistent occurrences were recognized at the base of Core 108-658A-19X. Sample 108-658A-19X-5, 143 cm, provided 21 specimens of *D. brouweri*, whereas Sample 108-658A-19X-7, 149 cm, provided 6 specimens of *D. brouweri*, 10 specimens of *D. surculus*, and 20 specimens of *Discoaster pentaradiatus*. Because this last species showed a less clear abundance pattern (compared with *D. surculus*), the top of Zone NN16 was considered more reliable than the top of Zone NN17. The range of uncertainty for the extinction of *D. pentaradiatus* covers the depth interval from Sample 108-658A-17H, CC through Sample 108-658A-19X-7, 149 cm (157.7–167.0 mbsf); however, *D. pentaradiatus* was present in sufficient numbers in Sample 108-658B-18H, CC to indicate an indigenous presence. This could decrease the range of uncertainty to between 157.7 and 163.8 mbsf.

Discoaster tamalis was observed at the top of Core 108-658A-22X. However, its rare occurrences in the lower half of that core and in the upper half of Core 108-658A-23X suggest that the top of Subzone CN12b can be only tentatively identified in terms of sub-bottom depth.

Recovery from Core 108-658A-32X was poor, making a precise determination of the extinction of *Reticulofenestra pseudoumbilica* (281.4–290.9 mbsf) and the top of Zone NN15 (3.56 Ma) impossible.

Eight cores were recovered from Hole 658C. Investigation of two core-catcher samples (108-658C-7H, CC and -658C-8H, CC) indicate that the extinction of *P. lacunosa* occurs within Core 108-658C-8H (63.4–72.9 mbsf).

Planktonic Foraminifers

Planktonic foraminifers were recovered from two holes at Site 658, with the deeper Hole 658A reaching the lower/upper Pliocene boundary. The fauna contains abundant, well-preserved foraminifers in the upper few cores, but below Cores 108-658A-8H and -658B-9H specimens are less common and less well preserved. Below Cores 108-658A-17H in Hole 658A and -658B-10H in Hole 658B more than one-half the core-catcher samples had too few specimens of planktonic foraminifers to make relative abundance estimates. The greater than 150- μm fraction of these organic-rich green clays consisted predominantly of mud pellets that resisted disaggregation in a 10% hydrogen peroxide bath. Although dissolution appears to have been extensive, most samples contained relatively few foraminifer fragments.

The Pleistocene assemblage, recovered above Cores 108-658A-13H, CC and -658B-12H, CC, is dominated by *Globorotalia inflata*, *Neogloboquadrina pachyderma* (d.), and *Globigerina bulloides*. The large numbers of *G. bulloides*, at times in excess of 30%, show that this site is located in an upwelling area. As at Site 657, tropical species are present in very low abundances and scattered influxes of cooler *N. pachyderma* (s.) are observed, more so in Hole 658A than Hole 658B. *Globigerinatella calida*, believed to have evolved in the late Pleistocene, is observed consistently in Hole 658B, and its FO in Sample 108-698B-9H, CC may define the base of Bolli and Saunders' (1985) undated *Globigerinatella calida* Zone. The FO of *Globorotalia truncatulinoides*, which should define the base of the *Globorotalia truncatulinoides* Zone at 1.9 Ma, was found in Samples 108-658A-13H, CC and -658B-13H, CC. However, we do not see the evolution of this species from its ancestor *Globorotalia tosaensis*, and in cool-water sites such as this, *G. truncatulinoides* is commonly absent during the early part of its range (Weaver and Clement, 1986). Ideally, there should be an overlap of *G. truncatulinoides*, which has an FO at 1.9 Ma, with *Globigerinoides obliquus*, which has its last occurrence (LO) at 1.9 Ma. At Site 658, however, neither species is present in Cores 108-658A-14H and -658A-15H, nor Cores 108-658B-10H through -658B-12H. These cores, therefore, cannot be dated. The *Globigerinoides obliquus* Zone (PL6) can be recognized in Samples 108-658A-16H, CC through -658A-17H-5, 111 cm, and Samples 108-658B-13H, CC through -658B-17H, CC. A single specimen of *G. obliquus* that occurs in Core 108-658A-11H, CC, approximately 19 m (or about 0.2 Ma) above the observed FO of *G. truncatulinoides*, may be reworked.

Below the Pliocene/Pleistocene boundary, the tropical zonal markers are rare owing to either dissolution or the cold-water environment, and thus zonal assignments are subject to error. The PL6/PL5 zonal boundary (2.2 Ma), as indicated by the last occurrence of *G. miocenica*, is above Samples 108-658A-17H, CC and -658B-18H, CC. Hole 658B does not extend beyond Core 108-658B-18H. The FO of *Globorotalia inflata* is also found in Sample 108-658A-17H, CC and its co-occurrence with *G. miocenica* thus may indicate an age slightly older than the observed age of 2.1 Ma for this datum in the North Atlantic (Weaver and Clement, 1986; Raymo et al., 1987).

The short PL4 Zone was observed in Sample 108-658A-25X, CC, which contained *Dentogloboquadrina altispira* but no *Sphaeroidinellopsis seminulina*. The LO of *S. seminulina* was in Sample 108-658A-26X, CC, but since this species was only observed in two samples in the entire hole, its nonoccurrence may be an artifact of dissolution. In the PL3 Zone, foraminifers continued to be scarce, and one sample was barren. The upper Pliocene assemblage is dominated by *N. pachyderma* (d.), *G. bulloides*, and *Globorotalia puncticulata*, *G. inflata*'s evolutionary predecessor. The deepest sample, 108-658A-33X, CC, contained a

few specimens of *G. margaritae*, indicating that the base of Hole 658A just reached the early Pliocene PL2 Zone.

Benthic Foraminifers

The benthic-foraminifer assemblage at Site 658A is characterized by its high diversity and abundant occurrence. The dominant species are *Pyrgo murrhyina*, *Melonis pompilioides*, *Melonis barleeanus*, *Bulimina aculeata*, *Gyrodinoides soldanii*, *Oridorsalis tener*, *Globobulimina auriculata*, *Cassidulina carinata*, *Cibicidoides kullenbergi*, *Planulina wuellerstorfi*, and *Uvigerina peregrina*. This assemblage suggests lower to upper bathyal depths.

The FO of *Hoeglundina elegans* occurs in Sample 108-658A-30X, CC. Although Schnitker (1979) assigned an age of 0.13 Ma to this event in the western North Atlantic, preliminary results at Site 658 suggest an age of about 3.4 Ma for this event. This age difference is assumed to result from different ecological conditions along the western and eastern North Atlantic continental margins.

Diatoms

Diatoms are present in all core-catcher samples examined from Holes 658A and 658B; their abundance and preservation vary from sample to sample. In general, the diatom assemblage in most samples consists of few specimens with poor preservation. However, some samples contain common to abundant, moderately well-preserved specimens.

The diatom assemblage is dominated by pelagic diatoms indicative of high surface-water productivity. Species consistently observed include *Actinocyclus octonarius*, *Actinoptychus senarius*, *Coscinodiscus marginatus*, *C. oculis-iridis*, *Hemidiscus cuneiformis*, *Nitzschia marina*, *Paralia sulcata*, *Thalassionema nitzschiooides*, *Thalassiosira eccentrica*, *T. leptopus*, *T. oestrupii*, and *Thalassiothrix longissima*. Resting spores, several varieties of freshwater *Melosira* spp., marine benthic diatoms, and opal phytoliths also were observed.

Age-diagnostic species are present but commonly have sporadic ranges resulting in tentative zonal assignments. Because of the sporadic occurrence of *Rhizosolenia praebergonii*, we are unable to recognize consistently the *Rhizosolenia praebergonii* Zone of Burckle (1977). Therefore, we will follow Baldauf (1984) and use the *Nitzschia marina* Zone for the interval corresponding to that of the *Rhizosolenia praebergonii* Zone. The *Nitzschia marina* Zone (Baldauf, 1984) is defined as the interval containing *N. marina* between the LO of *Nitzschia jouseae* and the FO of *Pseudoeunotia doliolus*.

Samples 108-658A-1H, CC through -658A-7H, CC and 108-658B-1H, CC through -658B-7H, CC are assigned to the late Pleistocene *Pseudoeunotia doliolus* Zone of Burckle (1977), based on the occurrence of *P. doliolus* stratigraphically above the LO of *Nitzschia reinholdii*.

Samples 108-658A-8H, CC through -658A-14H, CC and -658B-8H, CC and -658B-9H, CC are placed in the *Nitzschia reinholdii* Zone of Burckle (1977), based on the co-occurrence of *P. doliolus* with *N. reinholdii*. The LO of *N. reinholdii* was dated by Burckle (1972) and has an estimated age of 0.65 Ma in the eastern equatorial Pacific. In the middle and high latitudes of the North Atlantic, this biostratigraphic event has an assigned age of 0.44 Ma (Baldauf, 1987). The LO of *N. reinholdii* in Sample 108-658A-8H, CC is slightly above the LO of the calcareous nannofossil *Pseudoemiliania lacunosa*, which has an estimated age of 0.474 Ma. This suggests that the LO of *N. reinholdii* corresponds closely to the estimated age of its LO in the middle and high latitudes of the North Atlantic and significantly postdates that in the eastern equatorial Pacific. Although Samples 108-658B-10H, CC through -658B-14H, CC do not contain diagnostic species, their downhole positions relative to

Samples 108-658A-10H, CC through 108-658A-14H, CC (which contain *P. doliolus*) suggest an assignment to the *Nitzschia reinholdii* Zone.

Samples 108-658A-15H, CC through -658A-23X, CC and -658B-15H, CC through -658B-18H, CC are assigned tentatively to the *Nitzschia marina* Zone of Baldauf (1984). The occurrence of *Thalassiosira convexa* in Sample 108-658A-18H, CC allows placement of Samples 108-658A-15H, CC through -658A-17H, CC into Subzone "b" and Samples 108-658A-18H, CC through -658A-24X, CC into Subzone "a" of this same zone (Baldauf, 1987). The base of the *Nitzschia marina* Zone is placed in Sample 108-658A-24X, CC and corresponds to the LO of *N. jouseae*. Placement of this zonal boundary is, however, extremely tentative because of the rare occurrence of this species. The calcareous-nannofossil stratigraphy suggests that Sample 108-658A-24X, CC is slightly older (approximately 2.9 Ma), indicating that although Sample 108-658A-24X, CC is indeed equivalent to the *Nitzschia jouseae* Zone, the placement of the zonal boundary (*N. jouseae*/*N. marina*) should occur stratigraphically higher in the hole.

The occurrence of *Rhizosolenia praebergonii* in Sample 108-658A-18H, CC and Samples 108-658A-24X, CC through -658A-26X, CC and -658B-16H, CC allows placement of these samples into the *Rhizosolenia praebergonii* Zone of Burckle (1977). The sporadic occurrence of *R. praebergonii*, however, makes the use of this species unreliable for independent stratigraphic control. The occurrence of *N. jouseae* in Samples 108-658A-24X, CC through -658A-26X, CC allows placement of these samples into the *Nitzschia jouseae* Zone of Baldauf (1984).

Core-catcher samples examined from Cores 108-658A-27X through -658A-33X contain rare to common diatoms. Preservation is invariably poor. Because no age-diagnostic species were observed, these samples are unzoned.

PALEOMAGNETISM

Magnetostratigraphy

Experimental Procedures

We measured all possible cores through Core 108-658A-19H in Hole 658A and Core 108-658B-17H in Hole 658B with the pass-through cryogenic magnetometer. The cores were routinely demagnetized to 50 Oe after measuring the natural remanent magnetization (NRM). Discrete samples were taken from each core section for a total of approximately 200 samples. Most were measured using the cryogenic magnetometer in a discrete sample mode. The weak magnetization of the sediments was near the noise level of shipboard equipment. Therefore, we subjected each sample to several demagnetization steps in order to isolate the stable component while still maintaining measurable intensity.

Results

For the most part, the whole-core measurements were excellent and agreed well with the discrete-sample data and the expected magnetic inclination for the site (37°). As a typical example, we show the results from Core 108-658A-5H, in Figure 13. We plot the whole core data, the inclination data from the discrete samples, and the expected inclination for the site. An exception to the general correspondence of the results can be seen in the first section, which displayed extensive coring disturbance. Such coring disruption is quite common in core tops.

In contrast to the overall high quality of the whole-core measurements obtained at this site from APC cores, data from the XCB cores were less satisfying. In Figure 14 we show the results from Core 108-658A-19X. These are highly scattered, and we hesitate to interpret them in terms of polarity. Therefore, the

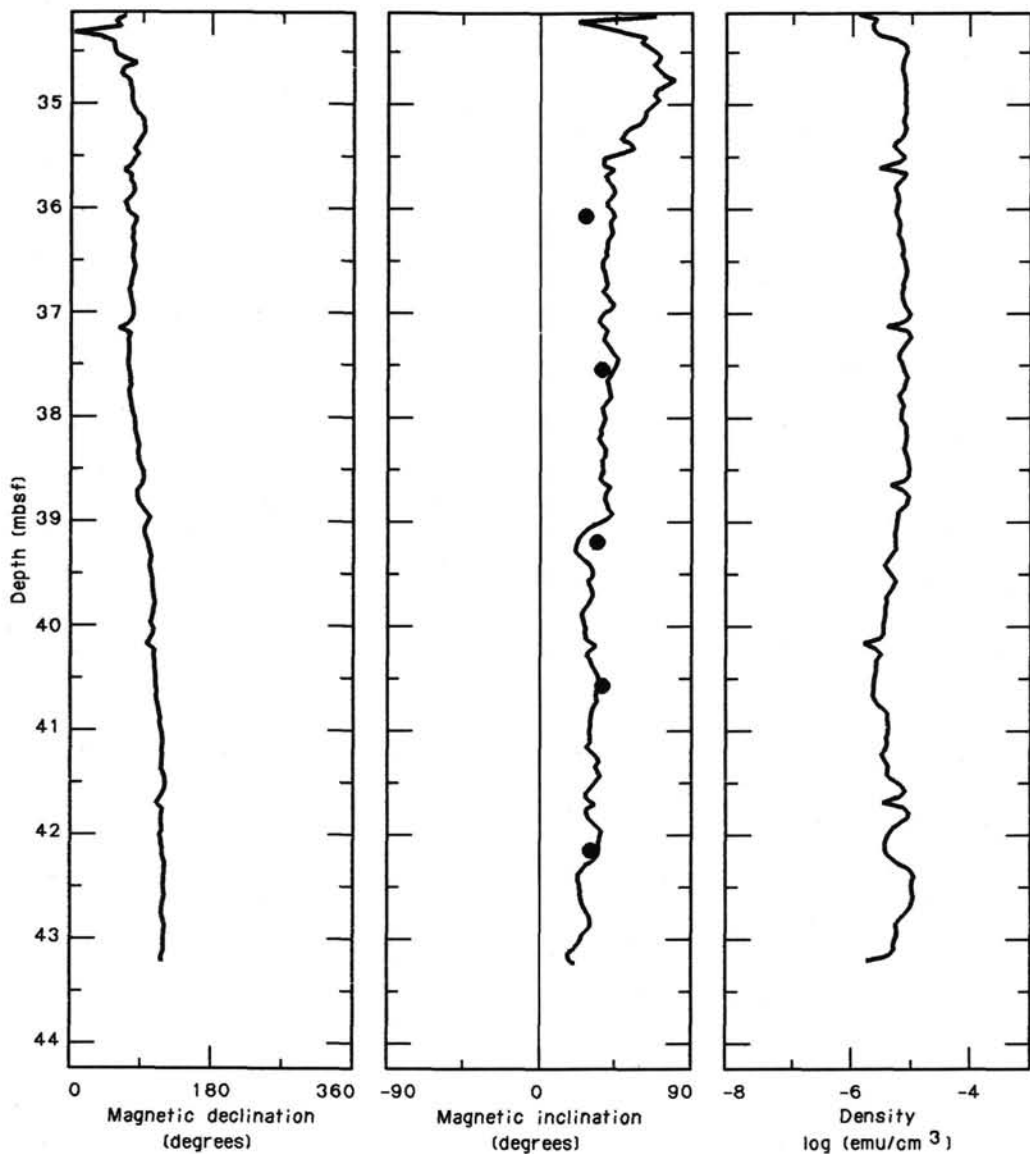


Figure 13. Declination, inclination, and intensity variations as a function of depth recorded in Core 108-658A-5H.

magnetostratigraphy from XCB cores is based entirely upon discrete-sample data.

In Figure 15, we show selected vector end-point diagrams. These diagrams indicate that the stable component is easily isolated, in most cases after 50 Oe. The magnetostratigraphic results are shown in Figures 16 and 17. These results are based on discrete-sample data selected by means of the following criteria: demagnetization behavior, circular standard deviation, and intensity. The appropriate demagnetization step, as judged from detailed curves, was chosen for each sample. Different criteria are necessary for data generated on the spinner and cryogenic magnetometers owing to sensitivity and procedural differences. Spinner-magnetometer data that had circular standard deviations in excess of 35 were excluded. Measurements with intensities of less than 10⁻⁶ emu were rejected for cryogenic-magnetometer data.

All results meeting the criteria mentioned are plotted in Figure 16 (Hole 658A) and Figure 17 (Hole 658B). Inclinations are interpreted in terms of polarity, based on the sign (positive being normal and negative reversed). Polarity intervals represented by a single specimen are indicated by arrows, as they are consid-

ered less reliable. Correlation with the time scale without independent evidence would present problems. However, when combined with the biostratigraphy, correlation is quite satisfactory and indicates that the upper part of Chron C1r is missing. A sampling density of one per section is inadequate to resolve the short events within Chron C2A (Kaena and Mammoth) and additional samples will be requested.

Magnetic Susceptibility

We measured whole-core volume susceptibility on Cores 108-658A-1H through -658A-20H (0-167.4 mbsf, about 0-2.5 Ma) and on Cores 108-658B-1H through -658B-9H (0-68.8 mbsf, about 0-0.5 Ma). The presence of numerous voids (resulting from gas expansion) below about Cores 108-658A-10H and -658B-10H made whole-core measurements troublesome. For this reason we did not continue these measurements below this level in Hole 658B.

Susceptibility values are generally low (less than 10⁻⁴ SI units). Despite the uniformity of lithology at this site, sufficient variation exists in the susceptibility stratigraphy to permit detailed correlations between Holes 658A and 658B down to about 80 mbsf. We have correlated more than 50 susceptibility peaks be-

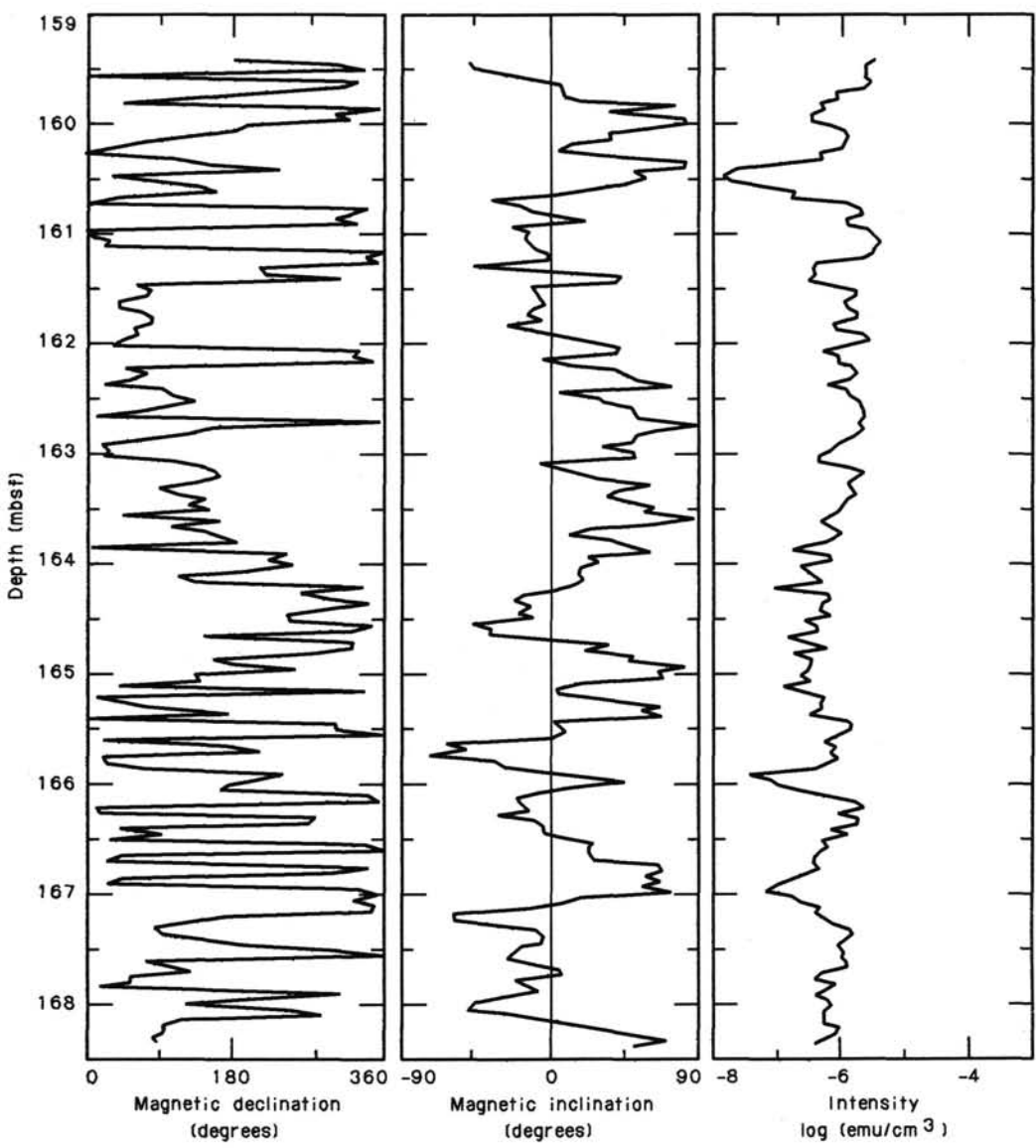


Figure 14. Example of scattered results obtained from XCB cores (Core 108-658A-19X).

tween the two holes over this interval. Figure 18 shows an example from Cores 108-658A-4H and -658A-5H and Cores 108-658B-4H and -658B-5H.

SEDIMENT-ACCUMULATION RATES

The sediment-accumulation rates of Hole 658A are reconstructed using 22 control points (Table 3 and Fig. 19). The combination of high productivity and continental proximity resulting in substantial input of terrigenous material causes high accumulation rates on the order of 70 to 150 m/m.y. The sediments at the bottom of Hole 658A (300.4 mbsf) are no older than about 3.7 Ma. The cored sequence contains one major hiatus, spanning the time interval from approximately 0.7 to 1.5 Ma. Depending on whether sedimentological, biostratigraphic, or magnetostratigraphic evidence is used, the hiatus occurs somewhere within the depth interval from 101.6 to 109.2 mbsf. Figure 19 shows the position of the hiatus as indicated by the magnetostratigraphic data.

The highest accumulation rate was found above the hiatus in the least compacted, uppermost 100 m of the sedimentary column (147 m/m.y.). Below this level, the sediments were accumulating at a rate of about 72 m/m.y. between 1.5 and 2.5 Ma, and

at a rate of 108 m/m.y. between 2.5 and 3.7 Ma. The decrease in sedimentation rate at 2.5 Ma may be related to the onset of moderate-scale glaciation in the Northern Hemisphere during this time.

The age/depth positions of eight biochronologic markers do not fall on the accumulation-rate curve suggested by the magnetostratigraphic reversal boundaries. These eight species events are discussed next.

The four diatom markers (LO of *Nitzschia reinholdii*, FO of *Pseudoeunotia doliolus*, LO of *Thalassiosira convexa*, and LO of *Nitzschia jouseae*) have anomalous positions relative to the suggested sedimentation-rate curve. These discrepancies may result from the influence of cooler water temperatures and upwelling at Site 658. The stratigraphic ranges of these species are similar to their ranges in middle to high latitudes rather than in low latitudes.

Burckle (1972) assigned an estimated age of 0.65 Ma for the LO of *N. reinholdii* in the eastern equatorial Pacific. Although Site 658 is located in the eastern equatorial Atlantic, the estimated age of the LO of *N. reinholdii* (Fig. 19) at this site is between 0.44 and 0.59 Ma. Baldauf (1987) estimated an age of 0.44 Ma for the LO of *N. reinholdii* in several DSDP sites in

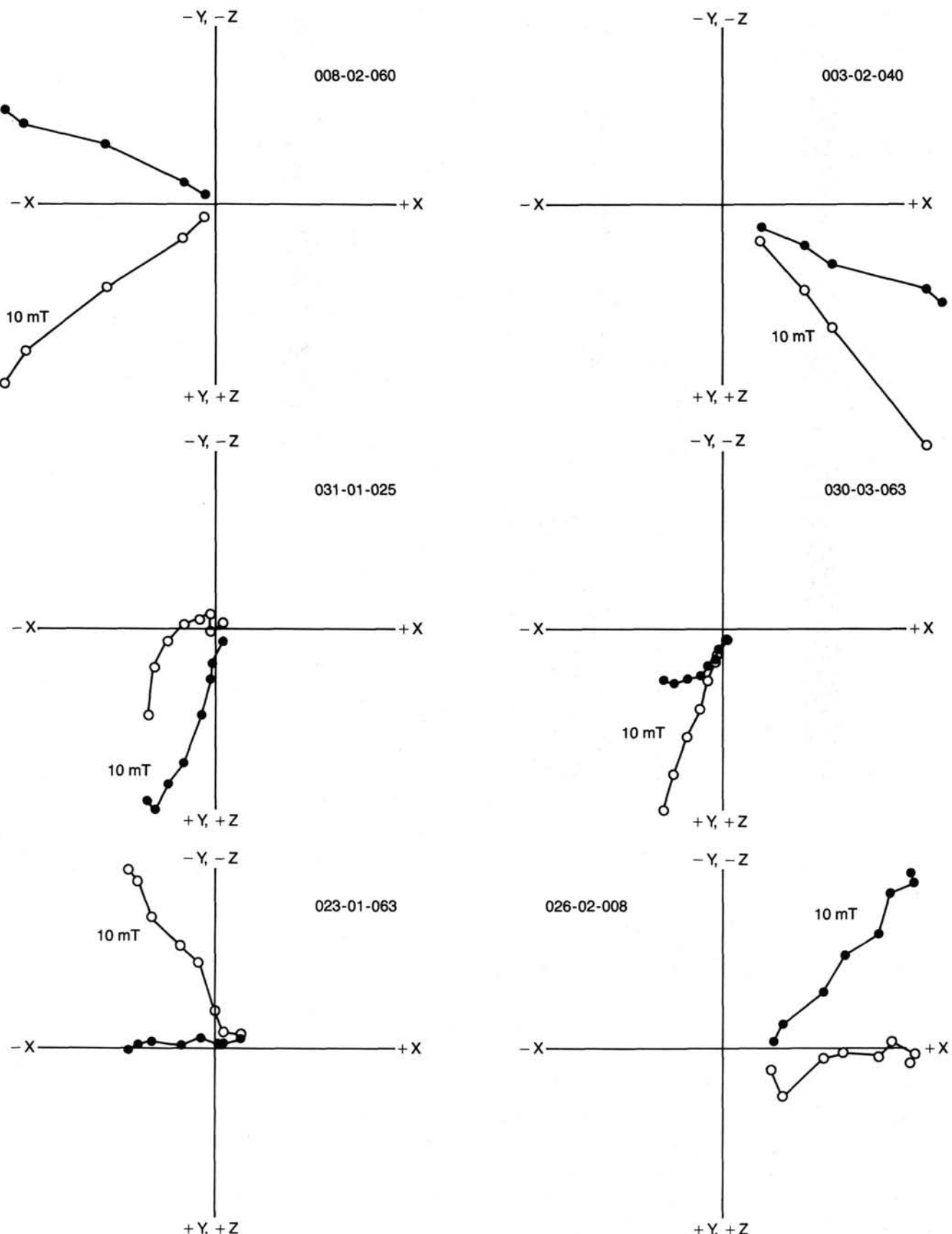


Figure 15. Typical ac demagnetization diagrams of samples from Hole 658A.

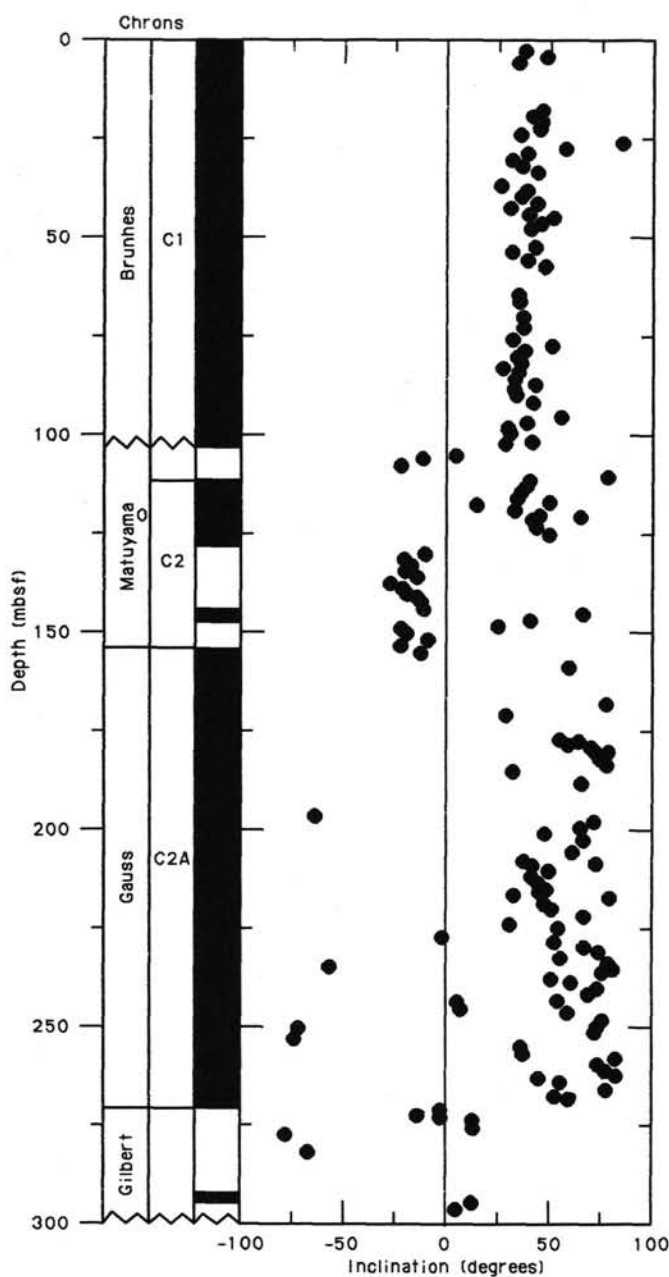


Figure 16. Magnetostratigraphic results interpreted from inclination variations in Hole 658A. Correlation with the geomagnetic polarity time scale given on the left of the figure has been obtained by combining it with biostratigraphic results.

middle and high latitudes of the North Atlantic. This suggests that at Site 658, *N. reinholdii* has a range similar to that of middle and high latitudes of the North Atlantic and thus may be responding to the cooler water conditions at Site 658.

The FO of *P. doliosus* is placed in Sample 108-658A-14H, CC. Such a placement suggests that this event is slightly older (by 0.16–0.3 m.y.) than the age of 1.8 Ma assigned to this event in both the equatorial Pacific (Burkle, 1977) and middle and high latitudes of the North Atlantic (Baldauf, 1986). The most likely explanation for this earlier occurrence is downhole contamination. Examination of calcareous nannofossils from Samples 108-658A-14H-4, -658A-14H-5, and -658A-14H, CC indicate that *Discoaster brouweri*, although present in Samples 108-658A-

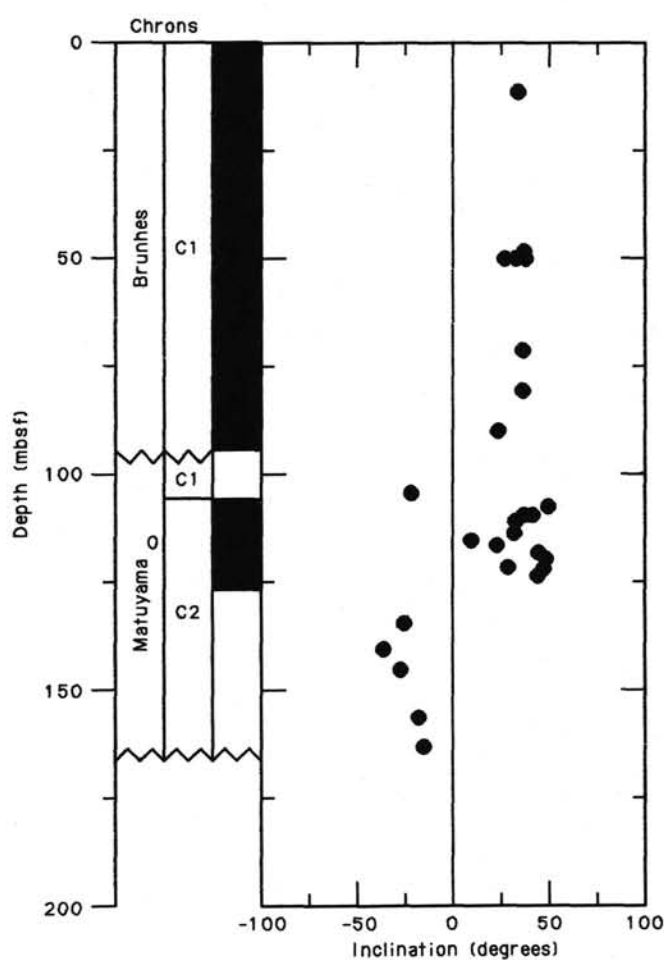


Figure 17. Magnetostratigraphic results interpreted from the inclination variations in Hole 658B.

14H-4 and -658A-14H-5, is absent from Sample 108-658A-14H, CC. This suggests contamination of the core-catcher material from a higher stratigraphic interval.

The last occurrences of *T. convexa* and *N. jouseae* seem to be significantly older at Site 658 than in other equatorial regions. Both these species have sporadic stratigraphic occurrences, which are most likely controlled by changing ecologic conditions. Therefore, these species are considered to be unreliable for biostratigraphic or biochronologic control at Site 658.

The planktonic foraminifer *Globorotalia miocenica* was not observed in sediment younger than about 2.35 Ma. This species may have disappeared from the area of Site 658 roughly 0.15 m.y. before its extinction at 2.2 Ma, or, more likely, strong dissolution in the samples above its disappearance could have caused its absence.

The aberrant age/depth position of the last observed occurrence of the calcareous nannofossil *Discoaster tamalis* may represent an early disappearance (about 0.15 m.y.) from Site 658 or may indicate that its highest consistent occurrence does not represent its true extinction level. A few specimens observed at the top of Core 108-658A-22X were interpreted to have been reworked. However, if this is not the case, the LO of *D. tamalis* would fall on the suggested sedimentation-rate curve.

The entire interval from 101.6 mbsf to the top of Hole 658A is normally magnetized. The age-depth positions of the two *Emiliania huxleyi* datums and the *Pseudoemiliania lacunosa* datum support the interpretation of this 101.6-m sequence as the

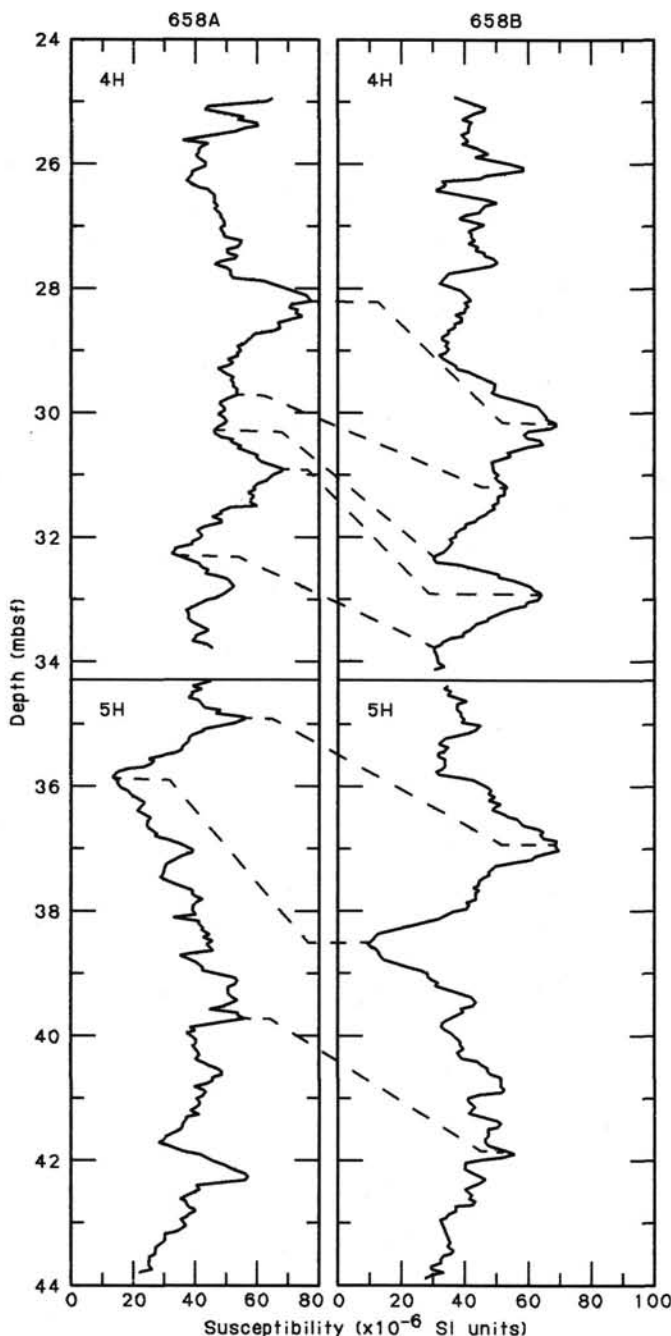


Figure 18. Between-hole susceptibility correlations.

Brunhes; the age of the 101.6-m level cannot be older than 0.73 Ma. Downhole extrapolation of the sedimentation rate from the *P. lacunosa* datum intercepts the 101.6-m level at about 0.69 Ma.

Calcidiscus macintyrei and *Helicosphaera sellii* both disappear 2.0–2.5 m above the 101.6-m level within Chron C1. This gives erroneous age estimates for their extinctions: 0.8 m.y. too young for *C. macintyrei* and 0.5–0.7 m.y. too young for *H. sellii*. Their positions above the indicated hiatus must represent reworking.

INORGANIC GEOCHEMISTRY

Interstitial-water samples were squeezed from six sediment samples taken routinely from approximately every 50 m in Hole

Table 3. Depth and age estimates of biostratigraphic and magnetostratigraphic indicators used to establish accumulation rates for Site 658.

	Datum	Depth (mbsf)	Age (Ma)
	<i>Emiliana huxleyi</i> acme	5.7–24.7	0.09
FO	<i>E. huxleyi</i>	34.2–43.7	0.28
LO	<i>Pseudoemiliana lacunosa</i>	68.7–70.2	0.47
LO	<i>Nitzschia reinholdii</i>	62.7–72.2	0.65
	Brunhes (within)	101.6–101.6	0.73
LO	<i>Calcidiscus macintyrei</i>	99.1–99.4	1.45
	Matuyama/Olduvai	109.2–109.8	1.66
	Olduvai/Matuyama	124.2–129.7	1.88
	<i>Discoaster brouweri</i>	124.2–127.2	1.89
FO	<i>Pseudoeunotia doliolus</i>	129.2–138.7	1.80
FO	<i>Discoaster triradiatus</i> acme	138.7–144.7	2.07
LO	<i>Globorotalia miocenica</i>	155.3–157.7	2.20
LO	<i>Thalassiosira convexa</i>	157.7–157.9	2.20
LO	<i>Discoaster surculus</i>	165.4–167.7	2.45
	Matuyama/Gauss	154.6–158.3	2.47
LO	<i>Discoaster tamalis</i>	197.4–203.3	2.65
LO	<i>Nitzschia jouseae</i>	205.4–214.9	2.65
LO	<i>Dentoglobularina altispira</i>	214.9–224.4	2.90
	Gauss/Gilbert	267.3–281.7	3.40
LO	<i>Reticulofenestra pseudoumbilica</i>	281.4–290.9	3.56

FO = first occurrence; LO = last occurrence.

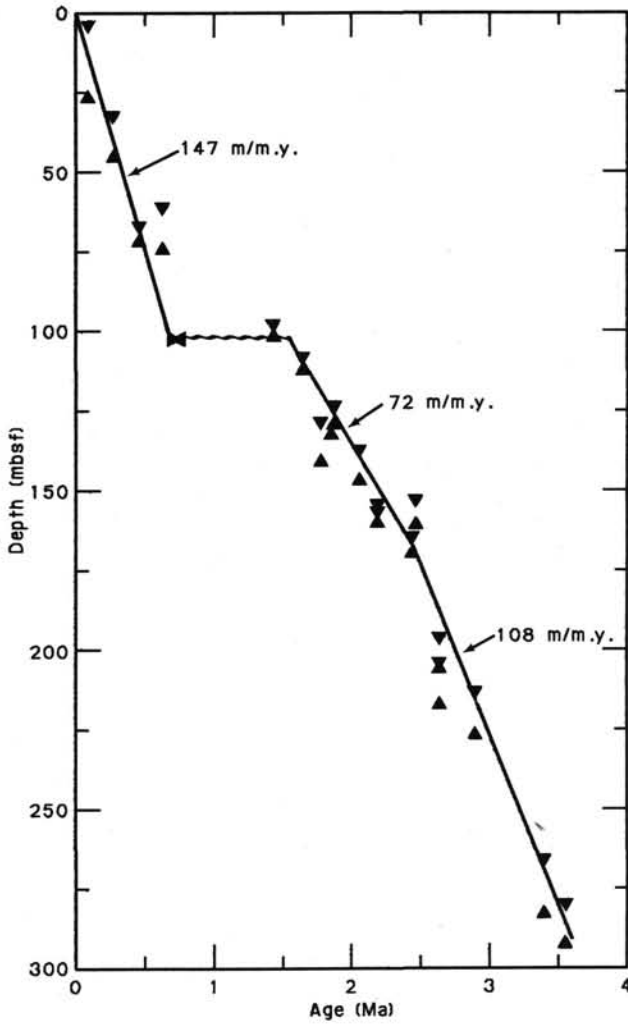


Figure 19. Accumulation-rate curve for Hole 658A.

658A (Cores 108-658A-21X and -658A-30X) and Hole 658B (Cores 108-658B-1H, -658B-6H, -658B-11H, and -658B-17H). Values for pH and alkalinity were measured in conjunction using a Metrohm 605 pH-meter, followed by titration with 0.1N HCl. Salinities were measured using an optical refractometer, and chlorinities were determined by titration with silver nitrate to a potassium chromate end point. Calcium, magnesium, and sulfate analyses were performed by ion chromatography on a Dionex 2120i instrument. Results from all analyses are presented in Table 4.

ORGANIC GEOCHEMISTRY

Site 658 was characterized by the high concentration of gas trapped in the sediments, which upon release of pressure expanded to form frequent voids in the cores. Samples of gas were obtained from most cores using vacutainers and analyzed immediately as a safety precaution.

Physical-property samples were used to determine total-organic-carbon (TOC) and carbonate contents for Hole 658A. Of these, a representative set of samples was also analyzed by Rock-Eval pyrolysis. Organic extracts of 17 sediment samples from the upper part of Hole 658A were analyzed by capillary gas chromatography.

Analysis of Hydrocarbon Gases

High concentrations of gas were encountered at Site 658, causing large and frequent voids in cores because of gas expansion during the release of pressure. This feature was particularly notable in Hole 658A, where voids made up almost 50% of the core liner volume. Gas samples were taken by piercing the core liner over a void and then collecting the gas in sealed, evacuated vacutainers for immediate gas chromatographic analysis. A small sample of the gas (0.25 mL) was injected into a Hewlett-Packard 5890 Gas Chromatograph fitted with DC200 and Porapak Q packed columns connected in series. The carrier gas was helium at 50-psi head pressure, and the oven temperature was maintained at 70°C. Hydrocarbons were detected using a flame ionization detector (FID). The resulting signal was plotted and peak areas calculated with a Hewlett-Packard 3392a integrator. Concentrations of methane (C_1) and ethane (C_2) were listed by the integrator after each analysis, and values of C_1/C_2 were calculated from peak area counts (Fig. 20). Because of difficulties with the instruments during the early stages of coring at Hole 658A, only minimum values of C_1/C_2 could be assigned; these are omitted from the plot but are listed in Table 5.

The upper cores from Holes 658A and 658B contained relatively low concentrations of methane and no detectable ethane. A low concentration of ethane was seen in Core 108-658B-6H, and after this point ethane increased considerably with depth, causing the methane/ethane ratio to fall toward 1000 (Fig. 20).

High concentrations of methane are common in organic-rich sediments such as these and arise from bacterial activity (so-called biogenic methane). In contrast, ethane and higher hydrocarbons are generally produced with depth as increasing temperature and pressure lead toward petroleum generation (Tissot and

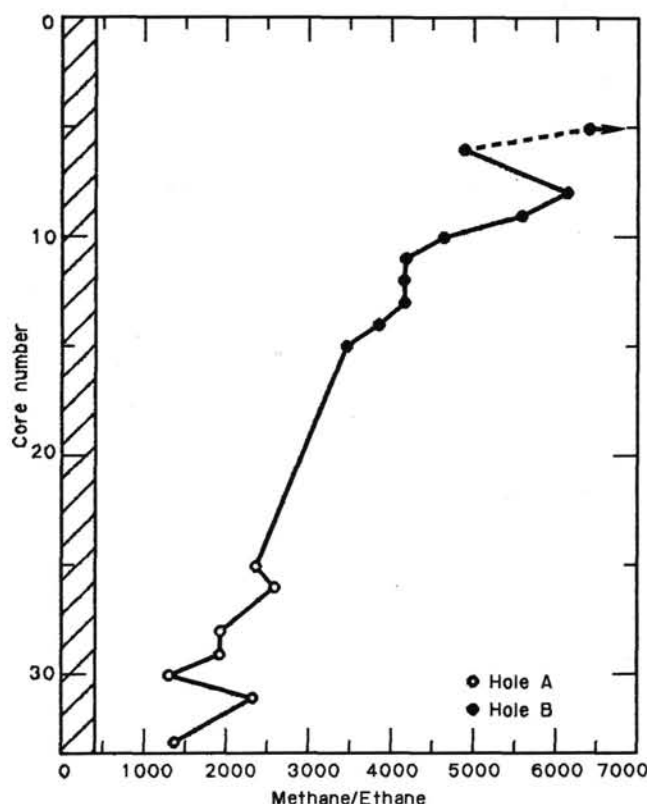


Figure 20. Plot of methane/ethane ratio vs. depth (as core number). The shaded region is generally considered to represent a relatively high-risk situation where drilling must be stopped.

Welte, 1984). Hence, the methane/ethane ratio may be monitored to assess the risk of encountering a dangerous accumulation of thermally generated hydrocarbons. The lowest C_1/C_2 value measured at Site 658 was 1311, which was near the bottom of Hole 658A and well above the ODP Safety Panel limit of 500. Hydrocarbons higher than ethane were not detected in any of the gas samples analyzed from this site.

Organic and Inorganic Carbon

Inorganic-carbon (IC) contents were measured on the Coulometrics Carbon Dioxide Coulometer, whereas total-carbon (TC) values were determined using the Perkin Elmer 240C Elemental Analyzer. TOC values were calculated by difference. Analytical methods are discussed and data presented in the Appendix (this volume).

TOC values at Site 658, Hole 658A, are consistently high throughout the section, ranging from 0.44% to 3.26%. The upper part (Cores 108-658A-1H through -658A-10H) is significantly lower in organic-carbon content than the lower levels,

Table 4. Results of inorganic-geochemical analyses conducted for Site 658.

Hole/core/ section	pH	Alkalinity (mmol/L)	Salinity (‰)	Chlorinity (mmol/L)	SO_4^{2-} (mmol/L)	Mg^{2+} (mmol/L)	Ca^{2+} (mmol/L)
B-1H-1	7.76	3.34	34.0	572	20.9	46.7	14.2
B-6H-5	7.43	33.52	33.8	587	0.0	39.9	^a low
B-11H-7	7.09	43.84	36.0	558	0.0	48.2	^a low
B-17H-7	7.54	43.50	37.2	636	0.0	35.6	^a low
A-21X-2	7.48	44.32	38.4	625	5.20	53.1	^a low
A-30X-3	7.76	38.00	42.1	691	5.45	50.1	^a low

^a Ca^{2+} cannot be detected in standards containing 7.24 mmol/L.

Table 5. Results of analyses of vacutainer gas samples at Site 658.

Hole 658A		Hole 658B	
Core no.	C ₁ /C ₂	Core no.	C ₁ /C ₂
6	^a n.m.	5	n.m.
		6	4903
		8	6174
9	n.m.	9	5613
		10	4671
11	>1600	11	4201
		12	4172
13	n.m.	13	4197
14	n.m.	14	3887
15	n.m.	15	3473
17	>2000		
19	n.m.		
20	>600		
21	>1800		
22	>500		
23	>850		
24	>500		
25	2365		
26	2630		
28	1940		
29	1949		
30	1311		
31	2330		
33	1367		

^a n.m. = not measurable (ethane was not detected).

Note: In some cases only minimum values could be assigned; true values may have been considerably higher.

where values around 3% are common (Fig. 21). Quasiperiodic cyclic variations in organic-carbon content are superimposed upon a gradual trend of increasing TOC with depth.

The carbonate curve (Fig. 21) tends to mirror that of TOC. The uppermost part of the section (through Core 108-658A-10H), corresponding to lithologic Unit I (see "Lithostratigraphy and Sedimentology" section, this chapter), displays higher average carbonate content (with a maximum of 68%) than do the lower levels. There is a general trend of decreasing carbonate content with depth upon which are superimposed quasiperiodic variations of up to 40%.

Rock-Eval Pyrolysis

Rock-Eval pyrolysis (Espitalié et al., 1977) was used to indicate the type and maturity of the organic matter of almost 40 samples taken from throughout the section. A van Krevelen plot (Fig. 22) shows that all samples exhibit relatively low hydrogen indexes (HI) and intermediate to high oxygen indexes (OI) and can be plotted in an area between fields II and III. This suggests that these samples contain mixed organic matter of marine and terrestrial origin (i.e., types II and III; Tissot and Welte, 1984).

The samples can be plotted in an area well away from the origin of the van Krevelen diagram, indicating the immaturity of their organic matter (Tissot and Welte, 1984). This feature is also shown by the low temperatures of maximum pyrolysis yield (T_{max}), which vary between 403° and 425°C (Table 6).

Gas Chromatography of Extractable Lipids

Seventeen sediment samples from Core 108-658-1H were freeze dried and ultrasonically extracted with methanol and dichloromethane to yield organic extracts that were subsequently analyzed by gas chromatography. The Hewlett-Packard 5890 Gas Chromatograph was operated in a splitless injection mode with an OV-1-type capillary column (cross-linked methyl silicone; 25 m × 0.20-mm inside diameter) and helium carrier gas. The

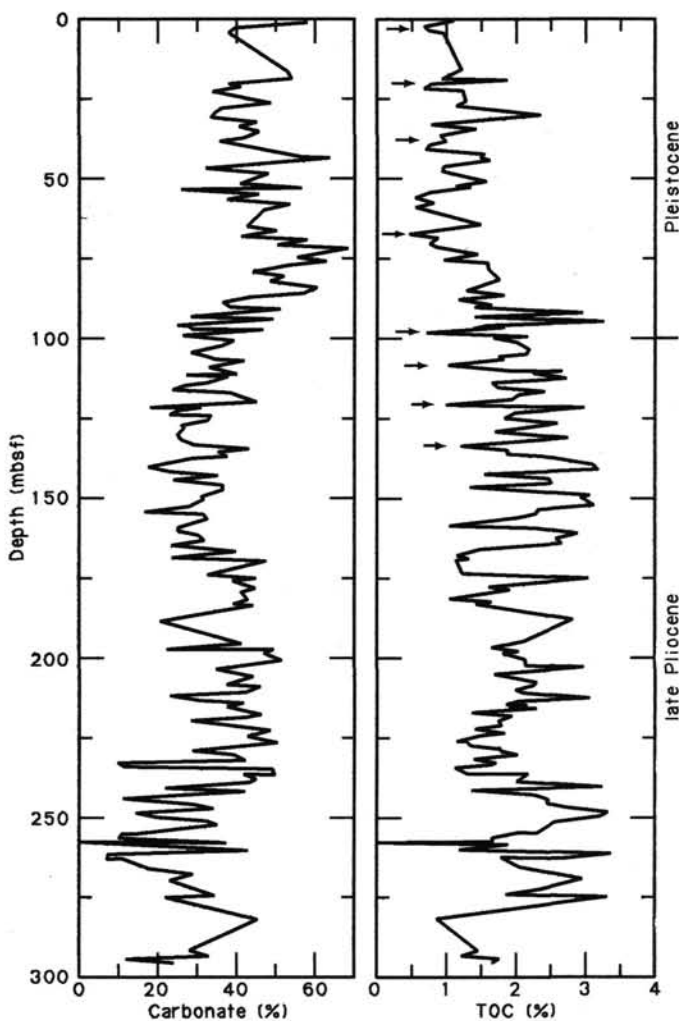


Figure 21. Organic-carbon and carbonate records of Site 658, Hole 658A. The arrows mark distinct minima in the TOC curve.

oven temperature was programmed from 50° to 220°C at 10°C/min and 220° to 300°C at 4°C/min. The FID signal was monitored by a Hewlett-Packard 3392 Integrator.

Generally, the organic extracts display similar chromatograms, with a complex mixture of low-molecular-weight compounds. An important feature to note, however, is the presence of two doublets in all samples, eluting in the high molecular weight range (Fig. 23). These compounds are C₃₇ and C₃₈ alkenones (long-chain unsaturated ketones; assigned by comparison with standard samples). A simple parameter, U₃₇^k, calculated from the relative abundances of two C₃₇ alkenones, differing only in their degree of unsaturation (A and B, Fig. 23), may be used to indicate variations in sea-surface temperatures (Brassell et al., 1986), where:

$$U_{37}^k = B/(B + A).$$

A plot of this unsaturation index vs. depth is shown in Figure 24.

The plot obviously displays cyclic or pseudocyclic variations in the unsaturation ratio and, hence, sea-surface temperature (Brassell et al., 1986). Based on an average sedimentation rate of 14.6 cm/1000 yr (see "Sediment-Accumulation Rates" section, this chapter), the equivalent of oxygen isotope Stage 1, the

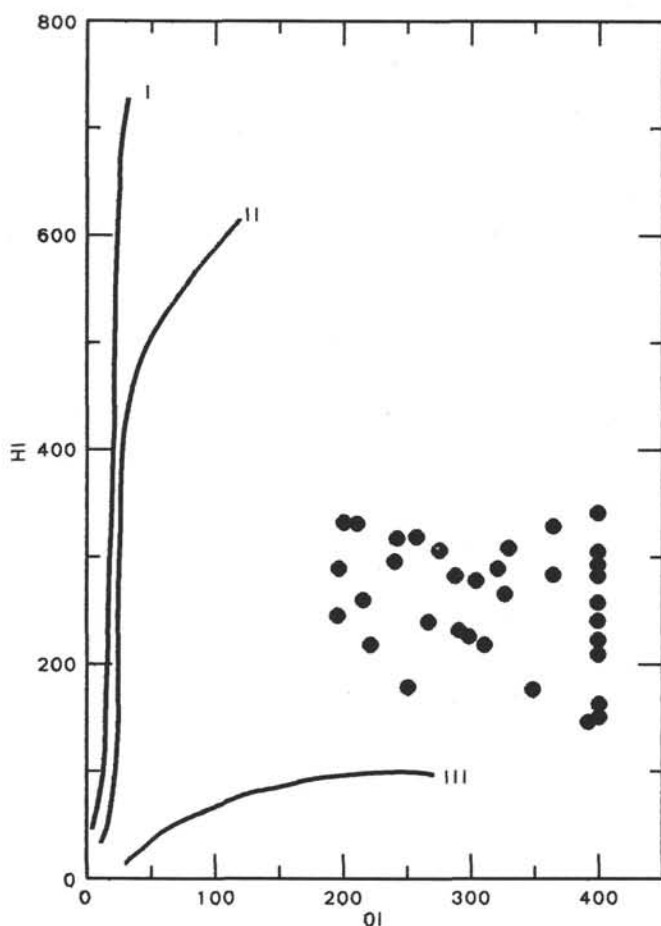


Figure 22. A van Krevelen plot of organic matter at Site 658, Hole 658A. HI = hydrogen index, OI = oxygen index (from Rock-Eval pyrolysis).

Table 6. Rock-Eval pyrolysis results and estimated amounts of marine organic matter (using Stein et al.'s method, 1986).

Sample interval (cm)	TOC (%)	HI	OI	T _{max}	Marine C _{org} (%)
658A-1-2, 120	1.09	149	394	415	40
658A-1-4, 34	0.96	285	442	415	60
658A-3-3, 120	0.92	297	527	416	60
658A-3-4, 120	0.77	260	492	414	55
658A-4-4, 120	2.36	284	287	411	60
658A-4-5, 120	1.54	310	329	414	65
658A-5-5, 120	0.67	281	510	411	55
658A-6-3, 120	0.92	308	441	425	60
658A-6-5, 120	1.57	277	329	416	55
658A-7-1, 120	0.72	247	458	415	55
658A-7-2, 120	0.53	172	630	403	40
658A-8-1, 120	1.47	182	305	412	40
658A-8-4, 120	0.86	344	628	412	65
658A-9-2, 120	0.95	238	468	415	50
658A-10-4, 120	1.16	243	402	415	50
658A-11-3, 96	3.26	337	208	416	65
658A-11-3, 102	2.87	324	241	417	65
658A-12-1, 24	2.02	247	267	414	55
658A-12-2, 118	2.18	222	219	418	50
658A-12-4, 102	1.71	313	275	422	60
658A-12-6, 82	1.02	218	311	415	50
658A-13-5, 120	2.40	300	241	411	60
658A-14-2, 94	2.97	336	200	408	65
658A-14-6, 85	2.59	182	251	419	45
658A-15-4, 88	1.19	222	408	417	50
658A-15-7, 34	2.34	282	305	415	60
658A-16-2, 120	3.17	262	214	411	55
658A-19-1, 84	1.03	170	403	409	40
658A-20-7, 84	1.19	212	400	414	50
658A-25-6, 64	1.39	329	364	415	65
658A-26-2, 96	1.27	282	365	420	60
658A-27-4, 86	1.96	236	291	417	50
658A-28-2, 120	2.42	230	297	407	50
658A-28-5, 118	3.18	251	194	422	55
658A-29-4, 101	1.64	293	323	412	60
658A-30-5, 119	2.94	294	195	420	60
658A-33-1, 120	1.45	185	348	421	45

TOC = total organic carbon, HI = hydrogen index, OI = oxygen index, T_{max} = maximum temperature, and C_{org} = organic carbon.

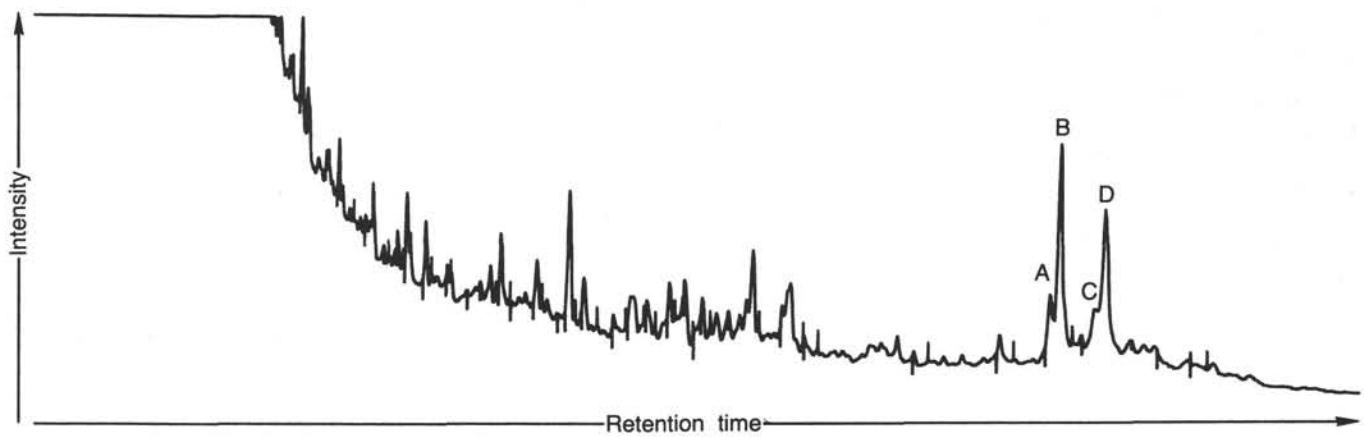


Figure 23. A gas chromatogram of the total organic extract (hexane-soluble fraction) of Core 108-658A-1H-1, 46-48 cm. A = C₃₇ alkatrienone (37:3), B = C₃₇ alkadienone (37:2), C = C₃₈ alkatrienone (38:3), D = C₃₈ alkadienone (38:2).

present interglacial stage is represented by high unsaturation indexes and began at around 10,000 yr (about 1.5 mbsf). After reaching maximum sea-surface temperatures at around 7000 yr (1.05 mbsf), evidence exists for a slight cooling toward the present time. The late Stage 2 glacial is represented by a distinct minimum in the curve at around 2.25 mbsf. Before this, the sig-

nal fluctuates between periods of cool and moderate sea-surface temperatures.

Discussion

The high concentrations of methane encountered at Site 658 were the result of subsurface bacterial degradation of organic

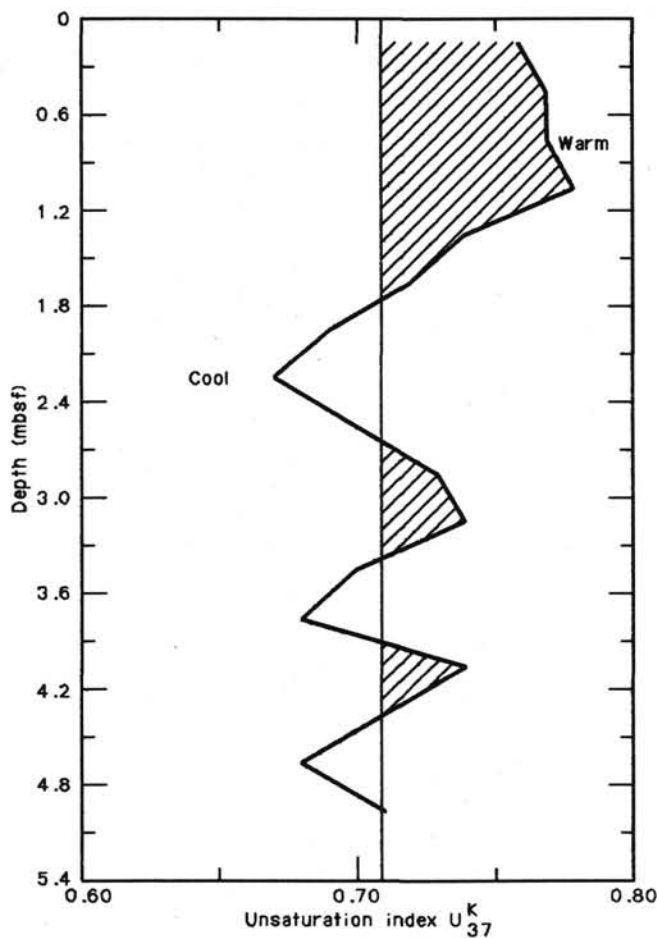


Figure 24. A plot of alkenone unsaturation index (U_{37}^k) vs. depth in Core 108-658A-1H. High unsaturation indices indicate warmer sea-surface temperatures.

matter. The low amounts of ethane that were observed probably arose from mixing early products of thermal evolution of kerogen with large amounts of biogenic gas.

The sediments at Site 658 are characterized by very high organic-carbon contents (0.44% to 3.26%), well above the normal values expected for a marine environment. Using the HI values obtained by Rock-Eval pyrolysis and Stein et al.'s method (1986), one can suggest values of 40% to 65% marine organic matter for the sediments at Site 658. However, this is hardly surprising, as the site lies underneath the permanent oceanic upwelling cell west of Cap Blanc. Thus, high oceanic productivity may have been the main factor controlling the accumulation of organic matter, although fluvial and eolian input of terrigenous organic matter may also have been important at Site 658.

The change in average carbonate and TOC values around the base of Core 108-658A-10H lies at about 0.6 Ma (see "Sediment-Accumulation Rates" section, this chapter) and is represented by a change in lithology with higher noncarbonate sediment beneath this level (see "Lithostratigraphy and Sedimentology" section, this chapter). Because the sedimentation rates are distinctly higher in the carbonate-rich upper part of the sequence (i.e., in Unit I), it appears that the lower carbonate content below Core 108-658A-10H may be caused by dissolution. The high-frequency variations in both TOC and carbonate content throughout Cores 108-658A-1H through -658A-10H may reflect climatic cycles of 100,000-yr duration, but higher resolution analyses are needed before this signal can be identified for certain.

PHYSICAL PROPERTIES

The techniques used for the shipboard physical-property measurements at Site 658 are outlined in the "Introduction and Explanatory Notes" (this volume). Tables 7 through 11 show data for the index properties, vane shear strength, and the limited compressional-wave velocity (Hamilton Frame) from Holes 658A and 658B. Only GRAPE measurements were performed on cores from Hole 658C. Most of these data for Holes 658A and 658B are presented graphically in Figures 25 through 31 (the calcium carbonate profile is shown in Figure 29 for comparison with the other properties). None of the data presented in this section were screened for bad data points.

Most cores recovered from this site contained significant amounts of gas, especially below 35 mbsf. It is unclear at this time if any of this gas exists in a free state, *in situ*, or whether it is all in solution. The large volumetric expansion during recovery caused sediment cores to expand significantly and to break into small sections. Consequently, many of the cores (which included the many voids) were recorded as being longer than the 9.5-m core barrel. As shown in Figures 25 through 31, the below seafloor depths were calculated for this preliminary report as follows. For Hole 658A, the core was "shortened" to 9.5 m, if necessary, by subtracting any excess length evenly from each of seven sections. For Hole 658B, the process was repeated but in addition any remaining voids were subtracted from the total length, which allowed for recoveries of less than 100%.

It is worth noting that during core splitting the sediment sections often moved within the core liner. Therefore, whole-core logs and "barrel sheets" certainly will not correlate. It would have been extremely helpful to the physical-properties scientists if permission had been granted to reassemble physically the obviously broken cores in Hole 658B. However, data about the voids have been entered on the computer so that the gaps in these cores can be closed "on paper" (see "Operations" section, this chapter).

Owing to a lack of pycnometer beakers, sample volumes (and thus some of the index properties) for Hole 658B were calculated by using wet and dry weights and an assumed average grain density of 2.66 g/cm³. The measured grain densities from Hole 658A vary between 2.9 and 2.2 g/cm³ (Fig. 29). These variations reflect the changes in composition among biogenic silica, biogenic carbonate, and terrigenous material. Only the biogenic silica has a significantly lower grain density; hence, variations in this component are chiefly responsible for the low average grain density between 125 and 175 mbsf.

Three distinct units can be identified in the porosity profile for Hole 658A shown in Figure 28 (and in profiles of closely related parameters; Figs. 25 through 27). Unit I extends from the mud line to a depth of about 100 mbsf and shows a normal reduction in porosity from 73% to 62% caused by the consolidation process. Unit II extends from 100 to 200 mbsf and shows an essentially constant porosity with increasing depth of about 62%. This apparent lack of consolidation with depth is typical of sediments with higher amounts of biogenic silica, which form rigid open structures more resistant to the normal processes of consolidation. In Unit III (200–300 mbsf) the porosity decreases from 65% to 55%. The low-carbonate, high-grain-density profile in this unit indicates a higher proportion of terrigenous components that exhibit a more normal consolidation curve.

Hand-held "Torvane" shear-strength measurements were performed on cores from Site 658. Much of the cored material had suffered a high degree of disturbance (caused by the expansion of gas); hence, the vane-shear-strength profiles (Fig. 30) do not indicate formation shear strength. The apparent vane-shear-strength profile has two distinct units: (1) 0–150 mbsf (0–60 kPa) and (2) 150–300 mbsf (20–70 kPa). The break between

Table 7. Index-properties data for Hole 658A.

Section	Interval (cm)	Depth (m)	Grain density (g/cm ³)	Wet-water content (%)	Dry-water content (%)	Wet-bulk density (g/cm ³)	Dry-bulk density (g/cm ³)	Porosity (%)
1-1	20-122	1.21	2.58	53.57	115.40	1.42	0.70	74.69
1-2	20-122	2.71	2.82	47.82	91.63	1.53	0.83	71.90
1-3	20-122	4.21	2.69	47.99	92.27	1.51	0.81	71.04
1-4	34-36	4.82	2.74	46.58	87.19	1.54	0.85	70.30
3-1	20-122	16.41	2.73	48.42	93.89	1.51	0.82	71.75
3-2	20-122	17.91	2.76	49.82	99.29	1.49	0.79	73.06
3-3	20-122	19.41	2.63	52.02	108.43	1.44	0.73	73.86
3-4	20-122	20.91	2.66	43.74	77.73	1.56	0.92	67.13
3-5	20-122	22.40	2.83	43.05	75.59	1.60	0.97	67.90
3-6	34-36	23.04	2.73	44.97	81.73	1.56	0.91	68.81
4-1	20-122	25.90	2.72	46.33	86.31	1.53	0.86	69.90
4-2	20-122	27.40	2.75	49.47	97.89	1.49	0.80	72.71
4-3	20-122	28.90	2.88	47.83	91.68	1.54	0.84	72.30
4-4	20-122	30.40	2.57	49.12	96.55	1.47	0.79	71.09
4-5	20-122	31.90	2.51	46.96	88.53	1.49	0.87	68.76
4-6	20-122	33.40	2.61	47.16	89.25	1.50	0.83	69.76
5-1	84-86	35.05	2.49	48.20	93.03	1.47	0.83	69.67
5-2	20-122	36.82	2.69	43.89	78.22	1.56	0.93	67.50
5-3	20-122	38.28	2.68	41.88	72.06	1.59	0.99	65.59
5-4	20-122	39.73	2.67	42.32	73.38	1.58	0.95	65.91
5-5	20-122	41.19	2.69	44.39	79.82	1.56	0.90	68.01
5-6	20-122	42.65	2.31	49.26	97.09	1.42	0.76	68.99
5-7	34-36	43.27	2.92	43.23	76.16	1.62	0.94	68.75
6-1	84-86	44.50	2.70	44.89	81.47	1.55	0.92	68.50
6-2	20-122	46.41	2.72	43.88	78.20	1.57	0.93	67.81
6-3	20-122	47.91	2.61	43.95	78.40	1.55	0.95	66.91
6-5	20-122	50.91	2.66	44.16	79.09	1.56	0.91	67.57
6-6	20-122	52.44	2.38	64.22	179.48	1.28	0.50	81.02
6-7	34-36	52.77	2.40	63.46	173.69	1.29	0.51	80.60
7-1	20-122	54.41	2.59	42.63	74.32	1.56	0.94	65.58
7-2	20-122	55.91	2.70	41.77	71.74	1.60	0.96	65.66
7-3	20-122	57.41	2.73	43.32	76.43	1.58	0.93	67.38
7-4	20-122	58.91	2.77	42.89	75.11	1.60	0.95	67.32
8-1	20-122	63.90	2.72	44.37	79.77	1.56	0.91	68.19
8-2	18-120	65.39	2.66	48.36	93.65	1.50	0.82	71.14
8-3	15-117	66.82	2.68	39.98	66.60	1.62	1.01	63.82
8-4	20-122	68.40	2.58	44.44	79.99	1.54	0.89	67.16
8-5	20-122	69.90	2.72	41.79	71.79	1.60	0.97	65.86
8-6	81-83	71.01	2.71	45.01	81.84	1.55	0.89	68.68
9-1	20-122	73.41	2.63	45.21	82.53	1.53	0.88	68.22
9-2	20-122	74.91	2.61	46.20	85.87	1.52	0.88	68.90
9-3	86-88	76.06	2.79	43.32	76.42	1.59	0.96	67.85
9-4	20-122	77.90	2.70	44.22	79.27	1.56	0.91	67.92
9-5	20-122	79.40	2.54	47.01	88.71	1.49	0.84	69.04
9-6	20-122	80.90	2.55	46.77	87.86	1.50	0.85	68.89
10-1	20-122	82.90	2.69	45.44	83.27	1.54	0.88	68.89
10-2	20-122	84.40	2.55	43.97	78.47	1.54	0.90	66.42
10-3	20-122	85.90	2.71	43.68	77.55	1.57	0.91	67.48
10-4	20-122	87.40	2.67	42.52	73.96	1.58	0.95	66.16
10-5	18-120	88.88	2.57	43.74	77.75	1.54	0.92	66.43
10-6	48-50	89.68	2.64	43.04	75.56	1.57	0.94	66.36
11-2	24-26	92.72	2.61	44.75	81.00	1.54	0.88	67.66
11-3	02-104	94.70	2.41	49.60	98.40	1.44	0.78	70.19
11-4	20-122	96.17	2.56	43.98	78.51	1.54	0.91	66.50
11-5	20-122	97.47	2.61	39.23	64.55	1.62	1.04	62.50
11-6	20-122	98.78	2.58	42.48	73.85	1.56	0.95	65.32
11-7	24-26	99.25	2.53	42.35	73.46	1.56	0.96	64.78
12-1	24-26	100.90	2.60	38.08	61.50	1.64	1.06	61.28
12-2	18-120	102.98	2.57	40.39	67.77	1.59	0.99	63.23
12-3	20-122	104.27	2.56	38.57	62.79	1.62	1.06	61.34
12-4	02-104	105.39	2.53	35.15	54.21	1.66	1.17	57.54
12-5	24-26	106.01	2.75	37.44	59.85	1.68	1.12	61.89
12-6	20-122	108.10	2.62	35.11	54.10	1.69	1.19	58.28
12-7	20-122	109.95	2.42	39.46	65.19	1.57	1.02	60.96
12-8	59-61	110.13	2.59	38.23	61.90	1.63	1.08	61.32
13-1	59-61	110.70	2.71	47.47	90.36	1.52	0.86	70.83
13-2	20-122	112.49	2.52	41.34	70.48	1.57	0.39	63.73
13-3	16-118	113.73	2.55	38.44	62.45	1.62	1.06	61.11
13-4	20-122	115.04	2.56	36.97	58.66	1.64	1.12	59.77
13-5	20-122	116.32	2.56	40.52	68.11	1.59	1.02	63.30
13-6	84-86	117.29	2.59	42.78	74.78	1.56	0.96	65.67
13-7	20-122	118.87	2.51	42.44	73.75	1.55	0.93	64.65
14-1	20-122	120.67	2.75	32.93	49.09	1.76	1.25	57.11
14-2	20-122	121.88	2.65	41.66	71.41	1.59	0.98	65.20
14-3	20-122	123.11	2.60	39.71	65.85	1.61	1.03	62.87
14-4	34-36	123.63	2.65	41.15	69.94	1.60	0.88	64.67
14-5	34-36	124.85	2.56	38.30	62.07	1.62	1.05	61.10
14-6	85-87	126.48	2.61	43.63	77.38	1.55	0.92	66.67
14-7	34-36	127.29	2.61	42.60	74.20	1.57	0.96	65.69
15-1	34-36	129.49	2.61	35.52	55.09	1.68	1.13	58.67
15-2	20-122	131.49	2.32	42.87	75.05	1.50	0.90	63.28
15-4	88-90	133.76	2.63	37.63	60.33	1.65	1.08	61.06
15-5	88-90	135.03	2.59	39.23	64.55	1.62	1.03	62.31
15-6	84-86	136.26	2.63	38.18	61.75	1.64	1.06	61.59
15-7	34-36	137.11	2.45	40.91	69.24	1.56	0.37	62.69
16-1	20-122	139.46	2.22	47.53	90.60	1.42	0.86	66.57
16-2	20-122	141.27	2.25	45.45	83.32	1.45	0.90	64.98
16-3	20-122	142.77	2.47	39.36	64.91	1.58	1.08	61.32
16-4	20-122	144.12	2.53	40.37	67.70	1.58	1.06	62.89
16-5	20-122	145.62	2.32	41.79	71.79	1.51	0.98	62.22

these units occurs where both the carbonate and grain-density profiles are at a minimum value (25% and 2.3 g/cm³, respectively).

The problems with gas at this site precluded measuring any complete compressional-wave-velocity profiles. The velocity decreased from about 1.59 km/s at the mud line to about 1.50

Table 7 (continued).

Section	Interval (cm)	Depth (m)	Grain density (g/cm ³)	Wet-water content (%)	Dry-water content (%)	Wet-bulk density (g/cm ³)	Dry-bulk density (g/cm ³)	Porosity (%)
16-6	20-122	147.12	2.53	34.06	51.66	1.68	1.24	56.30
17-1	20-122	148.18	2.41	47.41	50.14	1.46	0.88	68.24
17-2	34-36	150.04	2.57	46.69	57.57	1.50	0.86	69.02
17-3	20-122	152.40	2.25	41.51	70.97	1.50	0.97	61.25
17-4	20-122	153.90	2.21	42.33	73.40	1.48	0.95	61.60
17-5	34-36	154.54	2.46	39.87	66.30	1.57	0.99	61.75
17-6	34-36	156.04	2.40	40.96	69.38	1.54	1.00	62.24
19-1	84-86	158.59	2.47	36.31	57.01	1.63	1.09	58.17
19-2	34-36	160.08	2.16	43.89	78.21	1.45	0.87	62.65
19-3	84-86	160.88	2.24	41.61	71.26	1.49	0.98	61.21
19-4	20-122	162.61	2.29	42.50	73.92	1.50	0.96	62.67
19-5	84-86	163.26	2.67	39.07	64.14	1.64	1.03	62.85
19-6	34-36	164.38	2.47	41.57	71.14	1.55	0.96	63.46
19-7	20-122	166.34	2.47	40.75	68.78	1.56	0.98	62.71
20-1	20-122	168.15	2.51	42.12	72.78	1.55	0.96	64.35
20-2	34-36	169.29	2.41	46.51	86.97	1.48	0.86	67.53
20-7	84-86	173.58	2.49	36.91	58.51	1.63	1.17	59.02
20-8	20-122	174.32	2.43	45.02	81.90	1.50	0.88	66.30
20-9	84-86	175.46	2.31	43.54	77.12	1.49	0.90	63.80
21-1	10-112	177.80	2.50	42.33	73.39	1.55	0.95	64.49
21-2	84-86	178.81	2.59	43.35	76.54	1.55	0.92	66.26
21-4	10-112	181.46	2.67	39.11	64.23	1.64	1.03	62.88
21-5	20-122	182.76	2.49	42.59	74.17	1.54	0.92	64.64
21-6	54-56	183.45	2.52	39.35	64.88	1.60	1.01	61.81
21-7	71-73	188.34	2.44	43.17				

Table 8. Index-properties data for Hole 658B.

Section	Interval (cm)	Depth (m)	Wet-water content (%)	Dry-water content (%)	Porosity (%)	Wet-bulk density (g/cm³)	Dry-bulk density (g/cm³)
1-1	120-122	1.21	58.06	138.42	77.35	1.39	0.60
1-2	15-17	1.66	57.92	137.65	77.26	1.39	0.60
2-1	120-122	3.48	56.06	127.57	75.95	1.42	0.64
2-2	120-122	4.95	47.53	90.60	69.43	1.52	0.81
2-3	120-122	6.42	43.92	78.30	66.35	1.57	0.89
2-4	120-122	7.89	47.55	90.66	69.45	1.52	0.81
2-5	81-83	9.36	42.10	72.72	64.72	1.60	0.93
2-6	120-122	10.83	41.00	69.50	63.70	1.61	0.96
2-7	50-52	11.60	42.14	72.83	64.75	1.60	0.93
3-1	120-122	12.96	47.65	91.02	69.53	1.52	0.81
3-2	120-122	14.07	51.46	106.02	72.56	1.47	0.73
3-3	120-122	15.42	46.56	87.11	68.62	1.53	0.83
3-4	120-122	16.72	49.31	97.27	70.87	1.50	0.77
3-5	67-69	17.44	46.62	87.34	68.67	1.53	0.83
3-6	120-122	19.15	47.81	91.59	69.66	1.52	0.80
4-1	120-122	22.51	37.07	58.92	59.89	1.68	1.06
4-2	120-122	24.01	46.50	86.93	68.57	1.54	0.83
4-3	120-122	25.51	48.44	93.94	70.17	1.51	0.79
4-4	120-122	27.01	47.29	89.73	69.23	1.52	0.82
4-5	120-122	28.51	49.83	99.32	71.29	1.49	0.76
4-6	120-122	30.01	45.70	84.17	67.89	1.55	0.85
5-1	120-122	31.24	48.50	94.19	70.23	1.51	0.79
5-2	120-122	32.64	44.86	81.34	67.17	1.56	0.87
5-3	120-122	33.99	63.85	176.65	81.14	1.33	0.50
5-4	120-122	35.29	43.55	77.16	66.02	1.58	0.90
5-5	120-122	36.54	42.91	75.16	65.45	1.59	0.92
5-6	80-82	37.34	42.10	72.71	64.71	1.60	0.94
5-7	46-48	38.49	45.89	84.81	68.06	1.54	0.85
6-1	120-122	41.41	44.82	81.23	67.14	1.56	0.87
6-2	120-122	42.71	43.93	78.35	66.36	1.57	0.89
6-3	120-122	43.91	46.24	86.01	68.35	1.54	0.84
6-4	120-122	45.01	44.77	81.05	67.09	1.56	0.87
6-5	120-122	46.01	42.92	75.20	65.46	1.59	0.92
6-6	120-122	46.91	43.74	77.74	66.19	1.57	0.90
7-1	120-122	50.92	57.78	136.87	77.16	1.40	0.61
7-2	120-122	52.25	44.56	80.39	66.91	1.56	0.88
7-3	120-122	53.49	45.92	84.92	68.08	1.54	0.85
7-4	120-122	54.65	41.11	69.80	63.80	1.61	0.96
7-5	120-122	55.72	45.22	82.54	67.48	1.55	0.86
7-6	120-122	56.71	44.48	80.12	66.84	1.56	0.88
8-1	120-122	60.45	43.67	77.53	66.13	1.58	0.90
8-2	120-122	61.54	45.98	85.13	68.13	1.54	0.84
8-3	120-122	62.85	42.89	75.09	65.43	1.59	0.92
8-4	120-122	64.10	44.85	81.32	67.16	1.56	0.87
8-5	120-122	65.29	50.19	100.75	71.57	1.49	0.75
8-6	120-122	66.41	39.66	65.73	62.44	1.64	1.00
9-2	120-122	71.21	45.28	82.76	67.54	1.55	0.86
9-3	120-122	72.41	45.71	84.20	67.90	1.55	0.85
9-4	120-122	73.51	43.19	76.01	65.70	1.58	0.91
9-5	120-122	74.51	43.79	77.90	66.23	1.57	0.89
9-6	120-122	75.41	43.80	77.93	66.24	1.57	0.89
9-7	120-122	76.21	46.27	86.12	68.38	1.54	0.84
10-1	134-136	79.40	46.16	85.74	68.29	1.54	0.84
10-2	34-36	79.77	43.38	76.61	65.87	1.58	0.90
10-3	84-86	81.23	50.50	102.00	71.81	1.48	0.75
10-4	120-122	82.74	42.16	72.89	64.77	1.60	0.93
10-5	34-36	83.29	41.81	71.85	64.45	1.60	0.94
10-6	120-122	85.45	42.40	73.63	64.99	1.59	0.93
10-7	120-122	86.71	44.58	80.45	66.93	1.56	0.88
11-2	120-122	89.33	44.61	80.53	66.95	1.56	0.88
11-3	34-36	89.73	43.41	76.72	65.90	1.58	0.90
11-4	120-122	91.85	45.92	84.90	68.08	1.54	0.85
11-6	34-36	92.88	41.88	72.06	64.51	1.60	0.94
11-8	120-122	95.44	37.69	60.49	60.51	1.67	1.05
12-1	34-36	97.65	38.52	62.67	61.33	1.65	1.02
12-2	34-36	99.05	37.34	59.59	60.16	1.67	1.06
12-3	84-86	100.45	38.98	63.89	61.78	1.65	1.01
12-4	120-122	101.85	38.13	61.62	60.94	1.66	1.04
12-5	120-122	103.13	38.66	63.02	61.46	1.65	1.02
12-6	84-86	104.08	36.01	56.27	58.80	1.69	1.09
12-7	120-122	105.65	37.20	59.23	60.02	1.67	1.06
13-1	18-20	107.02	41.99	72.37	64.61	1.60	0.94
13-2	120-122	108.05	38.29	62.06	61.11	1.66	1.03
13-3	120-122	109.54	36.80	58.24	59.62	1.68	1.07
13-4	95-97	110.79	38.54	62.72	61.35	1.65	1.02
13-5	48-50	111.79	43.33	76.48	65.83	1.58	0.91
13-6	120-122	113.98	42.53	74.02	65.11	1.59	0.92
14-2	88-90	117.48	42.38	73.56	64.97	1.59	0.93
14-4	12-14	119.62	38.00	61.29	60.81	1.66	1.04
14-5	48-50	121.32	38.96	63.82	61.75	1.65	1.01
14-7	18-20	123.49	38.26	61.96	61.07	1.66	1.03
15-3	120-122	128.69	39.69	65.81	62.46	1.64	0.99
15-6	48-50	130.34	42.33	73.40	64.93	1.59	0.93
15-7	48-50	131.77	39.06	64.10	61.86	1.64	1.01
15-8	48-50	133.27	35.75	55.63	58.53	1.70	1.10
16-1	120-122	136.51	32.58	48.31	55.14	1.75	1.19
16-2	120-122	138.01	36.60	57.73	59.41	1.68	1.08

Table 8 (continued).

Section	Interval (cm)	Depth (m)	Wet-water content (%)	Dry-water content (%)	Porosity (%)	Wet-bulk density (g/cm³)	Dry-bulk density (g/cm³)
16-3	120-122	139.51	47.93	92.06	69.76	1.52	0.80
16-4	120-122	141.01	39.47	65.20	62.25	1.64	1.00
16-6	50-52	142.35	36.45	57.37	59.26	1.69	1.08
17-2	120-122	146.45	39.67	65.76	62.44	1.64	1.00
17-3	32-34	146.95	43.93	78.35	66.36	1.57	0.89
17-5	50-52	149.18	45.30	82.80	67.55	1.55	0.86
17-7	50-52	150.89	41.84	71.93	64.48	1.60	0.94
17-8	50-52	152.32	42.18	72.94	64.79	1.60	0.93
18-1	50-52	154.81	33.67	50.76	56.33	1.73	1.16
18-3	120-122	157.13	38.53	62.68	61.34	1.65	1.02
18-5	50-52	157.84	41.22	70.11	63.90	1.61	0.96
18-6	120-122	159.86	37.34	59.59	60.16	1.67	1.06
18-7	120-122	161.01	32.48	48.10	55.03	1.76	1.19
18-8	50-52	161.51	33.34	50.01	55.97	1.74	1.17

tively, could obtain results of sufficient accuracy. We attempted to calculate the volume of gas present in the sediment (excluding the expansion that caused large voids in the cores) by looking at the difference between the sample volume measured directly from the pycnometer and that calculated from wet and dry weights and grain density. However, these differences were so small that they were within the realm of experimental uncertainties. We concluded, therefore, that the free gas content of the cores in the laboratory was <2%. One possible interpretation of the seismic records indicates velocities as low as 900–940 m/s in the sediments between 32 and 227 mbsf. Only free gas *in situ* could account for such low velocities.

All the whole-core sections were continuously logged using the GRAPE, which, at this site, provided a good record of the positions of the voids before splitting the cores.

SEISMIC STRATIGRAPHY

Precision-depth-recorder (3.5- and 12-kHz) and 20- to 500-Hz reflection profiles were recorded at Site 658 (see “Background and Scientific Objectives” section, this chapter). The 3.5-kHz echogram was produced by a hull-mounted transducer and revealed a fairly uniform seismic section of two conformable sub-bottom reflectors down to approximately 40 mbsf (Fig. 32). The 20- to 500-Hz seismic record is characterized by a series of five, mostly conformable, seismic units with parallel internal reflectors (Fig. 33; Table 12). The base of the total series has a distinct bowl shape. The thin upper seismic unit (unit 1) with two conformable sub-bottom reflectors extends down to 0.04 s below the seafloor and is an artifact. Seismic unit 2 comprises 0.16-s two-way traveltimes and contains a transparent layer 0.025 s thick above and six strong conformable reflectors below. At their base is another thin transparent layer, occasionally with a faint reflector in the center. Seismic unit 3 is 0.065 s thick and consists of four strong reflectors enclosing two seismic layers that pinch out to the west; however, east of the site location each of these layers reaches 0.035 s thick. Seismic unit 4 consists of eight to nine reflectors that become fainter and more bowl-shaped with increasing sub-bottom depth in the 0.23-s-thick section. Seismic unit 5 is 0.25 s thick and again shows about seven strong, bowl-shaped reflectors, with one or two possible onlaps in the center.

The source of these reflectors was difficult to determine, primarily because of the probability of free gas in the sediments. On one hand, this gas prevented our measuring sound velocities in the sediment cores and created numerous artificial gaps. On the other hand, the gas did not allow us to apply “standard” sound velocities (e.g., 1500 m/s) to the interpretation of the seismic profile because these velocities must be much reduced

Table 9. Vane-shear-strength data for Hole 658A.

Section	Interval (cm)	Depth (m)	Vane shear strength (kPa)
1-1	120-122	1.21	4.00
1-3	120-122	2.71	2.00
1-4	34-36	4.21	10.00
3-1	120-122	4.82	1.95
3-2	120-122	17.91	1.00
3-3	120-122	19.41	15.00
3-4	120-122	20.91	12.00
3-5	120-122	22.40	3.00
3-6	34-36	23.04	16.00
4-1	120-122	25.90	12.00
4-2	120-122	27.40	21.50
4-3	120-122	28.90	33.30
4-4	120-122	30.40	32.00
4-5	120-122	31.90	21.00
4-6	120-122	33.40	11.00
5-1	84-86	35.05	22.00
5-2	120-122	36.82	8.00
5-3	120-122	38.28	18.00
5-4	120-122	39.73	11.00
5-5	120-122	41.19	11.50
5-6	120-122	42.65	38.00
5-7	34-36	43.27	40.50
6-1	84-86	44.50	28.00
6-2	120-122	46.40	24.50
6-3	120-122	47.91	19.50
6-6	120-122	52.40	30.00
6-7	34-36	52.77	10.50
7-1	120-122	54.41	12.50
7-2	120-122	55.91	21.00
7-3	120-122	57.41	18.00
7-4	120-122	58.91	11.00
8-1	120-122	63.90	12.00
8-2	118-120	65.39	12.00
8-3	115-117	66.82	12.00
8-4	120-122	68.40	15.00
8-5	120-122	69.90	12.00
8-6	81-83	71.01	14.00
9-1	120-122	73.41	13.00
9-2	123-125	74.91	12.00
9-3	86-88	76.06	25.00
9-4	120-122	77.90	35.00
9-5	120-122	79.40	62.00
9-6	120-122	80.90	52.00
10-1	120-122	82.90	16.00
10-2	120-122	84.40	12.00
10-3	120-122	85.90	15.00
10-4	120-122	87.40	10.00
10-5	118-120	88.80	34.00
10-6	48-50	89.68	28.00
11-2	24-26	92.72	12.00
11-3	102-104	94.70	14.00
11-4	120-122	96.17	27.00
11-5	120-122	97.47	16.00
11-6	120-122	98.78	34.00
11-7	24-26	99.25	23.00
12-1	24-26	100.90	34.00
12-2	118-120	102.98	34.00
12-3	120-122	104.27	37.00
12-4	102-104	105.39	41.00
12-5	24-26	106.01	54.00
12-6	120-122	108.10	31.00
12-7	120-122	109.95	53.00
12-8	59-61	110.13	36.00
13-1	59-61	110.70	28.00
13-2	120-122	112.49	54.00
13-4	120-122	115.04	47.00
13-3	116-118	113.73	40.00
13-5	120-122	116.32	53.00
13-6	84-86	117.29	50.00
13-7	120-122	118.87	28.00
14-1	120-122	120.67	33.00
14-2	120-122	121.88	25.00
14-3	120-122	123.11	60.00
14-4	34-36	123.63	30.00
14-5	34-36	124.85	41.00
14-6	85-87	126.48	48.00
14-7	34-36	127.29	37.00
15-1	34-36	129.49	39.50
15-2	120-122	131.49	54.00
15-3	120-122	132.99	40.50
15-4	88-90	133.76	50.00
15-5	88-90	135.03	54.50
15-7	34-36	137.11	51.50
16-1	120-122	139.45	51.00
16-2	120-122	141.27	51.00
16-3	120-122	142.77	43.00

Table 9 (continued).

Section	Interval (cm)	Depth (m)	Vane shear strength (kPa)
16-4	120-122	144.12	100.00
16-5	120-122	145.26	90.00
16-6	120-122	147.12	59.90
17-1	120-122	148.18	52.20
17-2	34-36	150.04	58.50
17-3	120-122	152.40	88.00
17-4	120-122	153.90	42.00
17-5	34-36	154.54	52.50
17-6	34-36	156.04	38.50
19-1	84-86	158.59	9.50
19-2	34-36	160.08	33.50
19-3	84-86	160.88	40.50
19-4	120-122	162.61	54.50
19-5	84-86	163.26	41.00
19-6	34-36	164.38	41.50
19-7	120-122	166.34	32.00
20-1	120-122	168.15	10.00
20-2	84-86	169.29	5.00
20-3	34-36	169.50	33.00
20-7	84-86	173.58	27.00
20-8	120-122	174.32	9.00
20-9	84-86	175.46	53.00
21-1	110-112	177.80	32.00
21-2	84-86	178.81	29.00
21-4	110-112	181.46	47.00
21-5	120-122	182.76	45.00
21-6	54-56	183.45	54.00
22-2	71-73	188.34	50.00
22-5	87-89	192.99	16.00
22-7	100-102	195.16	37.00
23-1	123-125	196.92	39.00
23-2	108-110	197.99	32.00
23-3	56-58	198.78	41.00
23-4	126-128	200.56	38.00
23-5	35-37	201.14	34.00
23-6	64-66	202.49	28.00
23-7	34-36	203.46	42.00
23-9	76-78	205.37	33.00
24-1	14-16	205.52	33.00
24-2	130-132	207.89	22.00
24-3	76-78	208.74	38.00
24-4	113-115	210.40	29.00
24-5	58-60	211.34	8.00
24-6	100-102	212.96	55.00
24-7	46-48	213.81	33.00
24-8	17-19	214.88	40.00
24-9	8-10	215.97	31.00
25-1	126-128	216.03	7.00
25-2	120-122	217.50	28.00
25-3	69-71	218.45	34.00
25-4	49-51	219.56	45.00
25-5	65-67	221.59	29.00
25-6	41-43	222.73	5.00
25-7	34-36	223.88	45.00
26-1	21-23	226.04	56.00
26-5	5-7	229.06	41.00
26-7	30-32	231.57	54.00
26-8	30-32	233.06	52.00
27-1	68-70	234.57	32.00
27-2	114-116	236.49	66.00
27-5	120-122	240.96	55.00
27-6	68-70	241.92	60.00
28-1	120-122	244.52	15.00
28-2	120-122	245.92	29.00
28-3	115-117	247.27	26.00
28-4	120-122	248.72	54.00
28-5	118-120	250.11	91.00
28-6	92-94	251.52	50.00
28-7	30-32	252.08	39.50
29-2	124-126	255.47	57.00
29-3	106-108	256.71	54.00
29-4	120-122	258.07	57.00
29-5	56-58	258.92	68.00
29-6	56-58	260.46	41.00
29-7	84-86	261.71	58.00
30-1	50-52	262.90	83.00
30-3	54-56	265.94	59.00
30-4	49-51	267.39	39.50
30-5	119-121	269.59	37.00
31-1	119-121	273.10	31.00
31-2	121-123	274.61	42.00
31-3	54-56	275.44	100.00
32-1	80-82	281.40	60.00
33-1	120-122	292.10	90.00
33-2	109-111	293.48	95.00
33-3	79-81	294.67	96.00
33-4	50-52	295.90	58.00

Table 10. Vane-shear-strength data for Hole 658B.

Section	Interval (cm)	Depth (m)	Vane shear strength (kPa)
1-1	120-122	1.21	3.20
2-1	120-122	3.48	3.60
2-2	120-122	4.95	2.40
2-3	120-122	6.42	4.60
2-4	120-122	7.89	10.10
2-5	81-83	9.36	7.80
2-6	120-122	10.83	6.20
2-7	50-52	11.60	14.20
3-1	120-122	12.96	12.40
3-2	120-122	14.07	5.40
3-3	120-122	15.42	12.60
3-4	120-122	16.72	13.60
3-5	67-69	17.44	19.60
3-6	120-122	19.15	11.00
4-1	120-122	22.51	8.00
4-2	120-122	24.01	16.60
4-3	120-122	25.51	10.60
4-4	120-122	27.01	18.00
4-5	120-122	28.51	17.50
4-6	120-122	30.01	19.20
5-1	120-122	31.24	12.20
5-2	120-122	32.64	16.80
5-3	120-122	33.99	7.20
5-4	120-122	35.29	14.60
5-5	120-122	36.54	18.20
5-6	80-82	37.34	16.60
5-7	46-48	38.49	12.00
6-1	120-122	41.41	34.00
6-2	120-122	42.71	37.50
6-3	120-122	43.91	29.50
6-4	120-122	45.01	33.00
6-5	120-122	46.01	36.00
6-6	120-122	46.91	34.00
7-1	120-122	50.92	24.50
7-2	120-122	52.25	30.00
7-3	120-122	53.49	28.00
7-4	120-122	54.65	28.00
7-5	120-122	55.72	30.00
7-6	120-122	56.71	42.00
8-1	84-86	60.45	35.50
8-2	84-86	61.54	49.50
8-3	84-86	62.85	47.00
8-4	120-122	64.10	34.00
8-5	34-36	65.29	40.50
8-6	120-122	66.41	34.00
9-2	120-122	71.21	31.00
9-3	120-122	72.41	40.00
9-4	120-122	73.51	35.00
9-5	120-122	74.51	35.50
9-6	120-122	75.41	39.50
9-7	120-122	76.21	40.50
10-1	34-36	79.40	40.00
10-2	34-36	79.77	40.50
10-3	84-86	81.23	35.00
10-4	120-122	82.74	34.00
10-5	34-36	83.29	34.00
10-6	120-122	85.45	12.50
10-7	120-122	86.71	41.00
11-2	120-122	89.33	31.00
11-3	34-36	89.73	35.50
11-4	120-122	91.85	38.50
11-6	34-36	92.88	45.00
11-8	120-122	95.44	29.00
12-1	34-36	97.65	52.00
12-2	34-36	99.05	30.00
12-3	84-86	100.45	51.00
12-4	120-122	101.85	53.50
12-5	120-122	103.13	64.50
12-6	84-86	104.08	34.00
12-7	120-122	105.65	15.00
13-1	28-30	107.02	51.00
13-2	120-122	108.05	84.00
13-3	120-122	109.54	51.00
13-4	95-97	110.79	60.00
13-5	48-50	111.77	51.00
13-6	120-122	113.98	61.00
14-1	88-90	115.14	51.00
14-2	88-90	117.48	52.00
14-4	12-14	119.62	51.00
14-5	48-50	121.32	85.00
14-7	18-20	123.49	55.00
15-3	120-122	128.69	98.00
15-4	110-112	129.80	78.00
15-5	120-122	129.85	99.00
15-6	48-50	130.34	45.00
15-7	48-50	131.77	71.00
15-8	48-50	133.27	66.00
16-1	120-122	136.51	79.00
16-2	120-122	138.01	86.00
16-3	120-122	139.51	82.00
16-4	120-122	141.01	92.00
16-6	50-52	142.35	73.00
17-2	120-122	146.45	37.00

Table 11. Compressional-wave velocity data for Site 658.

Section	Depth (m)	P-wave velocity (km/s)
Hole 658A		
1-1	1.21	1.61
1-2	2.71	1.56
1-3	4.21	1.57
1-4	4.82	1.57
3-1	16.41	1.54
3-2	17.91	1.53
3-3	19.41	1.51
3-4	20.91	1.56
3-5	22.40	1.57
3-6	23.04	1.55
Hole 658B		
1-1	1.21	1.55
1-2	1.66	1.60
2-1	3.48	1.56
2-2	4.95	1.64
2-3	6.42	1.57
2-4	7.89	1.60
2-5	9.36	1.57
2-6	10.83	1.55
2-7	11.60	1.57
3-1	12.96	1.54
3-2	14.07	1.63
3-3	15.42	1.62
3-4	16.72	1.62
3-5	17.44	1.54
3-6	19.15	1.49
4-1	22.15	1.59
4-2	24.01	1.50
4-3	25.51	1.49
4-4	27.01	1.54
4-5	28.51	1.55
4-6	30.01	1.55
5-1	31.24	1.50
5-2	32.64	1.52
5-3	33.99	1.55
5-4	35.29	1.50
5-5	36.54	1.48
5-6	37.34	1.52
5-7	38.49	1.10

by the presence of the gas. We were able to perform a first approximation for the actual sound velocities in two independent ways.

First, we were able to draw a chord across the bowl-shaped seismic structure (Fig. 33). This chord connects the base reflectors on either margin of the bowl and parallels *conformable* reflectors near the top of the section. Thus, this chord presents the theoretical depth of the base reflector in case the sediment thicknesses remain constant and the sound velocities do not decrease from the margin to the center of the bowl-shaped seismic section. Thus, the difference in traveltimes between the chord and the base reflector of the bowl-shaped structure corresponds to a mere delay of seismic signals, i.e., it allows us to calculate the actual reduced velocities in gaseous sediments. Based on this reasoning, the ratio of the traveltimes of intervals A-B and A-C at the site profile (1:1.59) is inversely proportional to that of the respective sound velocities, i.e., if we assume for interval A-B a theoretical velocity of 1500 m/s, which is characteristic of water, we obtain a probable velocity of about 950 m/s for interval A-C.

Our second approach to the problem with sound velocity was based on values of sediment depth for seismic units 1 and 2, as

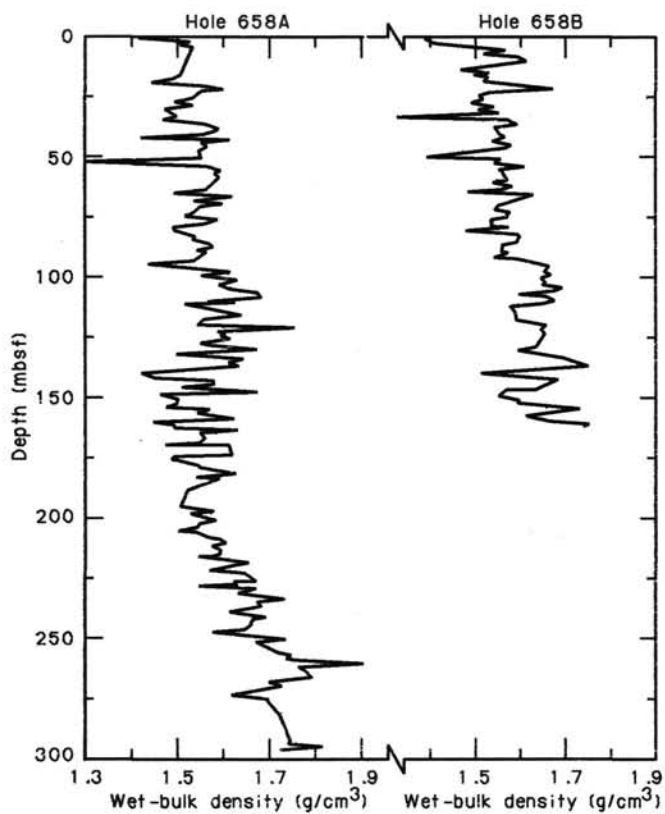


Figure 25. Wet-bulk-density profiles.

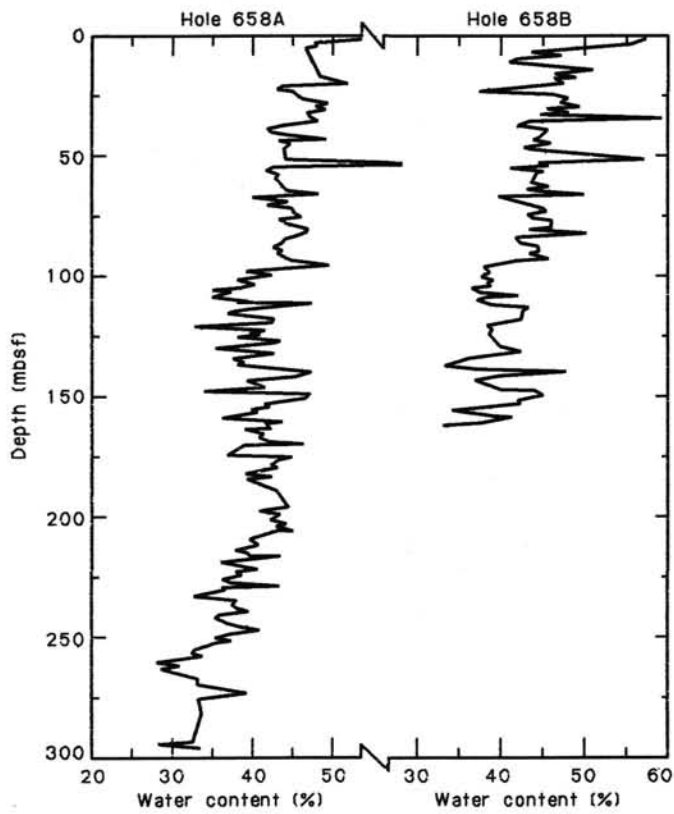


Figure 27. Water-content profiles.

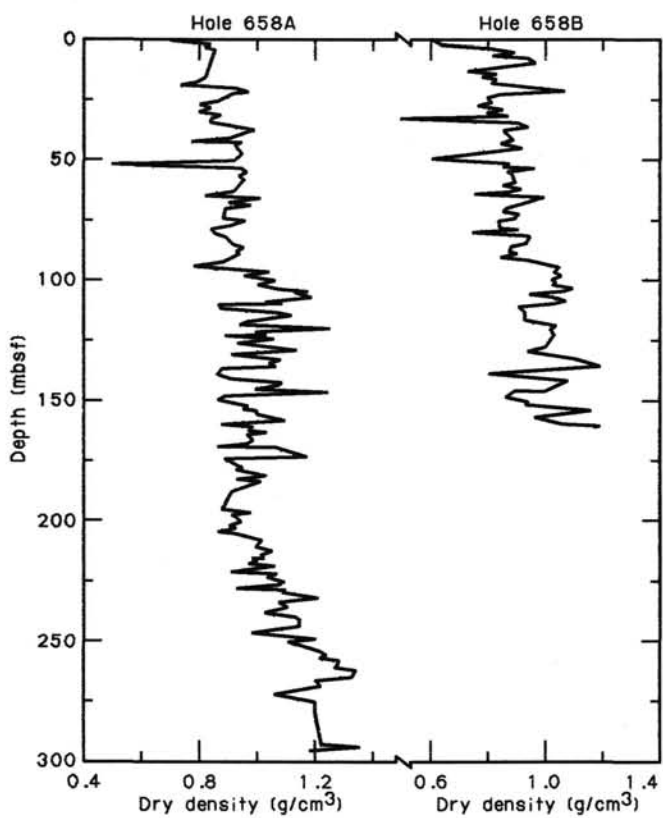


Figure 26. Dry-bulk-density profiles.

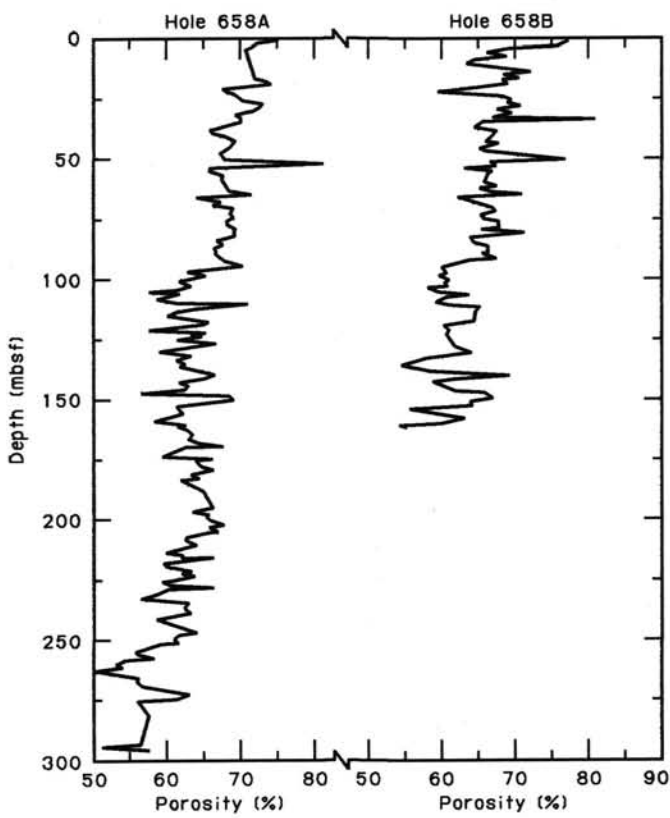


Figure 28. Porosity profiles.

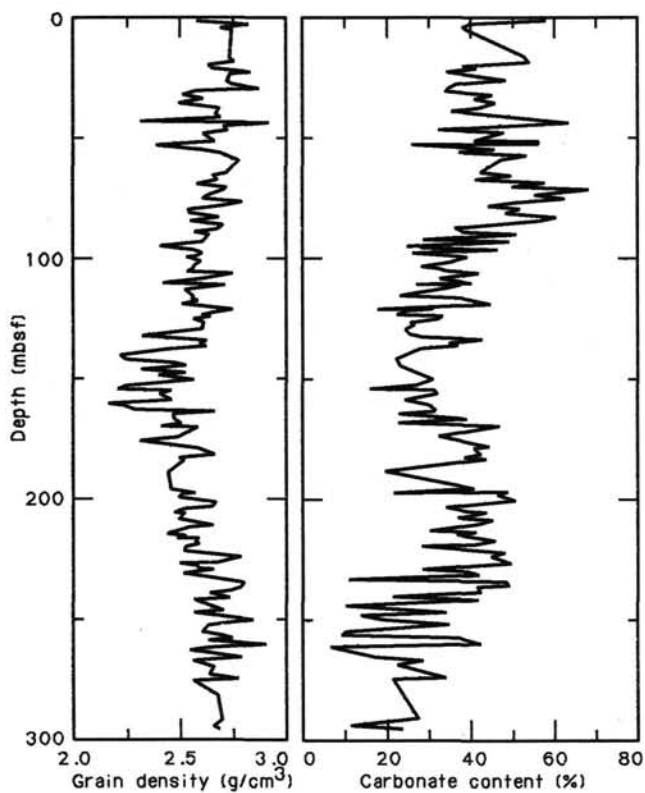


Figure 29. Grain-density and carbonate-content profiles for Hole 658A.

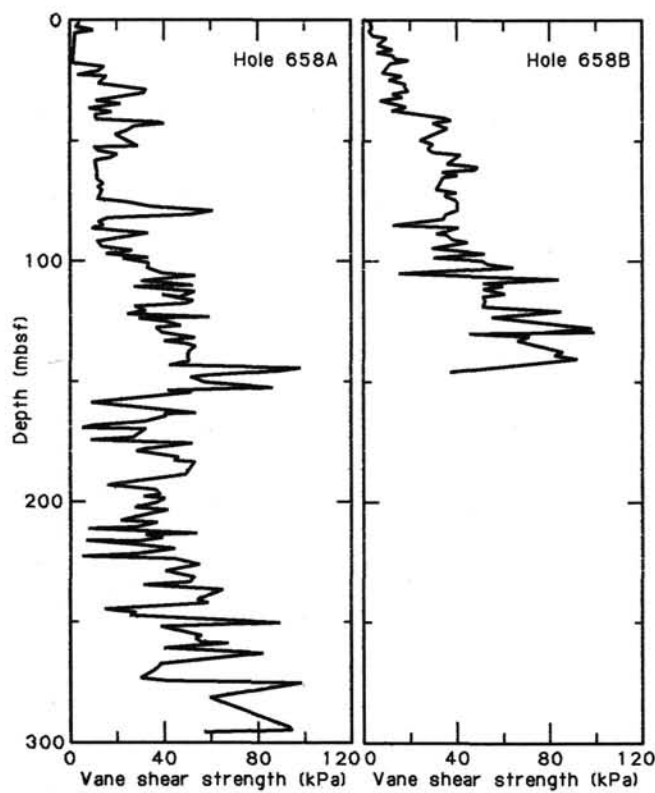


Figure 30. Vane-shear-strength profiles.

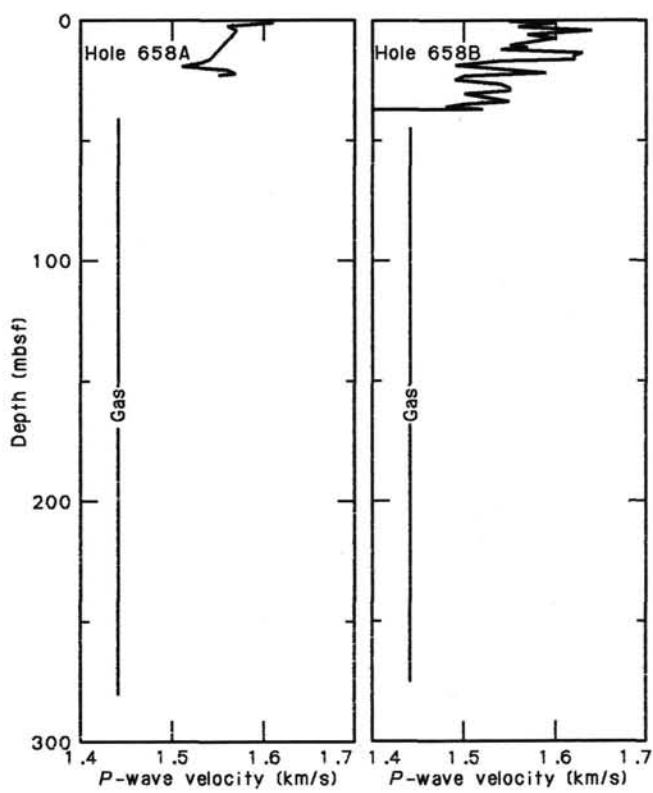


Figure 31. P-wave-velocity profiles.

revealed from the sediment record at Site 658. Here, the 31- to 34-m-thick lithostratigraphic Subunit IA with measured sound velocities of 1540–1500 m/s may correspond to seismic unit 1. The bottom of lithostratigraphic Subunit IB is a major hiatus near 100 mbsf (see “Lithostratigraphy and Sedimentology” and “Biostratigraphy” sections, this chapter), which probably correlates with the first distinct seismic unconformity at level A in Figure 33. Accordingly, the 70 m of lithologic Subunit IB would correspond to 0.16-s two-way traveltimes of seismic unit 2 and, thus, to a sound velocity of almost 900 m/s, a value slightly lower than the first raw estimate of the velocity between levels A and C.

We may try to interpret the middle part of the seismic section by extrapolating downcore the velocity estimate of 900 m/s. In this case, seismic unit 3 would be equal to a 30-m thickness and seismic unit 4 to a 95-m thickness. Both units combined would correspond to the thickness of lithostratigraphic Unit II. Lithostratigraphic Unit III would lie below level C, corresponding to the upper part of seismic unit 5, and would reach down to level D, assuming a somewhat higher sound velocity of 1050 m/s.

This attempted interpretation agrees with the gross seismic character of the profile. The bowl-shaped seismic unit 4 is increasingly transparent downward and may reflect the exceedingly high carbon and probable gas contents of lithostratigraphic Unit II. The stronger reflectors of seismic unit 5 may result largely from the high content of siliciclastic silt, i.e., the coarser grained zones in lithostratigraphic Unit III. In analogy with the geologically recent slump escarpment west of Site 658, the offlaps in seismic unit 3 are interpreted as another buried slump escarpment, the lost sediments of which may have been partially found in a contemporaneous mudflow unit in the upper sediment section at Site 657 (Site 657 chapter, this volume).

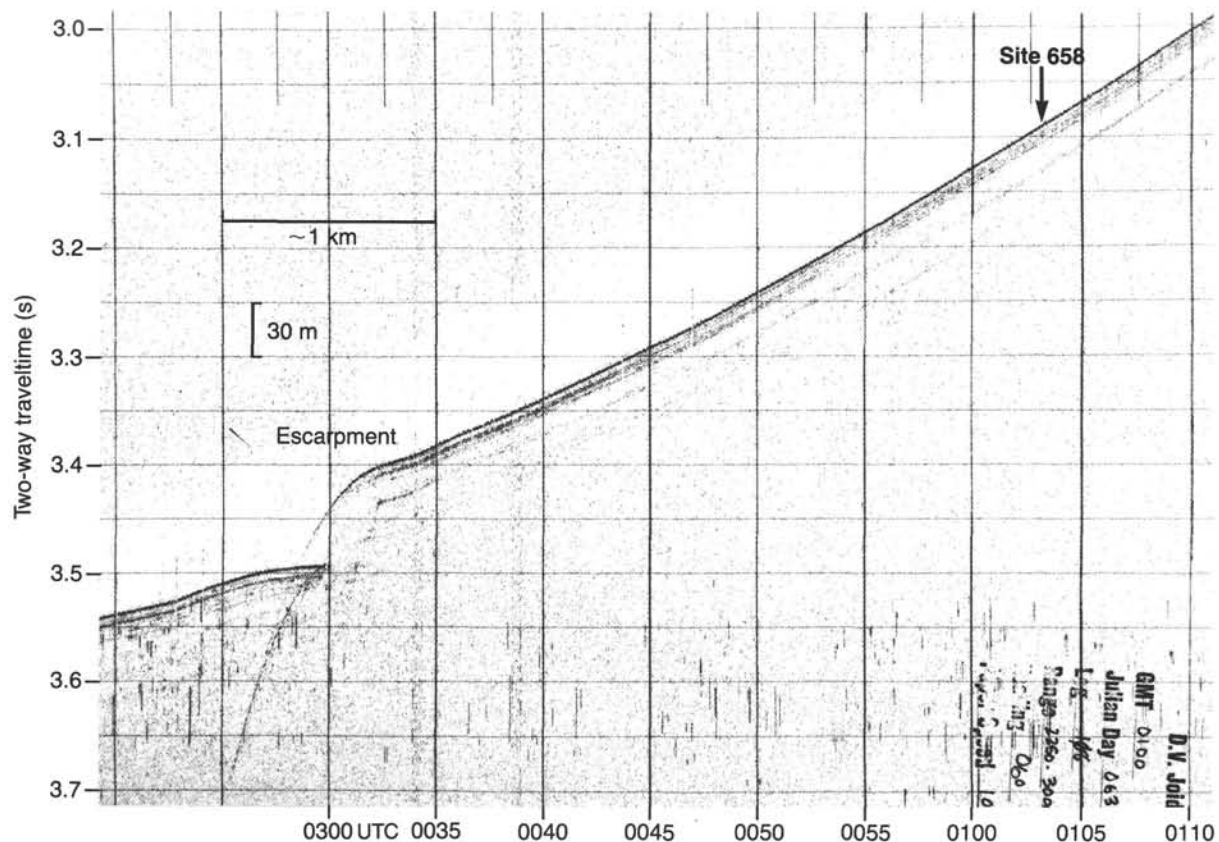
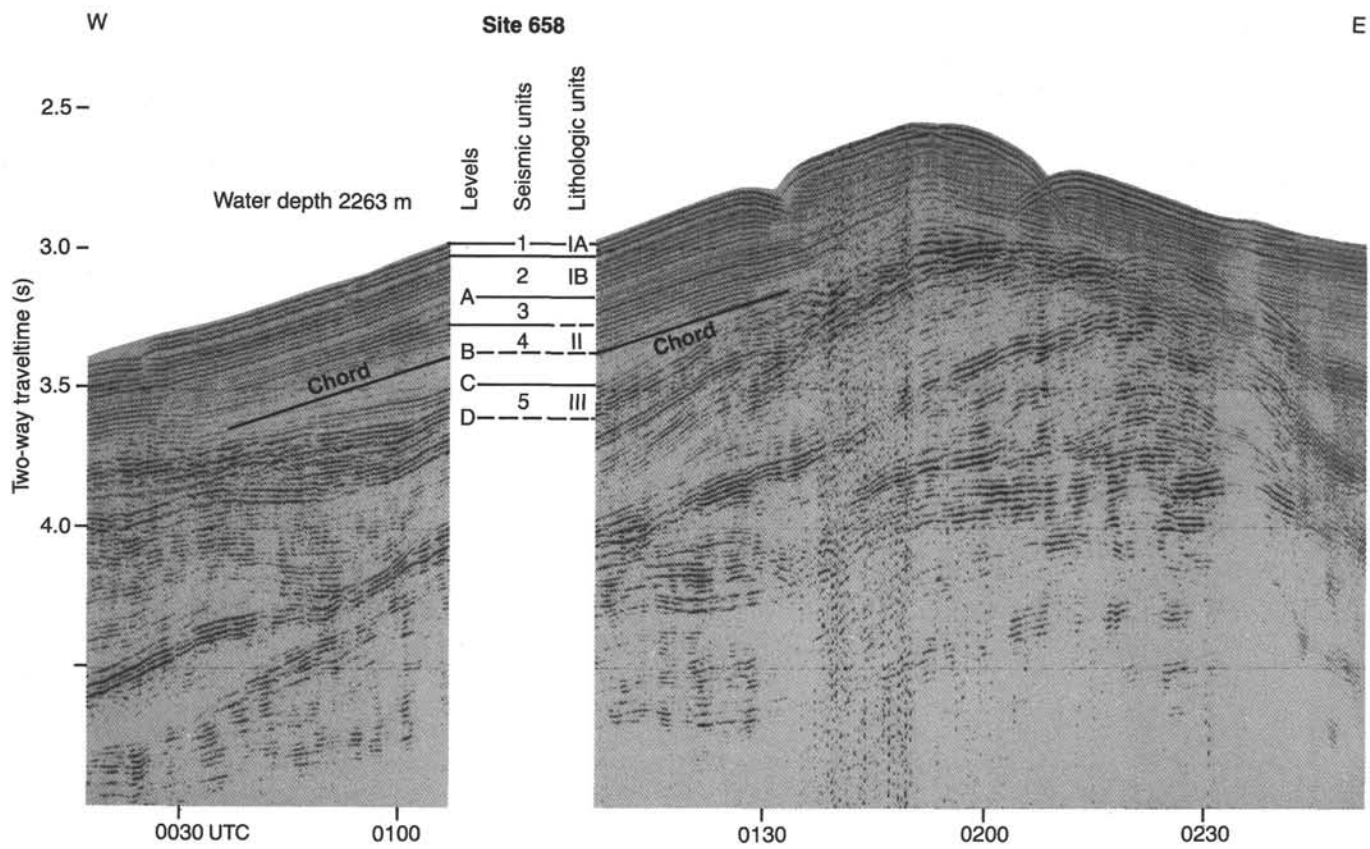
Figure 32. 3.5-kHz echogram of *JOIDES Resolution* over Site 658.

Figure 33. 50- to 500-Hz water-gun reflection profile over Site 658 showing the seismic sequence described in the text; summarized in Table 12.

Table 12. 50- to 500-Hz seismic correlations at Site 658.

Level	Base of seismic unit numbers	Reflector sub-bottom depth (s)	Depth (m) relative to preceding reflector			Cumulative depth (mbsf)	Source	Age (Ma)	Lithologic unit
			1520 m/s	≤ 900 m/s	~ 1050 m/s				
	1	0.04	32			32	Artifact	~ 0.23	—
(A)	2	0.20		70		102	Top of hiatus zone	< 0.7	—
	3	0.265		30		132	Base of hiatus zone	? ~ 2.0	II
(C)	4	0.48		95		227	Increase of siliciclastic silt	3.03	—
(D)	5	0.63			73	300	Total penetration depth		III
								> 3.6	—

COMPOSITE-DEPTH SECTION

At Site 658, two parallel holes were drilled with staggered core depths to obtain a complete hemipelagic sediment record (eight additional cores from Hole 658C were reserved for special organo-chemical studies and were not investigated on board ship). The 18 cores from Hole 658B overlap with those from Hole 658A down to about 164 mbsf. The recovered lithologic intervals are essentially identical in both holes (see "Lithostratigraphy and Sedimentology" section, this chapter); however, the high gas pressure at this site below about 35 mbsf caused numerous voids and, in part, strong disturbance of the core recovery, which markedly aggravated or prevented any correlation between Holes 658A and 658B. Nevertheless, we succeeded in correlating the uppermost 10 cores through to about 85 mbsf (approximately 0.6 Ma) in great detail by comparing continuous magnetic-susceptibility curves, which show marked short-term fluctuations (see "Paleomagnetism" section, this chapter, Fig. 18). No reliable markers were available for a between-hole correlation farther down.

The nominal sub-bottom depth (based on the drilling record) of the susceptibility-curve features is displaced by up to 2 m between Holes 658A and 658B. The direction of the offset changes somewhat downhole (Fig. 34). Because most gains and losses in core length are tied to breaks between succeeding cores or to the voids within, we regard them as artifacts related to the coring process, to contortions by release of gas pressure, or to ODP conventions of recording depths (see "Operations" section, this chapter).

Table 13 presents a correlation of core depths between both holes. The following criteria and rationales were applied to reach a complete and largely uncontorted composite-depth section:

1. The uppermost Cores 108-658A-1H and -658B-1H contain an equally well-preserved record of the uppermost sediment portion. We chose Hole 658A as the major reference unit for assembling a composite-depth section at this site because it posed fewer problems with the definition of nominal penetration depths.

2. Points in the undisturbed portion of the sediment cores that approximate the upper and lower boundary of those cores were used as switch points to generate a continuous "pathway" of between-hole correlation. However, we were unable systematically to accumulate gains and losses in core length downhole because it was impossible to adjust fully for voids.

3. Our correlations led to a complete overlap of sections of "good core" between both holes down to a composite depth of about 85 mbsf. This composite-depth section will be most valuable once the artificial gaps in the cores are closed "on paper,"

Table 13. Composite-depth levels used to correlate cores in Holes 658A and 658B.

Core/section (cm)	Depth (m)	Hole 658A		Composite depths (mbsf)
		Core/section (cm)	Depth (m)	
1H-1, 20	0.2	1H-1, 10	0.1	0.2
1H-2, 50	2.0	1H-2, 50	2.0	2.0
1H-3, 80	3.8	2H-1, 35	2.65	3.8
1H-4, 70	5.2	2H-1, 150	3.8	5.2
3H-1, 20	15.4	3H-2, 95	14.25	15.45
3H-5, 05	21.25	3H-7, 10	20.9	21.25
3H-6, 25	22.95	4H-1, 80	22.1	22.95
3H-6, 90	23.65	4H-1, 135	22.65	23.65
4H-1, 50	25.2	4H-2, 120	24.0	25.2
4H-5, 10	30.8	4H-6, 50	29.3	30.8
4H-5, 140	32.1	4H-6, 140	30.2	32.1
4H-6, 45	32.65	(?)5H-1, 70	31.5	32.65
5H-1, 60	34.8	5H-2, 120	33.5	34.8
5H-4, 95	39.85	5H-6, 10	38.4	39.85
5H-5, 140	41.6	(?)5H-6, 115	39.45	41.6
5H-6, 50	42.2	6H-1, 65	40.95	42.4
5H-7, 30	43.5	6H-2, 15	41.95	43.5
6H-1, 120	44.9	6H-3, 110	44.4	44.9
6H-4, 135	49.55	6H-6, 125	49.05	49.55
6H-5, 120	50.9	7H-1, 30	50.1	50.9
6H-6, 80	52.0	7H-1, 120	51.0	52.0
7H-1, 50	53.7	7H-2, 100	52.3	53.7
7H-4, 140	59.1	7H-6, 80	58.1	59.1
8H-1, 55	63.25	8H-2, 35	61.15	63.25
8H-1, 140	64.1	8H-2, 130	62.1	64.1
8H-2, 130	65.5	8H-5, 40	65.7	65.5
8H-4, 140	68.6	8H-7, 40	68.7	68.6
8H-5, -6	(?)	9H-1, -2	(?)	(?)
9H-1, 80	73.0	9H-3, 30	72.1	73.0
9H-2, 120	74.9	9H-4, 80	74.1	74.9
9H-4, 50	77.2	(?)9H-6, 80	77.1	77.2
9H-4, 120	77.9	9H-6, 135	77.65	77.9
10H-1, 80	82.5	(?)10H-4, 10	82.9	82.5
10H-2, 50	83.7	(?)10H-4, 140	84.2	83.7
			~ 87.0	

Note: Composite-depth levels equal to depth levels in Hole 658A.

based on detailed data about all voids. In Figure 23 the great number of voids and resulting core expansion (because of high gas content) were managed only by using a very general calculation approach.

Similar to other sites on this leg, the composite-depth section (Table 13, Fig. 34) shows how voids and contorted sections in cores with poor recovery can be bypassed successfully by sampling a companion hole.

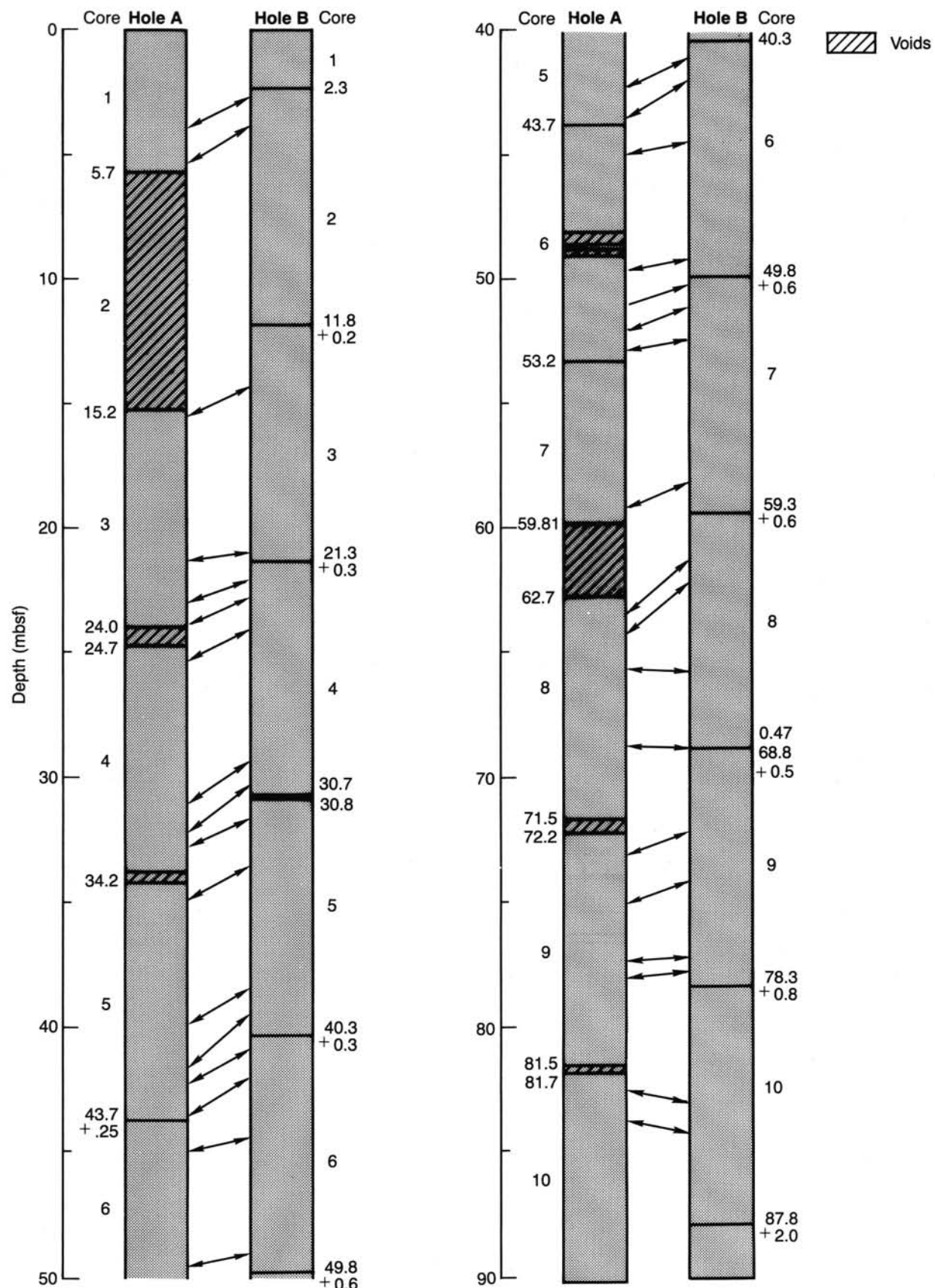
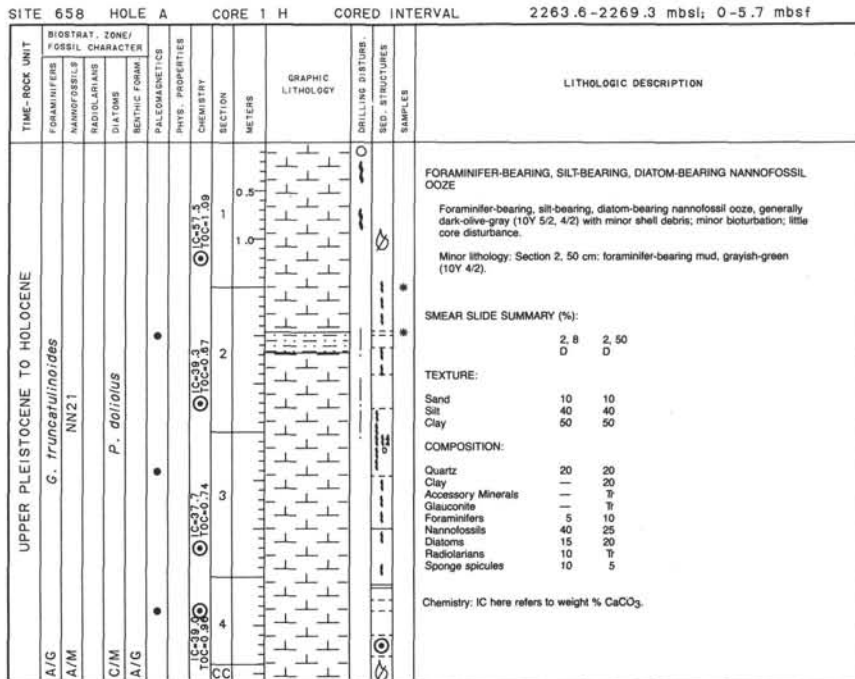


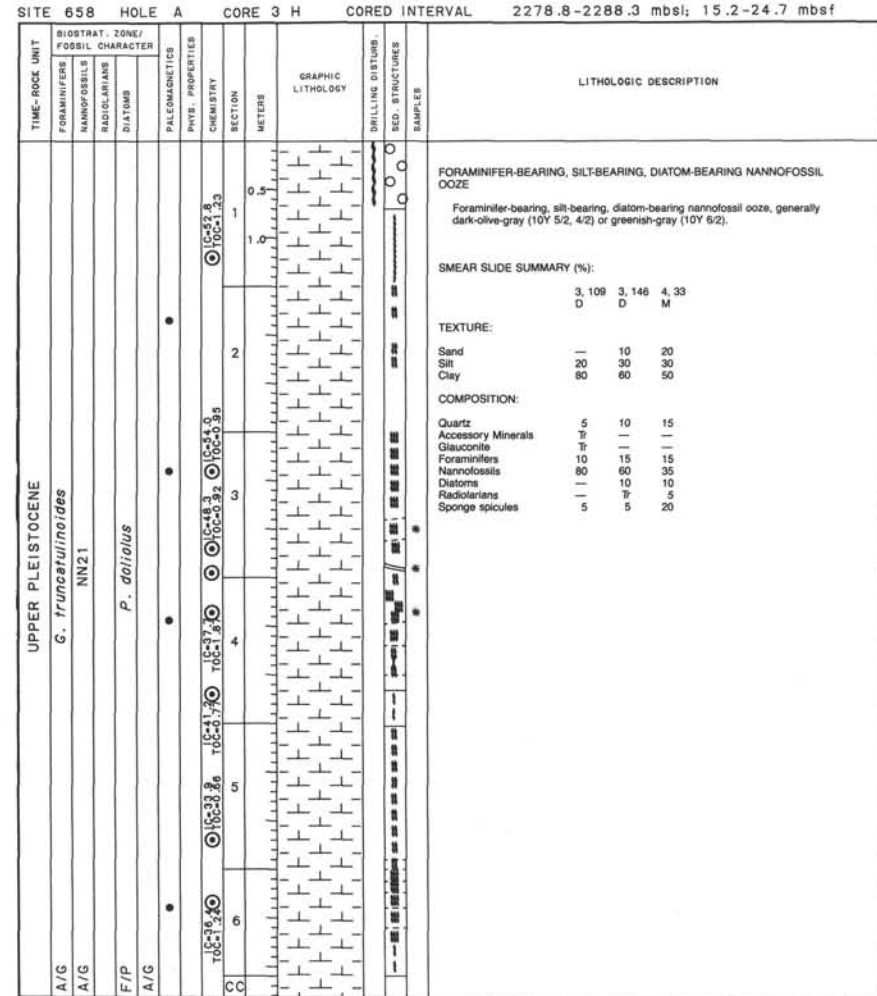
Figure 34. Depth correlation between Holes 658A and 658B through 85 mbsf. Nominal depth below seafloor of penetration and core numbers appear along the graphs of the single holes.

REFERENCES

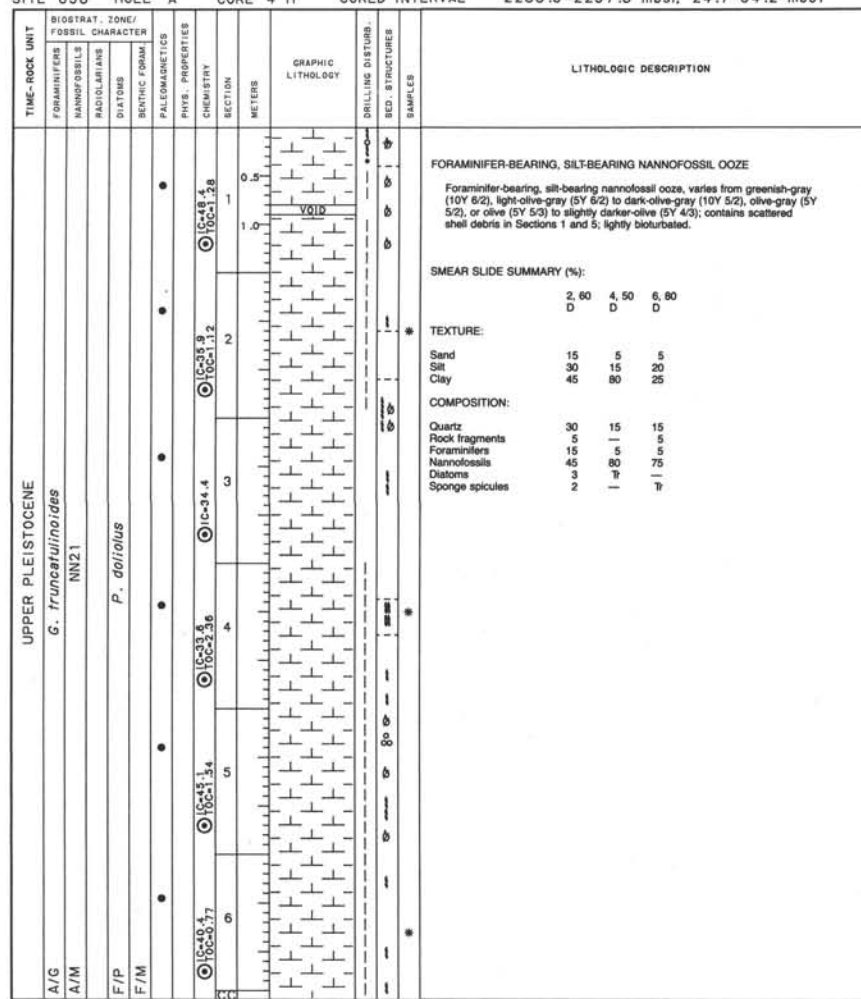
- Baldauf, J. G., 1984. Cenozoic diatom biostratigraphy and paleoceanography of the Rockall Plateau region, North Atlantic, Deep Sea Drilling Project Leg 81. In Roberts, D., Schnitker, D., et al., *Init. Repts. DSDP*, 81: Washington (U.S. Govt. Printing Office), 439-478.
- _____, 1986. Diatom biostratigraphic and paleoceanographic interpretations for the middle- to high-latitude North Atlantic Ocean. In Summerhayes, C. P., and Shackleton, N. J. (Eds.), *North Atlantic Paleoceanography*: Geol. Soc. London Spec. Publ., 21:243-252.
- _____, 1987. Diatom biostratigraphy of the middle- and high-latitude North Atlantic Ocean, Deep Sea Drilling Project Leg 94. In Ruddiman, W. F., Kidd, R. B., Thomas, E., et al., *Init. Repts. DSDP*, 94(Pt. 2): Washington (U.S. Govt. Printing Office), 729-762.
- Brassell, S. C., Eglington, G., Marlowe, I. T., Sarnthein, M., and Pflaumann, U., 1986. Molecular stratigraphy—a new tool for climatic assessment. *Nature*, 320:129-133.
- Burckle, L. H., 1972. Late Cenozoic planktonic diatom zones from the eastern equatorial Pacific. *Nova Hedw. Beihft.*, 39:217-250.
- _____, 1977. Pliocene and Pleistocene diatom datum levels from the equatorial Pacific. Republic of Indonesia. *Geol. Res. Devel. Centre. Spec. Publ.*, 1:25-44.
- Bolli, H. M., and Saunders, J. B., 1985. Oligocene to Holocene low latitude planktic foraminifera. In Bolli, H. M., Saunders, J. B., and Perch-Nielsen, K. (Eds.), *Plankton Stratigraphy*: Cambridge (Cambridge Univ. Press), 165-262.
- Cifelli, R., and Stern-Bernier, C., 1977. Planktonic foraminifera from near the west African coast and a consideration of faunal parcelling in the North Atlantic. *J. Foram. Res.*, 6:258-273.
- Codispoti, L. A., and Friederich, G. E., 1978. Local and mesoscale influences on nutrient availability in the northwest African upwelling region near Cabo Corbeiro. *Deep-Sea Res.*, 25:751-770.
- Espitalié, J., Madec, M., and Tissot, B. P., 1977. Source rock characterization method for petroleum exploration. *Proc. 9th Annu. Offshore Technol. Conf.*, Houston, May 2-5: 439-448.
- Raymo, M. E., Ruddiman, W. F., and Clement, B. M., 1987. Pliocene-Pleistocene paleoceanography of the North Atlantic at Deep Sea Drilling Project Site 609. In Ruddiman, W. F., Kidd, R. B., Thomas, E., et al., *Init. Repts. DSDP*, 94(Pt. 2): Washington (U.S. Govt. Printing Office), 895-901.
- Sarnthein, M., Thiede, J., Pflaumann, U., et al., 1982. Atmospheric and oceanic circulation patterns off northwest Africa during the past 25 million years. In von Rad, U., Hinz, K., Sarnthein, M., and Seibold, E. (Eds.) *Geology of the Northwest African Continental Margin*: Berlin-Heidelberg (Springer-Verlag), 545-604.
- Schemainda, R., Nehring, D., and Schulz, S., 1975. Ozeanologische Untersuchungen zum Produktionspotential der nordwestafrikanischen Wasserauftriebsregion 1970-1973. *Geod. Geophys. Veröff.*, 4(16):1-88.
- Schnitker, D., 1979. The deep waters of the Western North Atlantic during the past 24,000 years, and the re-initiation of the Western Boundary Undercurrent. *Mar. Micropaleontol.*, 4:265-280.
- Speth, P., Detlefsen, H., and Sierts, H.-W., 1978. Meteorological influence on upwelling off northwest Africa. *Deut. Hydrogr. Zschr.*, 31: 95-104.
- Stein, R., Rulkötter, J., and Welte, D., 1986. Accumulation of organic-carbon-rich sediments in the Late Jurassic and Cretaceous Atlantic Ocean—a synthesis. *Chem. Geol.*, 56:1-32.
- Thiede, J., 1975. Shell- and skeleton-producing plankton and nekton in the eastern North Atlantic ocean. *'Meteor' Forsch. Erg.*, C20:33-79.
- Thiede, J., Suess, E., and Mueller, P.J., 1982. Late Quaternary fluxes of major sediment components to the sea floor at the northwest African continental slope. In von Rad, U., Hinz, K., Sarnthein, M., and Seibold, E. (Eds.), *Geology of the Northwest African Continental Margin*: Berlin-Heidelberg (Springer-Verlag), 605-631.
- Tissot, B. P., and Welte, D. H., 1984. *Petroleum Formation and Occurrence*: Berlin-Heidelberg (Springer-Verlag).
- Tomczak, M., Jr., and Hughes, P., 1980. Three-dimensional variability of water masses and currents in the Canary Current upwelling region. *'Meteor' Forsch. Erg.*, A21:1-24.
- Weaver, P.P.E., and Clement, B. M., 1986. Synchronicity of Pliocene planktonic foraminiferal datums in the North Atlantic. *Mar. Micropaleontol.*, 10:295-307.



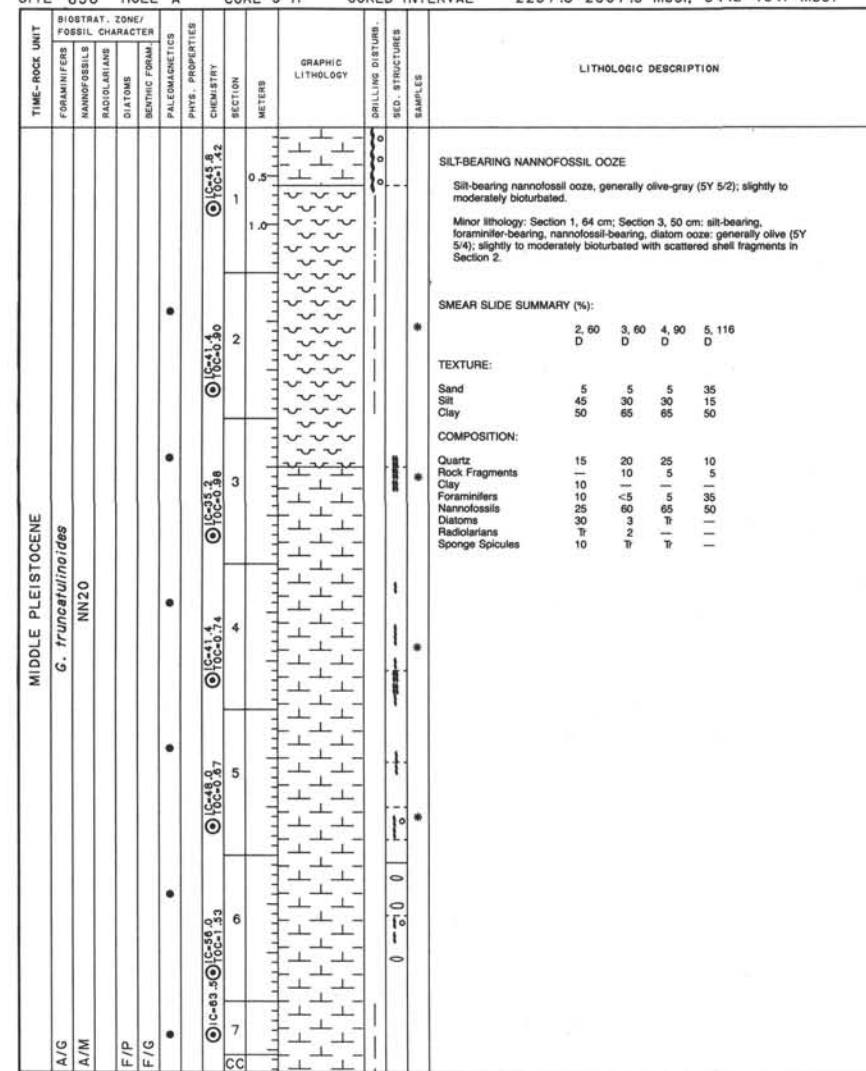
CORE 2H NO RECOVERY

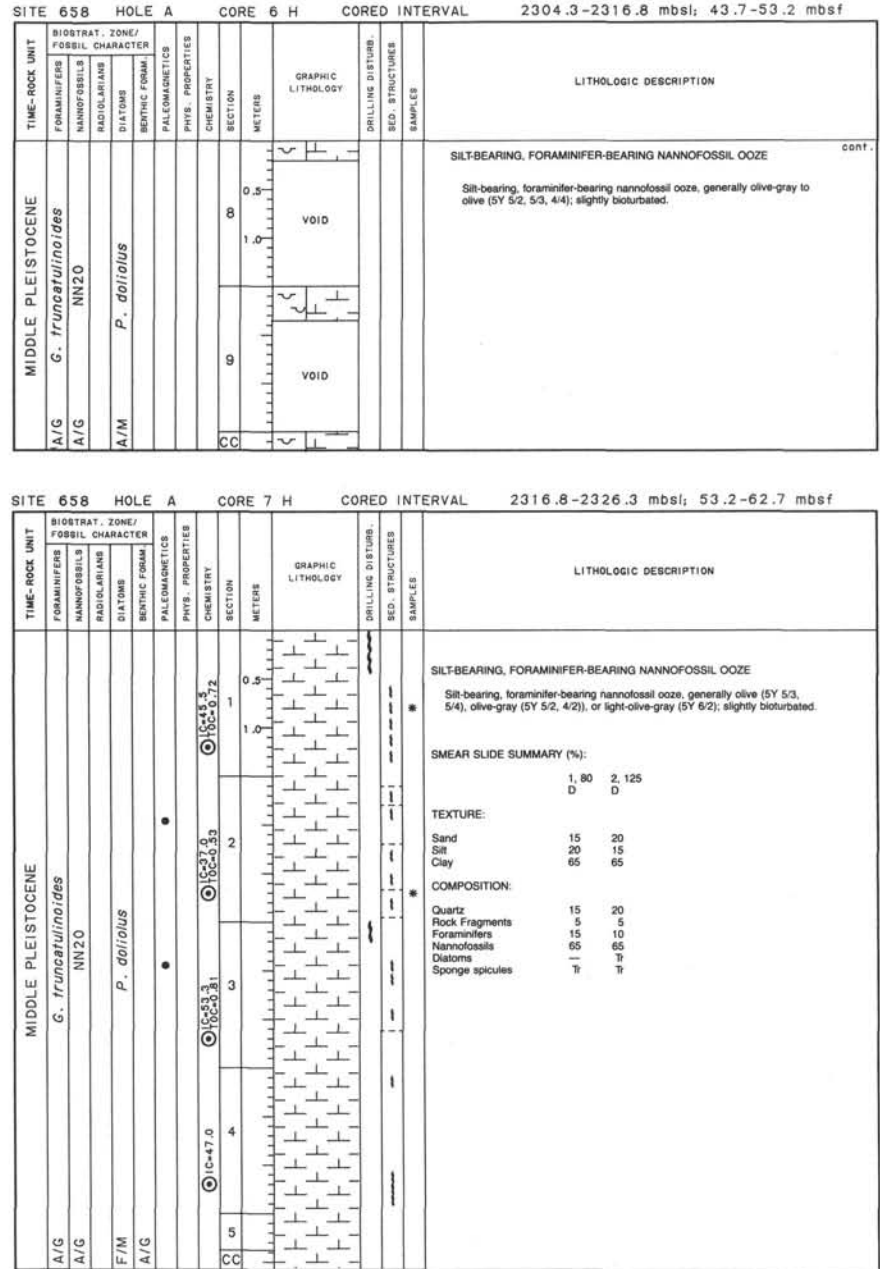
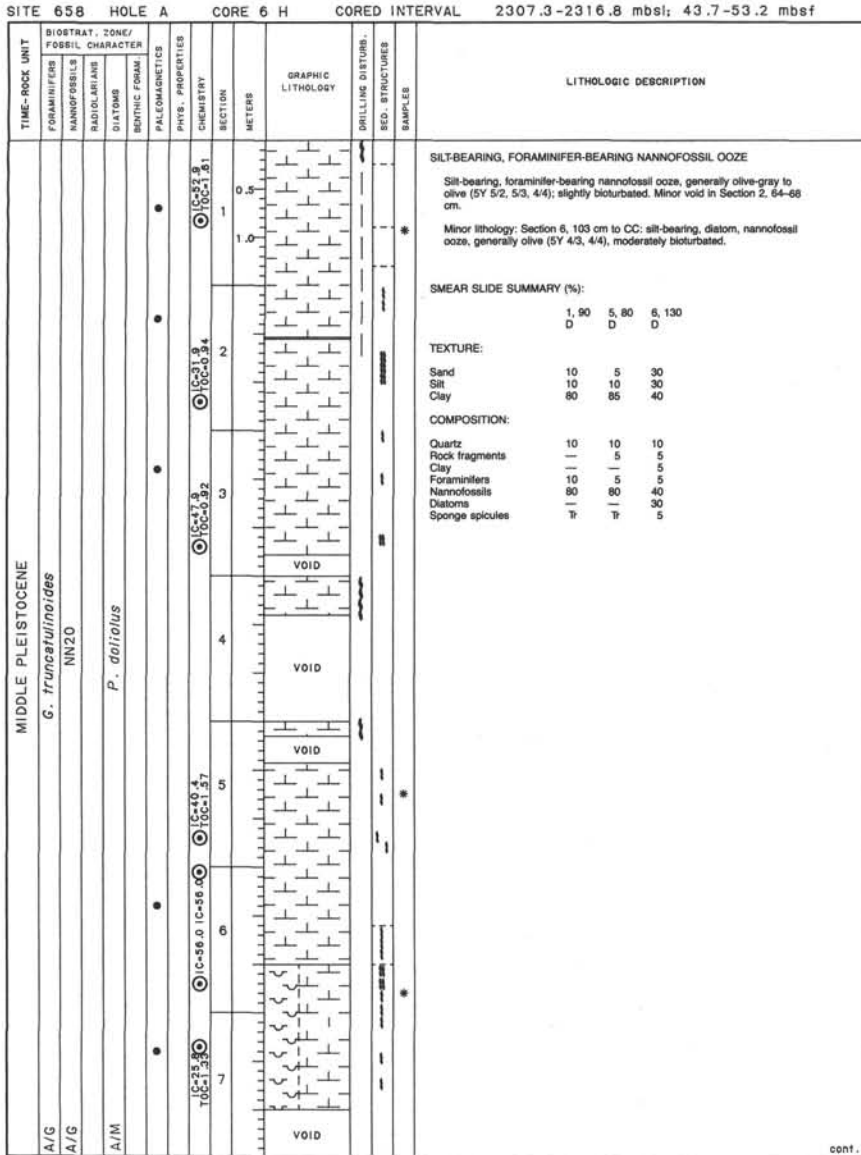


SITE 658 HOLE A CORE 4 H CORED INTERVAL 2288.3-2297.8 mbsl; 24.7-34.2 mbst



SITE 658 HOLE A CORE 5 H CORED INTERVAL 2297.8-2307.3 mbsf; 34.2-43.7 mbsf





SITE 658 HOLE A CORE 8 H CORED INTERVAL 2326.3-2335.8 mbsl; 62.7-72.5 mbst

TIME-ROCK UNIT	BIOSTRAT., ZONE/CHARACTER				LITHOLOGIC DESCRIPTION						
	FORAMINIFERS	NANOPROBOSSES	RADIOLARIANS	DIATOMS	PALaeOMAGNETICS	PHYS. PROPERTIES	GRAPHIC LITHOLOGY	DRILLING DISTANCE,	BED STRUCTURES	SAMPLES	
MIDDLE PLEISTOCENE											
A/G	<i>G. truncatulinoides</i>										
A/G	NN19										
C/M		<i>N. reinhardti</i>									
F/G											
6	●				● TC-68.0	● TC-50.0	● TC-57.6	● TC-50.56	● TC-41.0	● TC-42.47	
5											
4											
3											
2											
1											
CC											

NANNOFOSSIL Ooze
Nanofossil ooze, generally greenish-gray to light-greenish-gray (5GY 5/1, 6/1, 7/1), light-olive-gray (5Y 6/2), olive (5Y 4/3, 5/3), or olive-gray (5Y 5/2), slightly to moderately bioturbated. Minor void in Section 6, 15 cm.
Minor lithology: Section 2, 135-150 cm; Section 3, 0-50 cm: diatom nanofossil ooze, olive (5Y 4/3); moderately bioturbated.

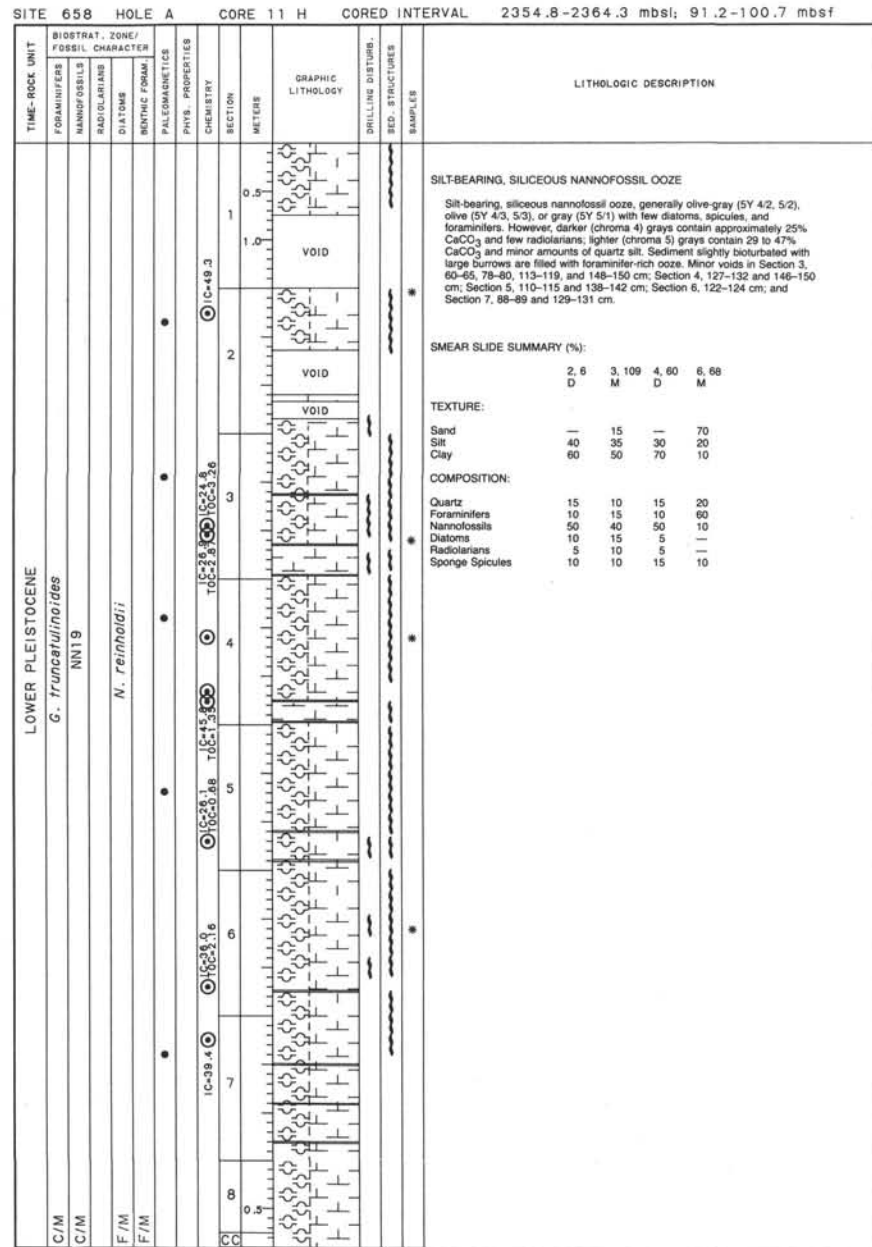
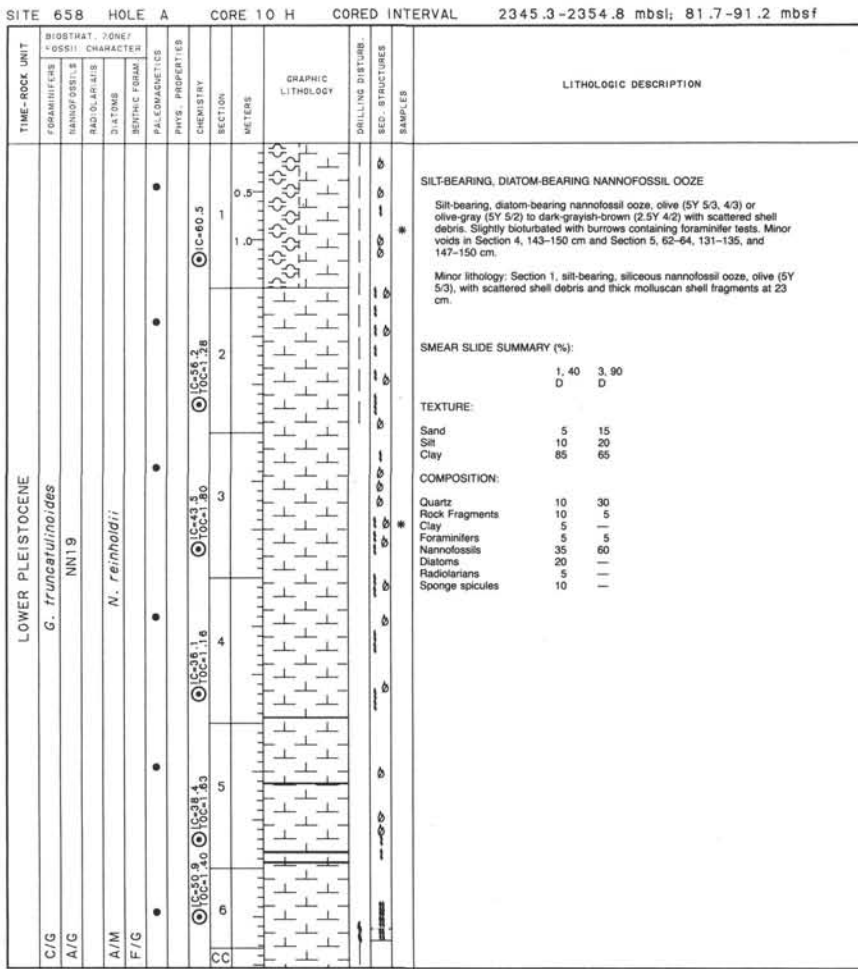
SMEAR SLIDE SUMMARY (%):

	1	90	3	10
D	—	—	D	—
Sand	—	—	—	—
Silt	10	—	10	—
Clay	90	—	90	—

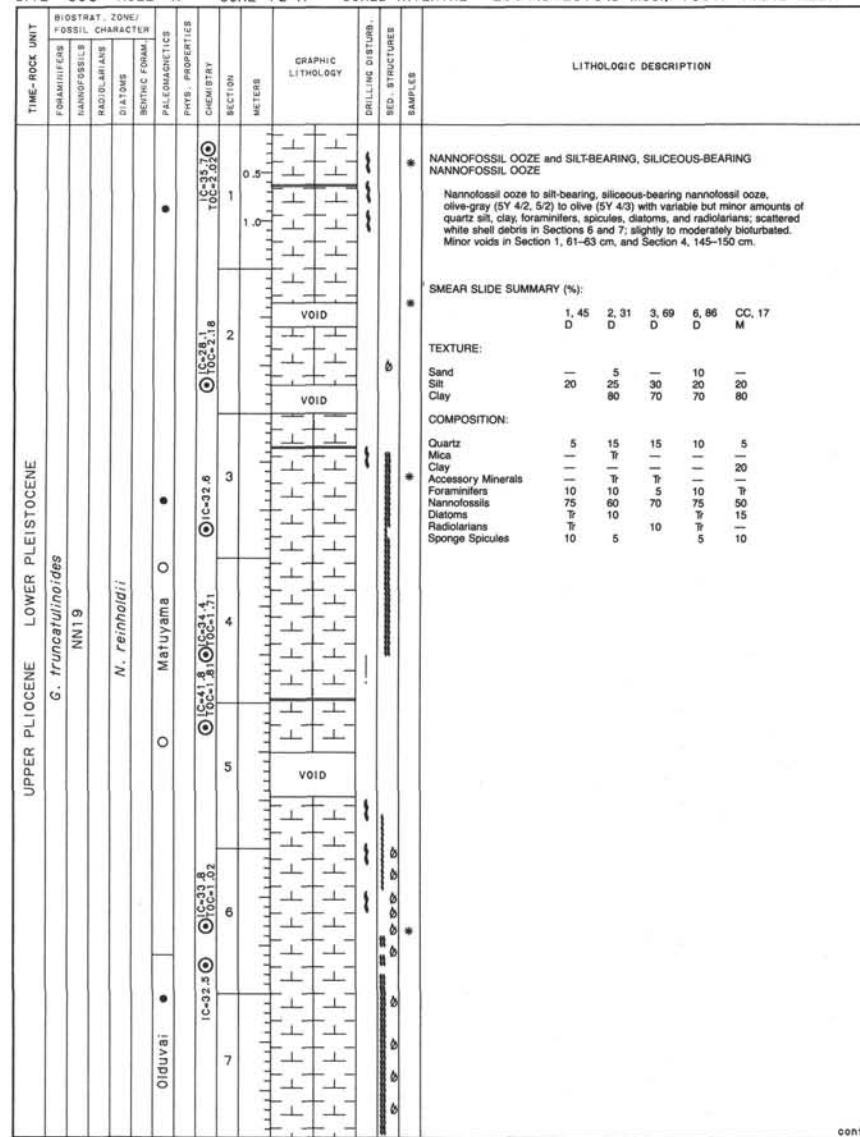
TEXTURE:

Quartz	<10	5
Rock Fragments	<5	—
Glauconite	<5	—
Foraminifers	Tr	Tr
Nanofossils	80	40
Diatoms	—	30
Radiolarians	—	10
Sponge spicules	—	15

COMPOSITION:

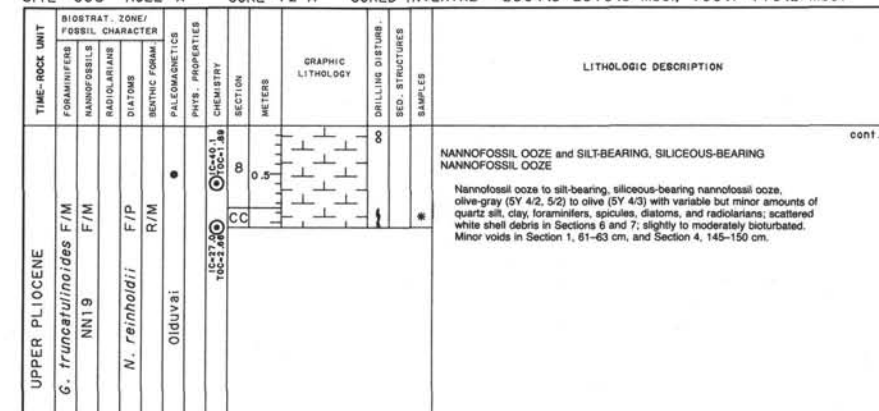


SITE 658 HOLE A CORE 12 H CORED INTERVAL 2364.3-2373.8 mbsl: 100.7-110.2 mbst



cont

SITE 658 HOLE A CORE 12 H CORED INTERVAL 2364.3-2373.8 mbsl; 100.7-110.2 mbst

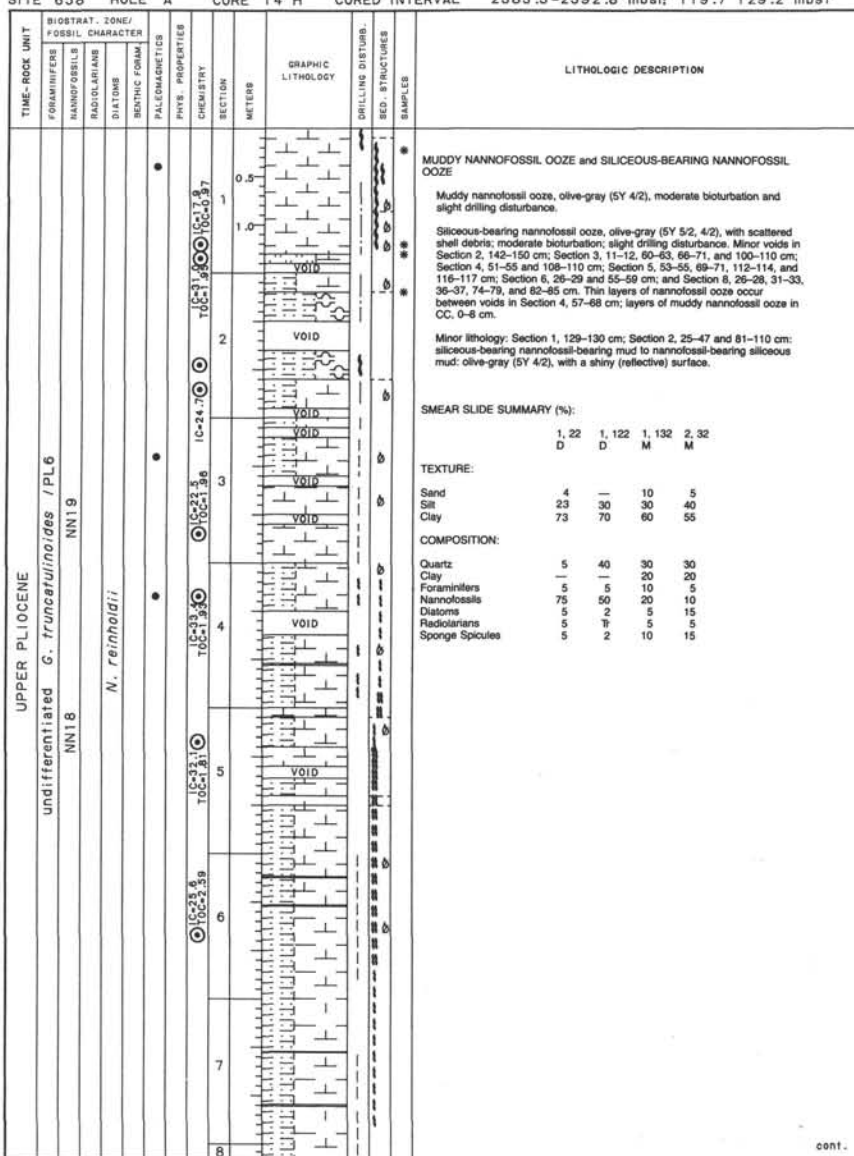


607

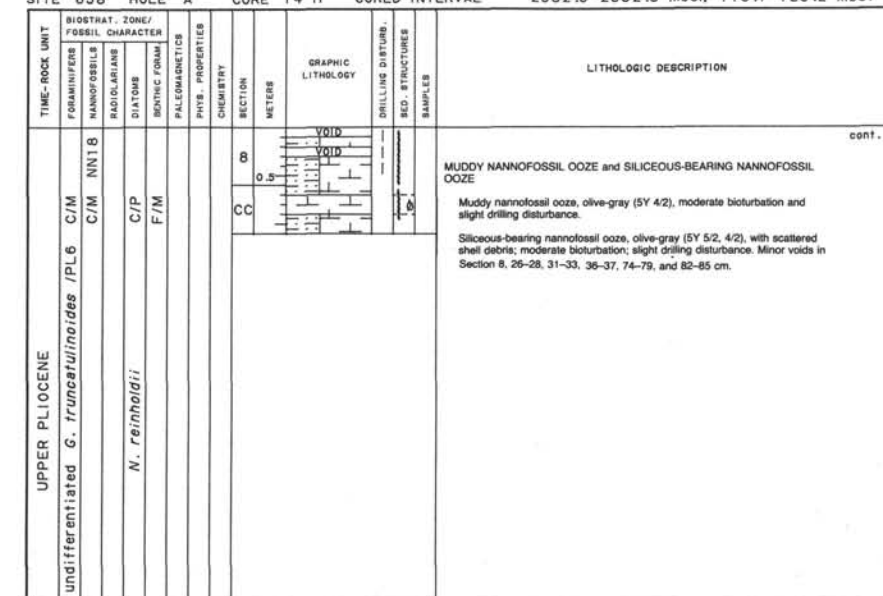
con

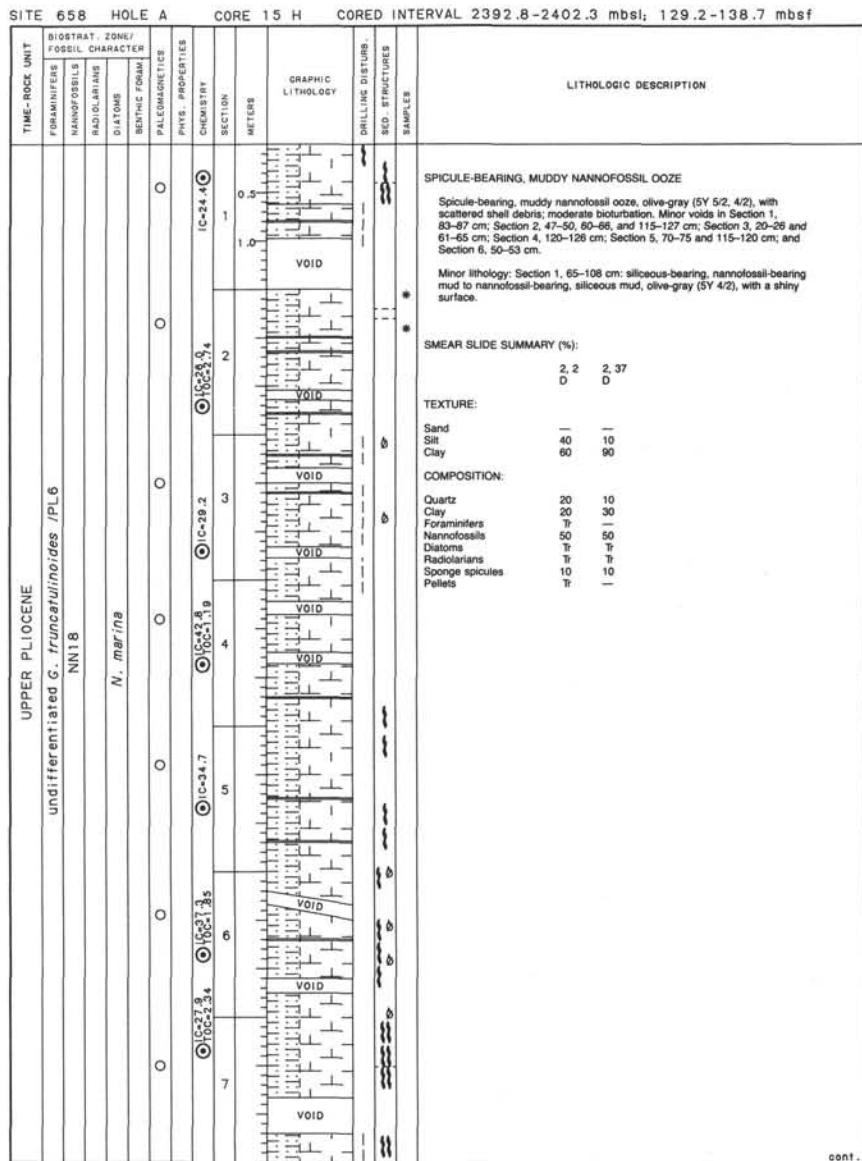
SITE 658

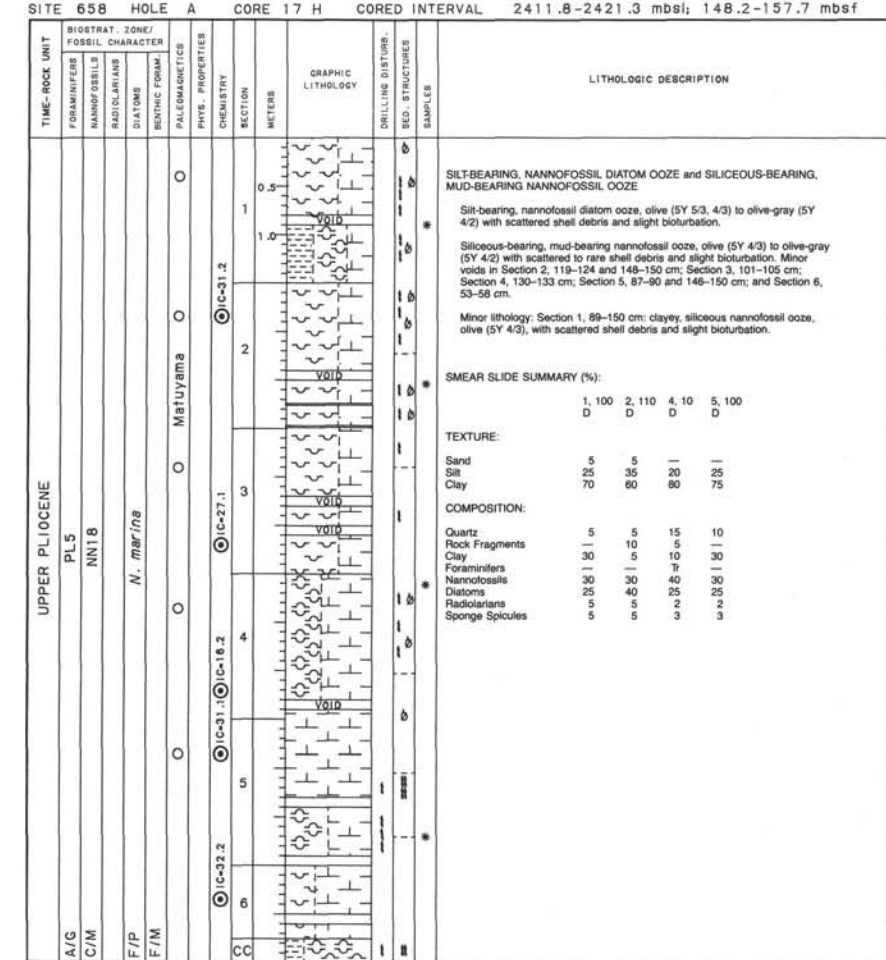
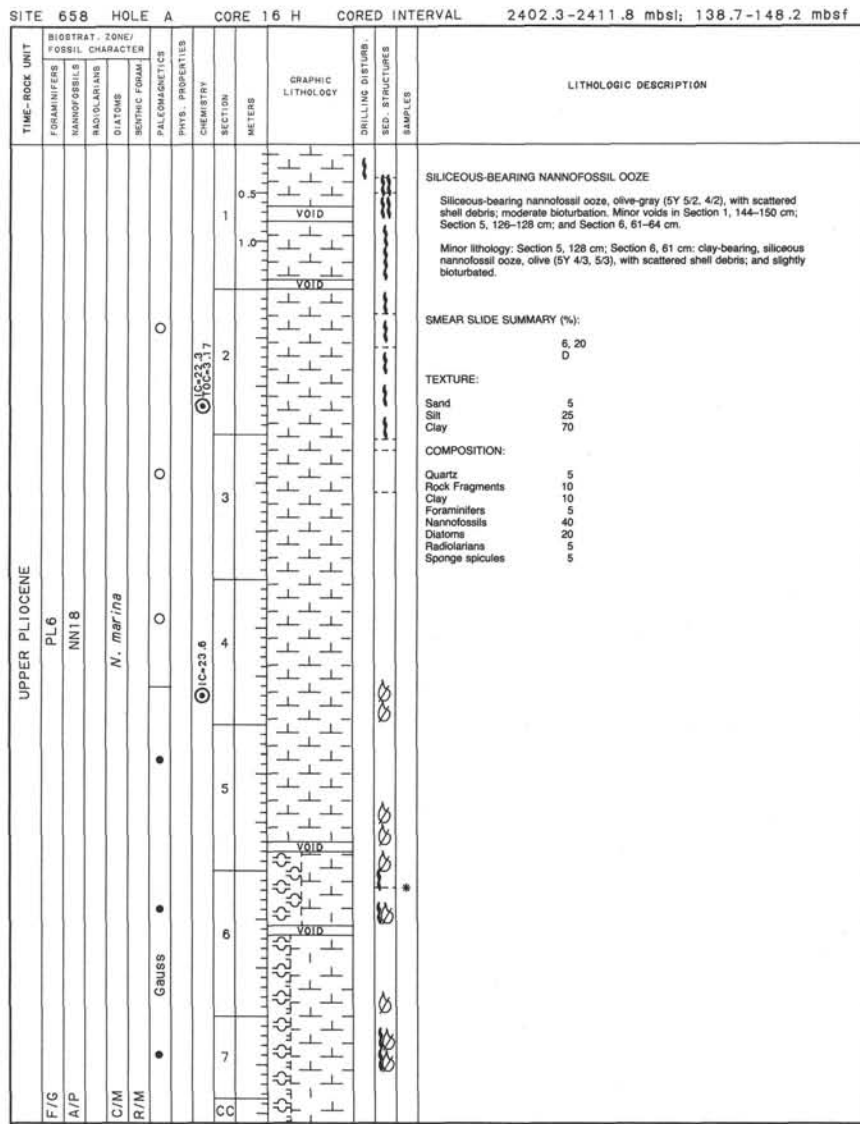
SITE 658 HOLE A CORED INTERVAL 2383.3-2392.8 mbsl; 119.7 129.2 mbst



SITE 658 HOLE A CORED INTERVAL 2382.3-2392.8 mbsl; 119.7-129.2 mbst







TIME-ROCK UNIT		CORE 19 X		CORED INTERVAL		2421.5-2431.0 mbsf; 157.9-167.4 mbsf	
FORMATION	ZONE/FOSSIL CHARACTER	PHYS. PROPERTIES	GRAPHIC LITHOLOGY	LITHOLOGIC DESCRIPTION			
BIOSTRAT.	RADIOLARIANS	PALaeOMAGNETICS	SECTION	METERS	DRILLING DISTURB.	BED. STRUCTURES	SAMPLES
DIA/OMB	BENTHIC FORAM	●	●	0.5			
NNANOFOSSILS		●	●	1			
PL5		●	●	1.0			
NN16		●	●	1.5			
GAUSS		●	●	2			
●		●	●	2.5			
●		●	●	3			
●		●	●	3.5			
●		●	●	4			
●		●	●	4.5			
●		●	●	5			
●		●	●	5.5			
●		●	●	6			
●		●	●	6.5			
●		●	●	7			
UPPER PLIOCENE							
SILICEOUS-BEARING, NANNOFOSSIL-BEARING MUD and SILT-BEARING, SILICEOUS-BEARING NANNOFOSSIL OOZE							
Siliceous-bearing, nannofoossil-bearing mud, generally olive (5Y 5/3, 5/4, 4/4) to olive-gray (5Y 4/2), with scattered shell fragments. Core greatly disturbed by drilling.							
Siliceous, siliceous-bearing nannofoossil ooze to silt-bearing, siliceous nannofoossil ooze, generally olive-gray (5Y 4/2, 5/2), slightly bioturbated with rare shell debris. Minor voids in Section 5, 32-36, 127-137, and 145-150 cm; and Section 7, 18-21 cm. Thin silt layers in Section 2, 115-119 and 141-146 cm.							
Minor lithology: Section 2: 0-97 cm; Section 3: 65-112 cm; hamnotossil-bearing, siliceous mud, olive (5Y 4/3) to olive-gray (5Y 5/2) with scattered shell debris. Core slightly disturbed by drilling. Section 6, 42-61 cm; clayey silty; siliceous nannofoossil ooze, olive-gray (5Y 4/2); slightly bioturbated.							
SMEAR SLIDE SUMMARY (%):							
	1, 70 D	2, 80 D	3, 80 D	7, 100 D			
TEXTURE:							
Sand	2	5	—	—			
Silt	33	35	30	30			
Clay	65	60	70	70			
COMPOSITION:							
Quartz	15	20	10	10			
Feldspar	Tr	Tr	—	—			
Rock Fragments	Tr	—	—	—			
Clay	20	10	20	10			
Accessory Minerals	40	20	25	15			
Foraminifera	Tr	—	—	—			
Nannofossils	15	15	15	35			
Diatoms	5	30	25	25			
Radiolarians	—	Tr	Tr	2			
Sponge Spicules	5	5	5	3			

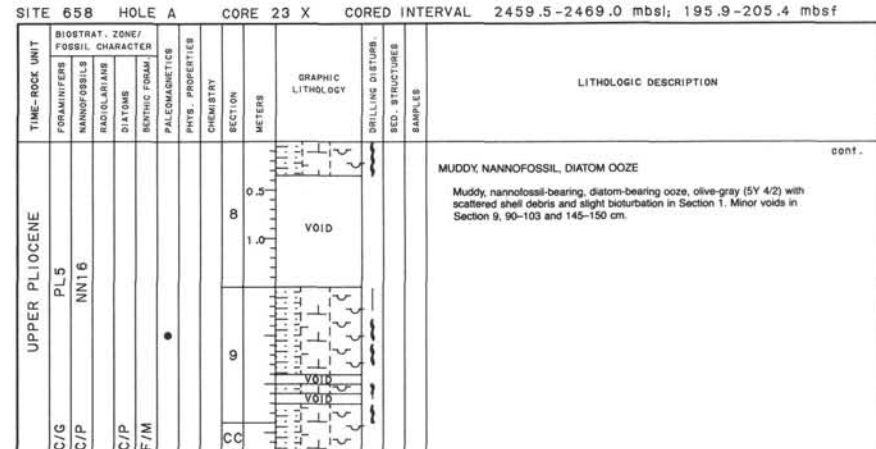
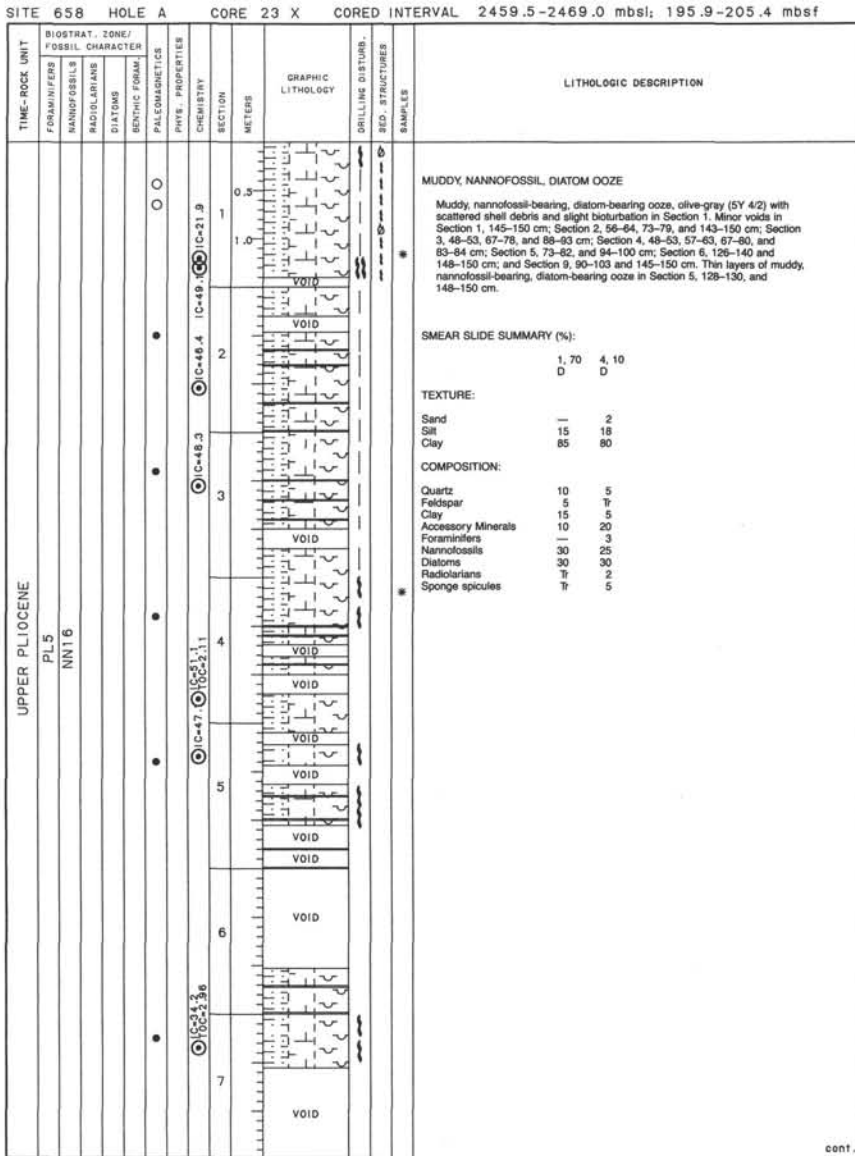
SITE 658 HOLE A CORE 29 X CORED INTERVAL 2431.0-2440.5 mbsf; 167.4-176.9 mbst

SITE 658 HOLE A CORE 20 X CORED INTERVAL 2431.0-2440.5 mbsl; 167.4-176.9 mbst

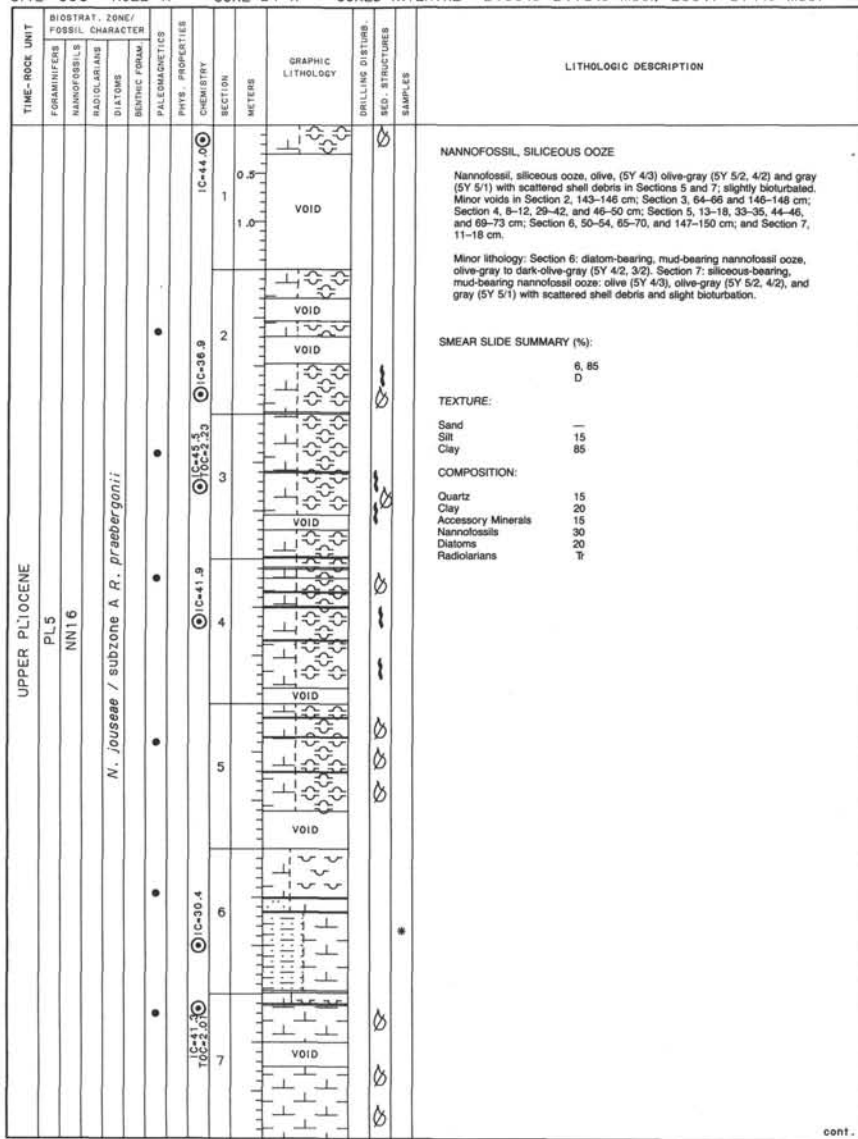
SITE 658 HOLE A		CORE 21 X	CORED INTERVAL	2440.5-2450.0 mbsf; 179.9-186.4 mbsf
TIME-ROCK UNIT				LITHOLOGIC DESCRIPTION
UPPER PLIOCENE				
R/M	PL-5	FORAMINIFERA BIOTRAT. ZONE/ FOSSIL CHARACTER		
C/P	NN16	NANNOFOSSILS		
		RADIOLARIANS		
F/I/P	●	DIATOMS SETHIC FORAM PALEOMAGNETICS		
R/M		PHYS. PROPERTIES CHEMISTRY		
		METERS	SECTION	GRAPHIC LITHOLOGY
		0.5		
		1.0		
	CC			DRAILLING DISTURBS. SED. STRUCTURES SAMPLES

SITE 658 HOLE A CORE 22 X CORED INTERVAL 2450.0-2459.5 mbsi; 186.4-195.8 mbst

TIME-ROCK UNIT	BIOSTRAT., ZONE/		CORED INTERVAL	PHYS. PROPERTIES	CHEMISTRY	SECTION	METERS	GRAPHIC LITHOLOGY	DRILLING DISTURBS.	SED. STRUCTURES	SAMPLES	LITHOLOGIC DESCRIPTION				
	FORAMINIFERS	NANNOFOSILS										BENTHIC FORAM.	PALaeONTOLOGIC			
UPPER PLIOCENE	PL5	NN16														
NANNOFOSSIL-BEARING, MUDDY, SILICEOUS OOZE																
Nannofossil-bearing, muddy, siliceous ooze, generally olive (SY 5-3), olive-gray (SY 5-2, 4/2), gray (SY 5-1), to dark-gray (SY 4-1) with scattered shell debris in Sections 1 and 7; slightly bioturbated. Minor voids in Section 3, 80-86, and 95-100 cm; Section 5, 67-70 cm; Section 6, 103-106 and 124-130 cm; and Section 7, 120-123 cm.																
SMEAR SLIDE SUMMARY (%):																
1, 100 2, 70 5, 80																
D D D																
TEXTURE:																
Sand — 5 —																
Silt 35 30 40																
Clay 65 65 60																
COMPOSITION:																
Quartz 25 20 15																
Clay 10 5 10																
Accessory Minerals 10 20 20																
Foraminifers — 1 5																
Nannofossils 20 25 20																
Diatoms 25 20 25																
Radiolarians 5 5 5																
Sponge spicules 5 5 —																
0.5																
1																
1.0																
1.5																
2																
2.0																
2.5																
3																
3.0																
3.5																
4																
4.0																
4.5																
5																
5.0																
5.5																
6																
6.0																
6.5																
7																
7.0																
CC																

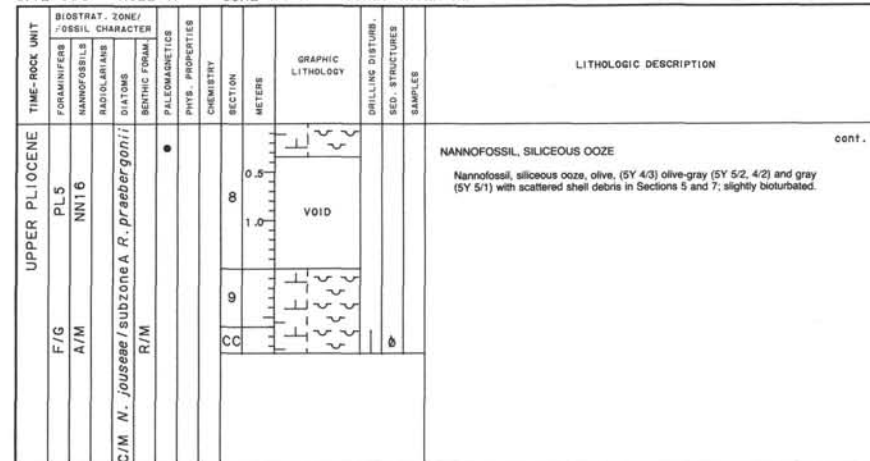


SITE 658 HOLE A CORE 24 X CORED INTERVAL 2469.0-2478.5 mbsl; 205.4-214.9 mbst



cont

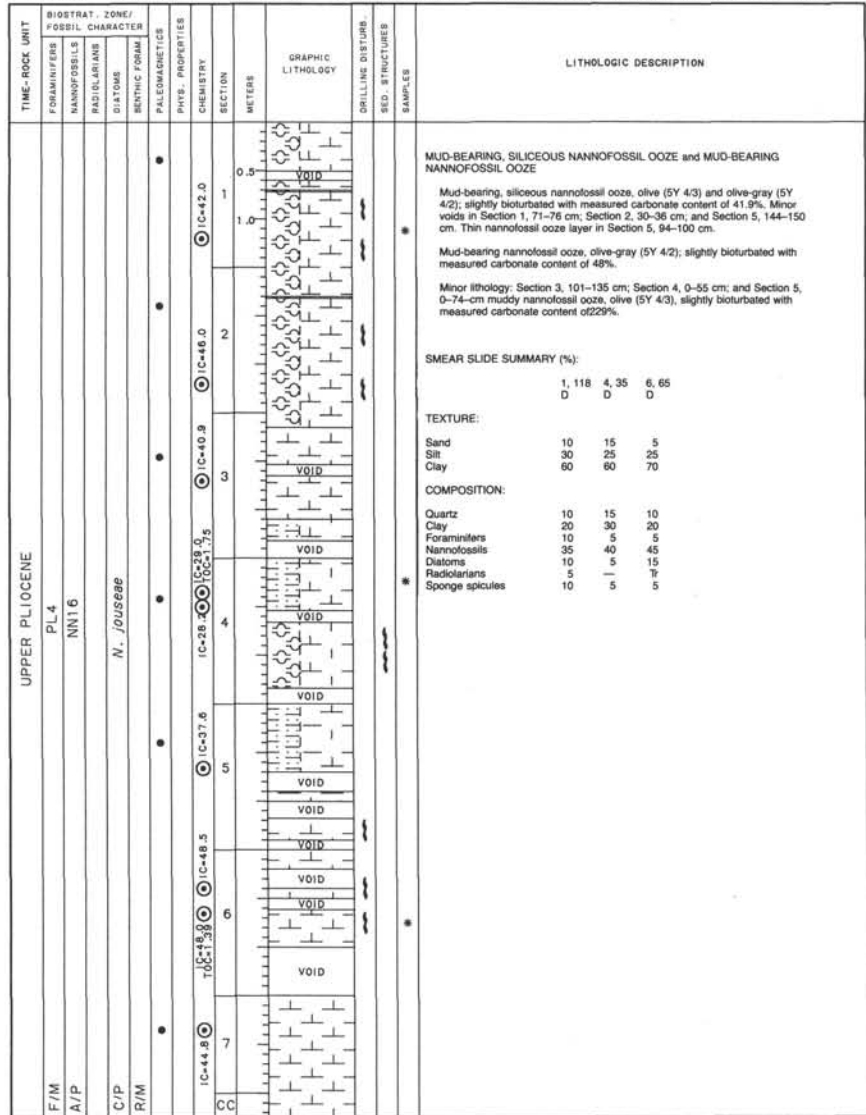
SITE 658 HOLE A CORE 24 X CORED INTERVAL 2469.0-2478.5 mbsl; 205.4-214.9 mbsf

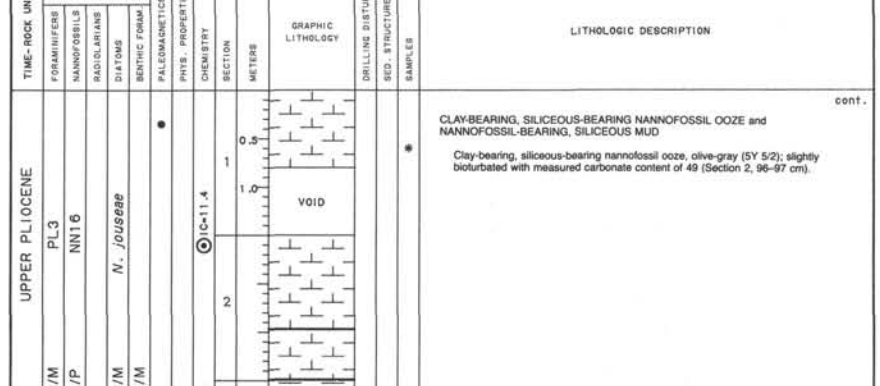
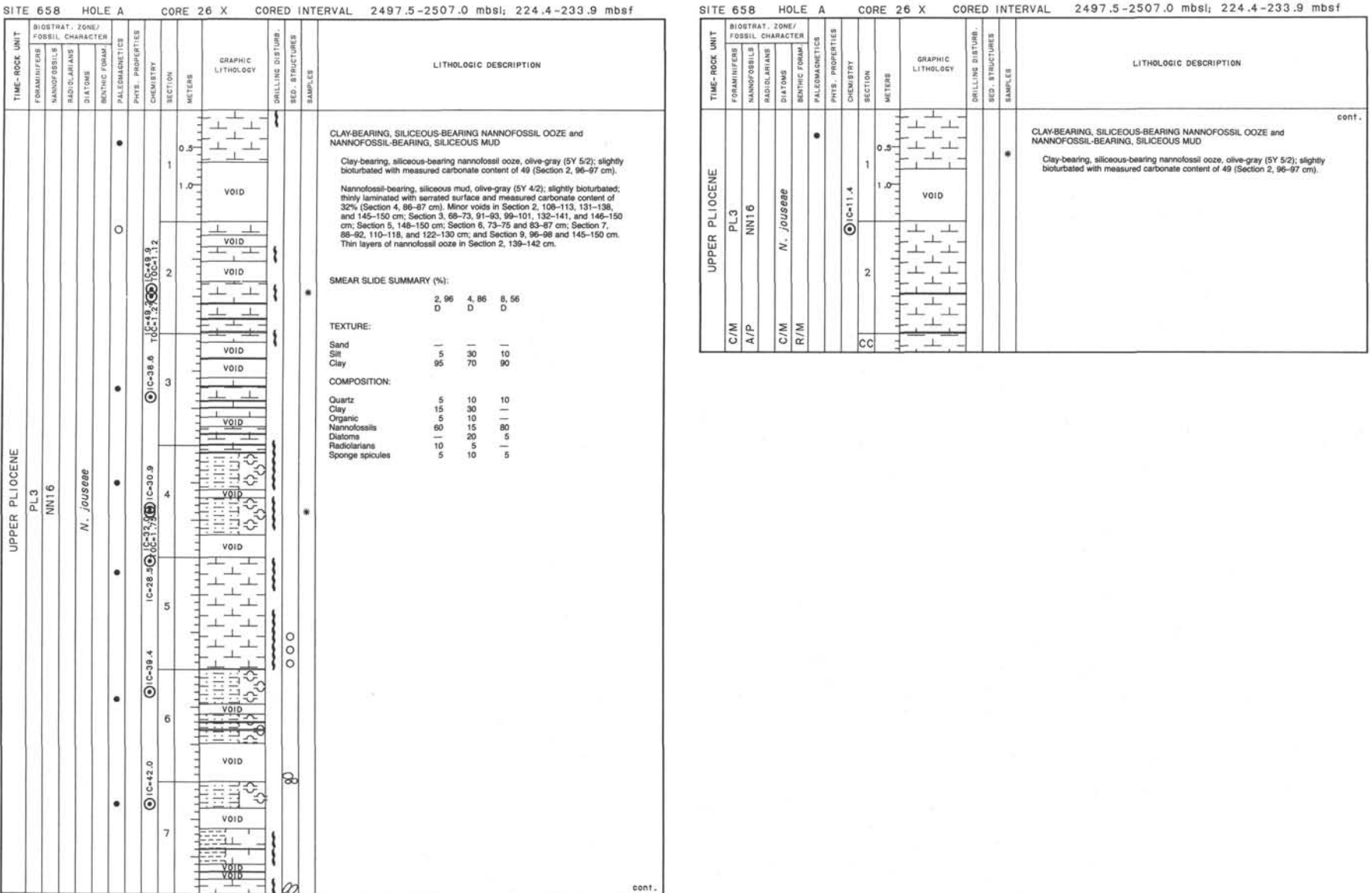


can

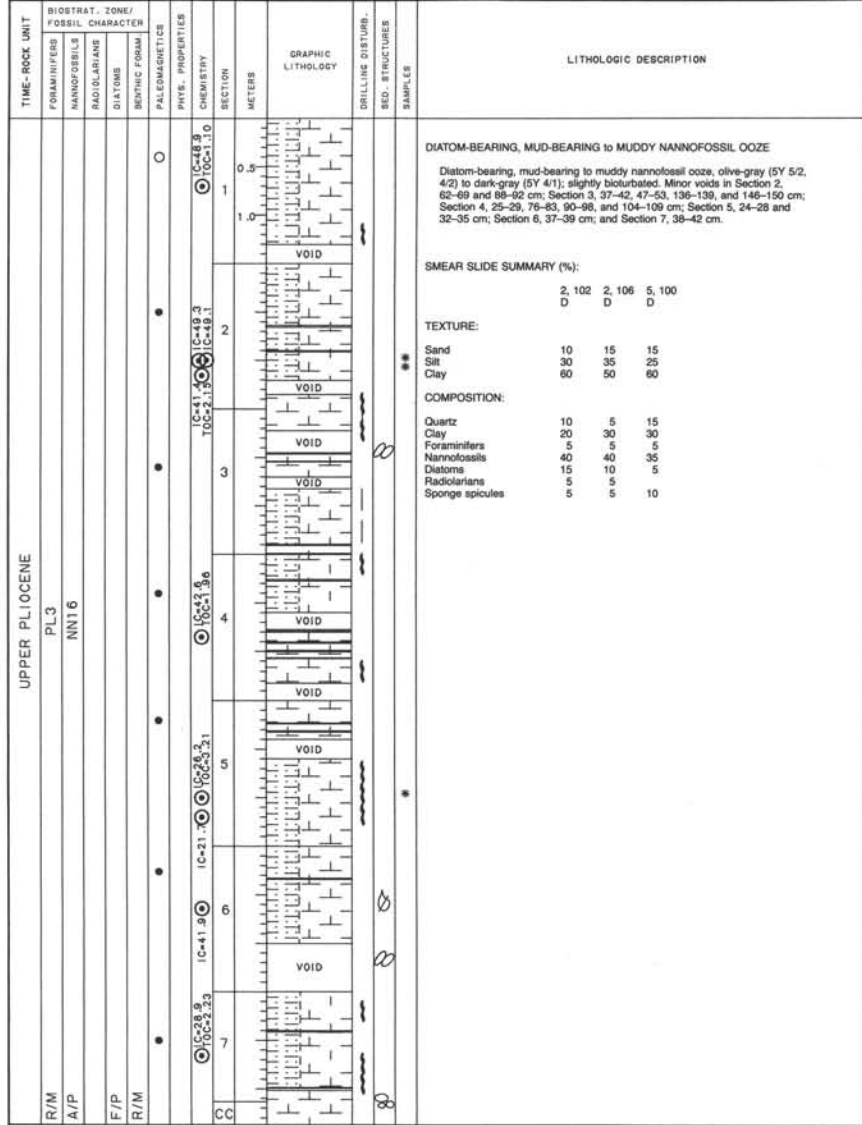
SIE 638

SITE 658 HOLE A CORE 25 X CORED INTERVAL 2478.5-2497.5 mbsl; 214.9-224.4 mbsf

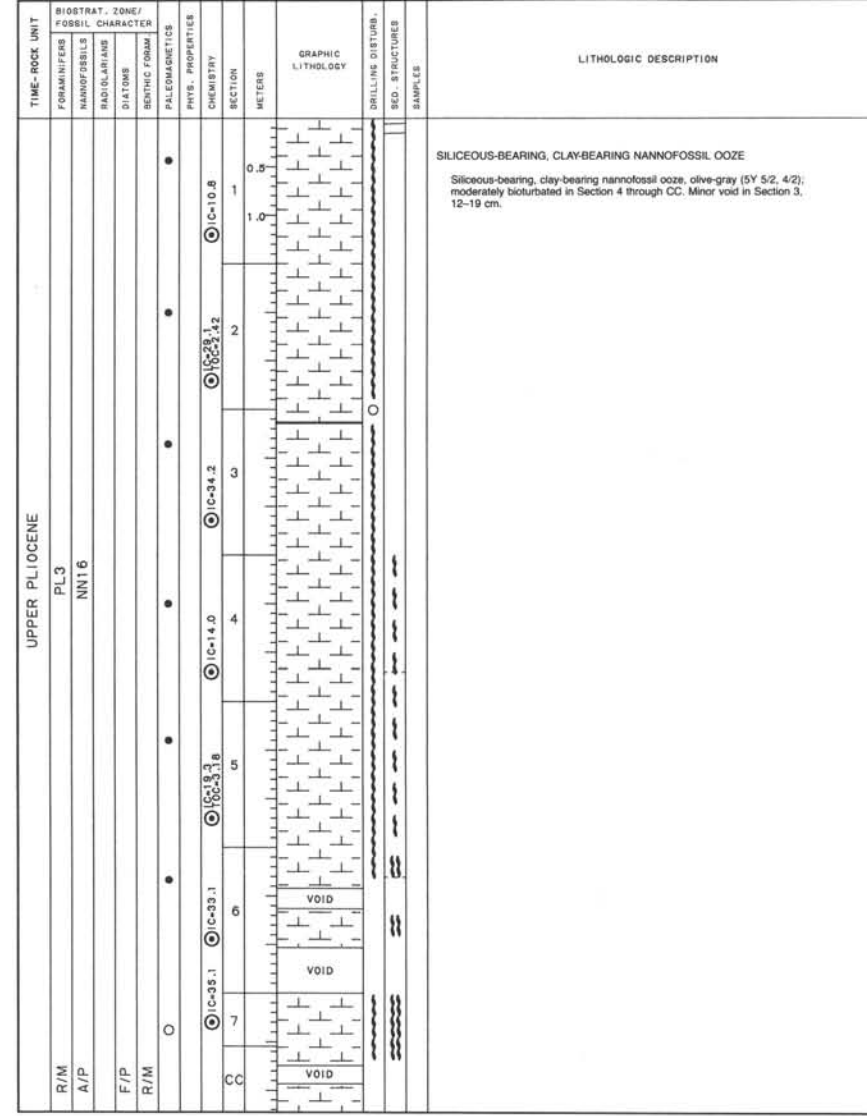


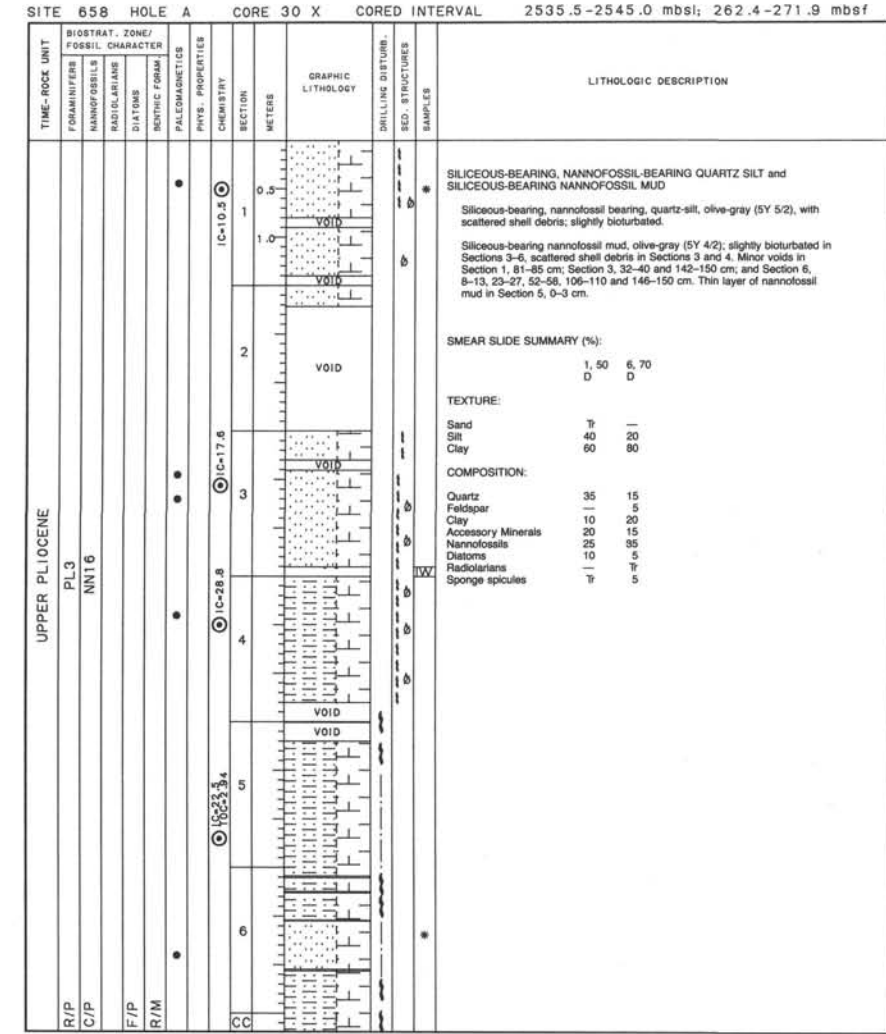
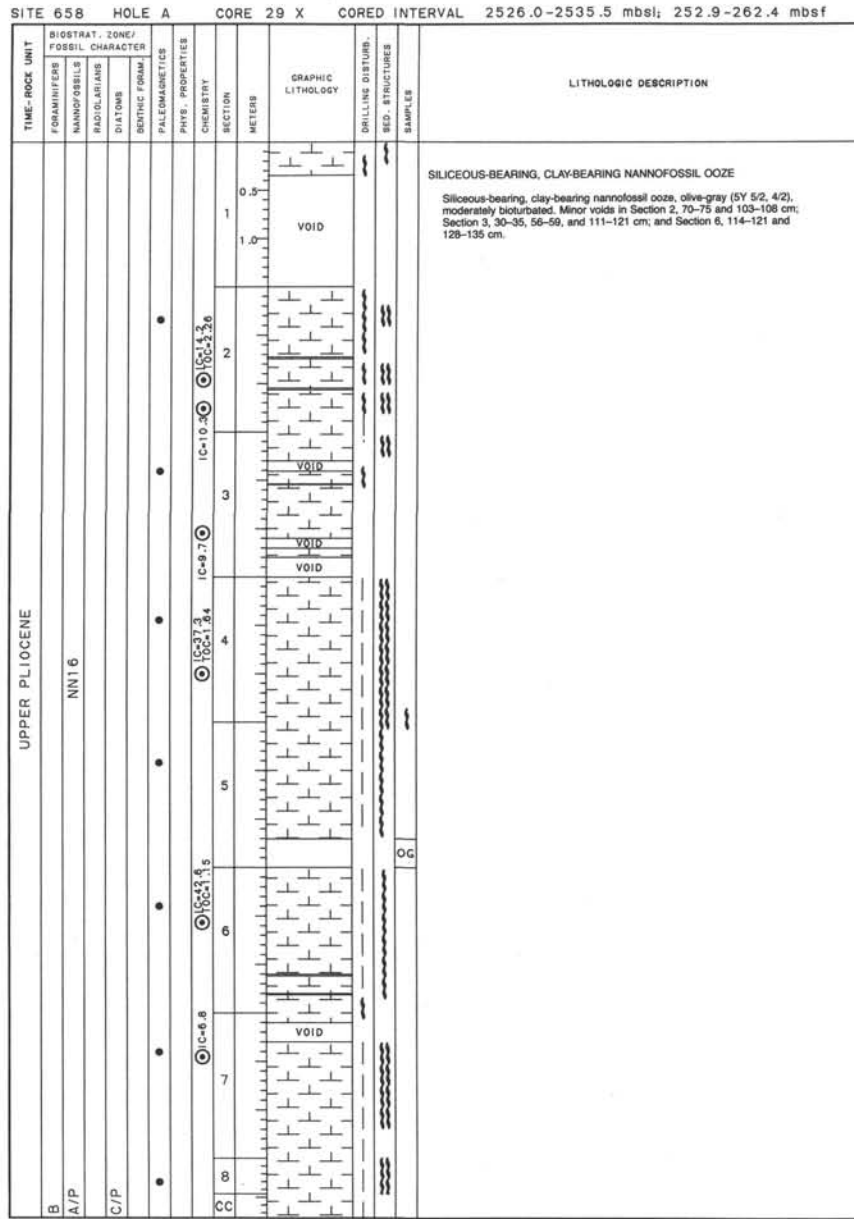


SITE 658 HOLE A CORE 27 X CORED INTERVAL 2507.0-2516.5 mbsl: 233.9-243.4 mbsf



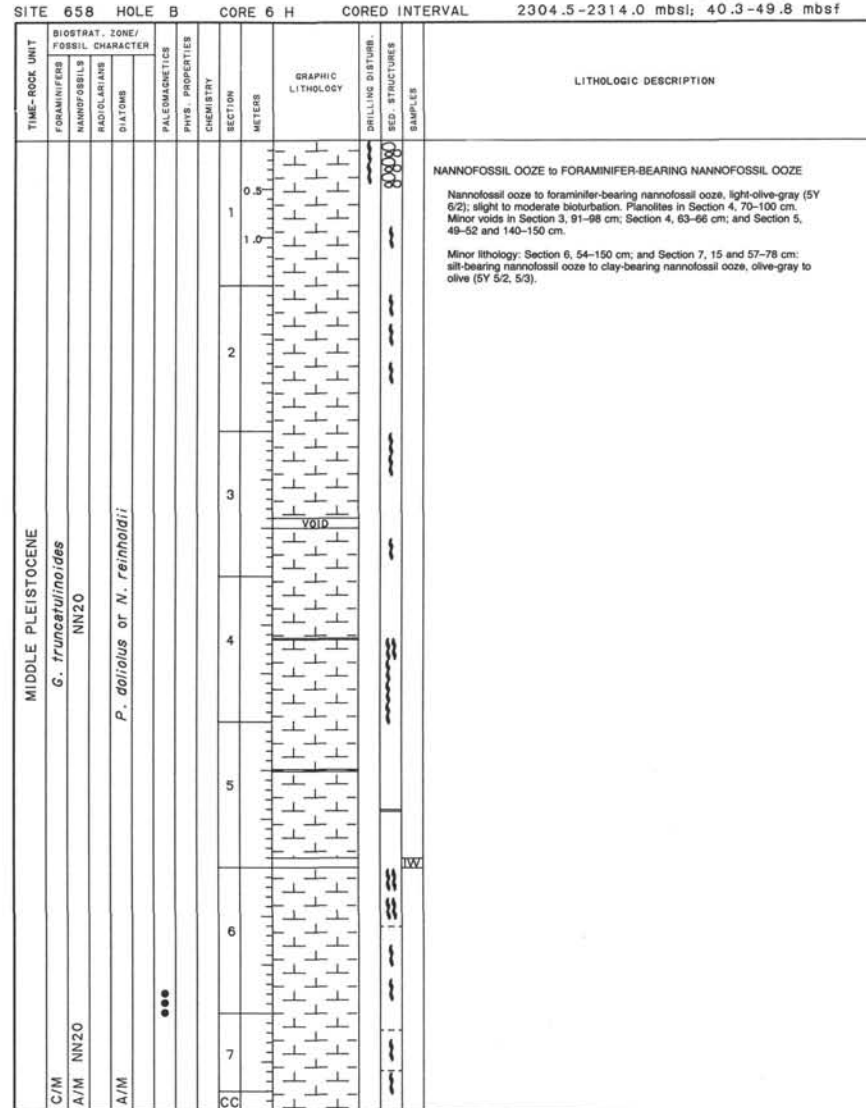
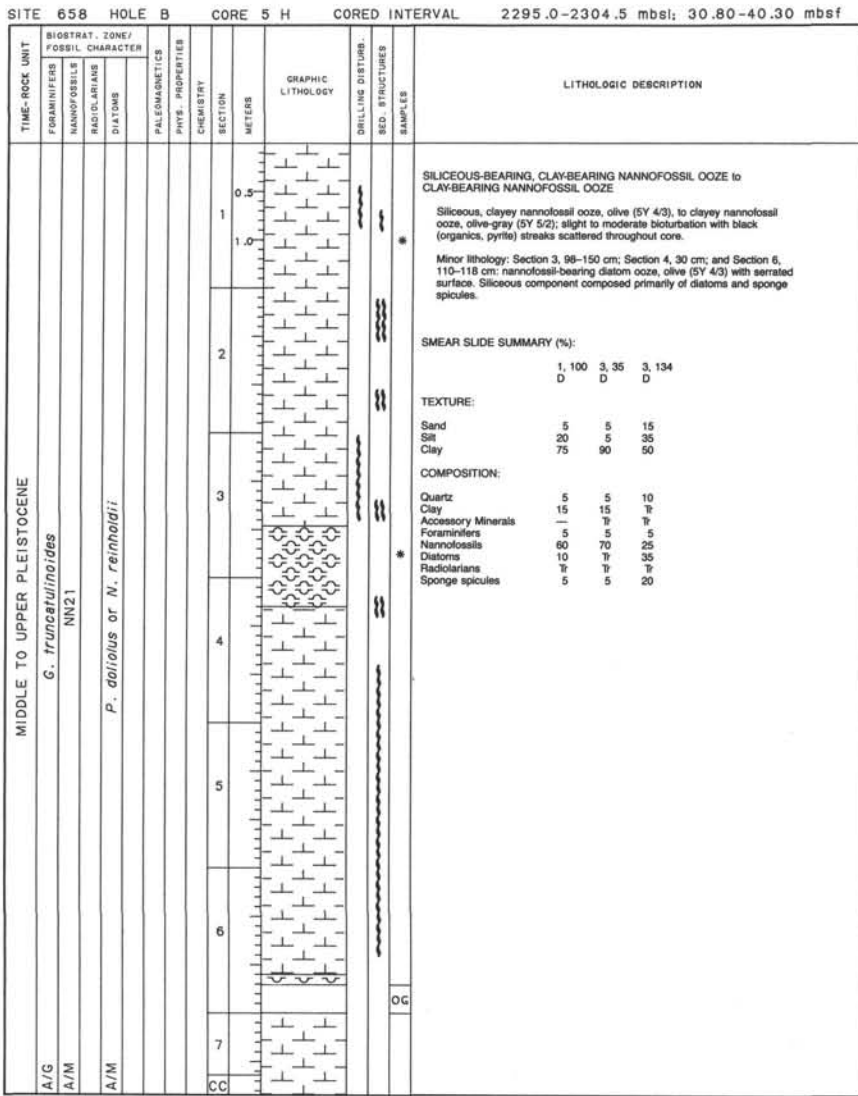
SITE 658 HOLE A CORE 28 X CORED INTERVAL 2516.5-2526.0 mbsl; 243.4-252.9 mbsl

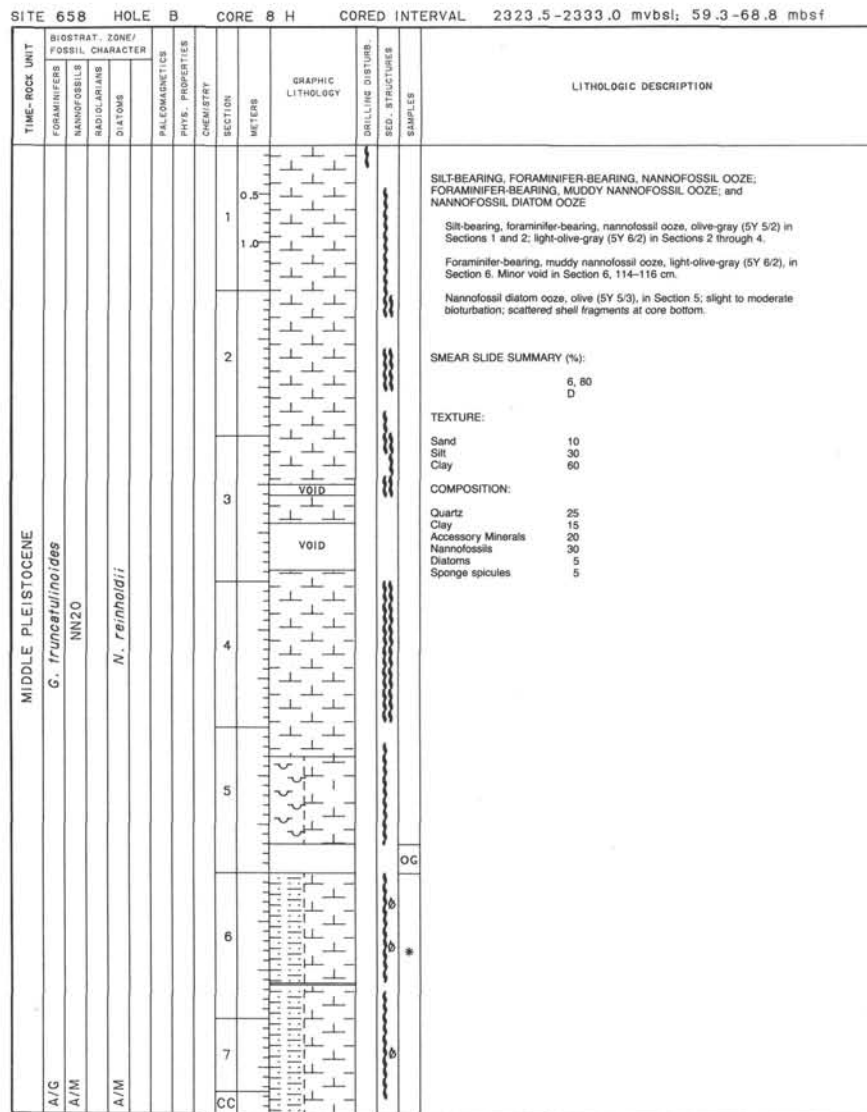
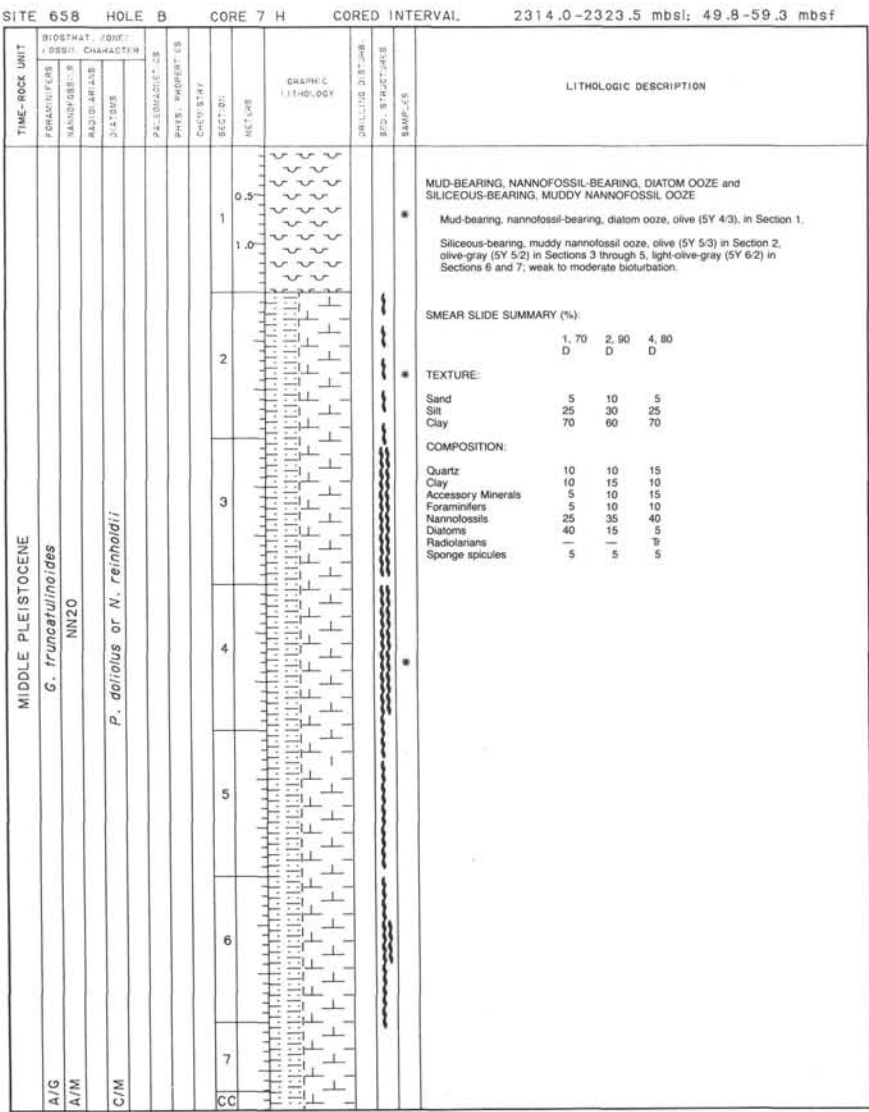




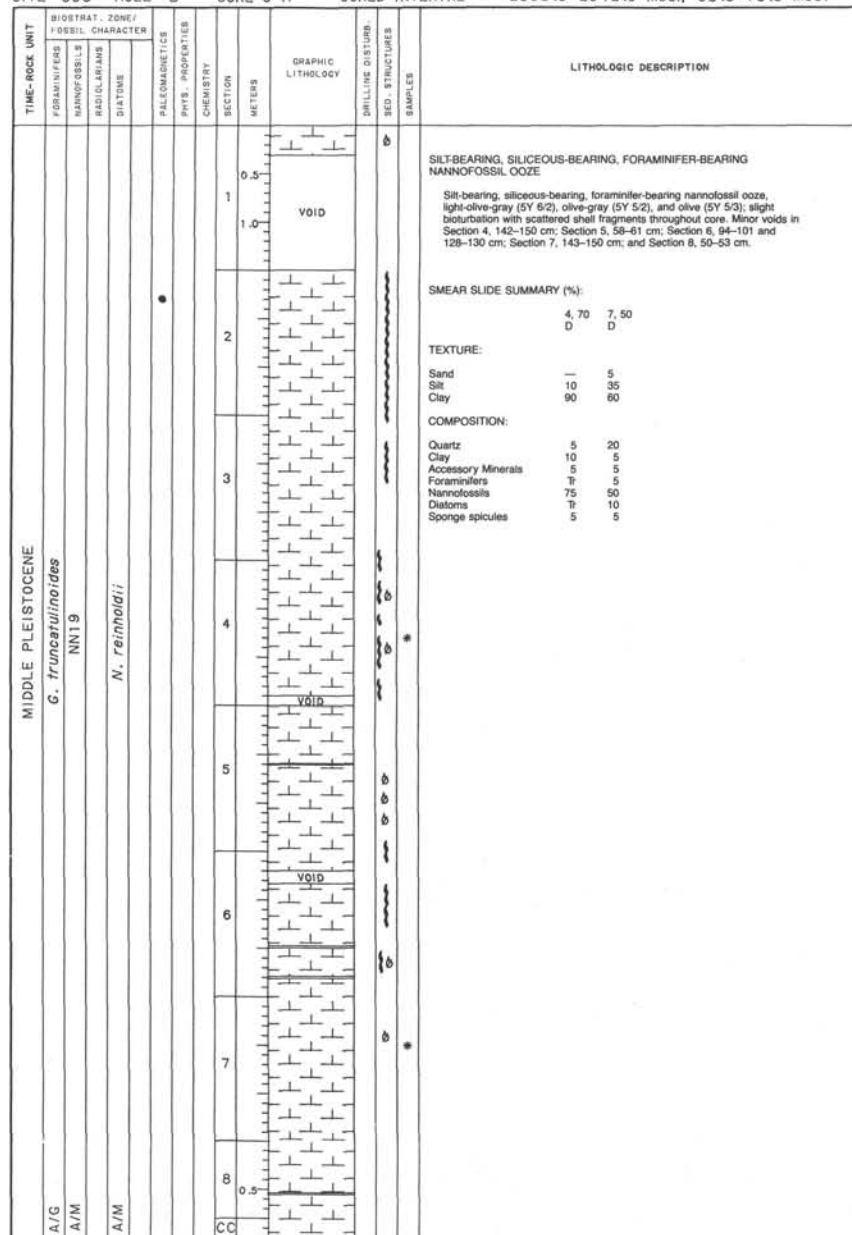
SITE 658 HOLE B		CORE 1 H	CORED INTERVAL	2264.2-2266.5 mbsl; 0-2.3 mbsf
TIME-ROCK UNIT	BIOSTRAT. ZONE/ FOSSIL CHARACTER			LITHOLOGIC DESCRIPTION
BIOSTRAT. ZONE/ FOSSIL CHARACTER				
FORAMINIFERS				
FLUOROCOPALS				
RADIOLARIANS				
DIATOMS				
PALaeOMAGNETICS				
PHYS. PROPERTIES				
CHAMBER				
SECTION				
METER				
0.5				
1				
1.0				
2				
CC				
A/G				
A/G				
NN21				
A/M				
<i>G. truncatulinoides</i>				
<i>P. doliosus</i> or <i>N. reinholdi</i>				
UPPER PLEISTOCENE TO HOLOCENE				
DIATOM-BEARING, MUDDY NANNOFOSSIL Ooze				
Diatom-bearing, muddy nannofossil ooze, olive-gray (SY 4/2); slightly bioturbated; moderately disturbed by drilling. Minor void in Section 1, 146-150 cm.				
DRILLING DISTURB. BED. STRUCTURES SAMPLES				
*				
W				
*				
SMEAR SLIDE SUMMARY (%):				
		1, 120	2, 30	
		D	D	
TEXTURE:				
Sand		5	—	
Silt		25	—	
Clay		70	65	
COMPOSITION:				
Quartz		10	15	
Rock Fragments		—	5	
Clay		10	5	
Accessory Minerals		20	10	
Foraminifers		5	5	
Nannofossils		35	40	
Diatoms		15	15	
Sponge spicules		5	5	

SITE 658 HOLE B		CORE 4 H	CORED INTERVAL	2285.5-2295.0 mbsl; 21.3-30.8 mbst
TIME-ROCK UNIT	BIOSTRAT., ZONE/ FOSSIL CHARACTER			LITHOLOGIC DESCRIPTION
A/M	FORAMINIFERS NANNOFOSILS RADULARIANS DIATOMS	PALaeOMAGNETICS	PHYS. PROPERTIES CHEMISTRY	DRILLING DISTURB. BED STRUCTURES SAMPLES
UPPER PLEISTOCENE				
G. <i>truncatulinoides</i>	NN21			SILICEOUS-BEARING, MUD-BEARING NANNOFOSSIL Ooze
P. <i>dolosus</i> or N. <i>reinholdii</i>				Siliceous-bearing, mud-bearing nannofossil ooze, olive-gray (SY 5/2, 4/2); slight to moderate bioturbation; scattered black (organics, pyrite) streaks.
				Minor lithology: Section 2, 58-128 cm; Section 3, 132-150 cm; and Section 4, 0-16 cm: siliceous nannofossil ooze, olive (SY 4/3).

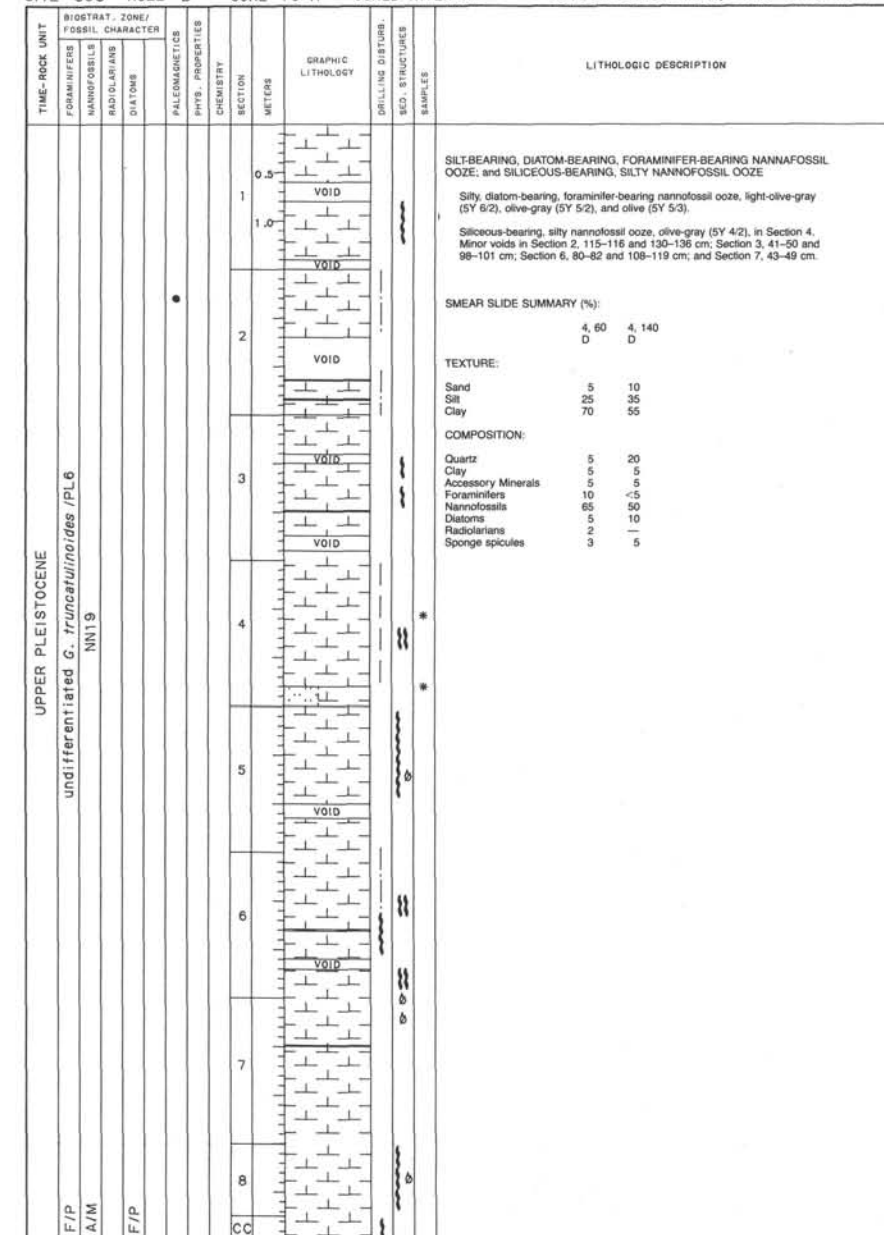




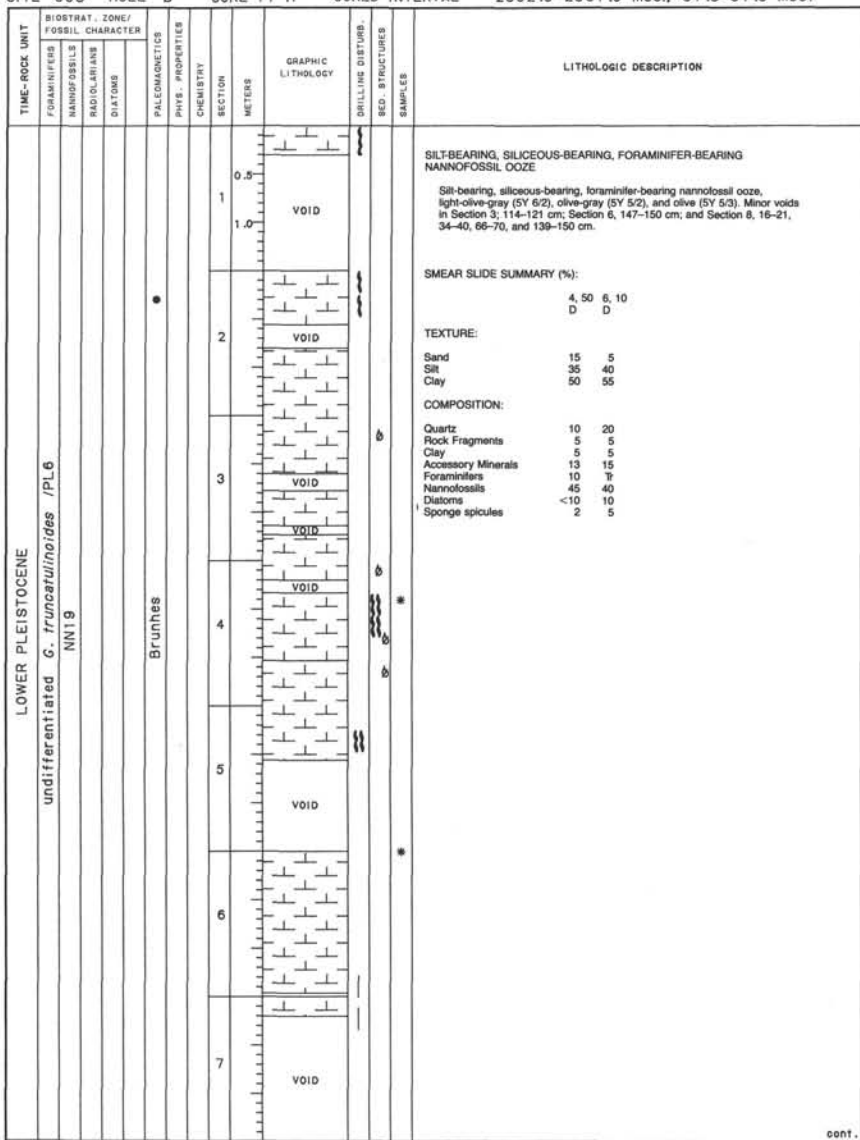
SITE 658 HOLE B CORE 9 H CORED INTERVAL 2333.0-2342.5 mbsl; 68.8-78.3 mbs



SITE 658 HOLE B CORE 10 H CORED INTERVAL 2342.5-2352.0 mbsl; 78.3-87.8 mbsf

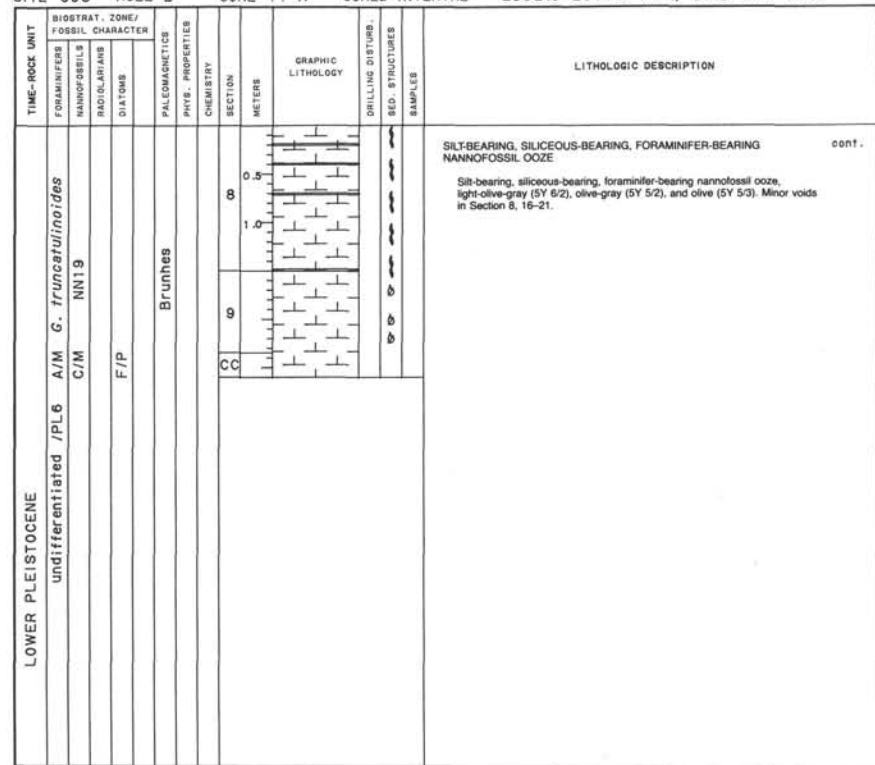


SITE 658 HOLE B CORE 11 H CORED INTERVAL 2352.0-2361.5 mbsl; 87.8-97.3 mbsf



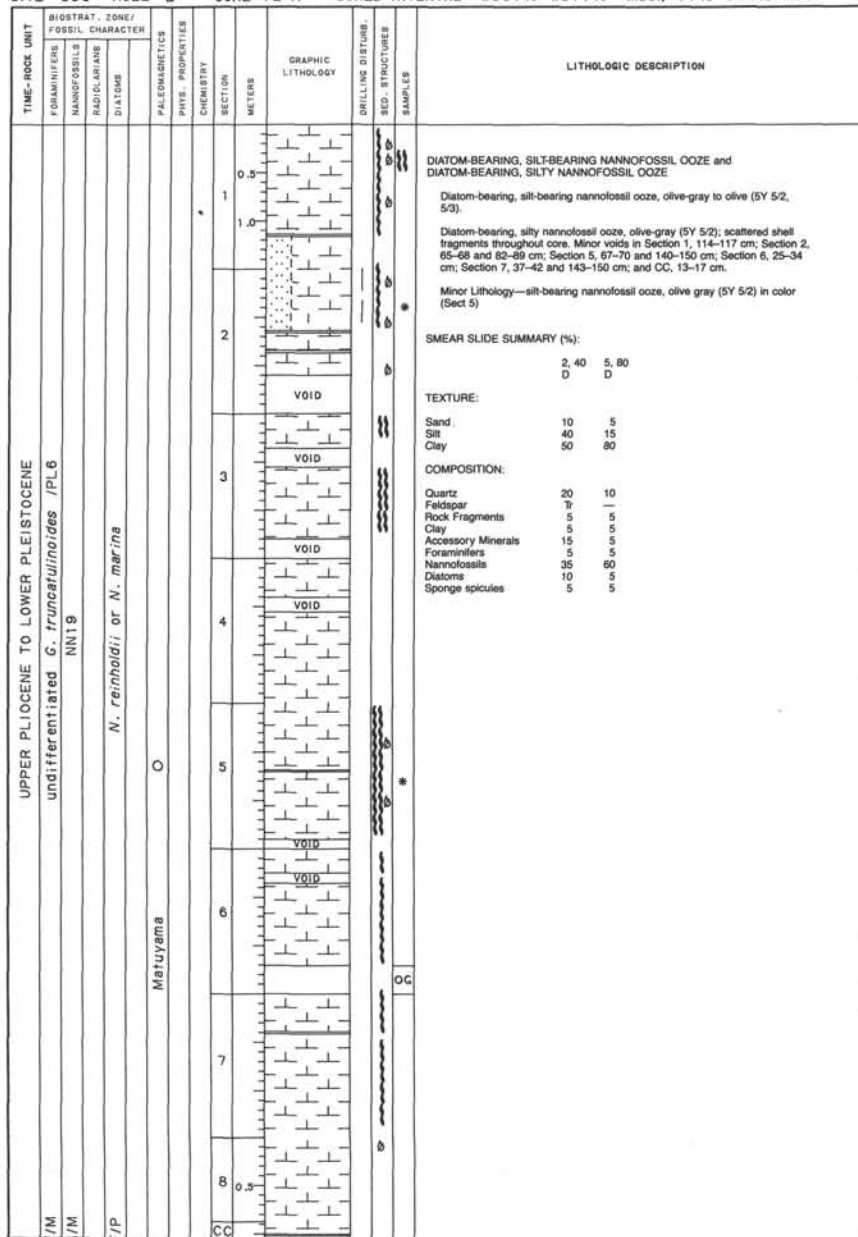
cont

SITE 658 HOLE B CORE 11 H CORED INTERVAL 2352.0-2361.5 mbsl; 87.8-97.3 msbf

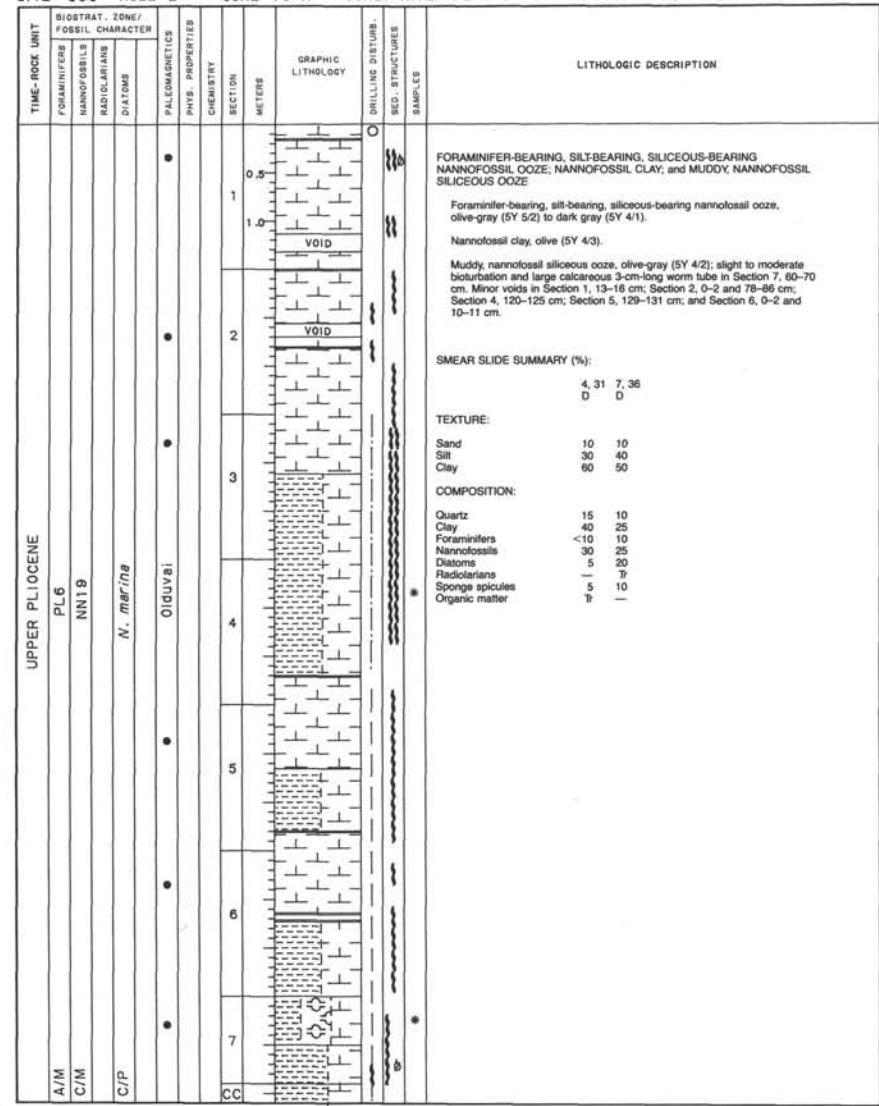


SITE 658

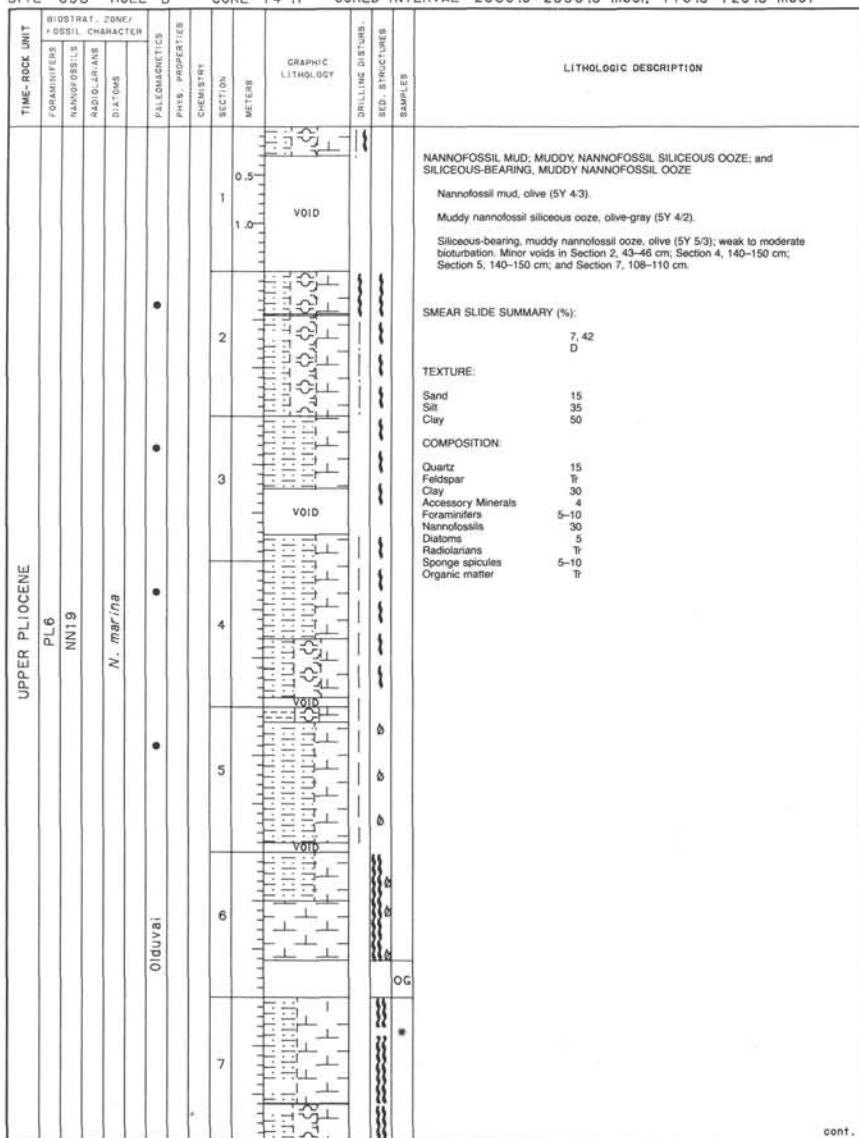
SITE 658 HOLE B CORE 12 H CORED INTERVAL 2361.5-2371.0 mbsf; 97.3-106.8 mbsf



SITE 658 HOLE B CORE 13 H CORED INTERVAL 2371.0-2380.5 mbsl; 106.8-116.3 mbst

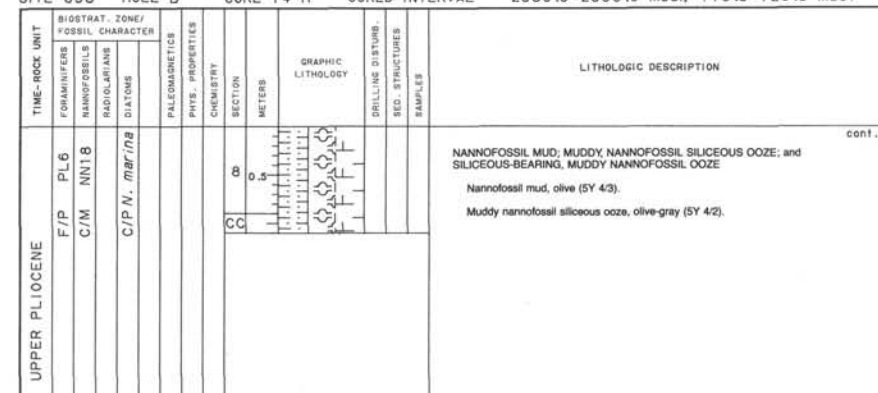


SITE 658 HOLE B CORE 14 H CORED INTERVAL 2380.5-2390.0 mbsf 116.3-125.8 mbst

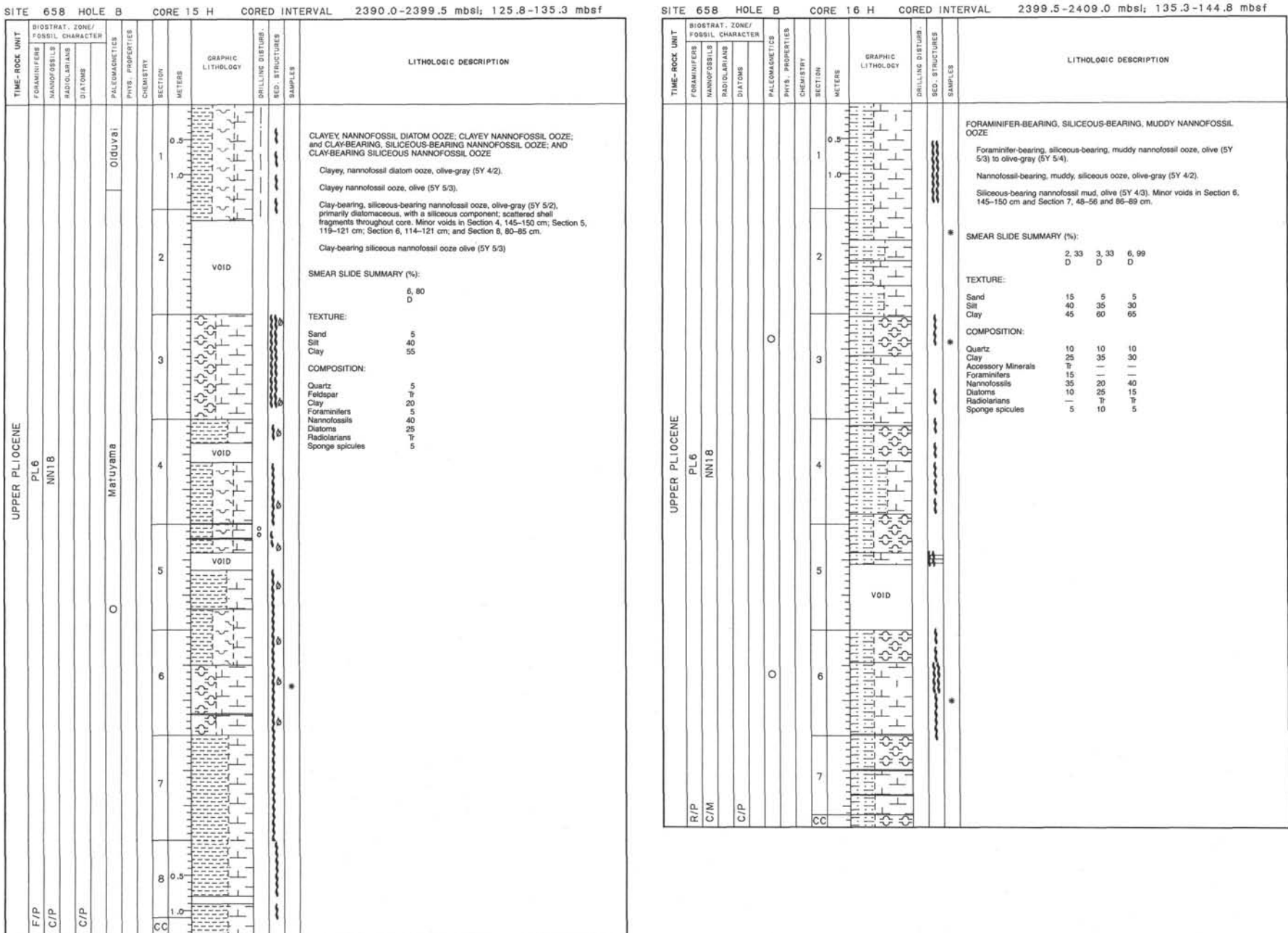


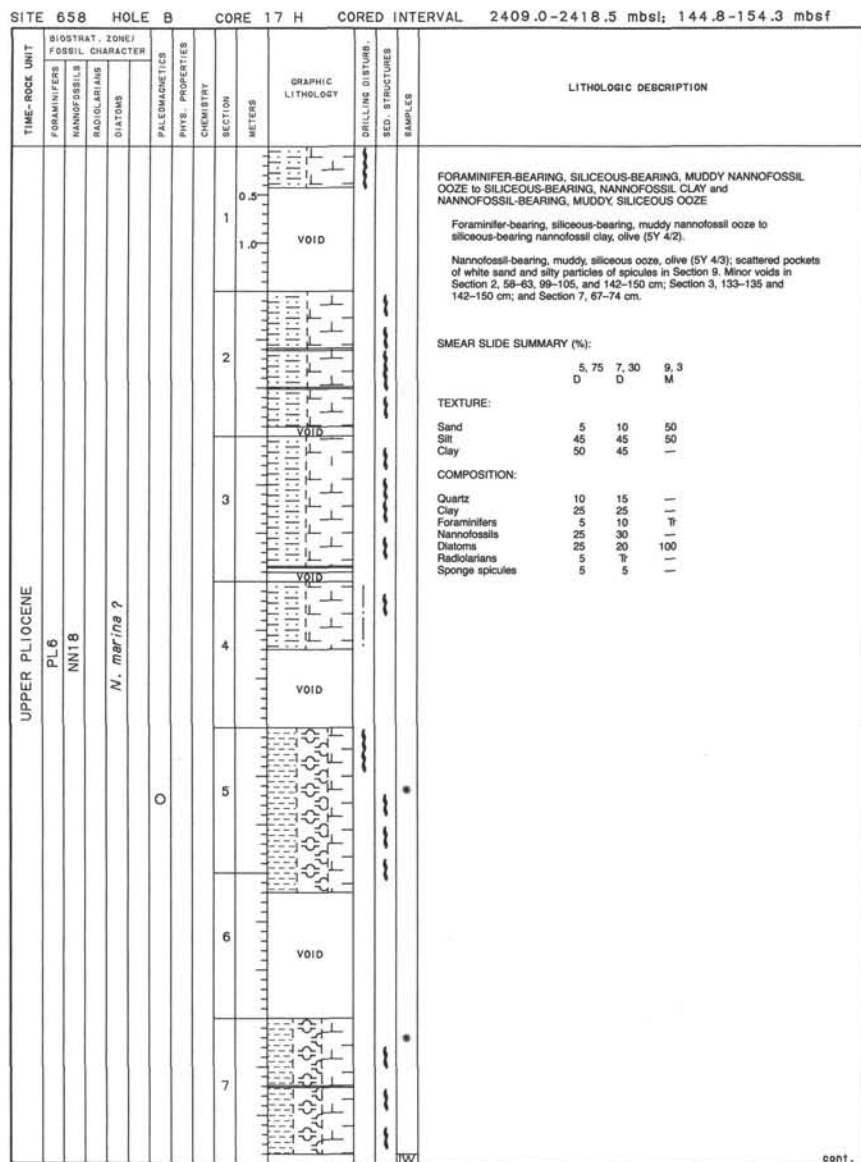
cont.

SITE 658 HOLE B CORE 14 H CORED INTERVAL 2380.5-2390.0 mbsl; 116.3-125.8 mbst

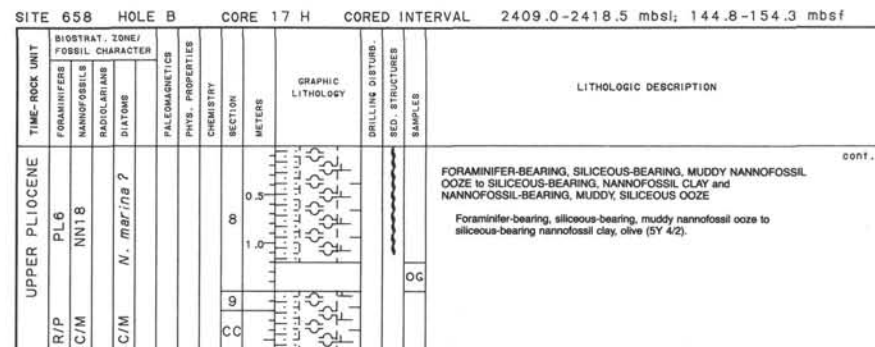


SITE 658





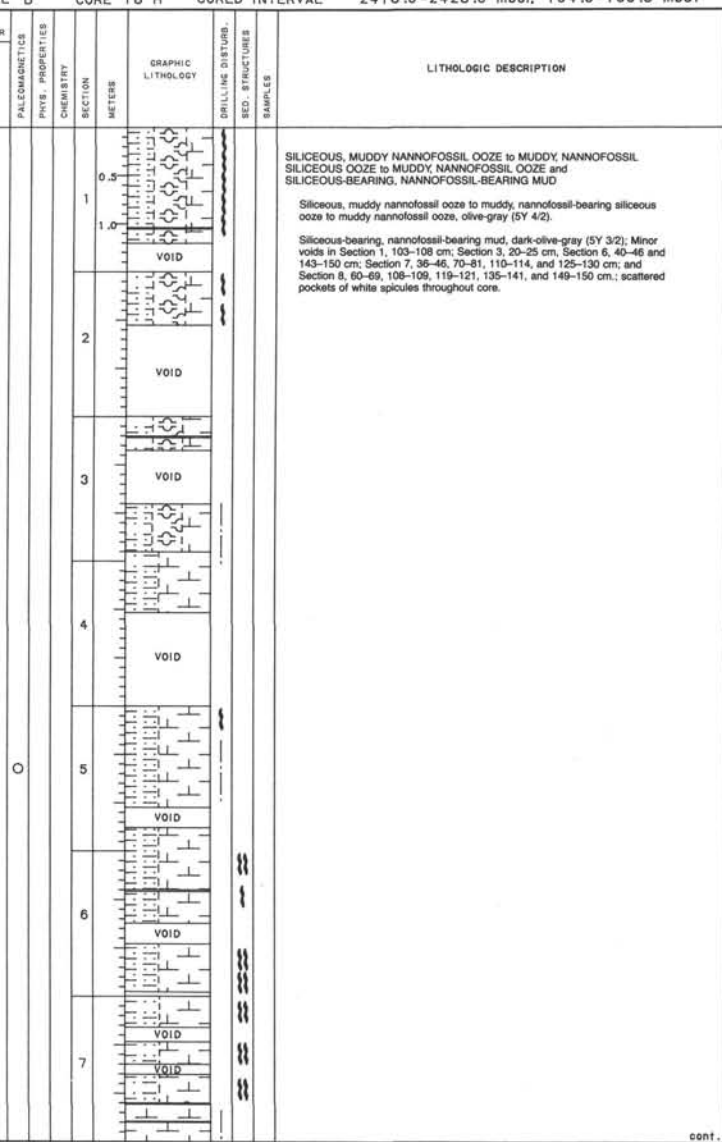
cont.



169

UPPER PLIOCENE
PL 5
ANAL. 9

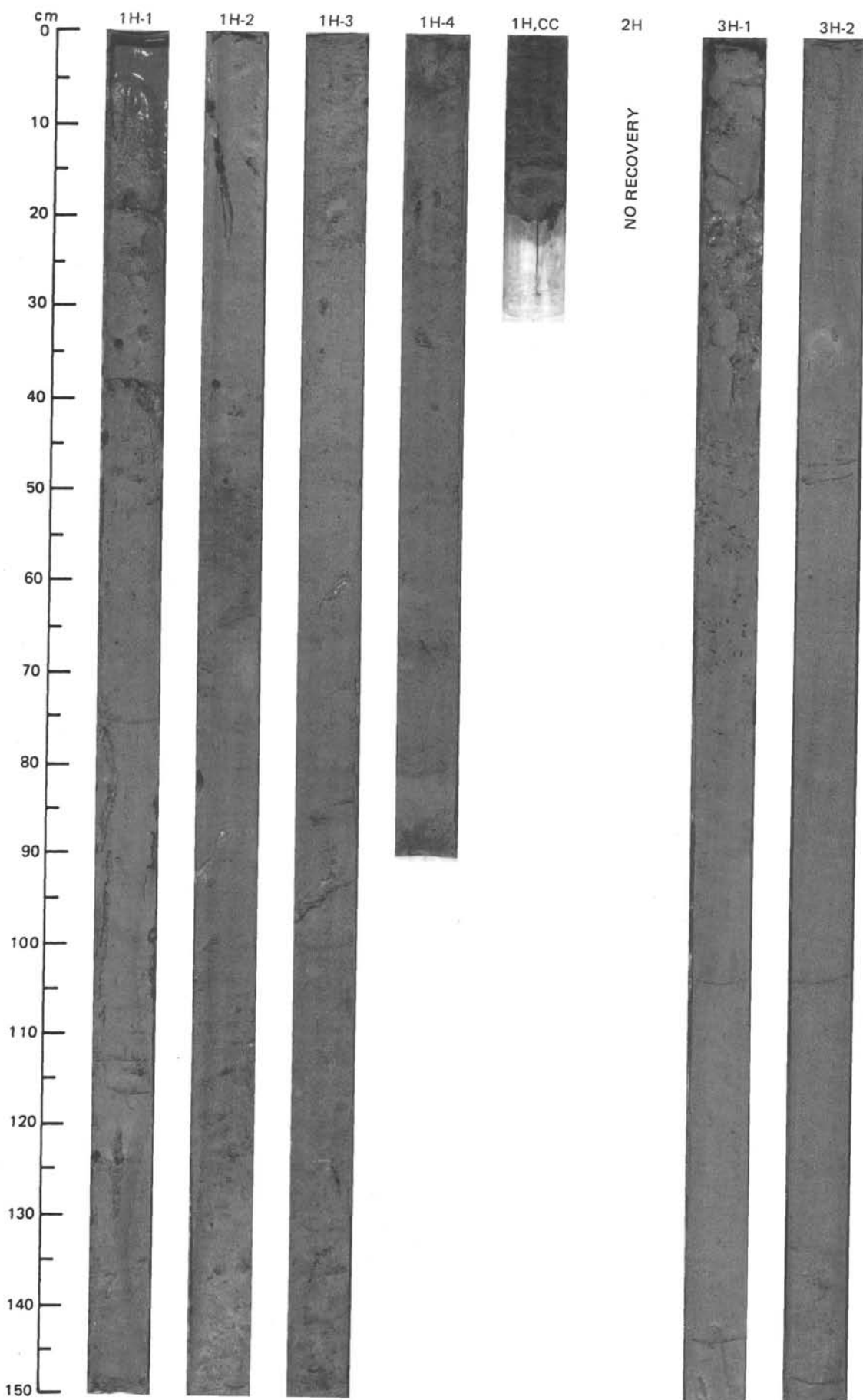
N. marina?

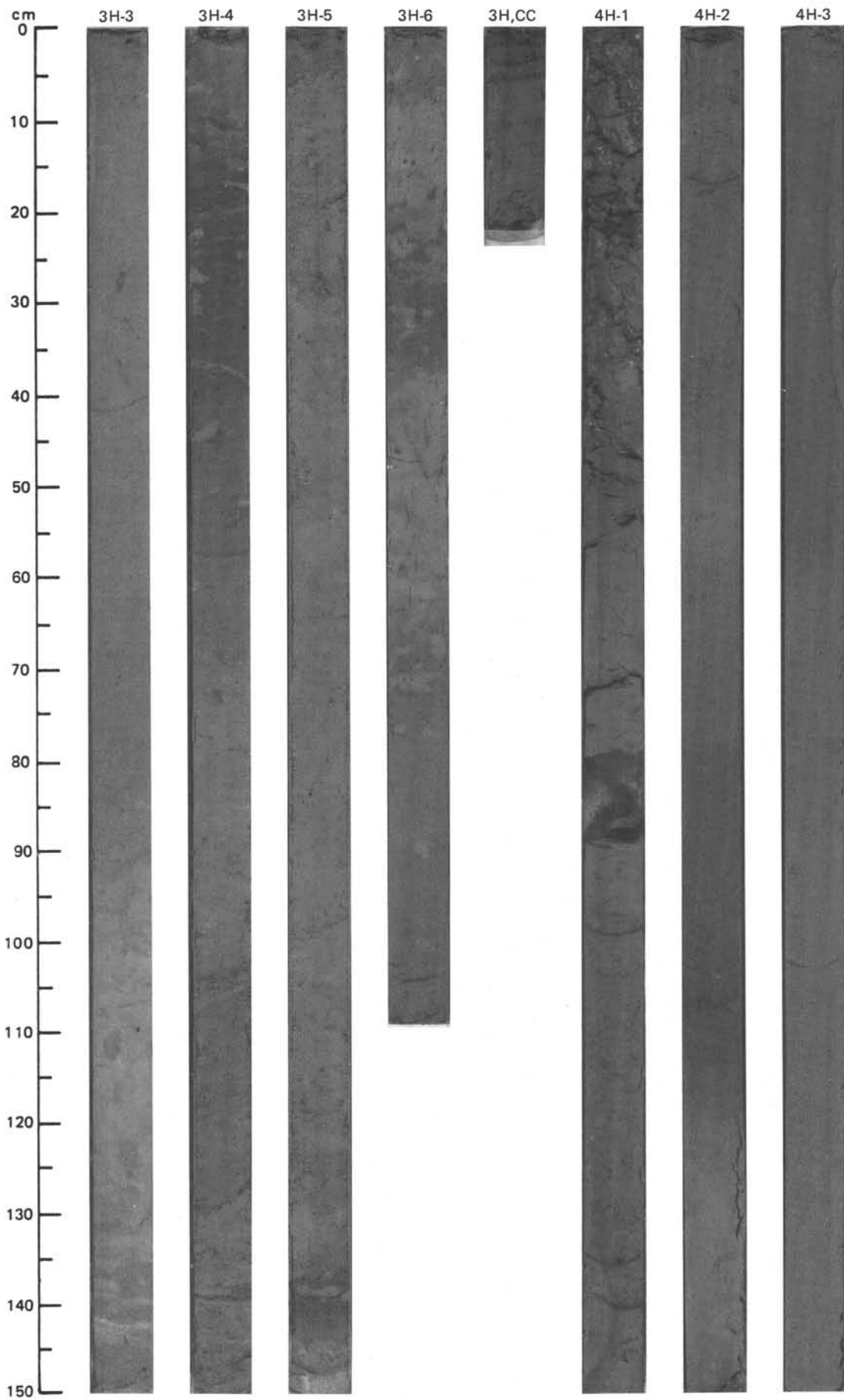


00

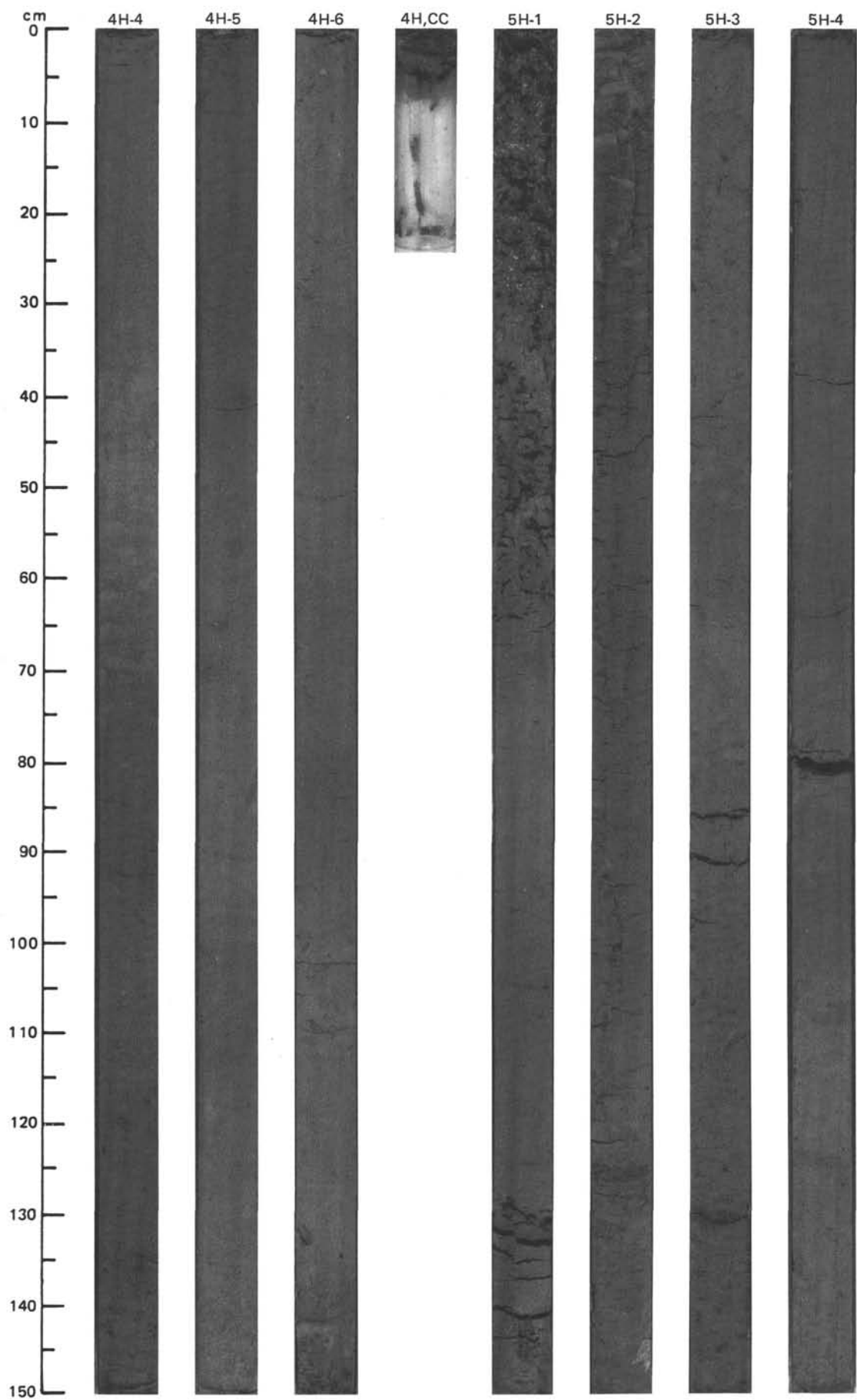
ce

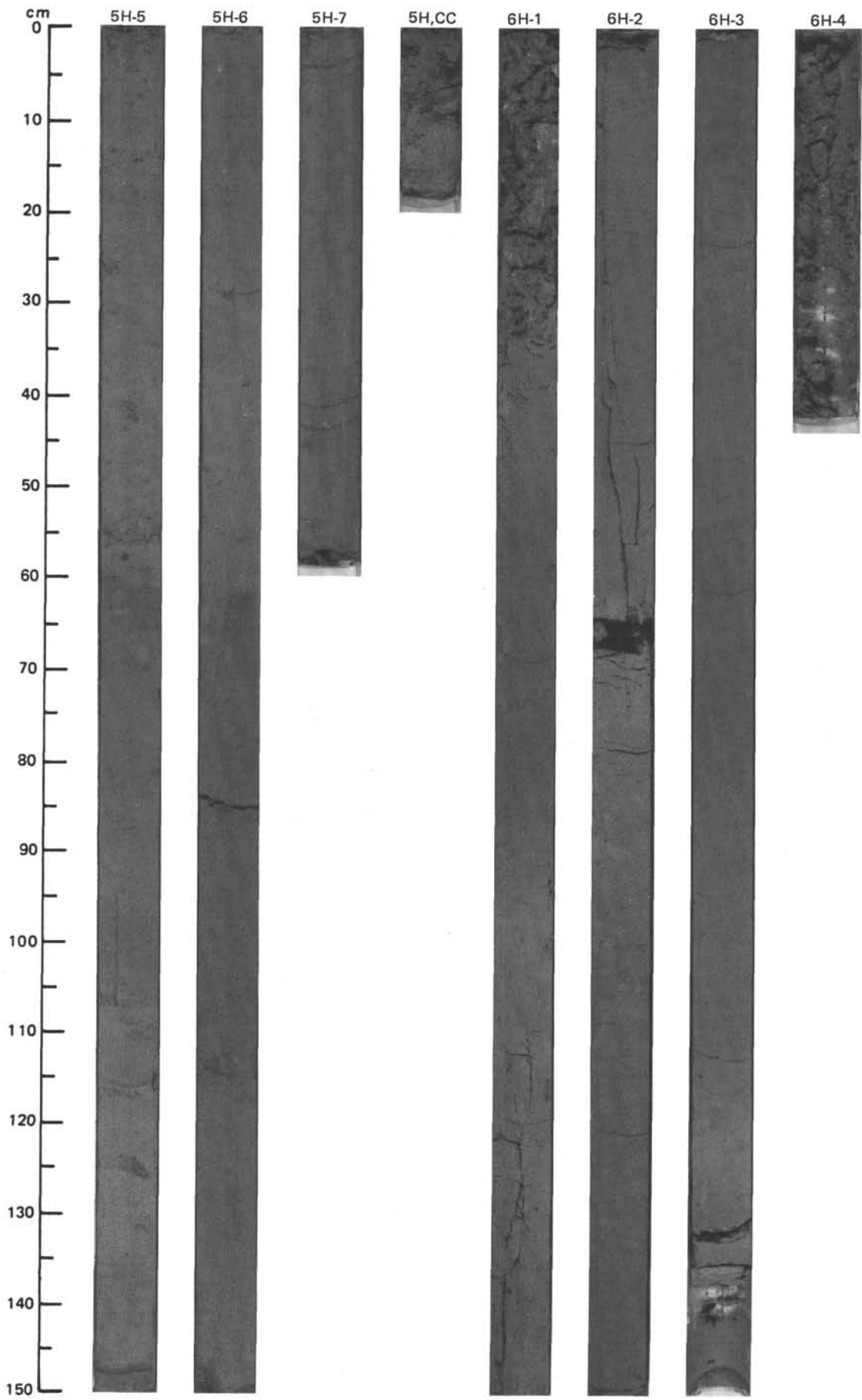
SITE 658 (HOLE A)





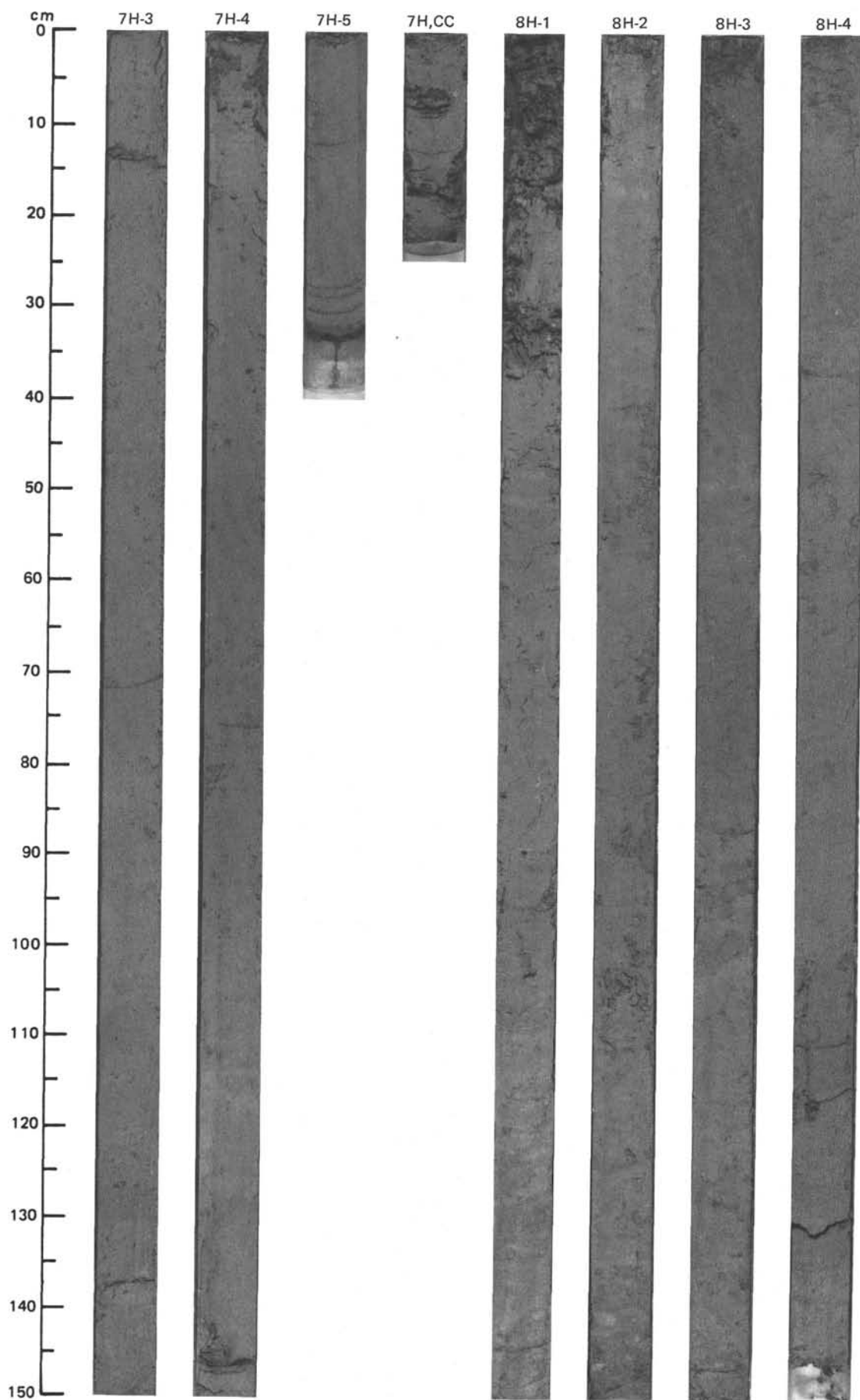
SITE 658 (HOLE A)



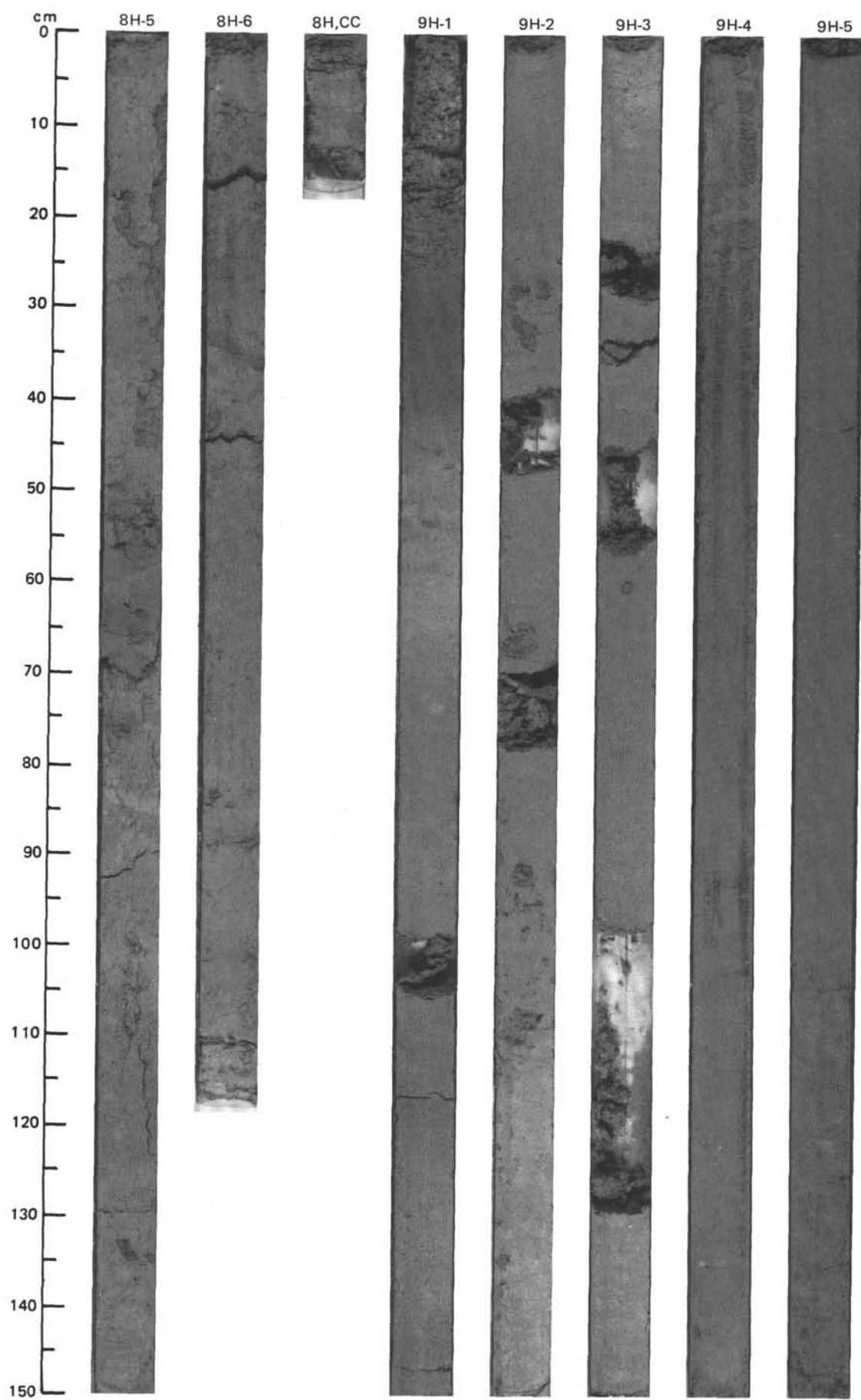


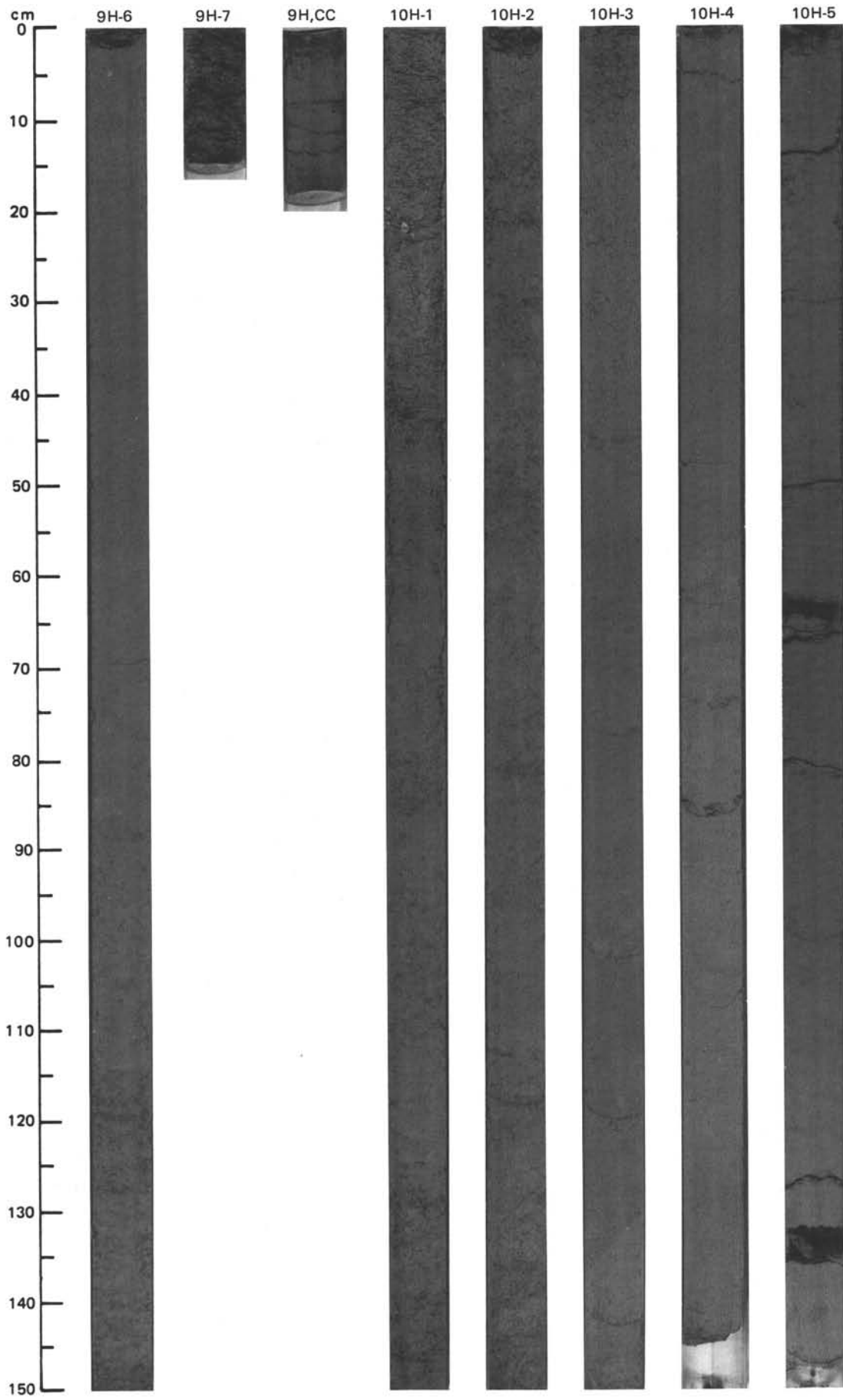
SITE 658 (HOLE A)



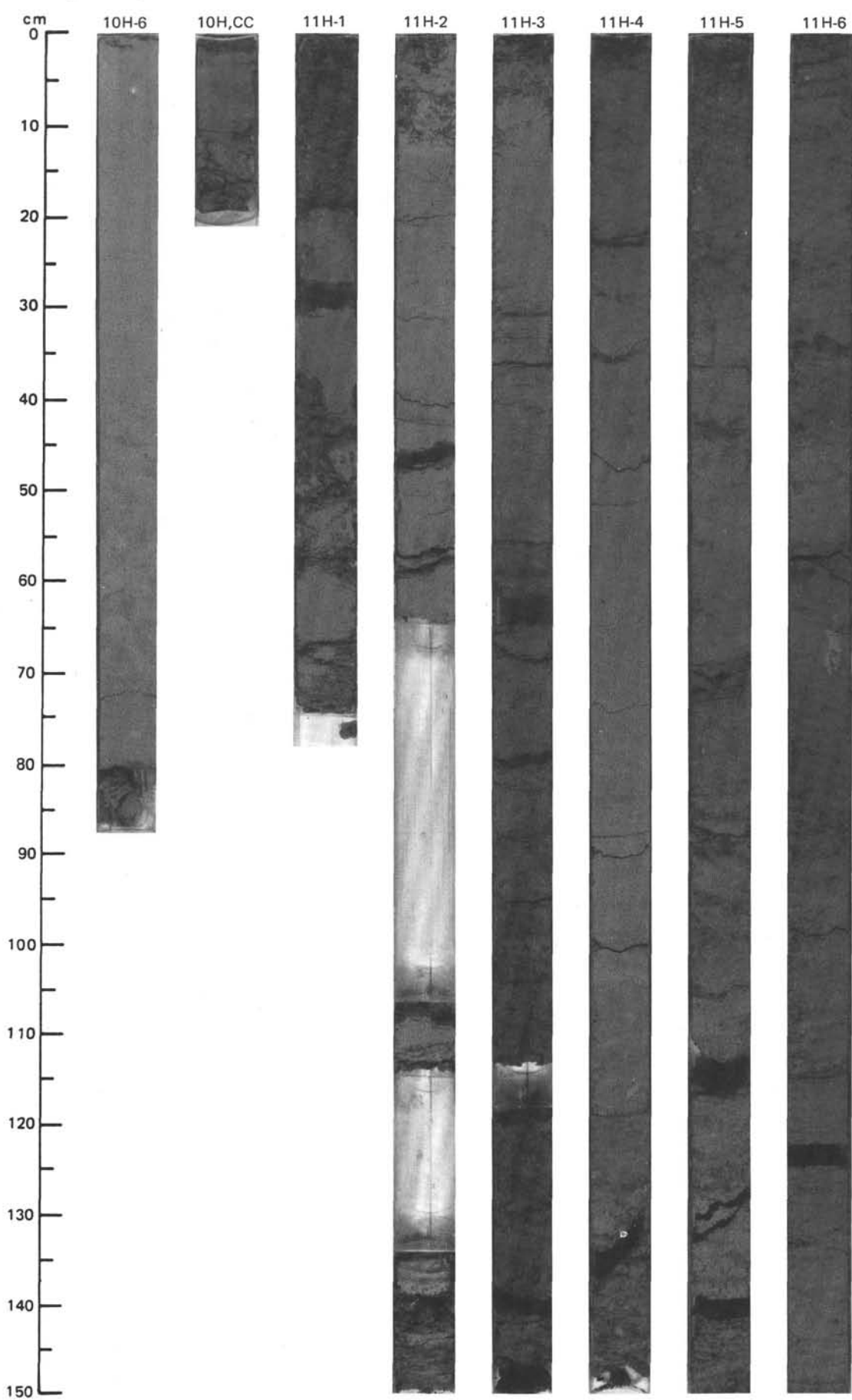


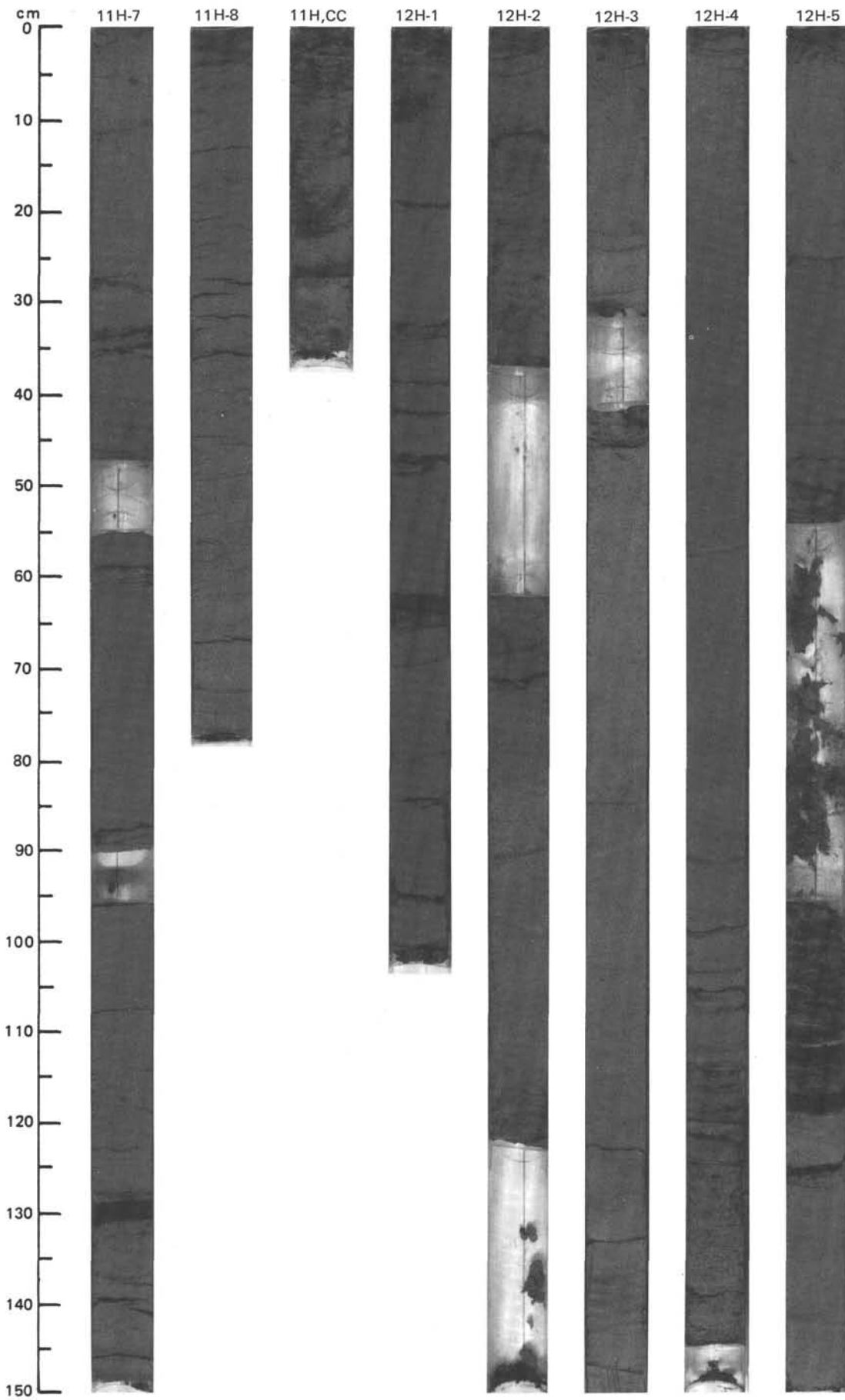
SITE 658 (HOLE A)



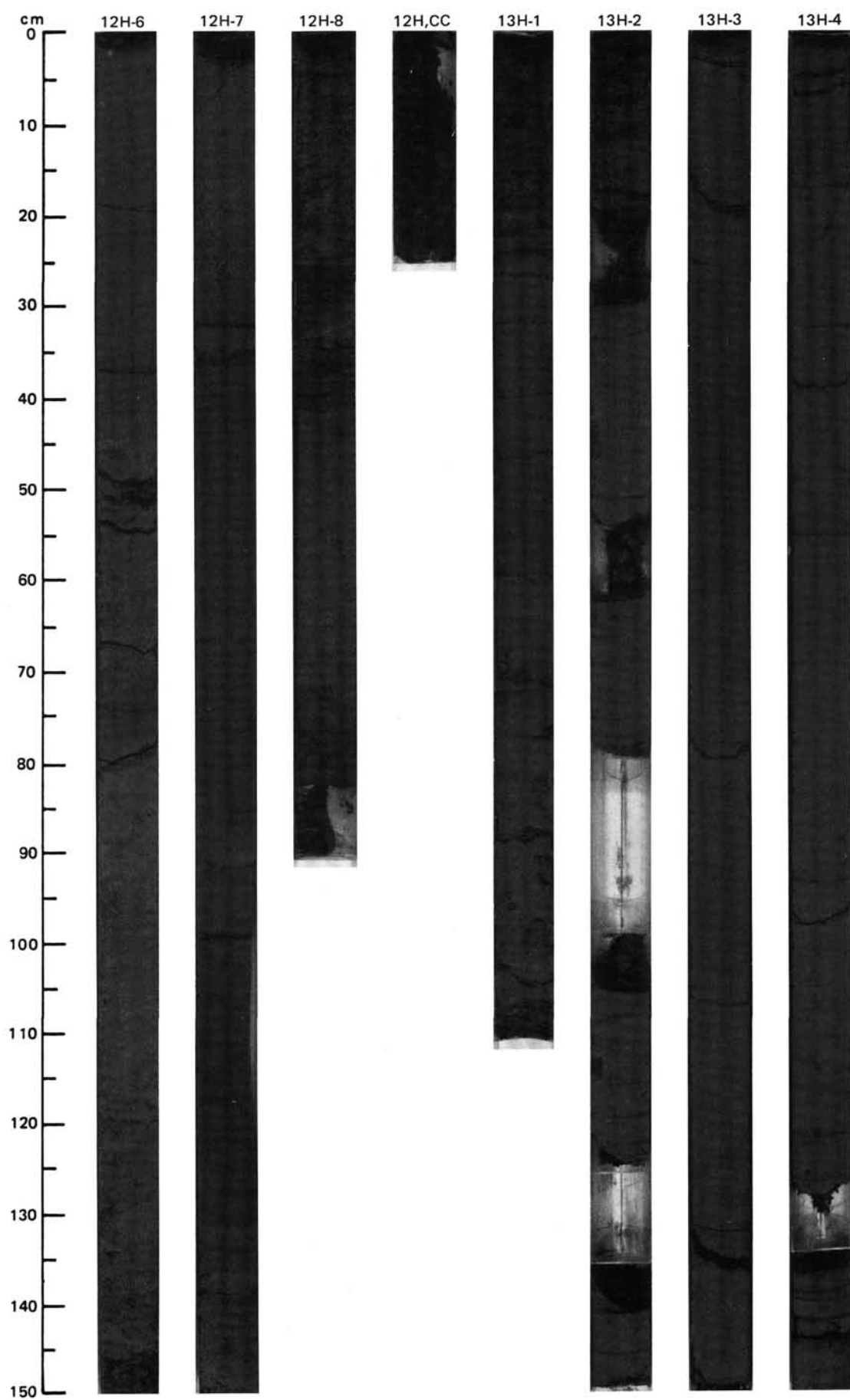


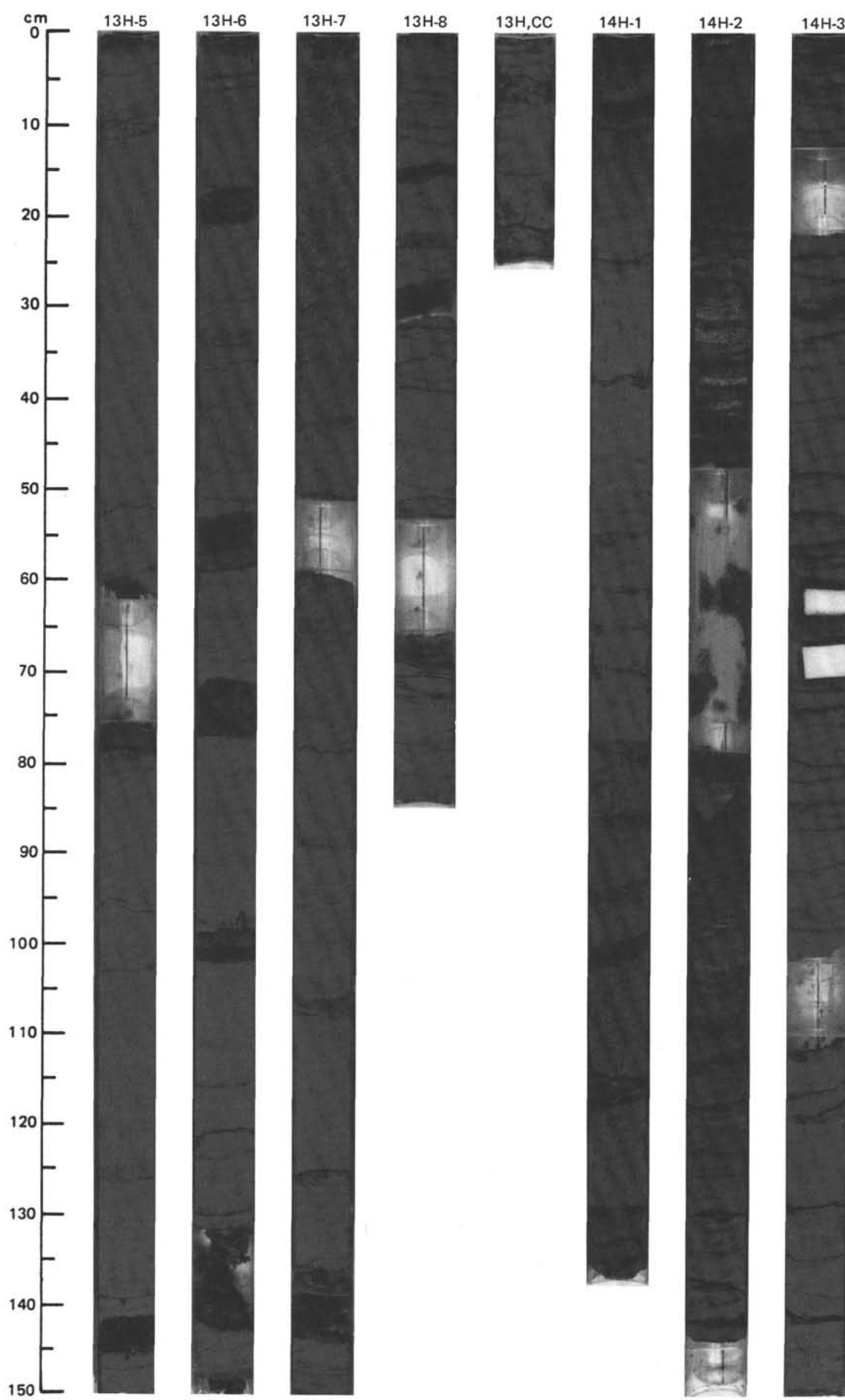
SITE 658 (HOLE A)



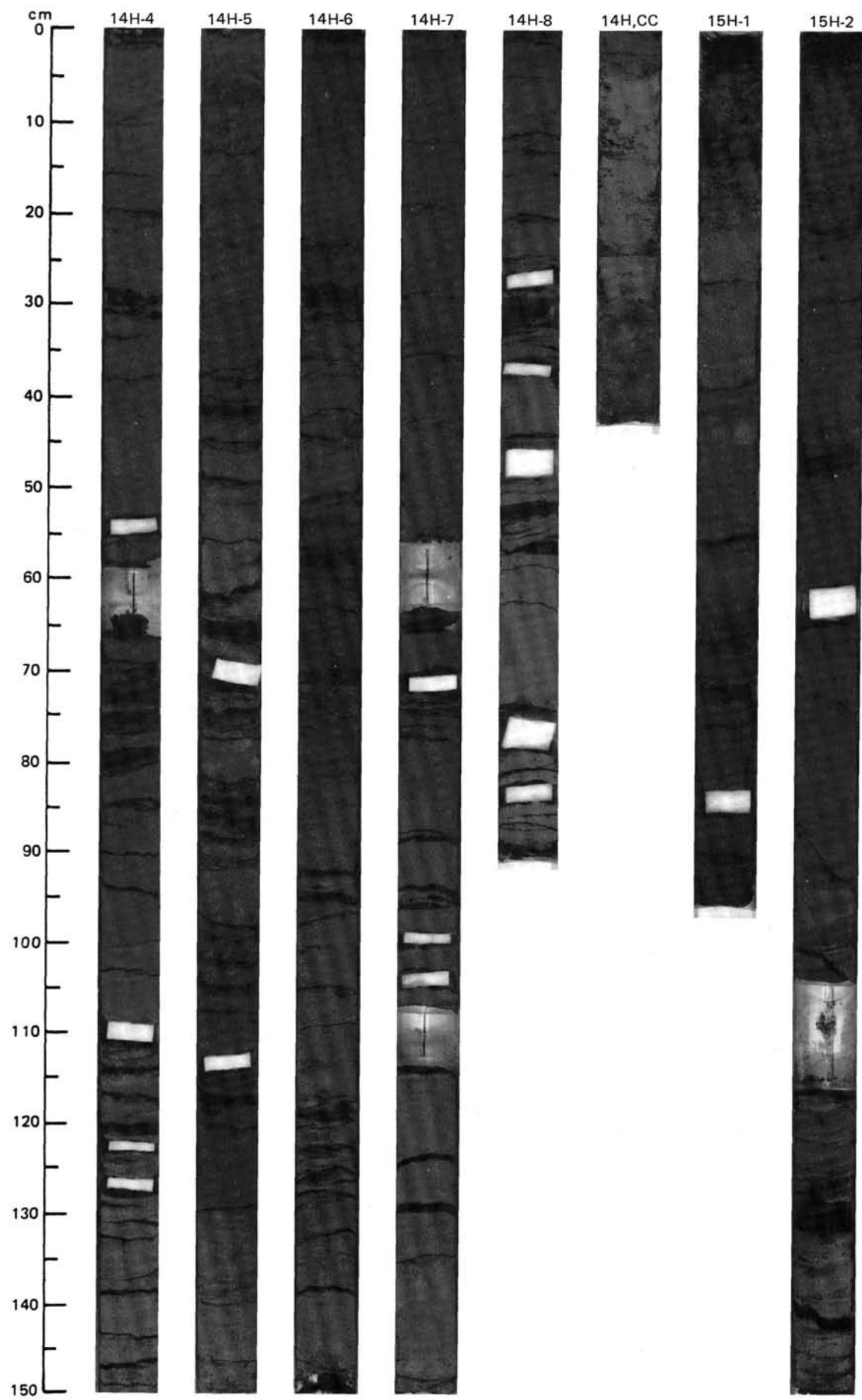


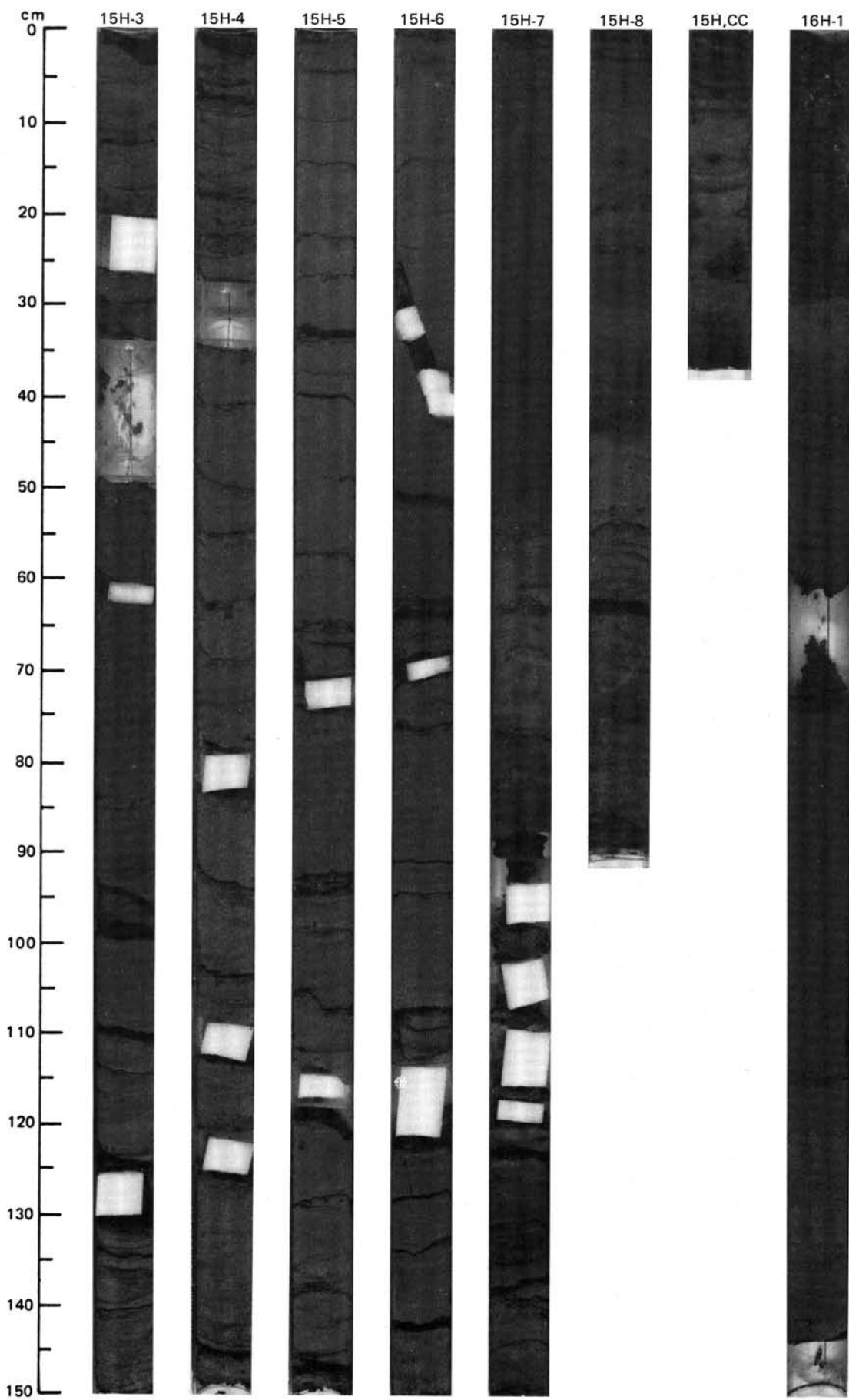
SITE 658 (HOLE A)



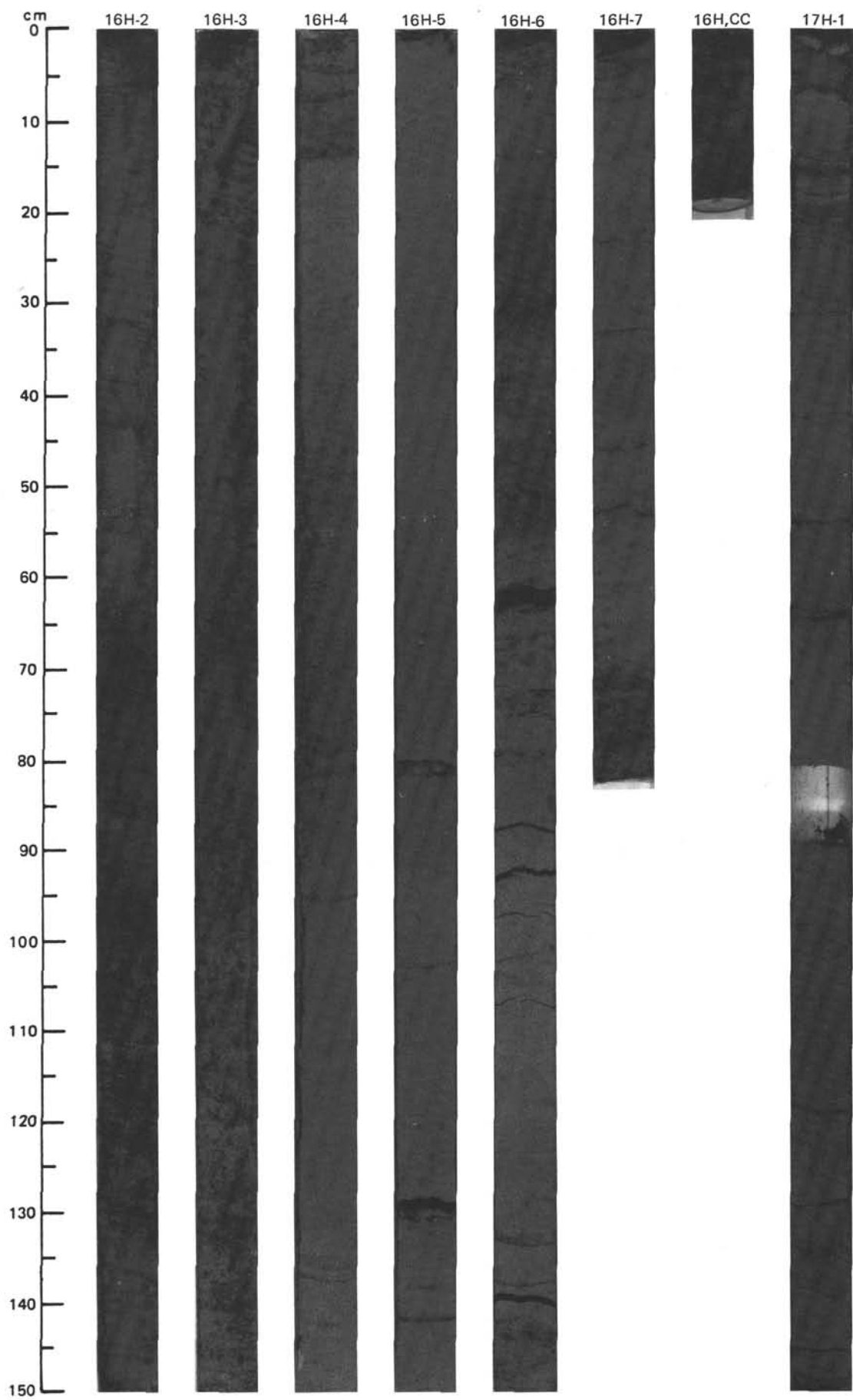


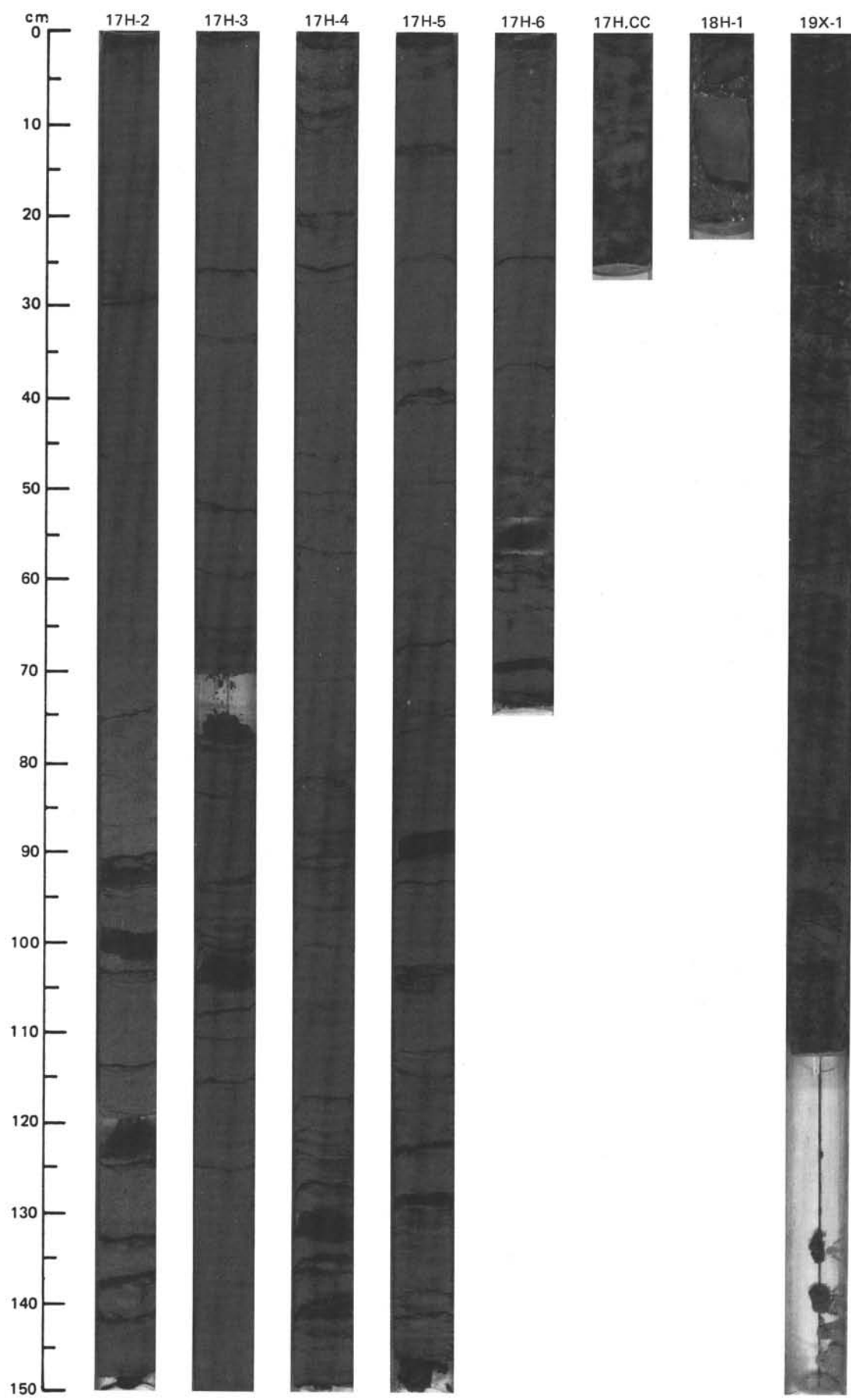
SITE 658 (HOLE A)



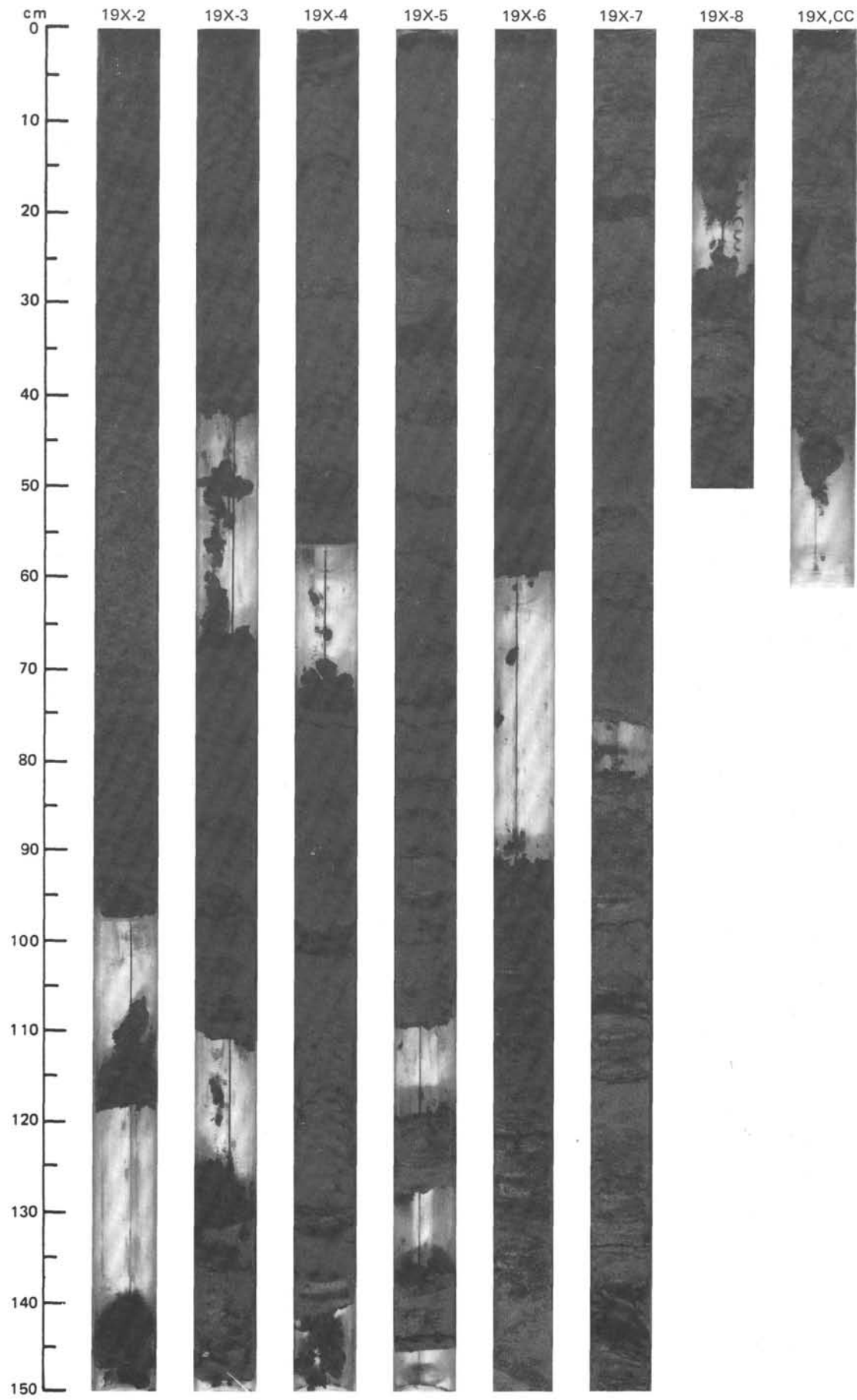


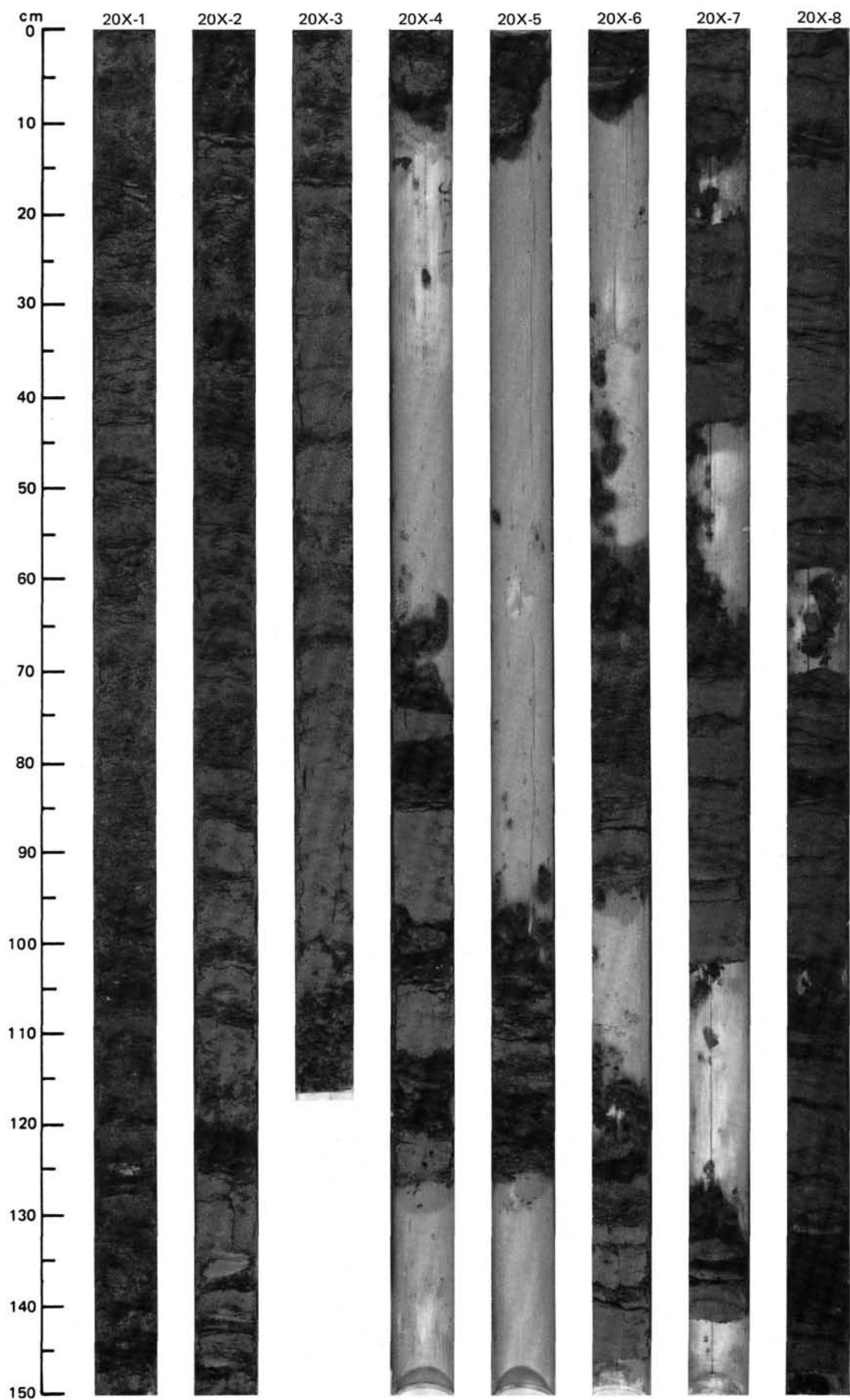
SITE 658 (HOLE A)



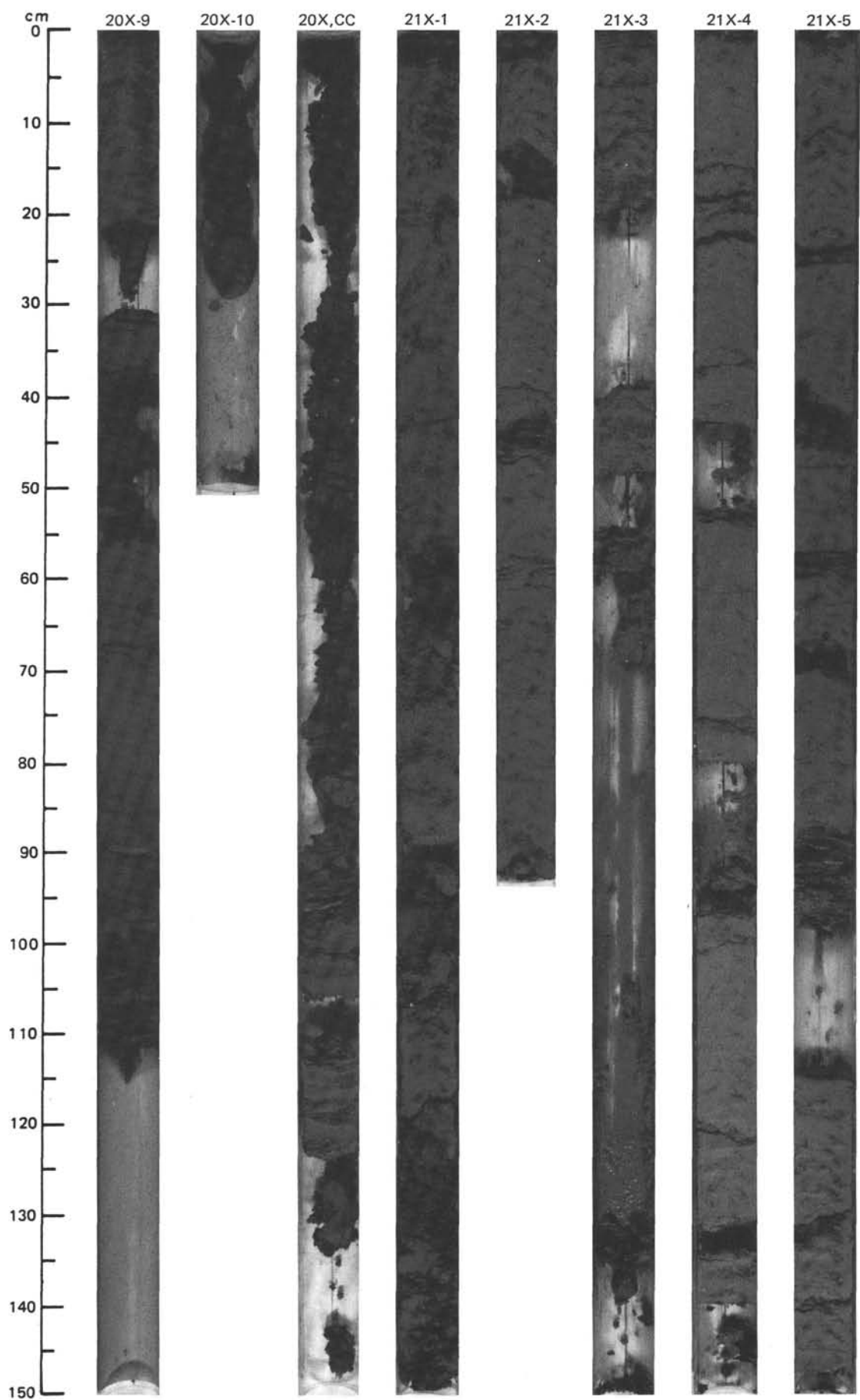


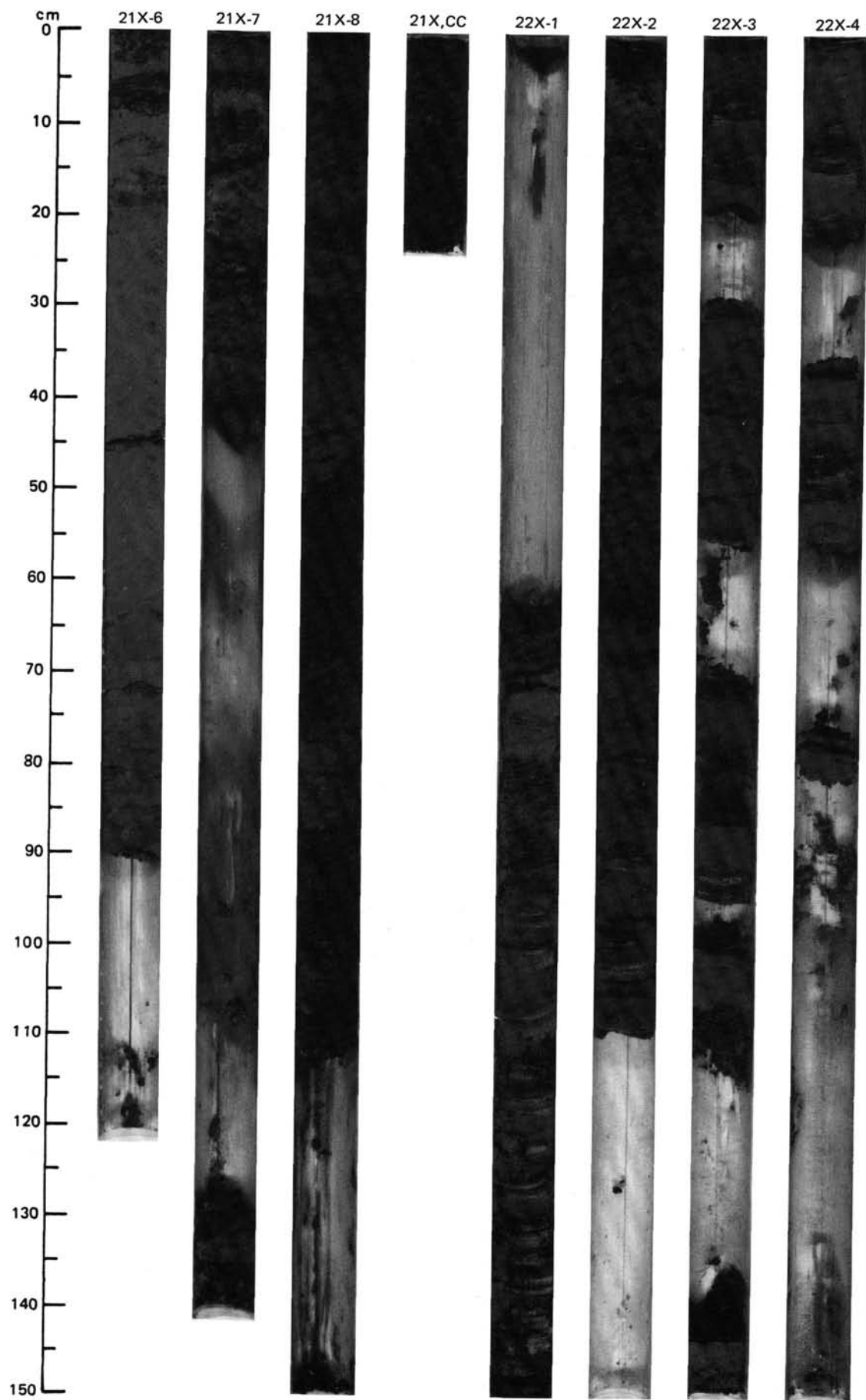
SITE 658 (HOLE A)



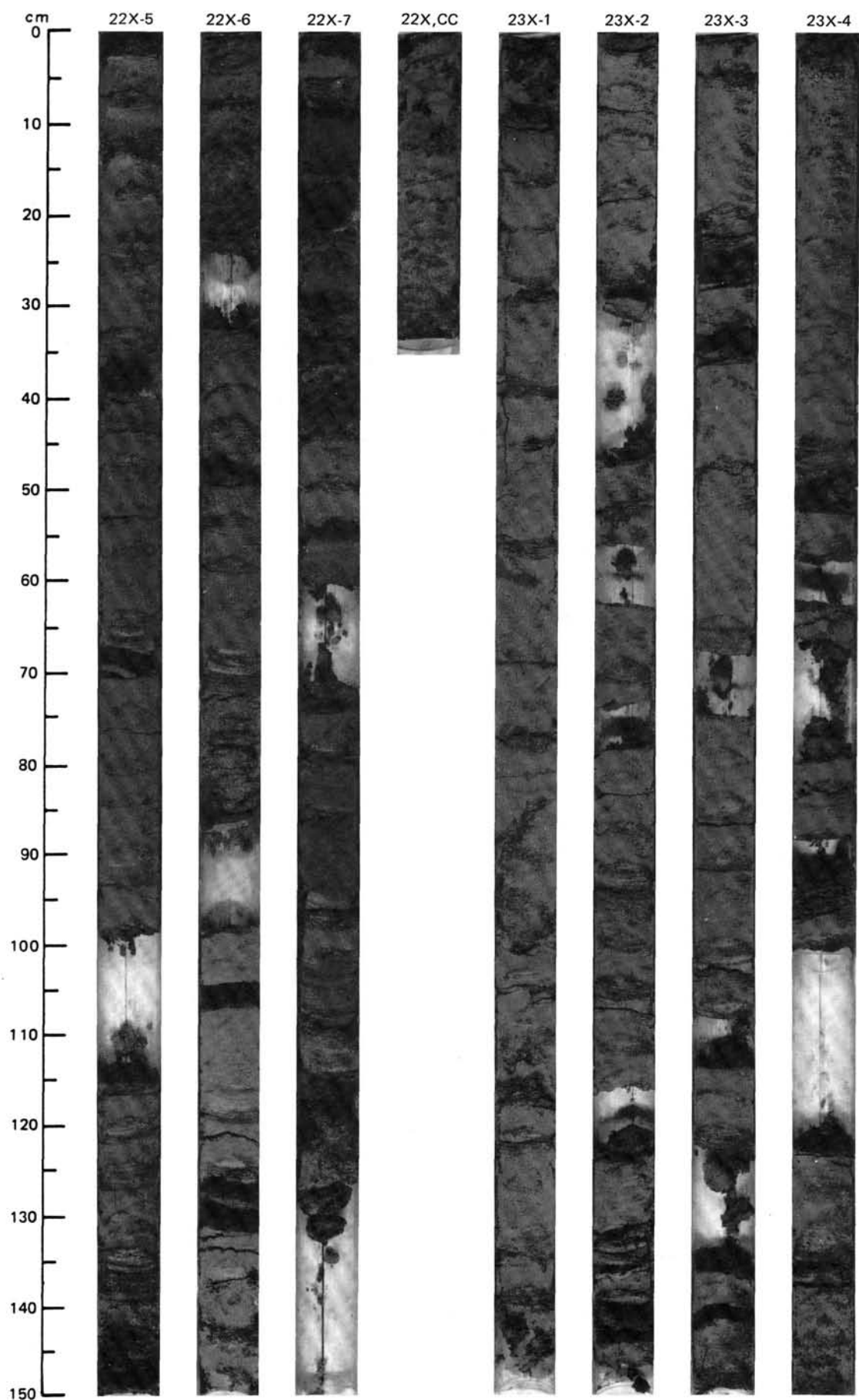


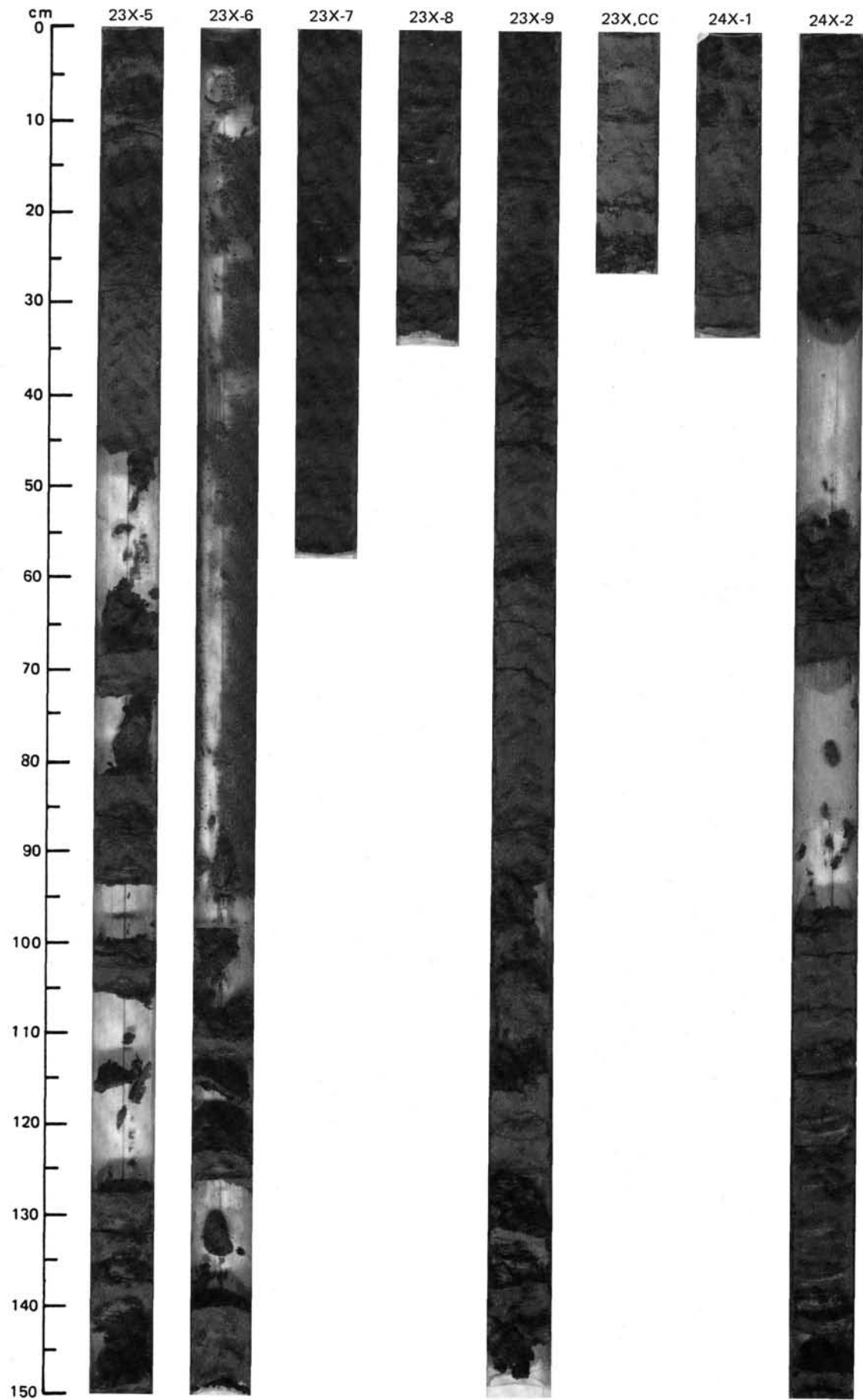
SITE 658 (HOLE A)



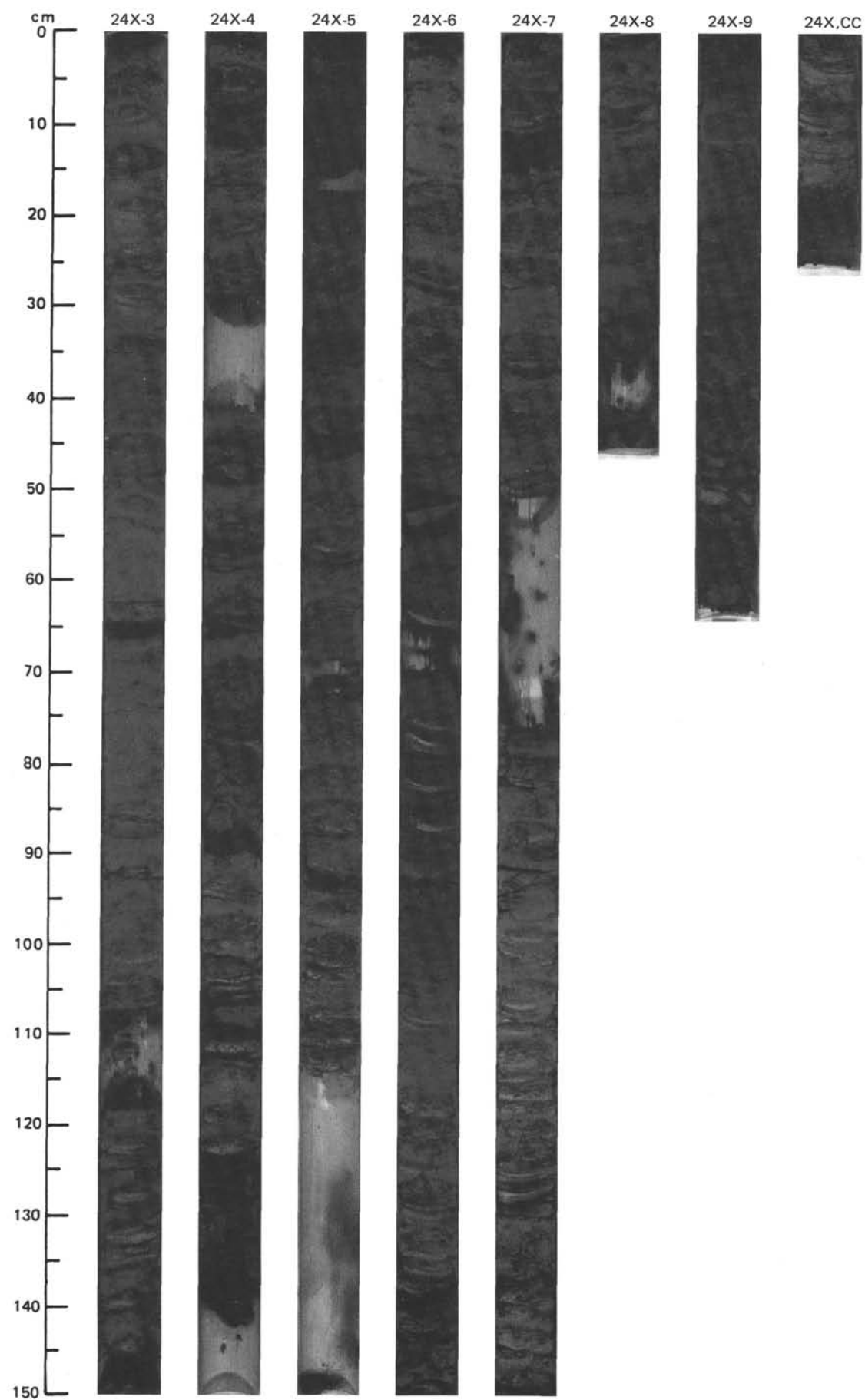


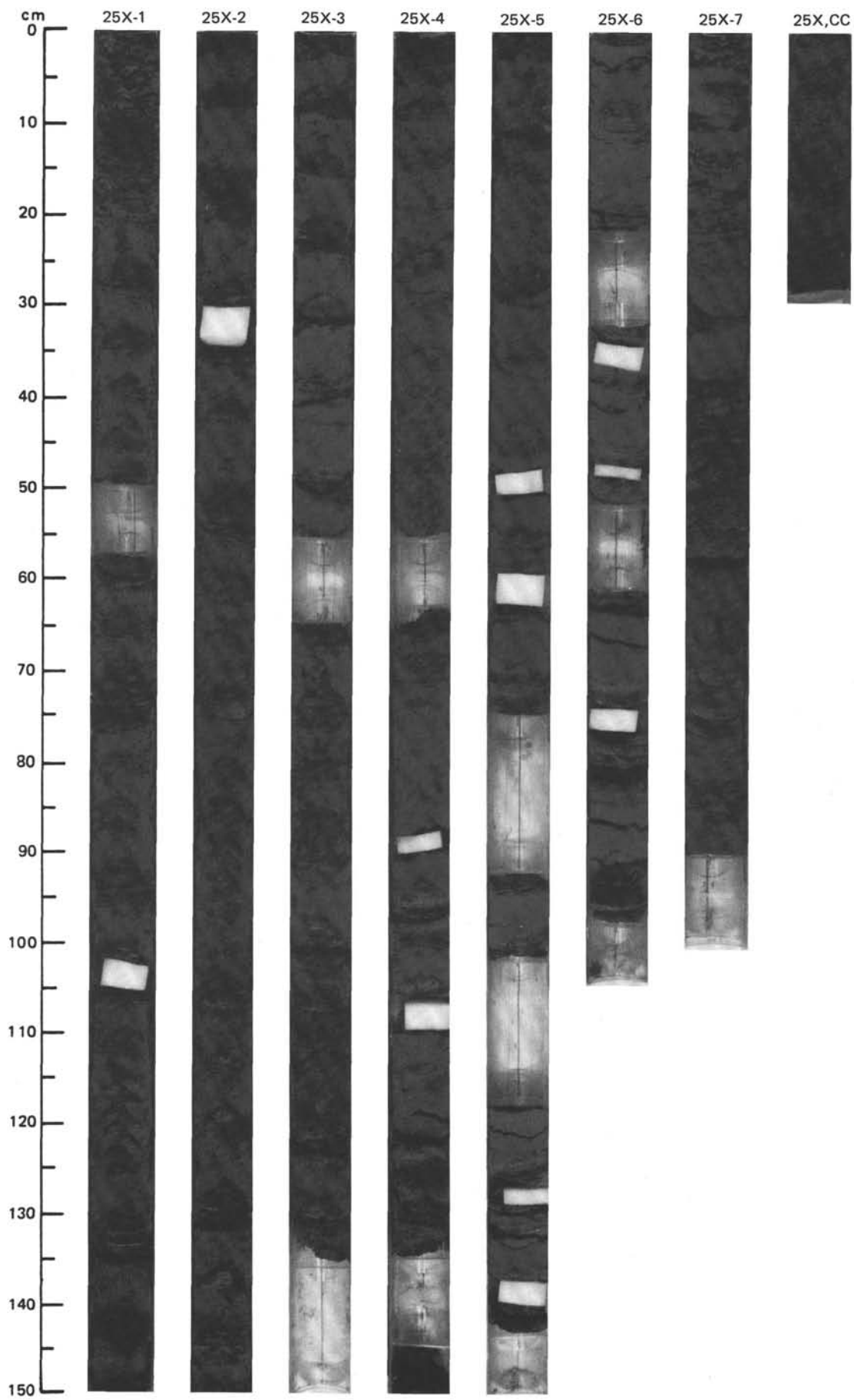
SITE 658 (HOLE A)



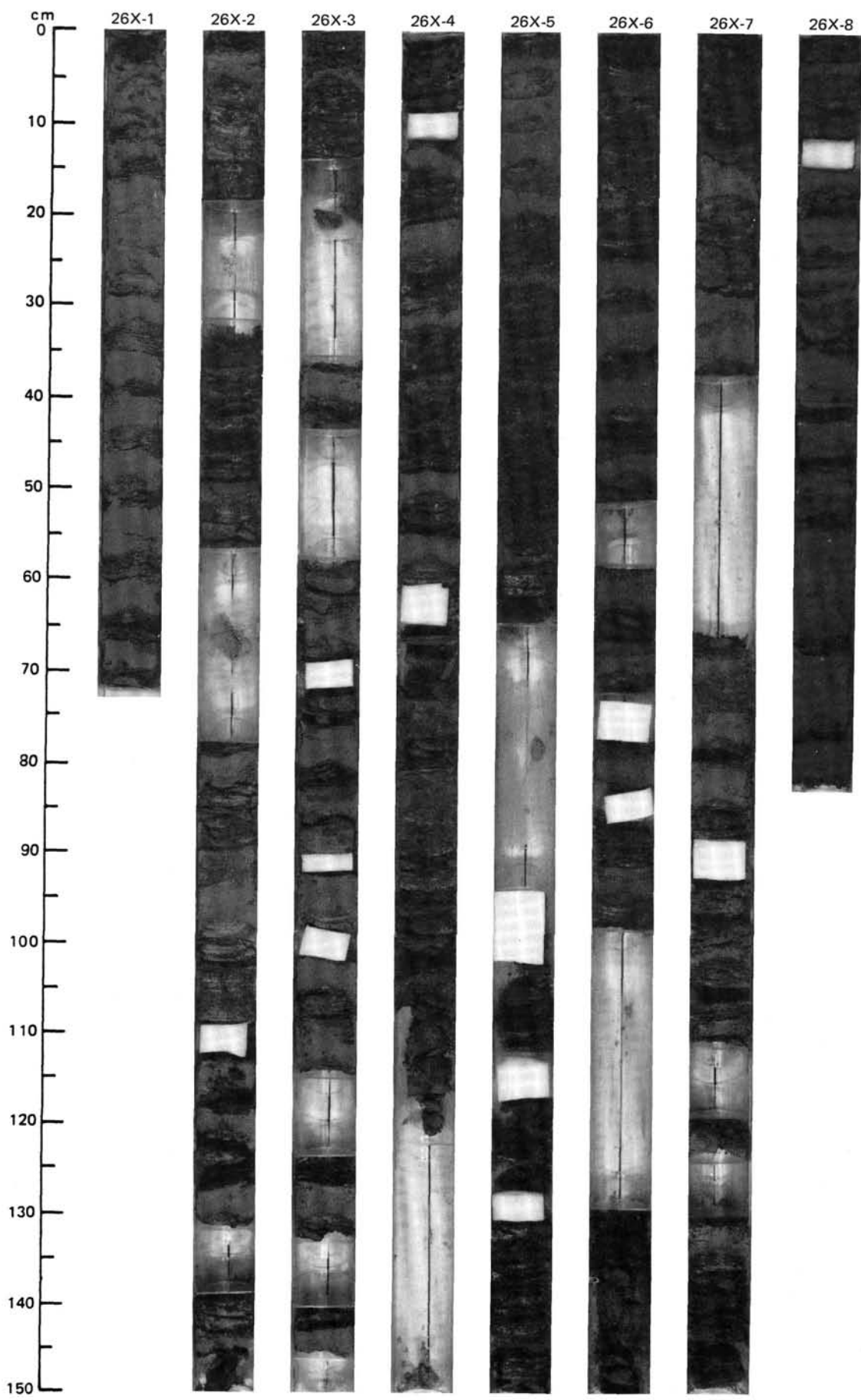


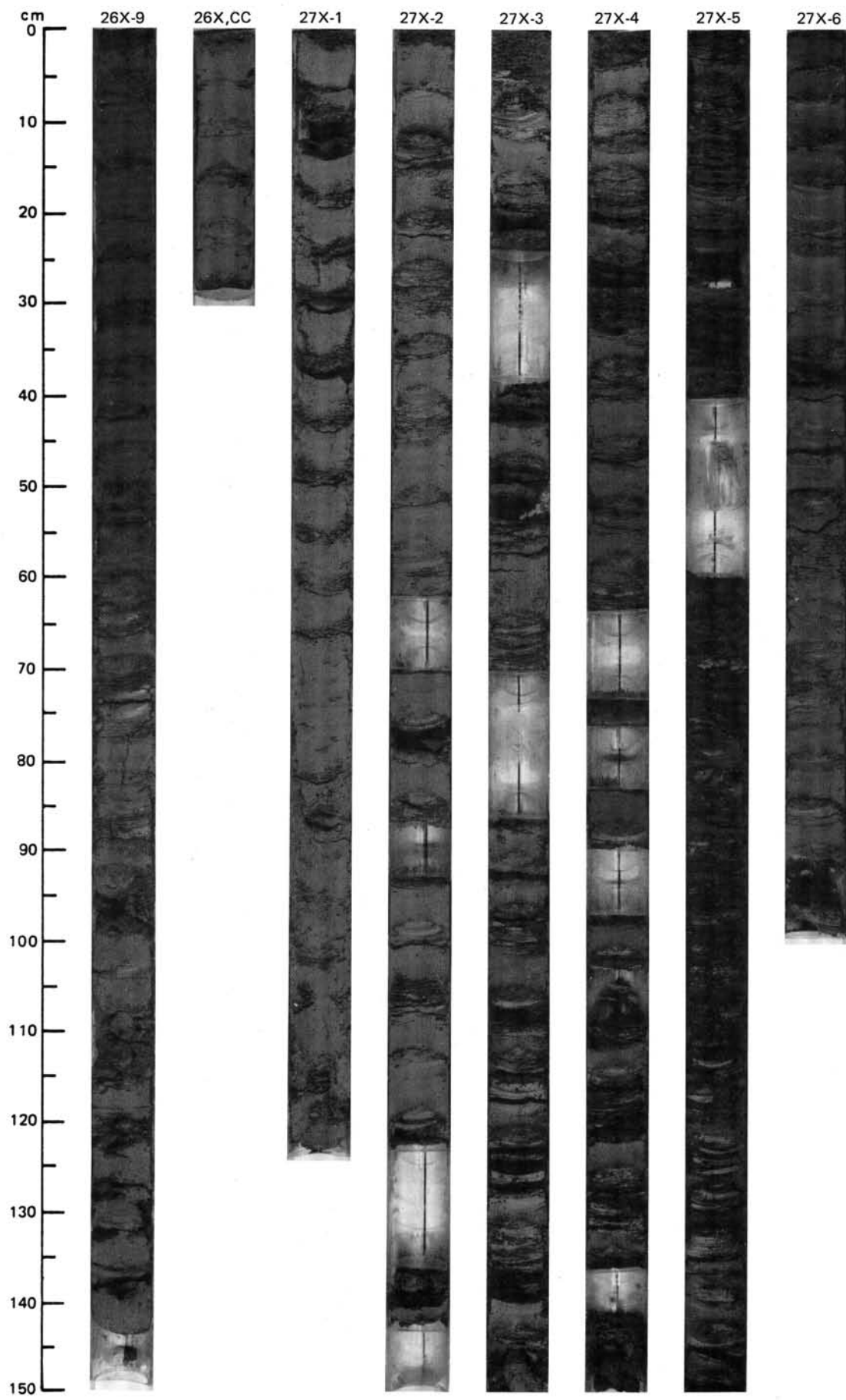
SITE 658 (HOLE A)



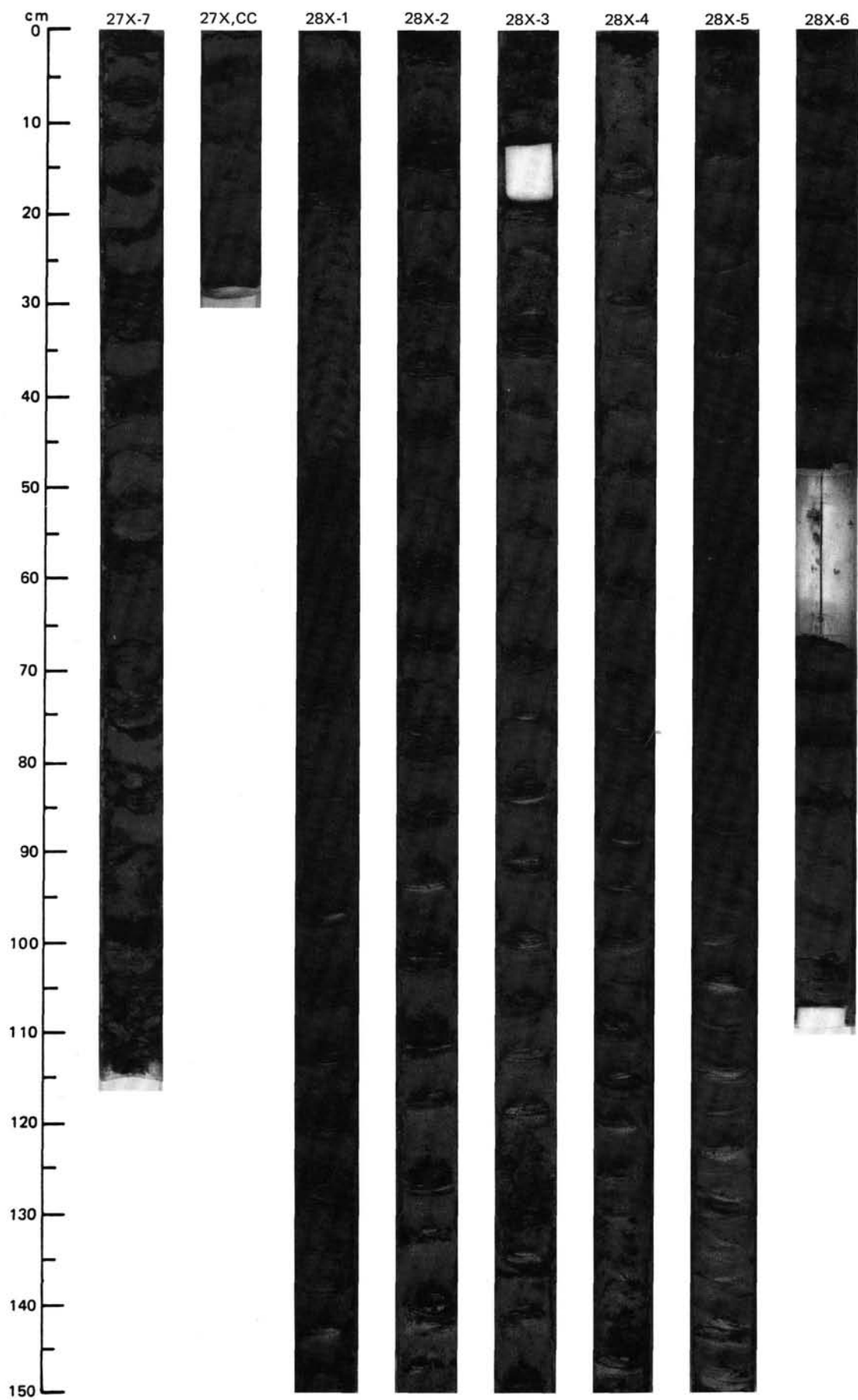


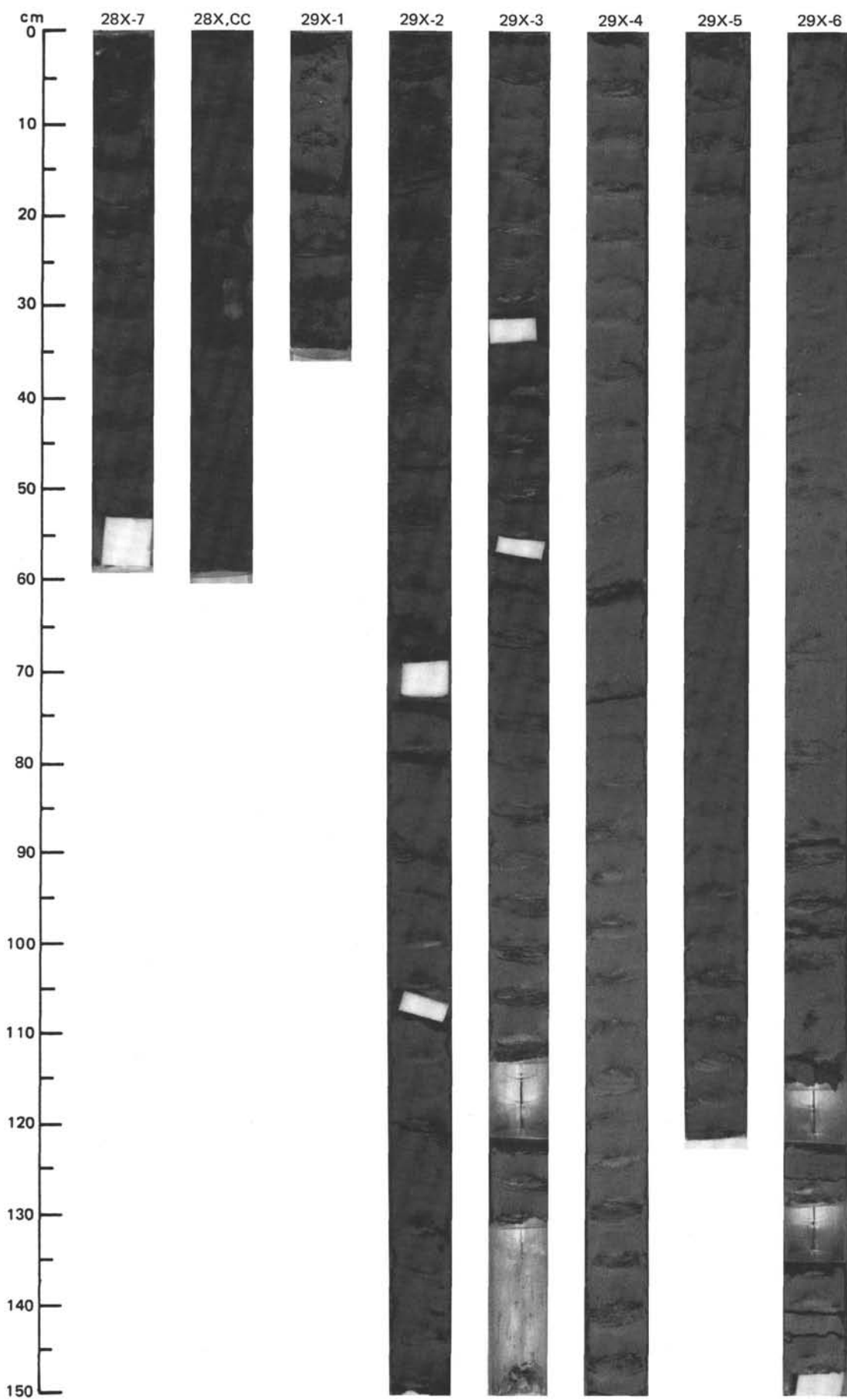
SITE 658 (HOLE A)



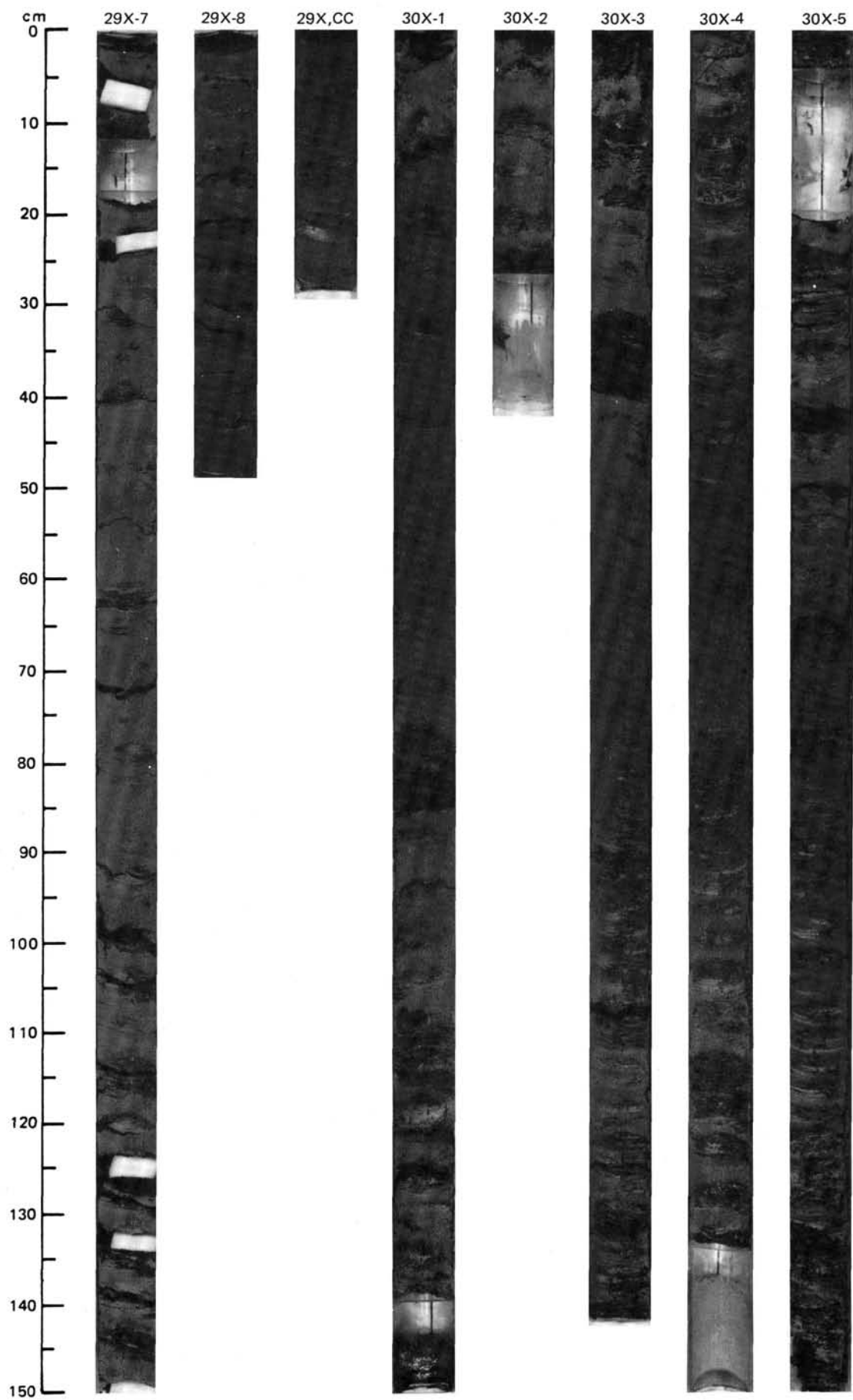


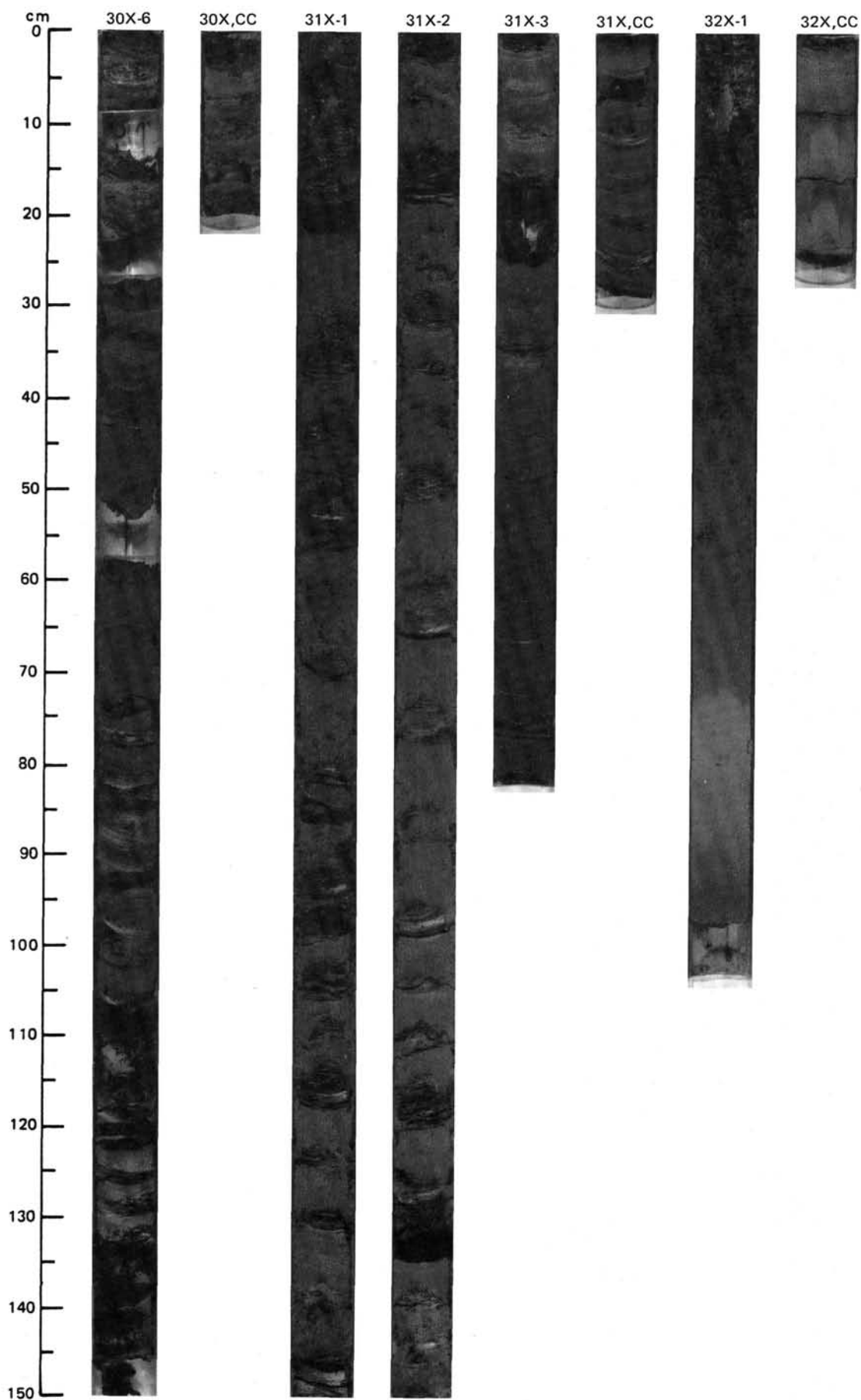
SITE 658 (HOLE A)



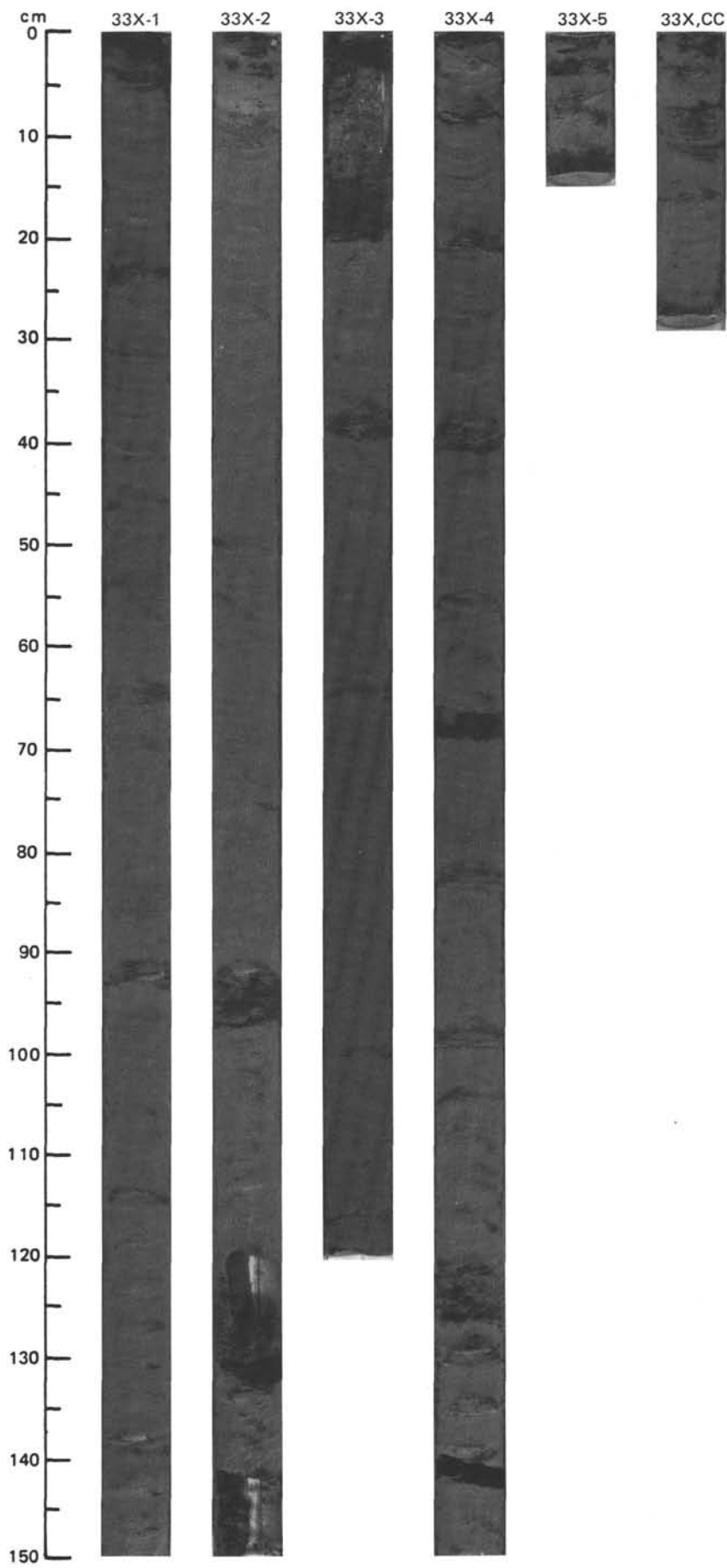


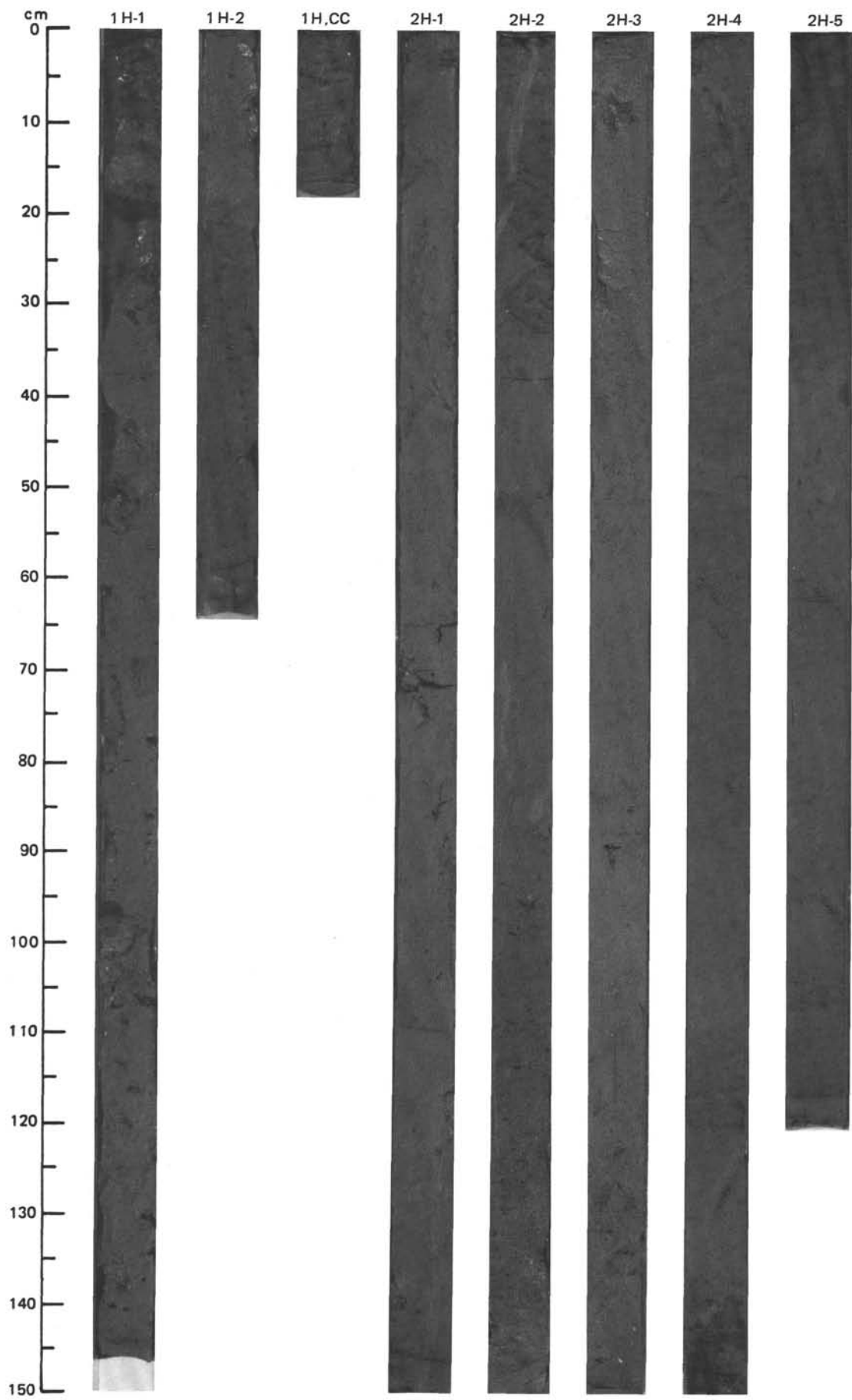
SITE 658 (HOLE A)



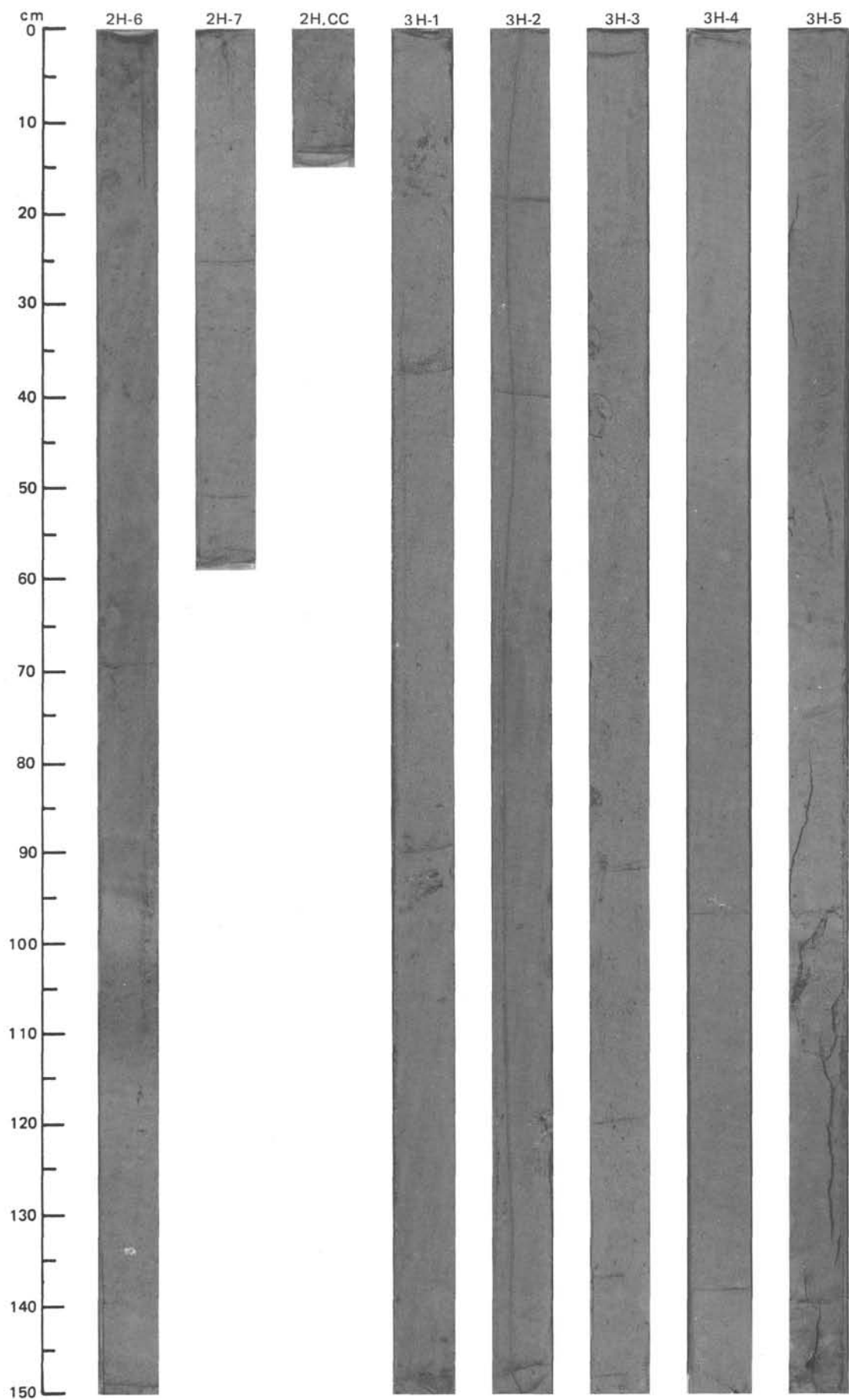


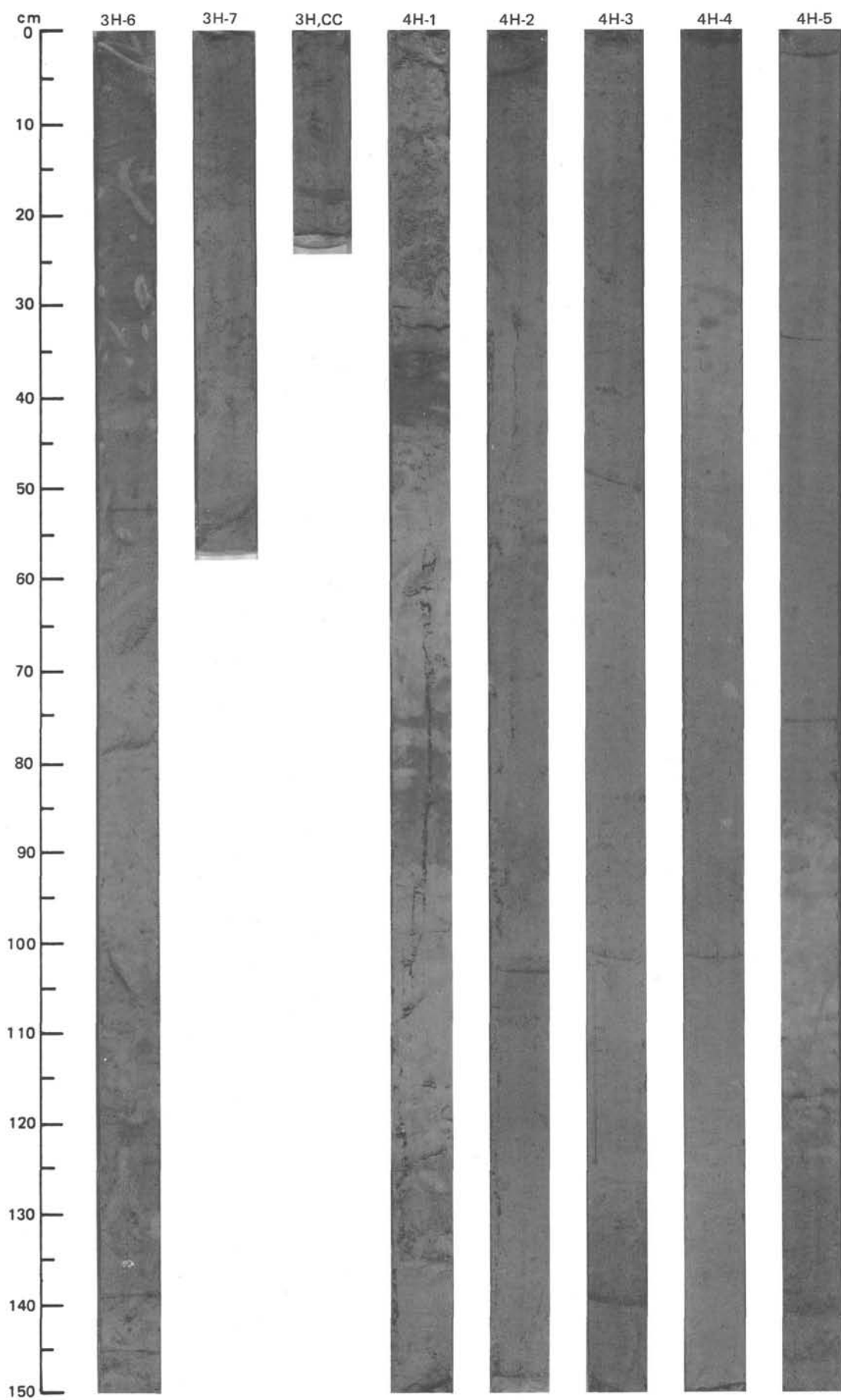
SITE 658 (HOLE A)



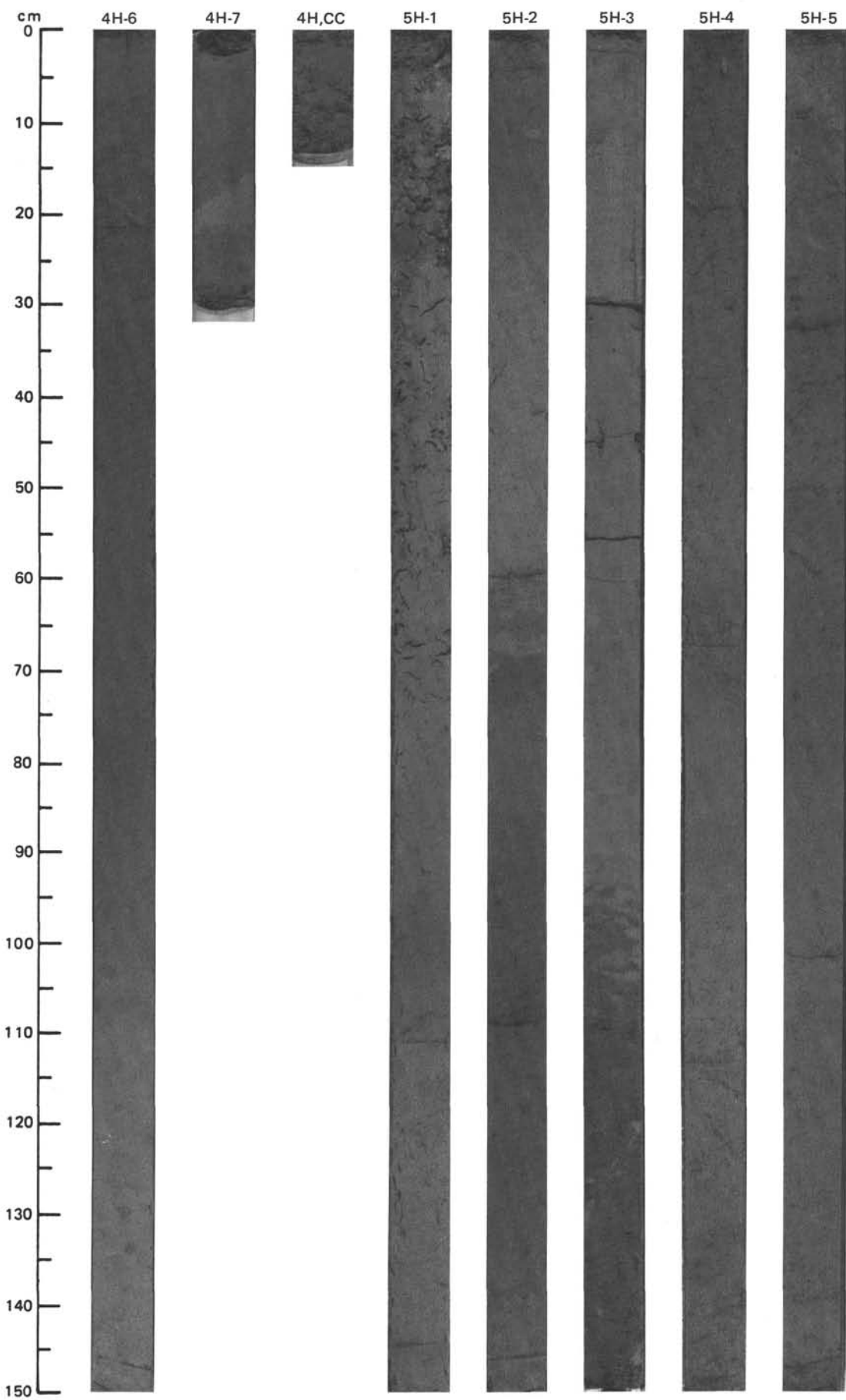


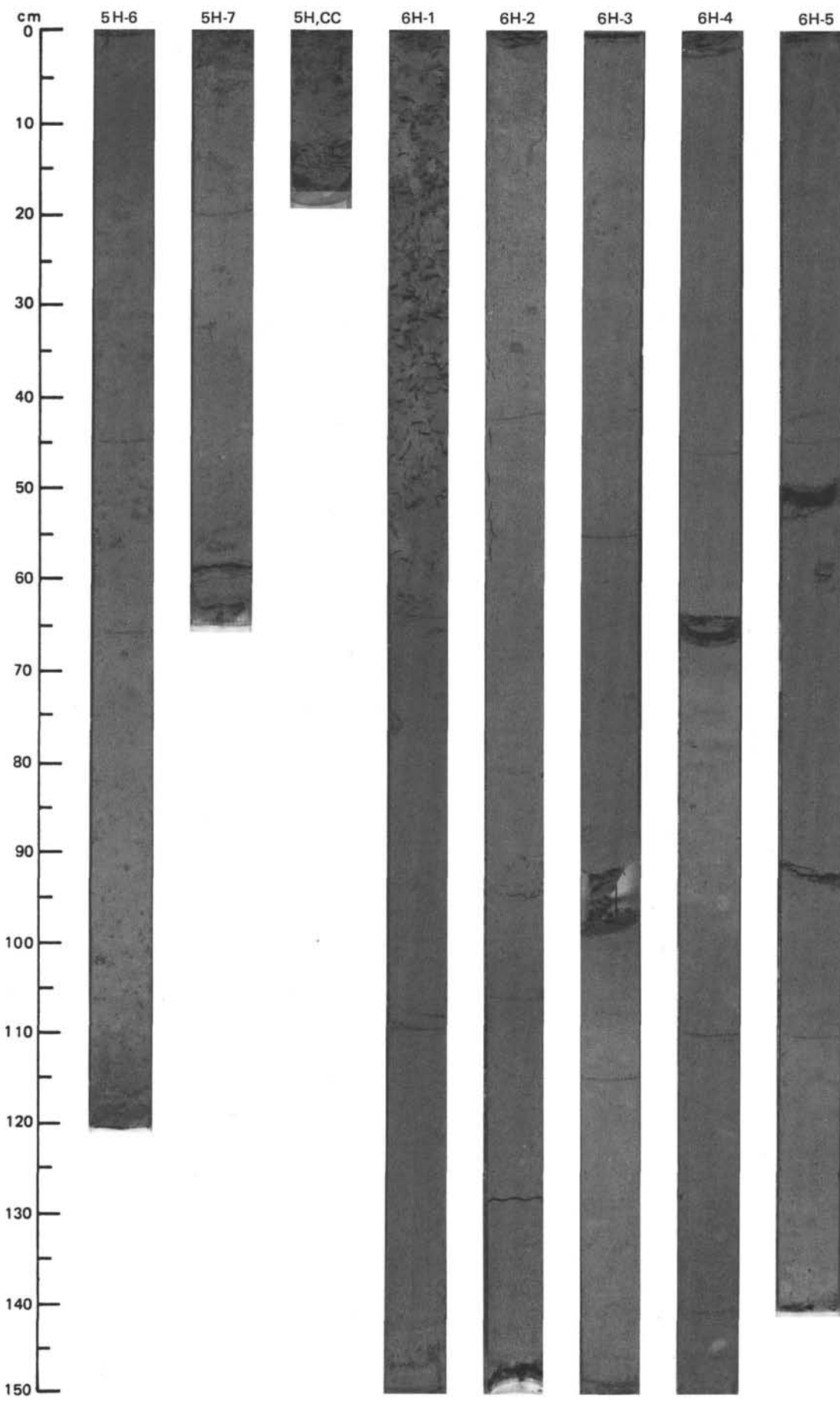
SITE 658 (HOLE B)



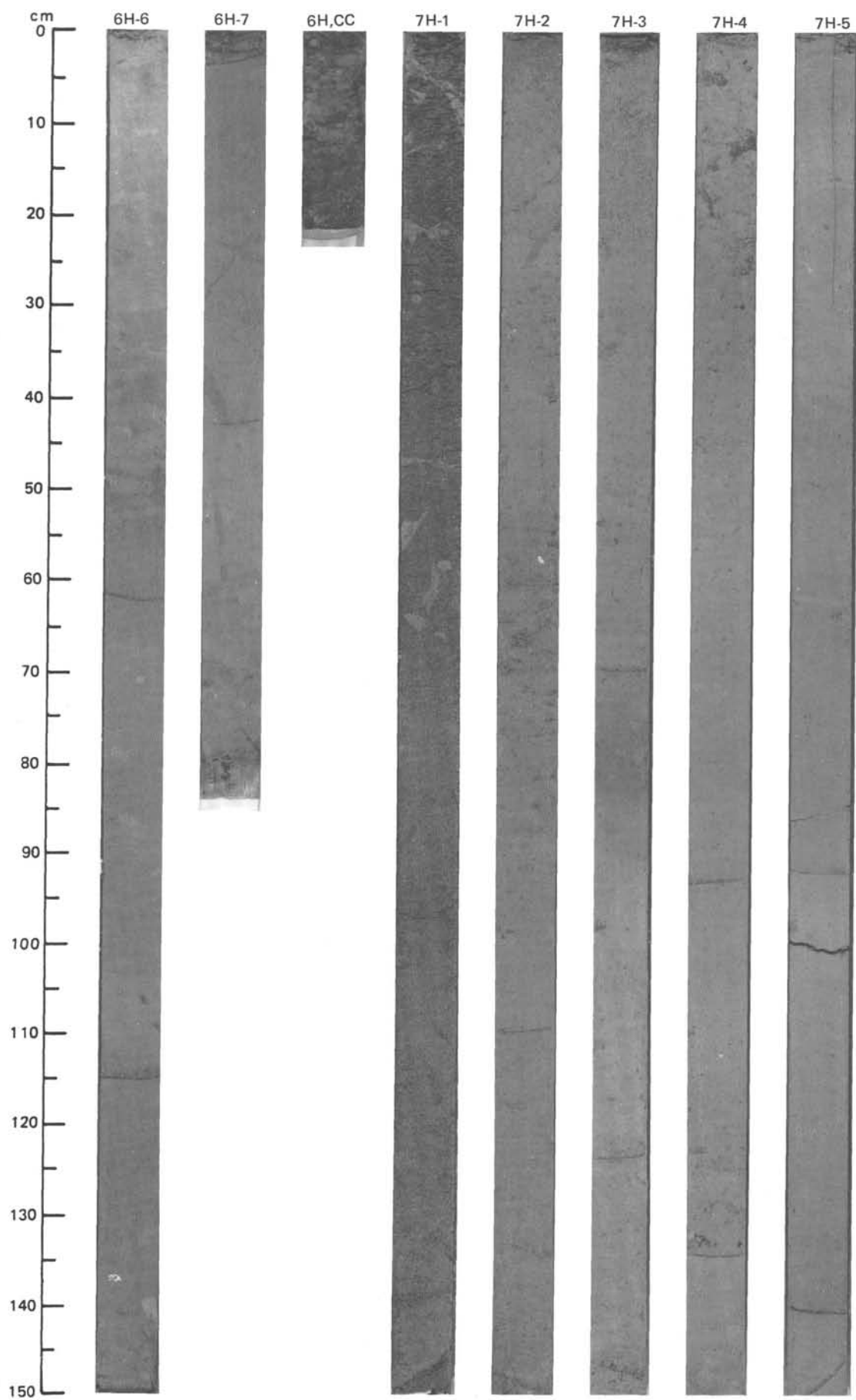


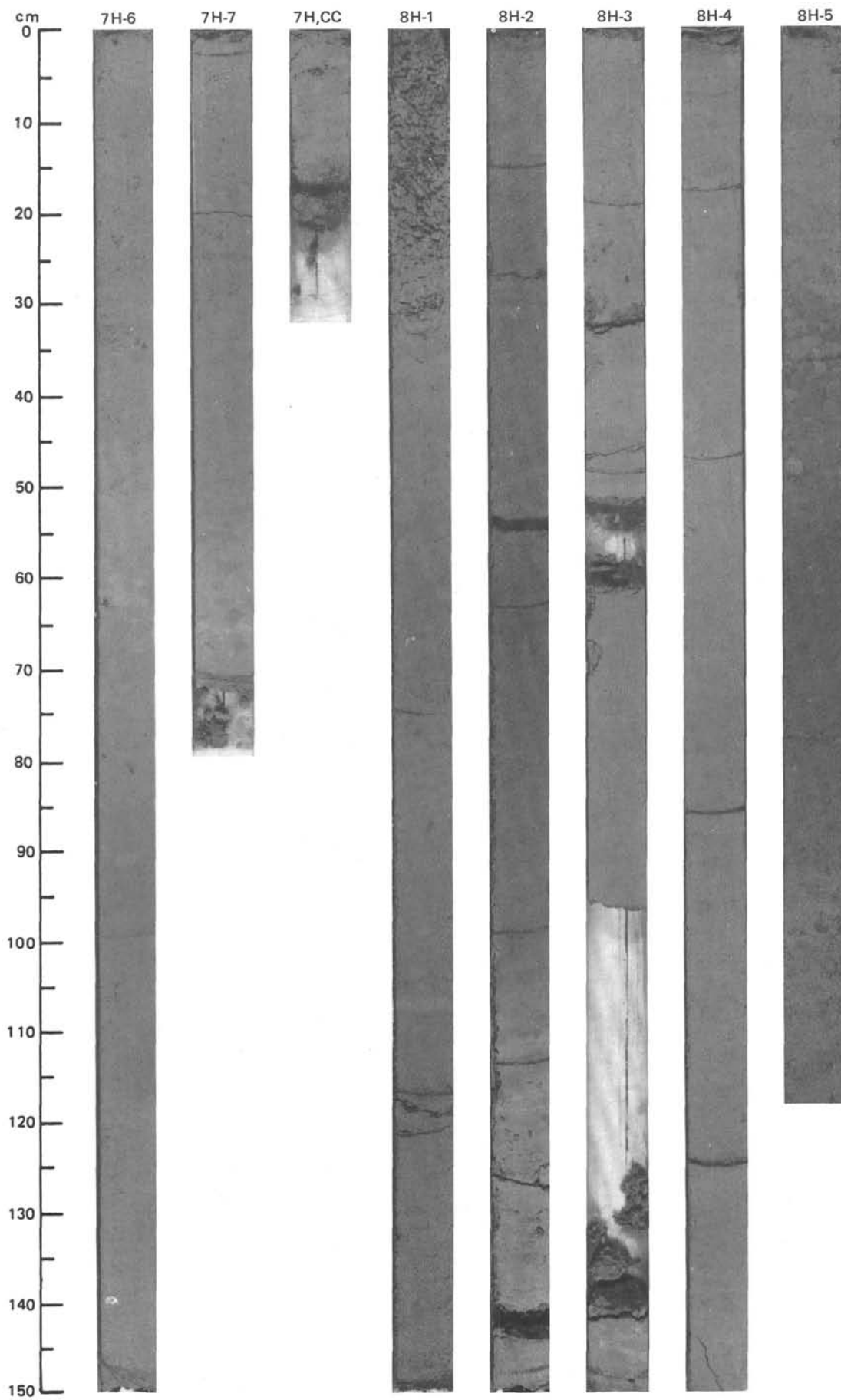
SITE 658 (HOLE B)



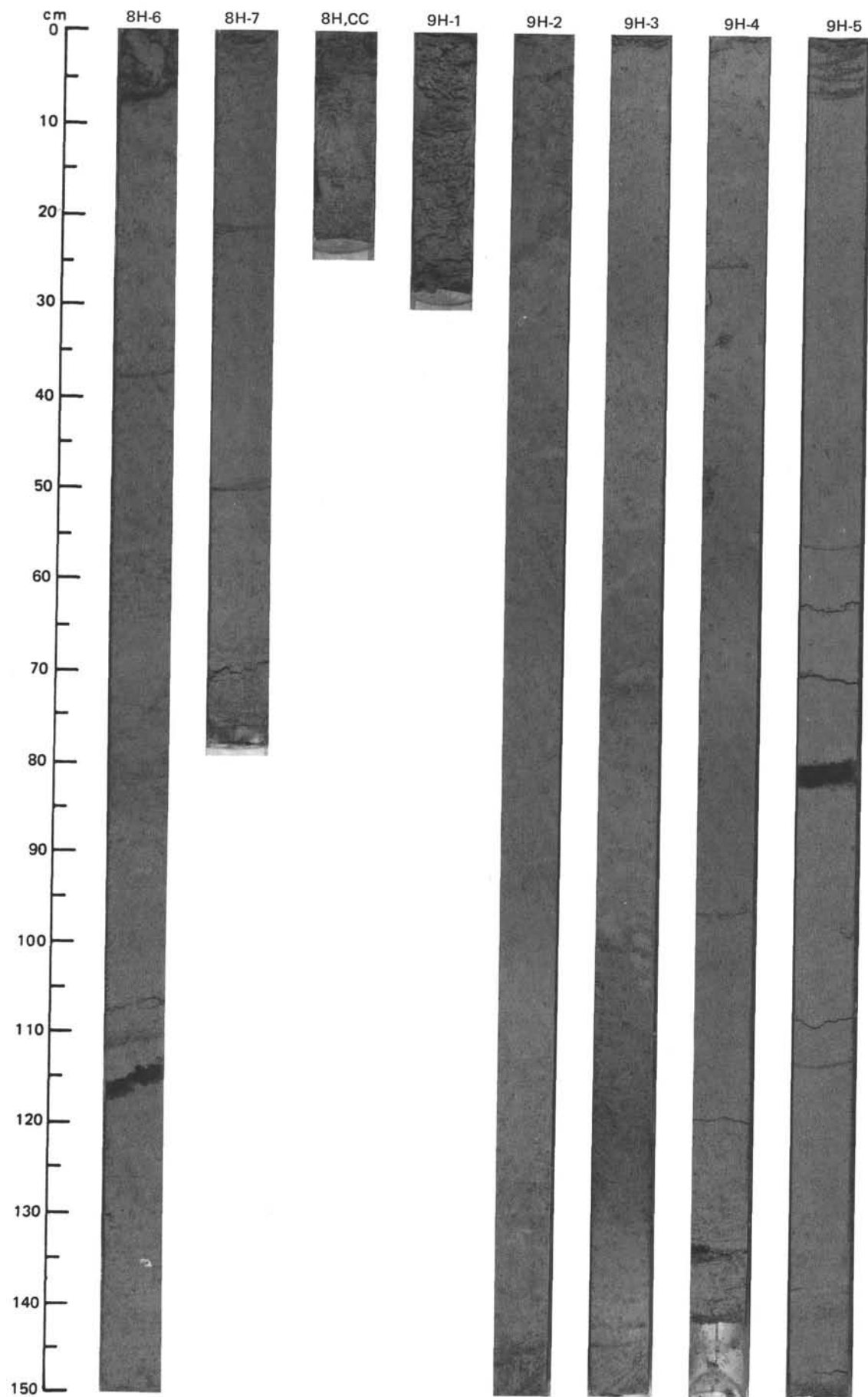


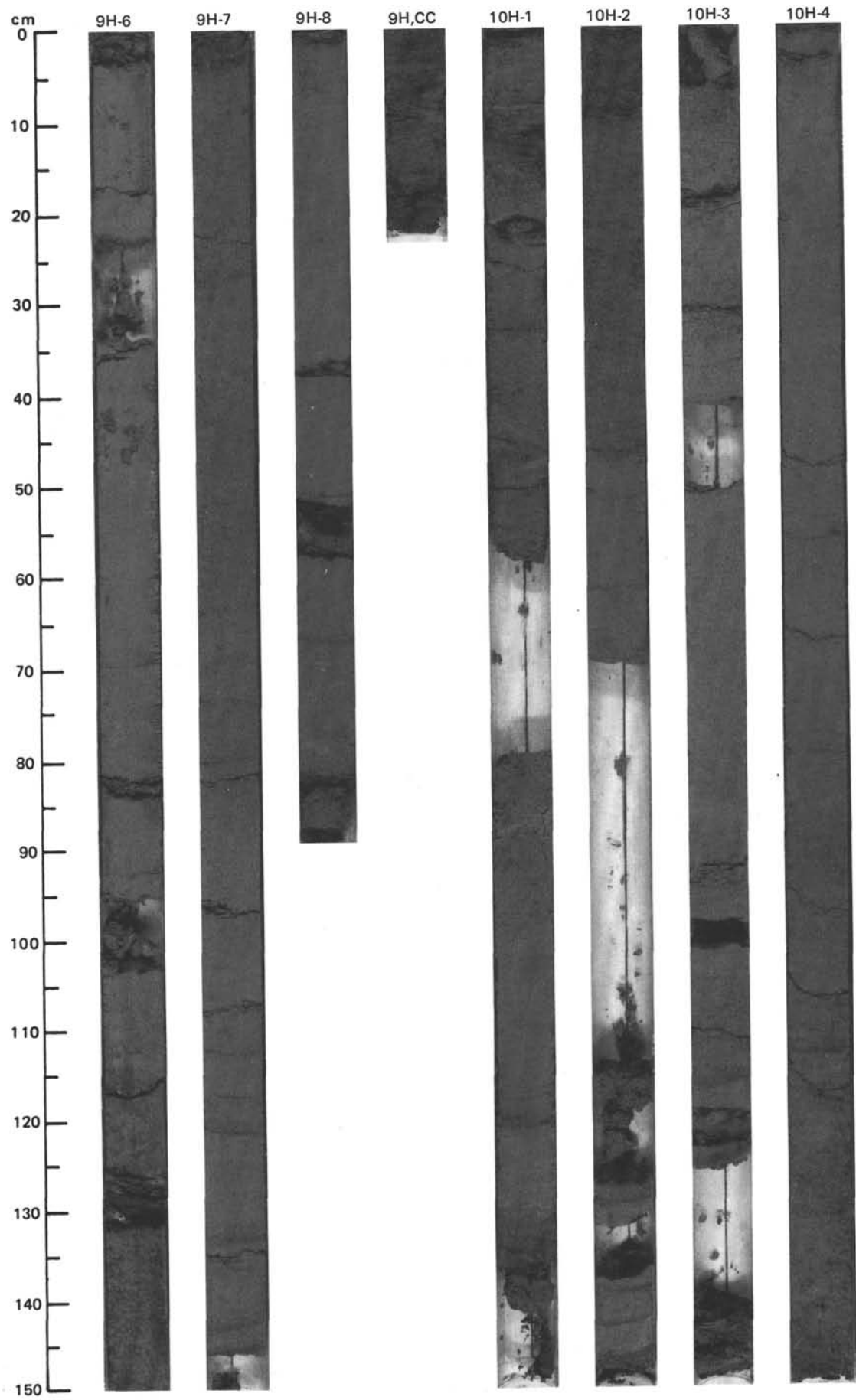
SITE 658 (HOLE B)



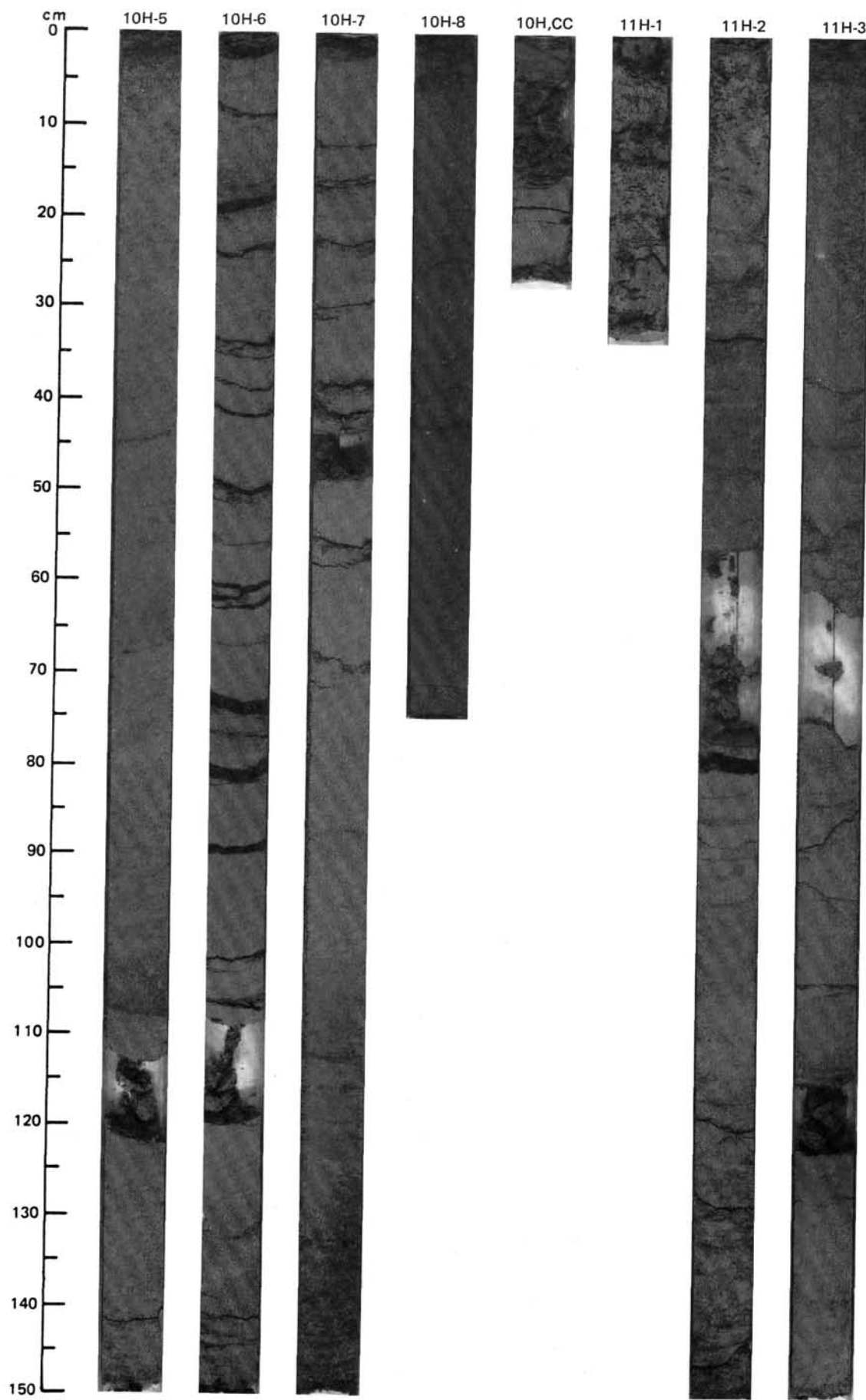


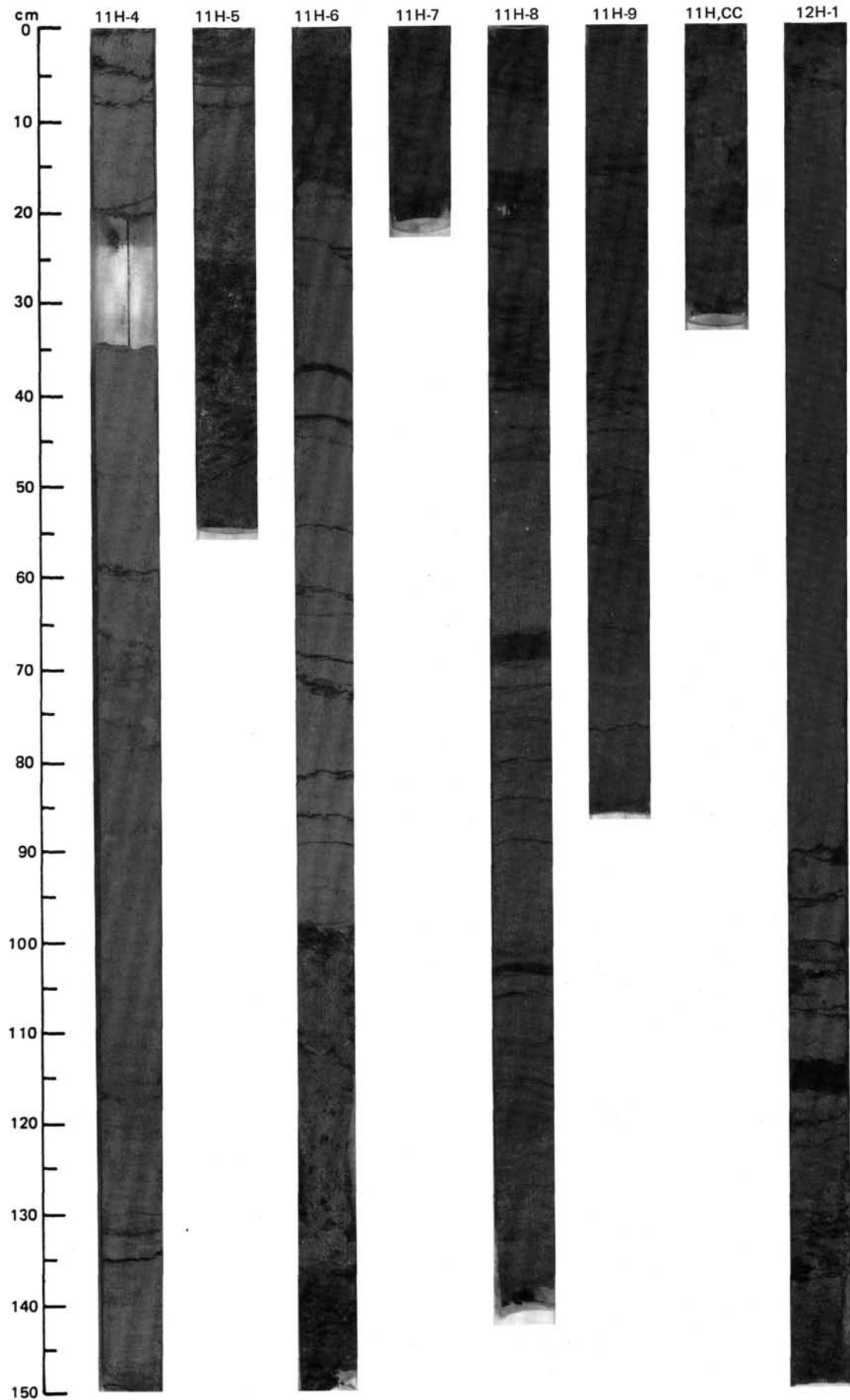
SITE 658 (HOLE B)



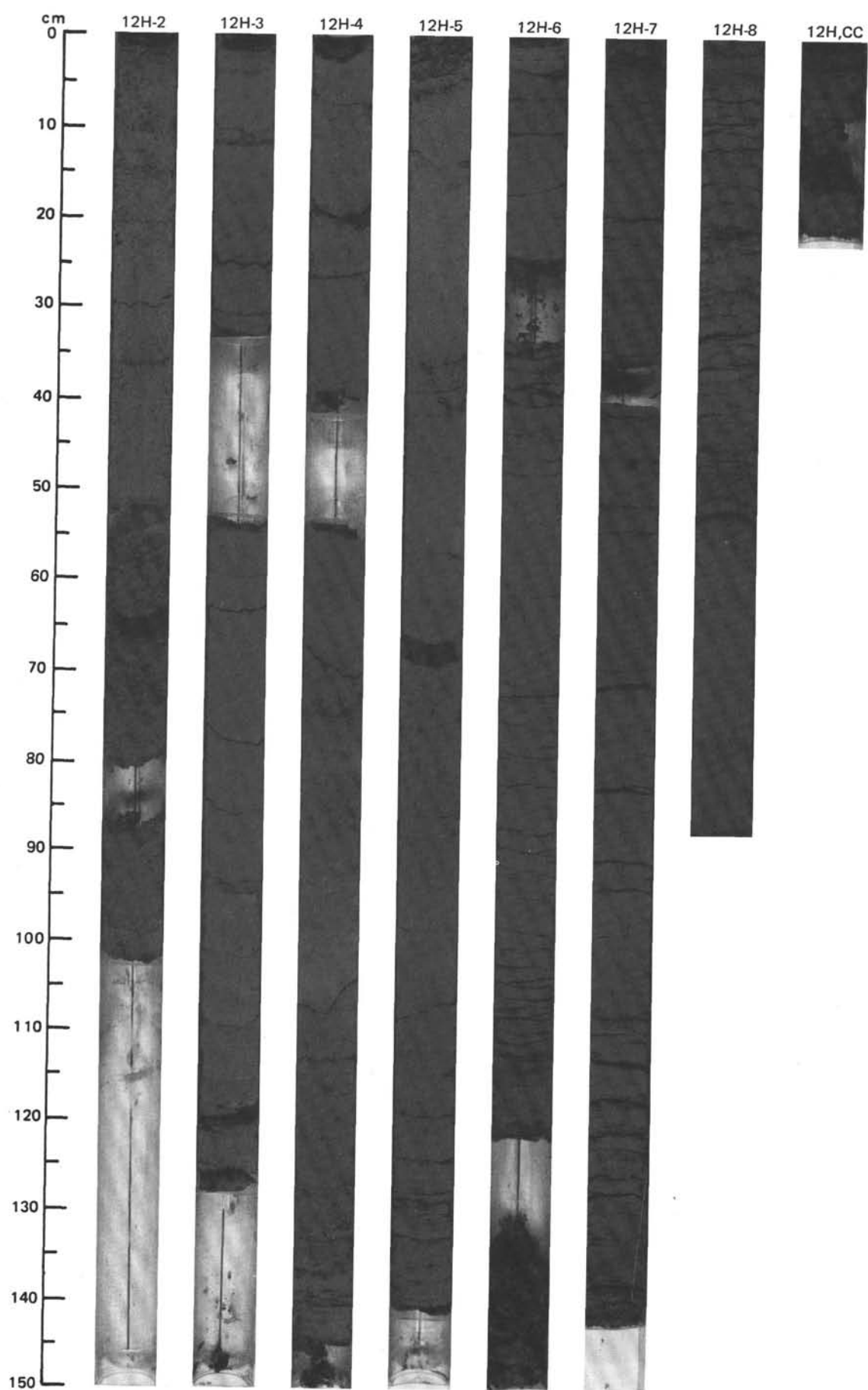


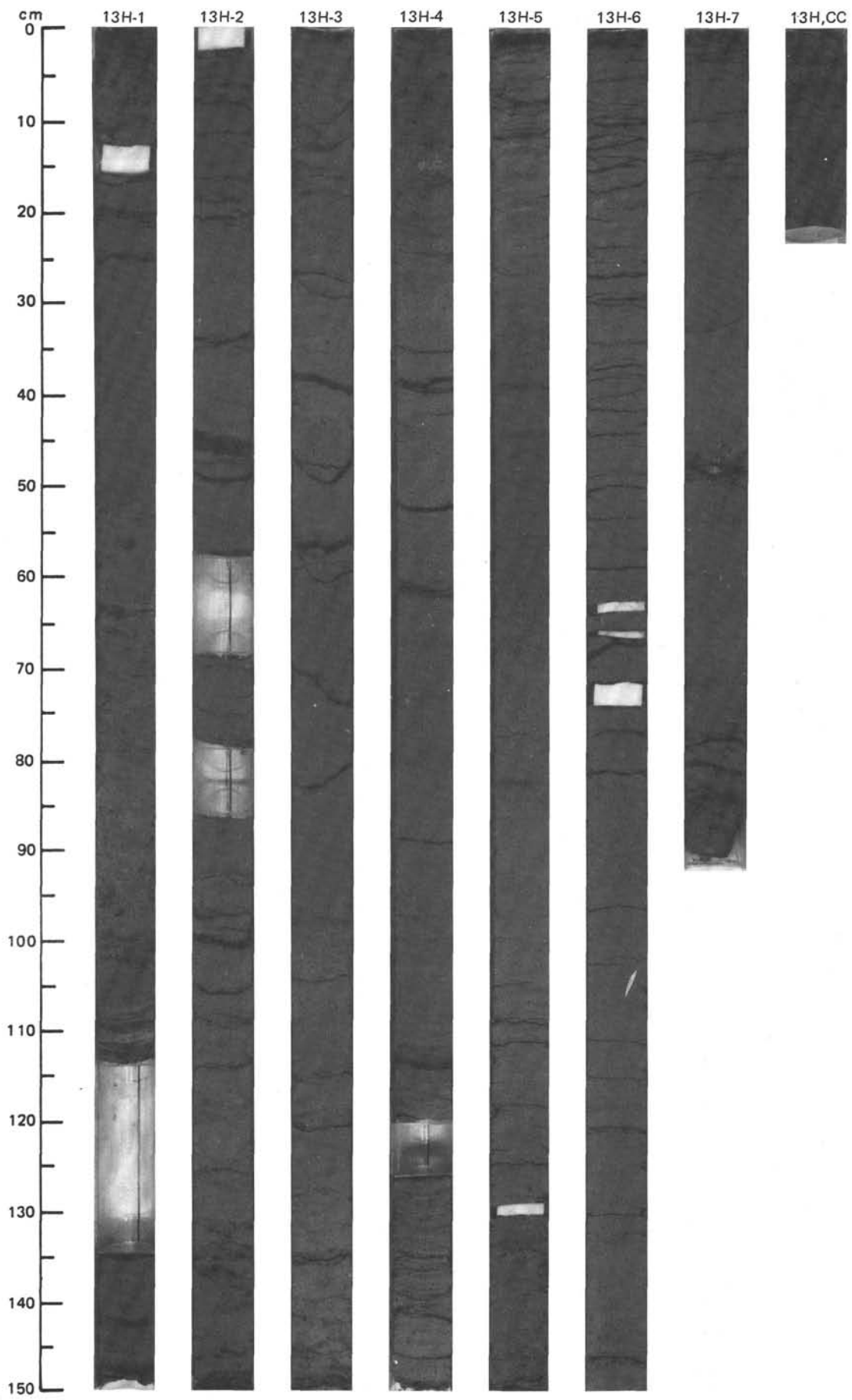
SITE 658 (HOLE B)



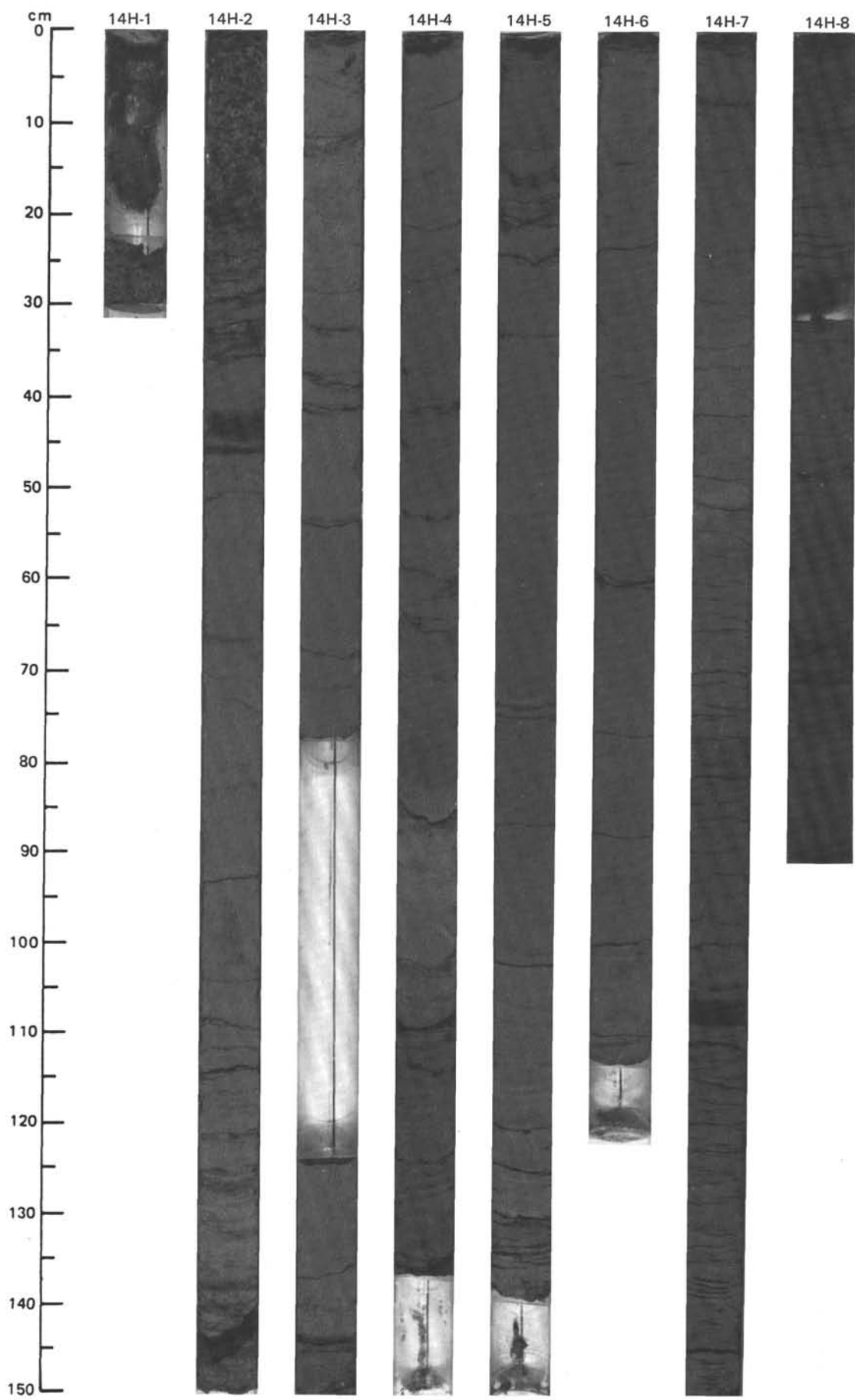


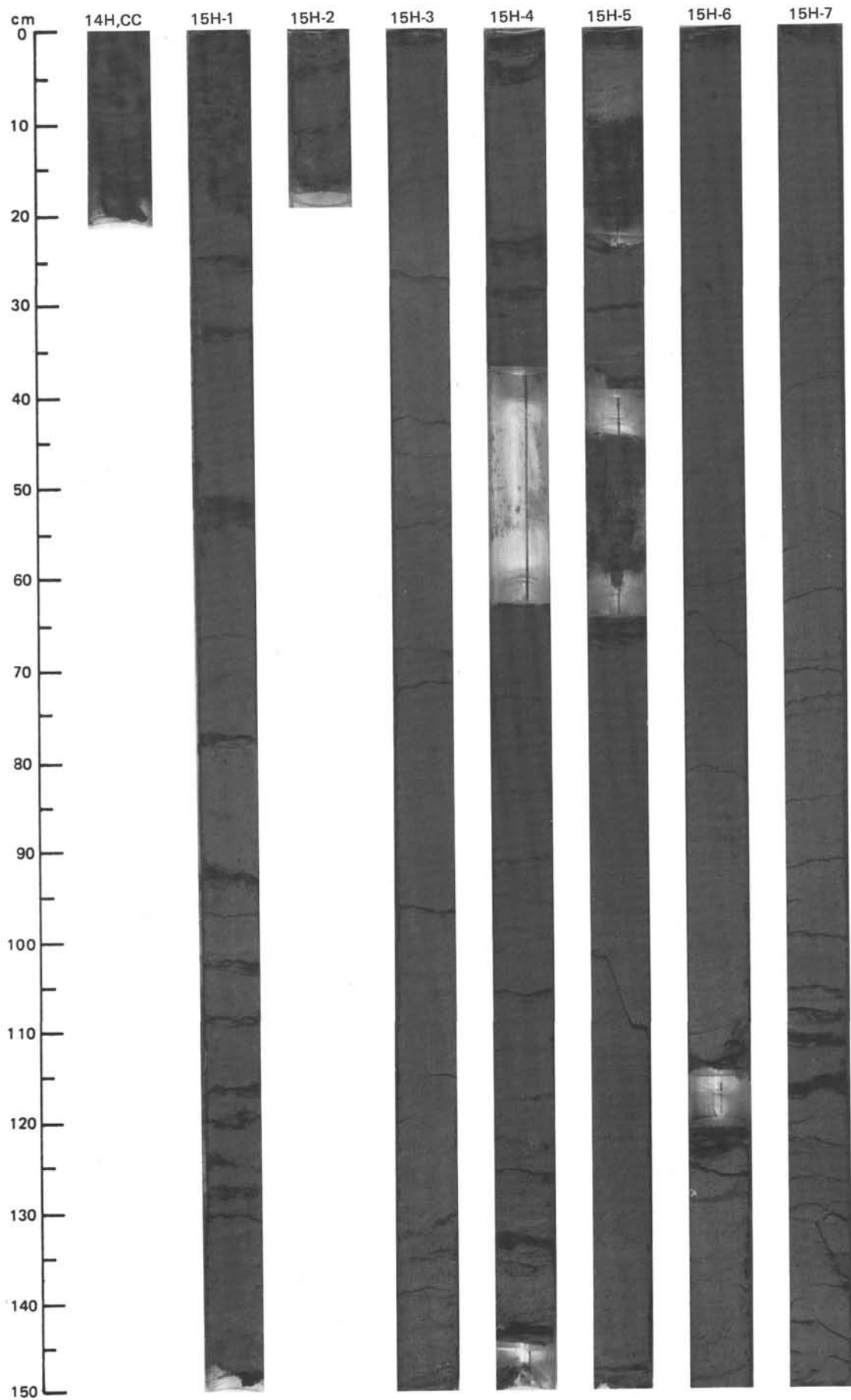
SITE 658 (HOLE B)



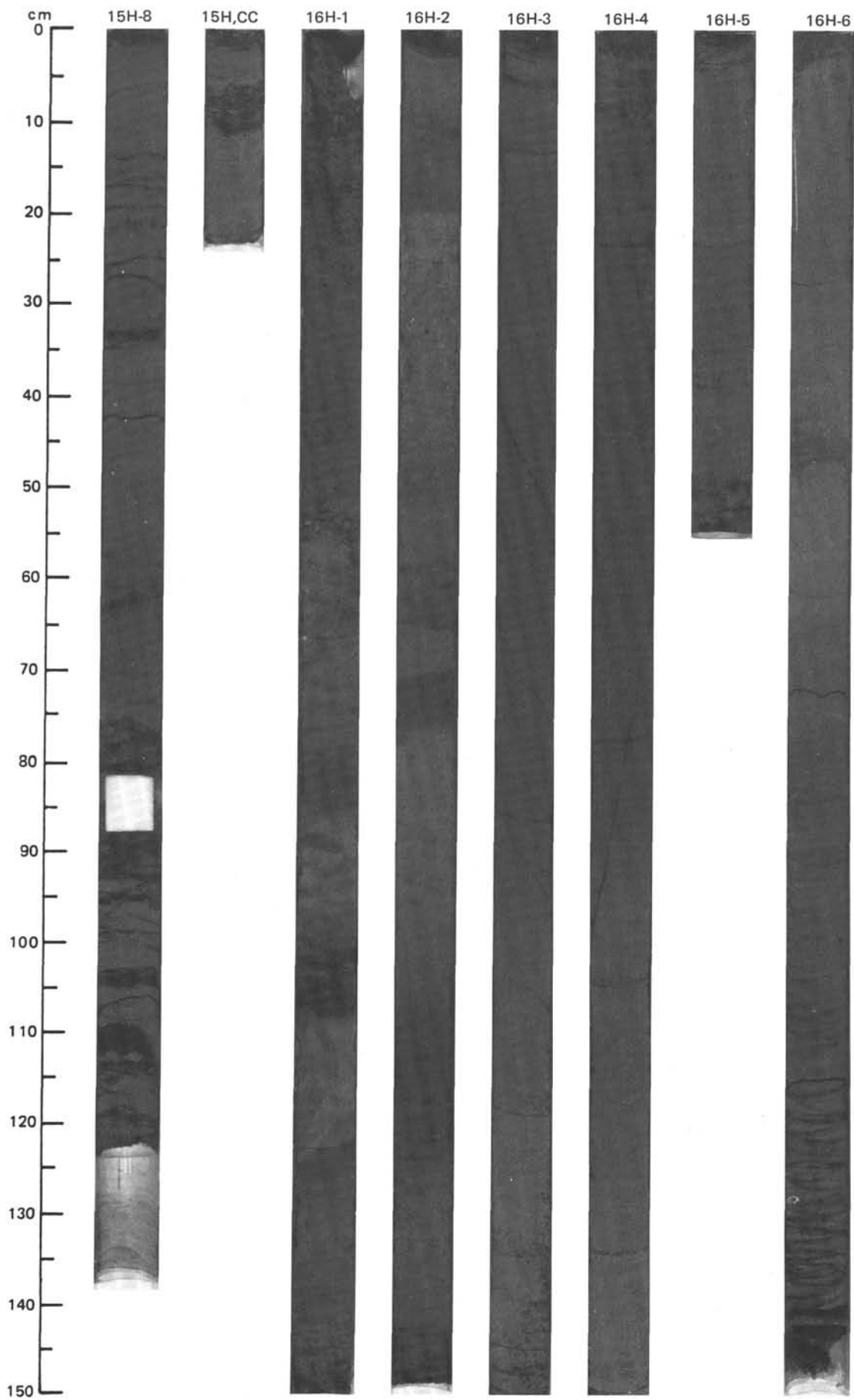


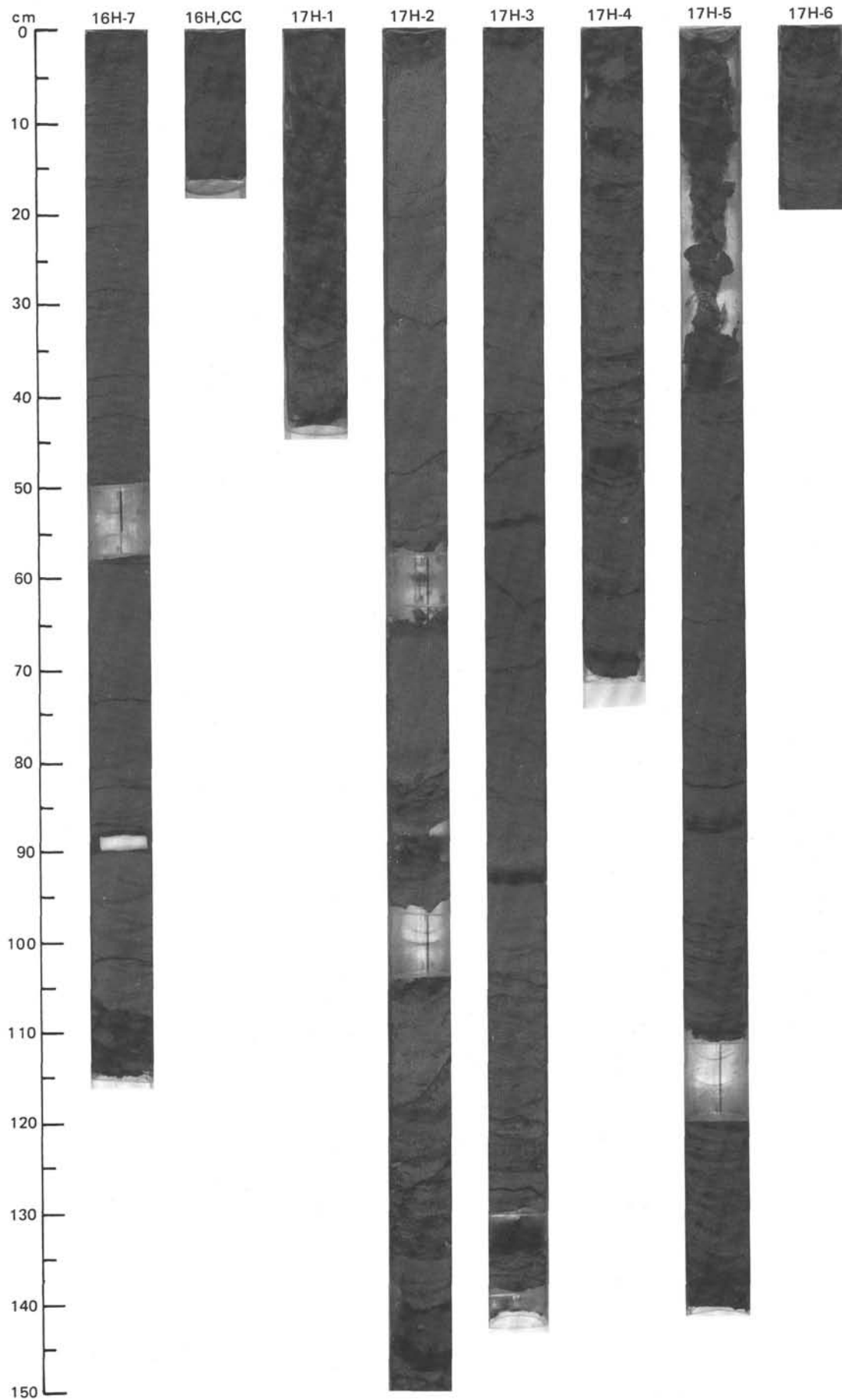
SITE 658 (HOLE B)





SITE 658 (HOLE B)





SITE 658 (HOLE B)

